

**CHARACTERISING THE MOLECULAR FUNCTION OF THE RHO  
GTPASE RHOJ IN ENDOTHELIAL CELLS**

**By**

**Eleanor Wilson**

A thesis submitted to the University of Birmingham for the Degree of  
DOCTOR OF PHILOSOPHY



School of Immunity and Infection

College of Medical and Dental Sciences

The University of Birmingham

April 2014

UNIVERSITY OF  
BIRMINGHAM

**University of Birmingham Research Archive**

**e-theses repository**

This unpublished thesis/dissertation is copyright of the author and/or third parties. The intellectual property rights of the author or third parties in respect of this work are as defined by The Copyright Designs and Patents Act 1988 or as modified by any successor legislation.

Any use made of information contained in this thesis/dissertation must be in accordance with that legislation and must be properly acknowledged. Further distribution or reproduction in any format is prohibited without the permission of the copyright holder.

## Abstract

RhoJ is an endothelial expressed Rho GTPase that localises to focal adhesions and regulates cell migration and tube formation. Previous work in our laboratory determined that RhoJ activation negatively regulates focal adhesion (FA) numbers, and interacts with the FA proteins GIT1 and  $\beta$ -PIX. The studies presented in this thesis aimed to characterise the role of RhoJ in modulating FA dynamics, further investigate its interactions with the GIT/PIX complex, and generate a RhoJ knockout mouse to determine its function *in vivo*.

Silencing RhoJ led to prolonged FA disassembly in migrating human umbilical vein endothelial cells (HUVEC), while adhesions in cells expressing a dominant active (da) mutant of RhoJ disassembled more rapidly. Interactions between daRhoJ and GIT1, GIT2 and  $\beta$ -PIX were identified, and the localisation of any member of the RhoJ/GIT/PIX complex to FAs was found to be dependent on each of the other components. daRhoJ expression increased levels of GIT2 protein, while silencing RhoJ reduced GIT2 Tyr 392 phosphorylation. *In vivo*, the growth of subcutaneous tumours was reduced in RhoJ knockout mice compared to wild type controls.

In conclusion, the data presented in this thesis show that RhoJ regulates FA disassembly, most likely in concert with the GIT/PIX proteins. This in turn influences endothelial cell migration and ultimately angiogenesis.

## Acknowledgements

Firstly, I would like to thank my supervisor Dr. Victoria Heath for her guidance and patience throughout the project. I greatly appreciate the help, advice and support you have given me and I feel lucky to have had the opportunity to be your student. I would also like to thank Prof. Roy Bicknell and Dr. Neil Hotchin for their suggestions and advice during my time in the lab. The British Heart Foundation has also been very generous in funding the project, and for that I am hugely grateful.

To the members of the Bicknell group past and present, thank you for creating such a welcoming and friendly environment to work in, and for answering my many questions over the past 3 years.

I would also like to thank the groups that attend the Heath lab meetings for their constructive criticisms and suggestions. In particular, the help I received from Dr. Josh Rappoport's laboratory and Dr. Natalie Poulter has been invaluable.

Finally, I thank my parents, family and friends for their encouragement and support through some difficult times along the way. Thank you for always being there, for your understanding, and for listening to every one of my presentations- I don't know what I would have done without you.



## Table of Contents

<b>CHAPTER 1</b>	<b>1</b>
<b>Introduction</b>	<b>1</b>
1.1 <i>Endothelial cells and angiogenesis</i>	2
1.1.1 Introduction	2
1.1.2 Mechanisms of angiogenesis	3
1.2 <i>Rho GTPases</i>	7
1.2.1 Introduction	7
1.2.2 Structure of Rho GTPases	8
1.2.3 Regulation of Rho GTPase activation	10
1.2.3.1 GEFs	11
1.2.3.2 GAPs	13
1.2.3.3 GDIs	14
1.2.3.4 Other methods of regulating Rho GTPase activation	14
1.2.4 Rho GTPase effectors	15
1.2.5 General functions of Rho GTPases	16
1.2.6 Rho GTPase function in endothelial cells and angiogenesis	17
1.3 <i>RhoJ</i>	19
1.3.1 Introduction	19
1.3.2 RhoJ in cytoskeletal rearrangements	19
1.3.3 RhoJ interactions and signalling	21
1.3.4 RhoJ in adipocyte differentiation and glucose transport	23
1.3.5 RhoJ in regulating endocytosis	23

1.3.6	RhoJ <i>in vivo</i>	24
1.4	<i>The cytoskeleton and cell migration</i>	26
1.4.1	Overview	26
1.4.2	Actin polymerisation, lamellipodia and filopodia	27
1.4.3	Adhesion to the extracellular matrix	28
1.4.4	Adhesion formation and maturation	30
1.4.5	Adhesion disassembly	34
1.4.6	Rho GTPase involvement in focal adhesion turnover	39
1.5	<i>The GIT/PIX complex</i>	40
1.5.1	Introduction to the GIT proteins	40
1.5.2	Domain structure of the GIT proteins	40
1.5.3	Introduction to the PIX proteins	42
1.5.4	Domain structure of the PIX proteins	43
1.5.5	General functions of the GIT and PIX proteins	44
1.5.5.1	The GIT/PIX proteins as regulators of GTPase activity	44
1.5.5.2	Roles in trafficking	45
1.5.5.3	Roles in the cytoskeleton	46
1.5.5.4	Roles in endothelial permeability	49
1.5.6	GIT and PIX <i>in vivo</i>	50
1.6	<i>Hypotheses and Aims</i>	52
<b>CHAPTER 2</b>		<b>55</b>
<b>Materials and Methods</b>		<b>55</b>
2.1	<i>Buffers and solutions</i>	56

2.2	<i>siRNA duplexes</i>	58
2.3	<i>Antibodies</i>	59
2.3.1	Primary Antibodies	59
2.3.2	Secondary Antibodies	61
2.4	<i>Oligonucleotides</i>	62
2.5	<i>qPCR primers</i>	64
2.6	<i>Plasmids</i>	65
2.7	<i>General tissue culture</i>	67
2.8	<i>Transfection</i>	68
2.8.1	RNAiMAX transfection	68
2.8.2	PEI transfection	69
2.9	<i>Lentiviral transduction of HUVEC</i>	70
2.9.1	Production of lentivirus	70
2.9.2	Infection of HUVEC with lentivirus	70
2.10	<i>Protein analysis</i>	71
2.10.1	Protein extraction	71
2.10.2	SDS Polyacrylamide gel electrophoresis	71
2.10.3	Western blotting	72
2.10.4	Stripping and reblotting membranes	72
2.11	<i>RNA Analysis</i>	73
2.11.1	RNA extraction from HEK293T and HUVEC	73
2.11.2	cDNA generation	74
2.11.3	qPCR	74

2.12	<i>GFP trap pulldown</i>	75
2.13	<i>Purification of GST fusion proteins</i>	76
2.14	<i>RhoJ activation assay</i>	77
2.15	<i>DNA manipulation</i>	78
2.15.1	Production and purification of plasmid DNA	78
2.15.2	Amplification of DNA fragments by PCR	78
2.15.3	Digestion of DNA with restriction enzymes	79
2.15.4	DNA electrophoresis	79
2.15.5	Gel purification	79
2.15.6	DNA ligation	79
2.15.7	Transformation of competent bacteria	80
2.15.8	Storage of plasmids and sequencing of DNA	80
2.16	<i>Yeast two-hybrid</i>	80
2.16.1	Yeast strain and media	80
2.16.2	Generation of yeast two-hybrid constructs	81
2.16.3	Transformation of yeast	82
2.16.4	Yeast two-hybrid spot assay	83
2.17	<i>Immunofluorescent staining</i>	83
2.18	<i>Monitoring of focal adhesions in fluorescent HUVEC by TIRF microscopy</i>	85
2.19	<i>Tube formation assay</i>	86
2.19.1	Co-culture tube formation assay	86
2.19.2	Staining of co-culture tubules	87
2.19.3	Matrigel tube formation assay	89

2.20	<i>Treatment of HUVEC with Src and FAK inhibitors</i>	89
2.21	<i>Phosphokinase array</i>	90
2.22	<i>Extraction and analysis of mouse protein and RNA</i>	90
2.22.1	Genomic DNA extraction from mouse samples	90
2.22.2	Genotyping of mouse genomic DNA	91
2.22.3	RNA extraction from mouse lung tissue	91
2.22.4	PCR of cDNA from mouse lung tissue	93
2.22.5	Tumour implantation in mice	93
2.23	<i>Image analyses</i>	93
2.24	<i>Statistical analyses</i>	94
<b>CHAPTER 3</b>		<b>96</b>
<b>The role of RhoJ in regulating focal adhesion dynamics</b>		<b>96</b>
3.1	<i>Introduction</i>	97
3.2	<i>Manipulation of RhoJ expression by RNA interference and lentiviral transduction</i>	99
3.3	<i>Optimisation of TIRF microscopy to monitor focal adhesion dynamics in HUVEC</i>	101
3.4	<i>Investigating the effect of RhoJ knockdown on focal adhesion dynamics</i>	109
3.5	<i>Investigating the effect of dominant active RhoJ expression on focal adhesion dynamics</i>	113
3.6	<i>Investigating the role of RhoJ in focal adhesion targeting by microtubules</i>	118
3.7	<i>Investigating the effect of RhoJ on focal adhesion size</i>	122
3.8	<i>Generation of a RhoJ biosensor</i>	126
3.9	<i>Discussion</i>	131

<b>CHAPTER 4</b>	<b>137</b>
<b>The physical and functional interaction of RhoJ with the GIT/PIX complex</b>	<b>137</b>
4.1 <i>Introduction</i>	138
4.2 <i>Mapping the interaction between RhoJ and GIT1</i>	140
4.3 <i>Profiling RhoJ, GIT and PIX expression in HUVEC, HMEC-1 and HEK293T</i>	141
4.4 <i>Pulldown of RhoJ partner proteins from GFP expressing HUVEC</i>	143
4.5 <i>Knockdown of RhoJ and its partner proteins in HUVEC</i>	145
4.6 <i>Determining co-localisation of RhoJ with GIT1, GIT2 and <math>\beta</math>-PIX</i>	147
4.7 <i>Investigating the effect of GFP-daRhoJ expression on GIT and PIX localisation to focal adhesions</i>	150
4.8 <i>Investigating the effect of knockdown of members of the RhoJ/GIT/PIX complex on recruitment to focal adhesions</i>	157
4.9 <i>Determining the effect of GIT and <math>\beta</math>-PIX knockdown on endothelial tube formation</i>	172
4.10 <i>Assessing the role of <math>\beta</math>-PIX in regulating RhoJ activation</i>	174
4.11 <i>The effect of dominant active RhoJ expression on GIT2 phosphorylation</i>	176
4.12 <i>The effect of RhoJ knockdown on GIT2 expression</i>	178
4.13 <i>Investigating the effect of Src and FAK inhibitors on GIT2 phosphorylation</i>	180
4.14 <i>Screening the effect of dominant active RhoJ expression on kinase phosphorylation</i>	182
4.15 <i>Discussion</i>	190

<b>CHAPTER 5</b>	<b>197</b>
<b>Generation of a RhoJ knockout mouse</b>	<b>197</b>
5.1 <i>Introduction</i>	198
5.2 <i>Generation of chimeras with germline transmission</i>	200
5.3 <i>Optimisation of a genotyping strategy to distinguish between the wild-type allele             and knockout cassette</i>	203
5.4 <i>Confirmation of splicing in wild-type, heterozygous and knockout mice</i>	206
5.5 <i>Breeding of RhoJ genetrap mice with PGK-Cre mice</i>	209
5.6 <i>Tumour growth in RhoJ knockout mice</i>	213
5.7 <i>Discussion</i>	215
<b>CHAPTER 6</b>	<b>219</b>
<b>General Discussion</b>	<b>219</b>
<b>References</b>	<b>231</b>
<b>APPENDIX: Re-print of the thesis related publication</b>	<b>254</b>

## List of Figures

### Chapter 1

Figure 1.1	A model of angiogenesis	5
Figure 1.2	The Rho GTPase family of Ras like G proteins	9
Figure 1.3	The Rho GTPase activation cycle	12
Figure 1.4	The cytoskeleton in a migrating cell	29
Figure 1.5	The composition of a focal adhesion	31
Figure 1.6	Methods of focal adhesion disassembly	35
Figure 1.7	The structure and interactions of the GIT/PIX complex	41

### Chapter 2

Figure 2.1	Co-culture tube formation assay procedure	88
Figure 2.2	Individual adhesions were outlined based on vinculin staining and the mean grey value of the partner protein measured on its corresponding channel	95

### Chapter 3

Figure 3.1	Knockdown of endogenous RhoJ by siRNA transfection, and stable expression of GFP-dominant active RhoJ in HUVEC	100
Figure 3.2	RhoJ knockdown results in increased focal adhesion numbers per cell area in HUVEC imaged by TIRF microscopy	103
Figure 3.3	Stable expression of RFP-Paxillin in HUVEC does not affect focal adhesion numbers per cell area	105
Figure 3.4	RFP-Paxillin co-localises with vinculin at focal adhesions	107
Figure 3.5	Focal adhesion lifetime in transduced HUVEC is not significantly different between cells	108
Figure 3.6	Focal adhesion lifetime in HUVEC is shortened upon expression of a dominant active mutant of RhoJ	111



Figure 3.7	Knockdown of RhoJ expression in HUVEC specifically prolongs focal adhesion disassembly.	114
Figure 3.8	Focal adhesion lifetime in HUVEC is shortened upon expression of a dominant active mutant of RhoJ	116
Figure 3.9	Dominant active RhoJ expression in RFP-Paxillin HUVEC leads to decreased focal adhesion disassembly time	119
Figure 3.10	Knockdown of RhoJ expression does not alter microtubule targeting of focal adhesions	121
Figure 3.11	GFP-daRhoJ expression increases focal adhesion size in HUVEC, compared to GFP control expressing cells	123
Figure 3.12	RhoJ knockdown results in decreased focal adhesion size in HUVEC, compared to siControl transfected cells	125
Figure 3.13	Construction and expression of a RhoJ biosensor	127
Figure 3.14	Pre- and post-bleaching images of adhesions from control and RhoJ biosensor expressing cells in the red and green channel	129
Figure 3.15	Green fluorescence subtly increases in RhoJ biosensor expressing cells after red-bleaching	130

## Chapter 4

Figure 4.1	wtRhoJ and daRhoJ interact with wtGIT1 in the yeast two-hybrid assay	142
Figure 4.2	Expression of RhoJ and its candidate partner proteins in endothelial and non-endothelial cells	144
Figure 4.3	GFP-daRhoJ interacts with $\beta$ -PIX, GIT1 and GIT2 in the GFP trap pulldown assay	146
Figure 4.4	Knockdown of RhoJ, $\beta$ -PIX and GIT1/2 with siRNA	148
Figure 4.5	Knockdown of RhoJ, $\beta$ -PIX and GIT1/2 with siRNA	149
Figure 4.6	$\beta$ -PIX primarily co-localises with GFP-daRhoJ at focal adhesions	151
Figure 4.7	GIT1 primarily co-localises with GFP-daRhoJ at focal adhesions	152
Figure 4.8	GIT2 co-localises with GFP-daRhoJ at focal adhesions, and with GFP-wtRhoJ to a lesser extent	153
Figure 4.9	Expression of GFP-daRhoJ increases recruitment of $\beta$ -PIX to	154

	focal adhesions	
Figure 4.10	Expression of both GFP-wtRhoJ and GFP-daRhoJ increases recruitment of GIT1 to focal adhesions	155
Figure 4.11	Expression of GFP-daRhoJ increases recruitment of GIT2 to focal adhesions	156
Figure 4.12	Knockdown of $\beta$ -PIX or GIT1/2 reduces recruitment of RhoJ to focal adhesions	159
Figure 4.13	Knockdown of RhoJ or GIT1/2 reduces recruitment of $\beta$ -PIX to focal adhesions	162
Figure 4.14	Knockdown of RhoJ or $\beta$ -PIX reduces recruitment of GIT1 to focal adhesions	165
Figure 4.15	Knockdown of RhoJ or $\beta$ -PIX reduces recruitment of GIT2 to focal adhesions	168
Figure 4.16	Knockdown of $\beta$ -PIX or GIT1/2 impairs tube formation	173
Figure 4.17	Knockdown of $\beta$ -PIX may partially impair VEGF-stimulated RhoJ activation	175
Figure 4.18	GFP-daRhoJ expression increases levels of GIT2, which is phosphorylated at Tyr 392	177
Figure 4.19	Knockdown of RhoJ reduces phosphorylation of GIT2 on Tyr 392 but has no effect on total GIT2	179
Figure 4.20	Inhibitors of Src and FAK reverse the GFP-daRhoJ induced increase in GIT2 phosphorylation on Tyr 392 but do not reduce the increase observed in total GIT2 levels	181
Figure 4.21	GFP-daRhoJ expression induces changes in phosphorylation of a panel of human kinases	184
Figure 4.22	GFP-daRhoJ expression induces changes in phosphorylation of a panel of human kinases	185
Figure 4.23	GFP-daRhoJ expression increases phosphorylation of JNK, EGF receptor, AMPK $\alpha$ 2, STAT5a and b, Hck and $\beta$ -Catenin	187
Figure 4.24	GFP-daRhoJ expression affects phosphorylation of MSK1/2, eNOS, HSP27 and PRAS40	188
Figure 4.25	GFP-daRhoJ expression led to a trend in increased phosphorylation of STAT5b, P38 $\alpha$ , Fyn, Lyn and CREB	189

## Chapter 5

Figure 5.1	ES cells containing the RhoJ knockout cassette were injected into blastocysts and implanted into pseudo-pregnant female mice, resulting in two good chimeras	202
Figure 5.2	Optimisation of genotyping strategy	205
Figure 5.3	Strategy to determine splicing events in the wild-type and knockout mice	207
Figure 5.4	RhoJ exon 1 is still splicing to exon 2 in the knockout mouse	208
Figure 5.5	Breeding of RhoJ knockout mice with PGK-Cre mice produced a line of mice with RhoJ exon 2 removed by Cre recombinase	211
Figure 5.6	Sequencing of the PCR product from PGK-Cre x RhoJ genetrap offspring	212
Figure 5.7	Preliminary data from <i>in vivo</i> tumour growth assays	214

## Chapter 6

Figure 6.1	RhoJ regulates angiogenesis by promoting focal adhesion disassembly in complex with GIT and PIX	222
Figure 6.2	The RhoJ/GIT/PIX interactions are functionally relevant to signalling and phosphorylation	226

## List of Tables

### Chapter 1

Table 1.1	General functions of Rho GTPases	16
Table 1.2	Roles of Rho GTPases in angiogenesis	18
Table 1.3	<i>In vivo</i> functions of the GIT and PIX proteins	52

### Chapter 2

Table 2.1	Common buffers	56
Table 2.2	siRNA duplexes	58
Table 2.3.1	Primary antibodies	59
Table 2.3.2	Secondary antibodies	61
Table 2.4	Oligonucleotides	62
Table 2.5	qPCR primers	64
Table 2.6.1	Cloned plasmids	65
Table 2.6.2	Other plasmids	66
Table 2.7	Volumes of OptiMEM and lipofectamine required to transfect various densities of HUVEC	69
Table 2.8	Cell densities used for immunofluorescent staining.	85

### Chapter 5

Table 5.1	Genotypes of black pups born from the germline-transmitting RhoJ chimera	203
-----------	--	-----

## List of abbreviations

3AT	3-amino-1,2,4-triazole
AP1	Activator protein 1
Arp2/3	Seven subunit protein containing the actin-related proteins 2 and 3
bp	Base pairs
BREC	Bovine retinal endothelial cells
BSA	Bovine serum albumin
CAP	c-Cbl associated protein
CAT	Cool-associated tyrosine-phosphorylated protein
cDNA	Complementary DNA
CREB	cAMP-response element-binding protein
CRIB	Cdc42/Rac-interactive binding domain
CZH	CDM-Zizimin homology
da	Dominant active
ddH <sub>2</sub> O	Double-distilled water
DEPC	Diethyl pyrocarbonate
DH	Dbl homology
DMEM	Dulbecco's modified Eagle's medium
DOCK	Dedicator of cytokinesis
dn	Dominant negative
dNTP	Deoxyribonucleotide
DTT	Dithiothreitol
E	Embryonic day
<i>E. coli</i>	<i>Escherichia coli</i>
ECL	Enhanced chemiluminescent substrate
EDL	<i>extensor digitorum longus</i>
EDTA	Ethylenediaminetetraacetic acid
EGF	Epidermal growth factor
EGFR	Epidermal growth factor receptor
eNOS	Endothelial nitric oxide synthase
ERK	Extracellular-signal regulated kinase

ES cells	Embryonic stem cells
FAK	Focal adhesion kinase
FBS	Foetal bovine serum
Fwd	Forward
g	Gravity
GAP	GTPase activating protein
GDI	Guanine nucleotide dissociation inhibitor
GDP	Guanosine diphosphate
GEF	Guanine nucleotide exchange factor
GFP	Green fluorescent protein
GIT	G-protein coupled receptor-kinase interacting target
GPCR	G-protein coupled receptor
GST	Glutathione S-transferase
GTP	Guanosine-5'-triphosphate
HDF	Normal human dermal fibroblasts
HEK293T	Human embryonic kidney 293T cells
HEPES	4-(2-Hydroxyethyl)piperazine-1-ethanesulphonic acid
Het	Heterozygous
HMEC-1	Human microvascular endothelial cell line-1
HRP	Horseradish peroxidase
HUVEC	Human umbilical vein endothelial cells
IF	Immunofluorescence
IHC	Immunohistochemistry
IPTG	Isopropyl $\beta$ -D-1 thiogalactopyranoside
ISG20	Interferon-stimulated gene 20 kDa protein
JNK	c-Jun N-terminal kinase
kDa	Kilodalton
KO	Knockout
LB agar/broth	Luria Bertani agar/broth
Leu	Leucine
MCE	Mitotic clonal expansion
MCF-7 cells	Michigan Cancer Foundation 7 cells

mDia	Mammalian diaphanous
MDM	Murine double minute
MLC	Myosin light chain
MMP	Matrix metalloproteinase
mRNA	Messenger RNA
MTOC	microtubule organising centre
NFκB	Nuclear factor kappa B
ns	no significant difference
OAS1	2'-5'-oligoadenylate synthetase 1
OD	Optical density
p value	Probability value
PAEC	Porcine aortic endothelial cells
PAK	p21 activated kinase
PBR	Polybasic region
PBS	Phosphate buffered saline
PBST	Phosphate buffered saline Tween-20
PCR	Polymerase chain reaction
PEI	Polyethylenimine
PH	Pleckstrin homology
PIX	PAK interacting exchange factor
PLC-γ	Phospholipase C-gamma
PMSF	Phenylmethyl sulphonyl fluoride
POPX1/2	PP2C-like serine/threonine phosphatase 1/2
PVDF	Polyvinylidene difluoride
qPCR	quantitative PCR
Rev	Reverse
RFP	Red fluorescent protein
ROCK	Rho kinase
SCD	Synthetic complete dextrose
SDS	Sodium dodecyl sulphate
SDS-PAGE	Sodium dodecyl sulphate polyacrylamide gel electrophoresis
Sema3E	Semaphorin 3E

Ser	Serine
SH3	Src homology 3 domain
siControl	Control small interfering RNA duplex
siRNA	Small interfering RNA
TAE	Tris acetate EDTA
TBS	Tris buffered saline
TBST	Tris buffered saline Tween-20
TCL	TC10-like
TIMP	Tissue inhibitor of MMP
TIRF	Total internal reflection fluorescence
Trp	Tryptophan
VEGF	Vascular endothelial growth factor A
VEGFR1/2	Vascular endothelial growth factor receptor 1/2
WASP	Wiskott-Aldrich syndrome protein
WAVE	WASP-family verprolin-homologous protein
WB	Western blotting
WT	Wild-type



## **CHAPTER 1**

### **Introduction**

## 1.1 Endothelial cells and angiogenesis

### 1.1.1 Introduction

Endothelial cells line the internal walls of vessels in both the vascular and lymphatic systems, enabling transport of amongst others, gases and nutrients around the body (Adams and Alitalo 2007). These cells are crucial in mediating immunity, vasomotor tone and vessel permeability, amongst other processes (Aird 2012).

Blood vessel formation during development initially occurs via vasculogenesis, which is the *de novo* formation and remodelling of vessels from haemangioblast progenitor cells in blood islands. Angiogenesis is the formation of blood vessels from the existing vasculature (Carmeliet 2003, Lamalice, Le Boeuf *et al.* 2007). These two methods of blood vessel formation are driven by different mechanisms; vasculogenesis is dependent on the differentiation of progenitors into endothelial cells, and angiogenesis is reliant on migration and proliferation of existing cells (Drake 2003).

The process of angiogenesis is vital in normal physiological functions including wound repair and the female menstrual cycle, and is tightly regulated by a balance of pro- and anti-angiogenic factors (Pandya, Dhalla *et al.* 2006). A so-called 'angiogenic switch' occurs when there is a misbalance of these factors, leading to dysfunction of endothelial cells and angiogenesis. This contributes to many pathological conditions, including cancer, asthma, obesity and atherosclerosis, which may be characterised by insufficient or excessive angiogenesis. Tumours, for example, are unable to grow more than approximately 1 mm<sup>3</sup> without developing their own blood supply and thus many cancers are found to have

excessive and disordered vessels. In atherosclerosis, insufficient development of collateral vessels subsequent to occlusion can lead to ischaemia and insufficient perfusion of the heart muscle (Carmeliet 2003, Koerselman, van der Graaf *et al.* 2003, Carmeliet 2005, Gupta and Zhang 2005).

Vessels in adult tissues are generally quiescent, with slow turnover of endothelial cells, and rarely form new sprouts except in the case of the female reproductive cycle and tissue repair. These cells maintain their ability to respond to extracellular cues, however, and in angiogenic scenarios they are capable of rapid proliferation in order to form new vessels (Alberts 2002, Potente, Gerhardt *et al.* 2011).

Endothelial cells are known to demonstrate a great amount of heterogeneity, with differences noted between vessels of varying size, age and environments (Cleaver and Melton 2003). In fact, endothelial cells that form arteries and veins are found to express distinct sets of genes which mark their individual fates (Aird 2012). While some of these distinct transcriptional patterns are fixed, many are determined by the environment the cell is found in and lost upon *in vitro* culture, highlighting the plasticity of endothelial cell fate and the ability to adapt to the milieu (Alberts 2002, Cleaver and Melton 2003, Aird 2012).

### **1.1.2 Mechanisms of angiogenesis**

Angiogenesis is initiated by endothelial cell sensing of pro-angiogenic signals from agents including growth factors like vascular endothelial growth factor (VEGF) and chemokines like IL-8 (Pandya, Dhalla *et al.* 2006, Adams and Alitalo 2007). VEGF in particular is a highly potent stimulator of angiogenesis and as such its expression is tightly controlled by

alternative splicing, local oxygen concentration and expression of inhibitory factors such as arresten (Adams and Alitalo 2007, Lodomery, Harper *et al.* 2007, Ribatti 2009).

Figure 1.1 demonstrates the process of sprouting angiogenesis. Upon activation of endothelial cells by these factors, pericytes surrounding and stabilising the vessel detach, cell-cell junctions are weakened, apical-basal polarity is reversed and the basement membrane is broken down by proteases such as MMPs. An extracellular matrix is produced by plasma proteins, providing a scaffold for endothelial cells to migrate upon. Tip cells are selected to lead the new sprout and these cells form filopodia to probe the environment. Tip cells are rich in VEGFR2, a receptor which binds VEGF, and are therefore able to guide the direction of growth towards this growth factor, in particular the splice variant VEGF<sub>165</sub>. A diffusible splice variant of VEGF, VEGF<sub>121</sub>, which is unable to bind heparin sulphate in the basement membrane, supports endothelial cell proliferation but is unable to regulate tip cell guidance (Adams and Alitalo 2007). Stalk cells follow tip cells, and have high levels of Notch signalling which is responsive to the Delta-like 4 ligand. High Notch signalling results in reduced filopodia formation, a process which is crucial in tip cell function; as a result, those cells with high Notch expression are excluded from the front of the sprout (Blanco and Gerhardt 2013). Stalk cells are highly proliferative, which enable the extension of the growing vessel. Notch signaling inhibits proliferation, and its activity must be regulated by other proteins, in particular the Notch-regulated ankyrin repeat protein (NRARP) (Potente, Gerhardt *et al.* 2011). Notch signaling also stimulates expression of VEGFR1. VEGFR1 is expressed in stalk cells, where it acts as a decoy receptor to trap VEGF and limit tip cell formation. Splicing of VEGFR1 generates a soluble form of the receptor sVEGFR1, which

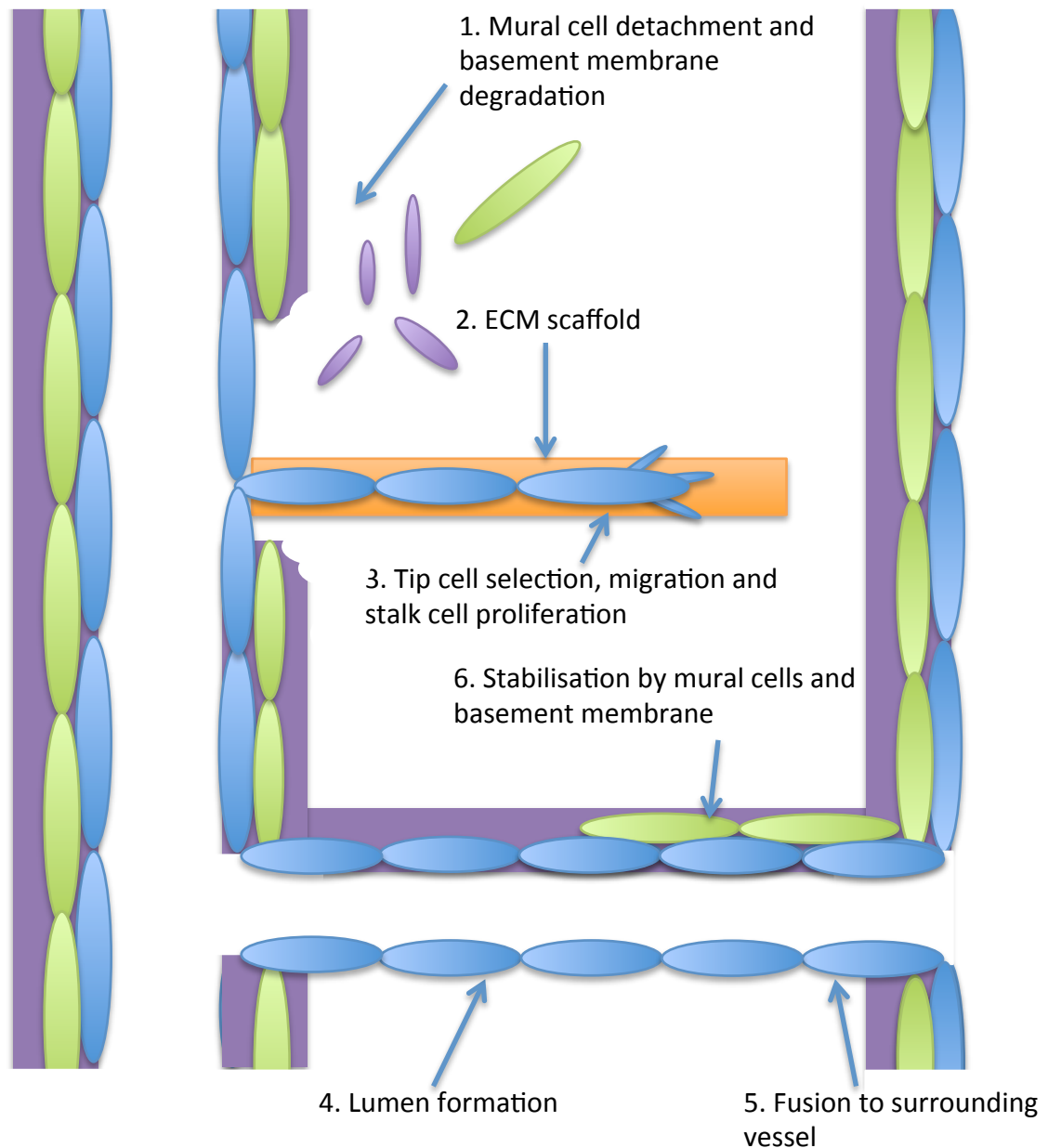


**Figure 1.1. A model of sprouting angiogenesis.** Endothelial cells are stimulated by pro-angiogenic factors such as VEGF, leading to release of proteolytic enzymes and subsequent basement membrane degradation/mural cell detachment. An extracellular matrix scaffold guides endothelial cells which migrate and proliferate towards stimuli, forming a basic tubule. A lumen forms and fusion to surrounding vessels occurs. Finally, the newly formed vessel is stabilised by the recruitment of supporting cells such as pericytes and the deposition of a basement membrane. Blue ovals: endothelial cells, green ovals: pericytes/mural cells; purple: basement membrane; orange: extracellular matrix scaffold.

similarly sequesters VEGF in the cytosol and prevents VEGFR2 activation (Potente, Gerhardt *et al.* 2011, Blanco and Gerhardt 2013).

Lumen form either by fusion of intracellular vacuoles or adjusting the shape and junctions of connected endothelial cells, enabling blood flow upon formation of a stable vessel. Eventually, the elongating sprout meets and fuses with a neighbouring vessel. This established vessel is subsequently stabilised by recruitment of pericytes and other mural cells, deposition of a basement membrane and initiation of blood flow. Increased availability of oxygen downregulates VEGF and as such tightens the junctions between cells (Adams and Alitalo 2007, Carmeliet and Jain 2011, Potente, Gerhardt *et al.* 2011). Finally, in order to form the most optimal vascular structure, vessels are subject to remodelling and pruning after their initial formation (Jain 2003, Wacker and Gerhardt 2011).

While sprouting angiogenesis is the most prevalent form of angiogenesis, vessels can also form by intussusceptive angiogenesis and in pathological scenarios via vessel co-option and vascular mimicry. Intussusceptive, or splitting, angiogenesis occurs when endothelial cells from opposite sides of a vessel migrate towards one another and form pillars which subsequently split and grow by merging with other pillars. This method of angiogenesis is faster than growth by sprouting and requires comparatively less energy, since there is little migration and proliferation. It is thought that while sprouting angiogenesis is responsible for the initial formation of a vascular network, intussusception is most prominent in the remodelling phase of vessel growth (De Spiegelaere, Casteleyn *et al.* 2012).

Vessel co-option is a mechanism most frequently seen in the early stages of tumour growth. Essentially, the tumour hijacks the vasculature of the normal tissue and does not induce an

angiogenic response itself. Later, a host defence response is triggered and vessel regression along with tumour necrosis is observed, however this is counteracted by angiogenesis at the edge of the tumour, providing a stable blood supply where co-option fails (Hillen and Griffioen 2007). As mentioned previously, vessel co-option is only seen in pathological conditions, however more recently Kilarski and colleagues observed a similar system in the rapid vascularisation occurring during wound healing. Activated fibroblasts or myofibroblasts contract the wound and the resulting tension leads to expansion of tissues that are already vascularised. Mature vessels are subsequently pulled towards the wound, and further remodelled by the more classical forms of angiogenesis outlined above (Kilarski, Samolov *et al.* 2009).

Finally, tumour cells can exploit their inherent plasticity in order to mimic endothelial cells and form vessels made entirely of tumour cells with an endothelial phenotype (Hillen and Griffioen 2007). This is a mechanism only seen in aggressive tumours, which are made up of cells with marked plasticity, and is thought to be similar to vasculogenesis. Vascular mimicry is associated with a poor prognosis for patients, and is particularly problematic for therapies that are designed to target the vasculature (Paulis, Soetekouw *et al.* 2010, De Spiegelaere, Casteleyn *et al.* 2012).

## **1.2 Rho GTPases**

### **1.2.1 Introduction**

Rho GTPases are a subclass of the Ras-like G protein superfamily which act as molecular switches cycling between an active GTP-bound state and an inactive GDP-bound state. In

total, there are 20 mammalian Rho GTPases and these are sub-divided into a further 8 groups according to sequence and domain homology: Rho-like (RhoA, RhoB and RhoC), Rnd (Rnd1, Rnd2 and Rnd3/RhoE), Rac-like (Rac1, Rac2, Rac3 and RhoG), Cdc42-like (Cdc42, TC10/RhoQ, TCL/RhoJ, Wrch1/RhoU and Chp/Wrch2/RhoV), RhoBTB (RhoBTB1 and RhoBTB2/DBC2), RhoD, Rif/RhoF and TTF/RhoH (Burridge and Wennerberg 2004, Boureux, Vignal *et al.* 2007, Vega and Ridley 2007, Heasman and Ridley 2008). There are 3 further proteins sometimes classed as Rho GTPases: RhoBTB3, Miro-1 (RhoT1) and Miro2 (RhoT2), although these are much more divergent than the core 20 proteins and consequently there is some dispute about whether they are true Rho GTPases. A dendrogram depicting the Rho family of GTPases is shown in Figure 1.2, with a star signifying those proteins where a knockout mouse has been described.

### **1.2.2 Structure of Rho GTPases**

All 20 Rho GTPases contain a Rho specific insert domain, along with an effector domain (also called switch I). Most Rho proteins also contain regions involved in binding GDP or GTP, which enables activation and inactivation of downstream signalling. There are however some atypical members (including the Rnd and RhoBTB families as well as RhoH) that do not exchange nucleotides; these are generally found in the GTP bound state due to amino acid substitutions (Vega and Ridley 2007, Heasman and Ridley 2008). Binding of Rho GTPases to GDP or GTP leads to changes in conformation of two N-terminal regions of the protein called switch I and switch II (Wheeler and Ridley, 2004). These regions are responsible for interacting with the  $\gamma$ -phosphate group of GTP, while the conserved p-loop interacts with nucleotides and the associated  $Mg^{2+}$  ions (Cherfils and Chardin 1999).



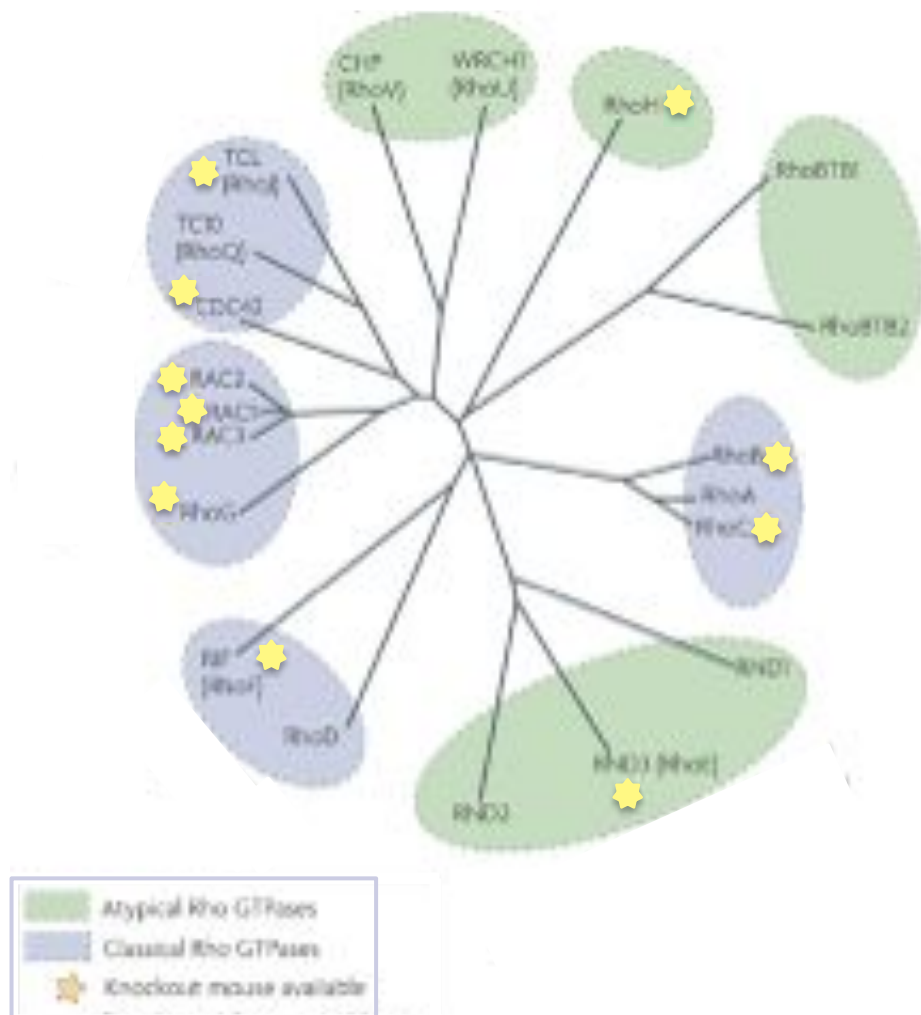


**Figure 1.2. The Rho GTPase family of Ras like G proteins.** The Rho GTPase family of proteins can be split into 8 subfamilies based on sequence and domain homology. The Rho GTPases in green circles are classed as atypical while those in blue are classical family members. A star signifies where a knockout mouse has been published for the protein. Adapted from Heasman and Ridley, 2008.

Most members of the Rho family of GTPases, with the exception of RhoV, RhoU and RhoBTB contain a CAAX box domain (where C is cysteine, A is any aliphatic amino acid and X is any amino acid), which is the site of isoprenylation, enabling association with the lipid membrane and regulating intracellular localisation. Within the CAAX box, the final amino acid is known to be important in determining the type of modification added, which may be farnesylation or geranylgeranylation. RhoJ for example is farnesylated (Roberts, Mitin *et al.* 2008) while RhoA is geranylgeranylated (Adamson, Marshall *et al.* 1992).

The region upstream of the CAAX box is also important in the localisation of the Rho GTPases, where a polybasic region (PBR, a group of basic amino acids) or palmitoylation of cysteine residues are required for proper membrane targeting (Boulter, Estrach *et al.* 2012).

While there is between 40-95% sequence identity between members of the Rho GTPase family (Wennerberg and Der 2004), specific function and localisation of Rho proteins is often determined by a hypervariable region at the C terminus (Michaelson, Silletti *et al.* 2001).

### **1.2.3 Regulation of Rho GTPase activation**

Rho GTPase activity is regulated by a number of mechanisms. Primarily, the exchange of GDP for GTP and subsequent activation is regulated by guanine nucleotide exchange factors (GEFs). When active, Rho GTPases are able to bind to their effectors and carry out downstream functions. In contrast the inactivation of Rho proteins i.e. the hydrolysis of GTP to GDP due to the intrinsic GTPase activity of the protein, which serves to terminate signalling, is promoted by GTPase activating proteins (GAPs). Rho guanine nucleotide dissociation inhibitors (RhoGDIs) meanwhile prevent further exchange and hydrolysis by

binding to the lipid tail of Rho GTPases and sequestering them in the inactive conformation in the cytosol (Jaffe and Hall 2005, Boulter, Estrach *et al.* 2012, Cherfils and Zeghouf 2013). Thus far, over 80 GEFs, approximately 70 GAPs and 3 GDIs have been identified for Rho GTPases (Cherfils and Zeghouf 2013). Figure 1.3 outlines the activation cycle of Rho GTPases and the various regulatory proteins that act to control this cycle.

#### **1.2.3.1 GEFs**

Guanine nucleotide exchange factors (GEFs) are known to facilitate the release of GDP and enable binding of GTP to Rho GTPases, thereby activating the protein and allowing downstream signalling.

There are 2 distinct families of Rho GEFs; those containing a Dbl homology (DH) domain which interacts with the switch regions and catalyses the exchange of GDP for GTP, and DOCK180-related proteins (also called CZH proteins) which contain a Dock homology region 2 (DHR2) domain that is distinct from the DH domain and regulates the exchange reaction in these proteins instead (Rossman, Der *et al.* 2005, Cote and Vuori 2007). Dbl-type GEFs also include a region called the Pleckstrin homology domain (PH), which coordinates protein localisation to the membrane (although it is also thought to play a role in activation of the Rho GTPase), while the DHR1 domain is responsible for this function in the DOCK family of GEFs. In addition to these core domains, GEFs frequently contain other diverse domains relating to their specific roles within the cell. Around 40% of human Rho GEFs contain PDZ-binding domains at their C-terminus, enabling binding to target proteins which contain this PDZ motif. This is thought to direct the localisation of GEFs to specific areas of the cell, thus fine-tuning the site of their activities (Garcia-Mata and Burridge 2007).

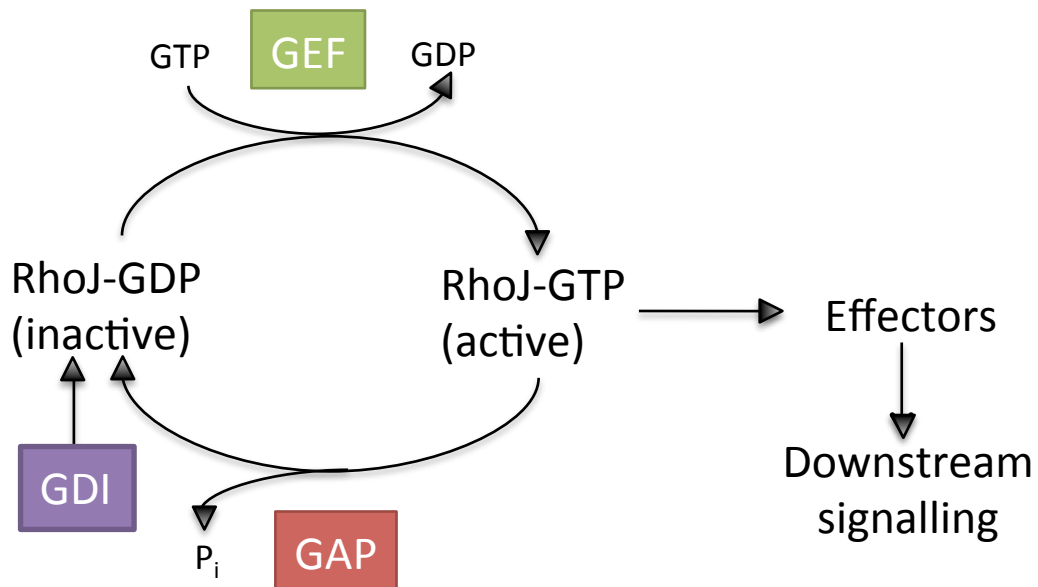


**Figure 1.3. The Rho GTPase activation cycle.** Rho GTPases generally cycle between an active GTP-bound form and an inactive, GDP-bound conformation. This cycle is controlled by several regulatory proteins including: guanine nucleotide exchange factors (GEFs), which stimulate the release of GDP and binding of GTP; GTPase activating proteins (GAPs), which stimulate the intrinsic GTPase activity of the Rho protein releasing  $P_i$  thus converting GTP to GDP; and guanine nucleotide dissociation inhibitors (GDIs), which bind the inactive form of the protein, sequestering it in the cytosol.

Approximately 70 DH-PH GEFs have been identified while only around 10 DOCK-180 related proteins have been described (Cote and Vuori 2007), and these act on members of the Rac and Cdc42 subfamilies specifically (Rossman, Der *et al.* 2005). The number of GEFs is vastly more than the number of Rho GTPases, meaning that multiple GEFs are capable of activating the same Rho protein. However, it is also known that some GEFs can activate several different GTPases (Garcia-Mata and Burridge 2007), the DH-PH GEF  $\beta$ -PIX for example has been shown to regulate the activities of both Rac and Cdc42 (Feng, Baird *et al.* 2006, ten Klooster, Jaffer *et al.* 2006).

In order for their activities to be regulated, GEFs are frequently subject to autoinhibition. The PH domain for example is able to inhibit some members of the DH-PH family of GEFs by steric hindrance, while binding of the DH domain by an N-terminal SH3 domain inhibits others. In DOCK proteins, the SH3 domain primarily coordinates inhibition. There are several methods that may be employed to relieve this autoinhibition, including binding by other proteins or phosphorylation at specific residues (Cherfils and Zeghouf 2013).

#### **1.2.3.2 GAPs**

GTPase-activating proteins (GAPs) are, in contrast to GEFs, regulators of Rho inactivation that enhance the intrinsic GTPase activity of the Rho protein and as such convert GTP to GDP. Additionally, they reverse effector binding, leading to the termination of downstream signalling (Ellenbroek and Collard 2007, Tcherkezian and Lamarche-Vane 2007).

Much like GEFs, GAPs are known to be multidomain proteins, with a RhoGAP core region that defines the family. Over 70 eukaryotic GAPs have been described so far; again, this is much greater than the number of Rho GTPases they regulate. Some GAPs are known to be

specific for particular tissues or signalling pathways; for example p73RhoGAP is restricted to the vascular endothelium and regulates Rho GTPases in angiogenesis (Su, Hahn *et al.* 2004). Furthermore, it is possible that the GAP domain acts as a recognition site for Rho GTPases with some GAPs acting as scaffold or effector proteins, rather than regulating inactivation (Tcherkezian and Lamarche-Vane 2007).

While the autoinhibition of RhoGAPs has yet to be described for many proteins of this family, it is likely to be regulated by protein-protein interactions (Cherfils and Zeghouf 2013). Additionally, the activity of these proteins can be regulated by phosphorylation and lipid modification (Tcherkezian and Lamarche-Vane 2007, Cherfils and Zeghouf 2013).

#### **1.2.3.3 GDIs**

Rho guanine nucleotide dissociation inhibitors (GDIs) are a family of proteins that bind to the GDP bound forms of Rho GTPases and impair the ability of the Rho protein to release its nucleotide, rendering it inactive. This regulation is vital in generating a reservoir of inactive Rho GTPases in the cytosol that can be released and activated when necessary. The RhoGDIs consist of 3 mammalian members, and each interacts with multiple targets (Garcia-Mata, Boulter *et al.* 2011).

#### **1.2.3.4 Other methods of regulating Rho GTPase activation**

In addition to GAPs, GEFs and GDIs, several other approaches have been identified recently to regulate Rho GTPase activity. RhoA, RhoG and Cdc42 for example may be removed from the membrane (and as such inactivated) by phosphorylation, which disrupts the hydrophobic interactions that form between the protein and the membrane. Furthermore, oxidation of a cysteine (C20 in RhoA) in the p-loop is able to facilitate nucleotide exchange in

the absence of GEFs (Boulter, Estrach *et al.* 2012), while SUMOylation has been shown to further stabilise active Rac (Castillo-Lluva, Tatham *et al.* 2010). Finally, the crosstalk between Rho GTPases has been shown to up- and down-regulate the activities of certain members of the family. RhoJ for example has been shown to mediate the activation of Rac1 and Cdc42 and RhoA (Yuan, Sacharidou *et al.* 2011).

#### **1.2.4 Rho GTPase effectors**

Upon activation of Rho GTPases, binding of effector proteins triggers downstream signalling pathways. Over 100 targets have been identified thus far, including kinases (serine/threonine, tyrosine and lipid), lipases, oxidases and scaffold proteins (Jaffe and Hall 2005, Hall 2012). Each GTPase is able to bind many effector proteins leading to the activation of a multitude of signalling cascades, and specific residues in the Rho protein enable binding of a specific effector (Bustelo, Sauzeau *et al.* 2007). However, it is also known that some effectors interact with more than one Rho GTPase (Ellenbroek and Collard 2007); Par6 for example is able to bind both Rac1 and Cdc42 in order to exert its effects on the cytoskeleton and cell polarity (Qiu, Abo *et al.* 2000).

The association of the effector protein to the membrane is necessary for its activation, and binding by Rho GTPases is thought to enable this activation by relaxation of intramolecular autoinhibitory interactions (Bishop and Hall 2000). Effector proteins also indirectly regulate their own activation, since some contribute to feedback loops which control Rho GTPase activity (Bustelo, Sauzeau *et al.* 2007).

### 1.2.5 General functions of Rho GTPases

Studies of the Rho GTPases frequently focus on the functions of RhoA, Rac1 and Cdc42, and while it is clear that the subfamilies related to these proteins regulate similar pathways, differences have also been noted. It is however evident that almost all Rho GTPases exert effects on the cytoskeleton (Vega and Ridley 2007); Table 1.1 outlines the general functions of Rho GTPases.

**Table 1.1 General functions of Rho GTPases**

Subfamily	Rho GTPase	General functions	References
Rho-like	RhoA	Stress fibre (SF) and focal adhesion (FA) formation; cell contractility; formation of membrane ruffles; elongate, stabilise and cross-link actin and myosin filaments	(Ridley and Hall 1992, Mellor, Flynn <i>et al.</i> 1998, Jaffe and Hall 2005, Kurokawa and Matsuda 2005, Pertz, Hodgson <i>et al.</i> 2006, Vega and Ridley 2007, Karlsson, Pedersen <i>et al.</i> 2009)
	RhoB	SF and FA formation; contractility; elongate, stabilise and cross-link actin and myosin filaments; endocytic trafficking; potential tumour suppressor	
	RhoC	SF and FA formation; contractility; elongate, stabilise and cross-link actin and myosin filaments; promotes metastatic behaviour and invasiveness in cancers	
Rac-like	Rac1 Rac2 Rac3	Formation of lamellipodia and focal complexes; actin polymerisation; stabilisation and elongation of microtubules (MTs); stabilisation of lamellipodia; FA turnover	(Ridley, Paterson <i>et al.</i> 1992, Kraynov, Chamberlain <i>et al.</i> 2000, Gumienny, Brugnera <i>et al.</i> 2001, Kiosses, Shattil <i>et al.</i> 2001, Burridge and Wennerberg 2004, Jaffe and Hall 2005, Vega and Ridley 2007, Heasman and Ridley 2008)
	RhoG	As per Rac1/2/3; activation of DOCK GEFs regulating cytoskeletal rearrangements in the particle engulfment stage of phagocytosis	
Cdc42-like	Cdc42	Filopodia formation; Golgi and MTOC reorientation; chemotaxis; MT stabilisation and elongation;	(Nobes and Hall 1995, Allen, Zicha <i>et al.</i> 1998, Millard, Sharp <i>et al.</i> 2004, Cau and



		generation of branched actin filament networks	Hall 2005, Jaffe and Hall 2005)
	RhoQ	Filopodia formation, glucose transport	(Chiang, Baumann <i>et al.</i> 2001, Vega and Ridley 2007)
	RhoJ	Outlined in Section 1.3	
	Wrch1	Filopodia formation; SF and FA disassembly	(Saras, Wollberg <i>et al.</i> 2004, Chuang, Valster <i>et al.</i> 2007, Vega and Ridley 2007)
	Wrch2	Filopodia formation	(Vega and Ridley 2007)
Rnd	Rnd1	SF and FA turnover	(Nobes, Lauritzen <i>et al.</i> 1998, Chardin 2006)
	Rnd2	Regulation of neurite outgrowth/branching	(Chardin 2006)
	RhoE	SF and FA turnover	(Guasch, Scambler <i>et al.</i> 1998, Chardin 2006)
RhoBTB	RhoBTB1 RhoBTB2	Candidate tumour suppressors	(Aspenstrom, Ruusala <i>et al.</i> 2007, Vega and Ridley 2007)
RhoD	RhoD	Filopodia formation; SF and FA disassembly; vesicular trafficking	(Murphy, Saffrich <i>et al.</i> 1996, Murphy, Saffrich <i>et al.</i> 2001, Aspenstrom, Fransson <i>et al.</i> 2004)
RhoF	RhoF	Filopodia formation	(Aspenstrom, Fransson <i>et al.</i> 2004)
RhoH	RhoH	Inhibits RhoA, Rac1 and Cdc42; regulates T cell maturation	(Li, Bu <i>et al.</i> 2002, Dorn, Kuhn <i>et al.</i> 2007)

### 1.2.6 Rho GTPase function in endothelial cells and angiogenesis

The general functions of Rho GTPases mainly concern regulation of the cytoskeleton, which is an important part of migration. In turn, endothelial cell migration is a key part of angiogenesis, since cells must be able to move in order to form new vessels. Several members of the Rho GTPase family have been shown to have roles in regulating various aspects of angiogenesis, from remodelling of the extracellular matrix to mediating endothelial barrier function (Bryan and D'Amore 2007). While much investigation has been

performed *in vitro*, knockout mice and other *in vivo* techniques have also been employed to elucidate the roles of this family of proteins in vessel formation. Table 1.2 outlines the angiogenic functions identified thus far for the Rho family of small GTPases.

**Table 1.2 Roles of Rho GTPases in angiogenesis**

Subfamily	Rho GTPase	Known roles in angiogenesis	References
Rho-like	RhoA	Activation increases VEGF expression and regulates MMP production via AP1 and NFκB, regulates VEGF-stimulated endothelial migration, tube formation, promotes endothelial cell organisation and survival, disrupts adherens junctions	(Wojciak-Stothard, Potempa <i>et al.</i> 2001, Davis, Bayless <i>et al.</i> 2002, Hippenstiel, Schmeck <i>et al.</i> 2002, Park, Kong <i>et al.</i> 2002, Abecassis, Olofsson <i>et al.</i> 2003, Hoang, Whelan <i>et al.</i> 2004, Wojciak-Stothard, Tsang <i>et al.</i> 2006, Bryan and D'Amore 2007, Bryan, Dennstedt <i>et al.</i> 2010, Ma, Xue <i>et al.</i> 2012)
	RhoB	Regulates capillary morphogenesis and endothelial cell survival, mediates tube formation, KO mice have impaired vessel outgrowth from the optic disc	(Adini, Rabinovitz <i>et al.</i> 2003)
Rac-like	Rac1	Activation increases VEGF expression and regulates MMP production via AP1 and NFκB, upregulates TIMP, regulates endothelial motility, tube formation and invasion, mediates assembly of capillary like tubes, involved in lumen formation, maintains adherens junctions and inhibits endothelial permeability, EC specific KO is lethal with embryos lacking branched vessels as well as abnormal heart structure	(Perona, Montaner <i>et al.</i> 1997, Engers, Springer <i>et al.</i> 2001, Wojciak-Stothard, Potempa <i>et al.</i> 2001, Bayless and Davis 2002, Connolly, Simpson <i>et al.</i> 2002, Wojciak-Stothard, Tsang <i>et al.</i> 2006, Bryan and D'Amore 2007, Tan, Palmby <i>et al.</i> 2008, Vader, van der Meel <i>et al.</i> 2011, Ma, Xue <i>et al.</i> 2013)
Cdc42-like	Cdc42	Activation increases VEGF expression and regulates MMP production via AP1 and NFκB, regulates branching and sprouting	(Perona, Montaner <i>et al.</i> 1997, Bayless and Davis 2002, Davis, Bayless <i>et al.</i> 2002, Kouklis, Konstantoulaki <i>et al.</i> 2004,

		of tubes, involved in lumen formation, restores barrier function after thrombin treatment, EC specific KO is lethal due to reduced vessel growth	Bryan and D'Amore 2007, Ispanovic, Serio <i>et al.</i> 2008, Hu, Chen <i>et al.</i> 2011, Ma, Xue <i>et al.</i> 2013)
	RhoJ	Regulates endothelial migration and tube formation, further outlined in Section 1.3.6	(Kaur, Leszczynska <i>et al.</i> 2011, Yuan, Sacharidou <i>et al.</i> 2011, Takase, Matsumoto <i>et al.</i> 2012, Kim, Yang <i>et al.</i> 2014)
RhoH	RhoH	Inhibits NFκB so may reduce MMP production	(Li, Bu <i>et al.</i> 2002)

## 1.3 RhoJ

### 1.3.1 Introduction

RhoJ, also known as TCL (TC10-like), is a member of the Cdc42-like subfamily of Rho GTPases with high sequence similarity to RhoQ (TC10, 74.15% as calculated by ClustalW) and Cdc42 (61.78% as calculated by ClustalW). First identified by Vignal *et al.* in 2000, RhoJ is encoded by 5 exons on human chromosome 14 (Vignal, De Toledo *et al.* 2000).

### 1.3.2 RhoJ in cytoskeletal rearrangements

A multitude of experiments have indicated a role for RhoJ in regulating the cytoskeleton. Studies in REF-52 fibroblasts, mouse fibroblasts and endothelial cells have demonstrated that expression of active mutants of both human and mouse RhoJ leads to a reduction in numbers of stress fibres (Vignal, De Toledo *et al.* 2000, Abe, Kato *et al.* 2003, Fukushima, Okada *et al.* 2011, Kaur, Leszczynska *et al.* 2011). Additionally, endogenous RhoJ was shown to localise to focal adhesions in endothelial cells and mediates their numbers (Kaur,

Leszczynska *et al.* 2011), and others have reported that overexpressed RhoJ localises to membrane blebs and vesicles (Fukushima, Okada *et al.* 2011).

Several groups have also identified a function for RhoJ in actin polymerisation. Expression of a dominant active mutant of RhoJ (human and mouse) induced accumulation of f-actin in fibroblasts and it was postulated that this is due to an interaction with N-WASP leading to activation of the Arp 2/3 complex (Vignal, De Toledo *et al.* 2000, Abe, Kato *et al.* 2003). In porcine aortic endothelial cells, active RhoJ expression led to the formation of actin filament bundles and focal adhesions at the cell periphery (Aspenstrom, Fransson *et al.* 2004). In addition, RhoJ has been implicated in the formation of podosomes in porcine aortic endothelial cells (PAEC). These are actin assemblies induced by adhesion and known to be regulated by GTPase activity, often Cdc42 (Billottet, Rottiers *et al.* 2008).

Kaur *et al.* also demonstrated that RhoJ is involved in mediating contractility in endothelial cells, with knockdown of endogenous protein inducing increased levels of phospho-myosin light chain, suggesting a link between RhoJ and Rho kinase (ROCK) which modulates this phosphorylation (Kaur, Leszczynska *et al.* 2011, Kim, Yang *et al.* 2014).

Since RhoJ regulates various aspects of the cytoskeleton, it is logical that this translates to regulation of migration, tube formation and lumen formation. These processes were all found to be impaired in endothelial cells upon knockdown of RhoJ, while inhibition of ROCK or non-muscle myosin II rescued migration and tube formation, further suggesting a role for RhoJ in regulating contractility (Kaur, Leszczynska *et al.* 2011, Yuan, Sacharidou *et al.* 2011, Kim, Yang *et al.* 2014). Reduced migration and invasion has also been noted in melanoma cells with diminished RhoJ expression (Ho, Soto Hopkin *et al.* 2013).

### 1.3.3 RhoJ interactions and signalling

Since it was first identified, several interacting partners have been described for RhoJ. Many of these are known to be Cdc42 effectors, with PAK1B, PAK4, p50RhoGAP, JamB and MT1-MMP all published, as well as Cdc42 itself (Aspenstrom, Fransson *et al.* 2004, Yuan, Sacharidou *et al.* 2011). Additionally, active RhoJ is known to bind to the Cdc42/Rac1-interacting binding domain (CRIB), which is found in WASP as well as some PAK proteins (Vignal, De Toledo *et al.* 2000).

In endothelial cells, a direct interaction has been found between RhoJ and the focal adhesion protein GIT1. GIT also binds to  $\beta$ -PIX, another adhesion protein and a GEF for Cdc42, and it is thought that RhoJ associates with  $\beta$ -PIX as a result of its interaction with GIT. Furthermore, it appears the recruitment of these proteins to focal adhesions is interdependent, since silencing of any member of the complex negatively affects recruitment of the others (Katarzyna Leszczynska, PhD thesis). The GIT/PIX complex has previously been shown to play a role in regulating adhesion dynamics (Zhao, Manser *et al.* 2000, Nayal, Webb *et al.* 2006, Feng, Baird *et al.* 2010, Kuo, Han *et al.* 2011) and thus its interaction with RhoJ may be related to the observation that RhoJ mediates focal adhesion numbers (Kaur, Leszczynska *et al.* 2011).

Recently, RhoJ was identified as a target for the transcription factor ERG, which is involved in mediating lumen formation. Knockdown of ERG was associated with a 75% decrease in RhoJ expression, and 3 conserved binding sites for ERG were found in the proximal promoter of RhoJ (Yuan, Sacharidou *et al.* 2011).

It also appears that RhoJ regulates the activity of and itself is regulated by other Rho GTPases. Dominant negative mutants of Rac1 and Cdc42 inhibited the activity of RhoJ in REF-52 cells, while knockdown of RhoJ reduced Rac1 and Cdc42 activation but increased active levels of RhoA in endothelial cells (Vignal, De Toledo *et al.* 2000, Yuan, Sacharidou *et al.* 2011).

Kaur *et al.* also reported that levels of active RhoJ increase upon stimulation of endothelial cells with VEGF after 15 min, while Fukushima and colleagues describe an inhibition of activation after treatment with this growth factor for 2 min (Fukushima, Okada *et al.* 2011, Kaur, Leszczynska *et al.* 2011). These differences are likely to be due to the time-points analysed, suggesting an initial inactivation of RhoJ activity immediately after VEGF treatment, followed by a later, sustained activation from 15 min to 1 h. Fukushima *et al.* also describe activation of RhoJ by Sema3E, and stimulation with this protein induced the transport of endogenous RhoJ from the cytoplasm to membrane blebs; they postulate that RhoJ mediates Sema3E in the retraction of filopodia (Fukushima, Okada *et al.* 2011).

More recent studies performed by Kusuhara *et al.* in 2012 have further described RhoJ inactivation in endothelial cells. The endothelial expressed guanine nucleotide exchange factor Arhgef15, along with a truncated form of the protein made up of the DH and PH GEF domains were found to significantly inactivate RhoJ when co-transfected in HEK293T cells (Kusuhara, Fukushima *et al.* 2012).

#### **1.3.4 RhoJ in adipocyte differentiation and glucose transport**

Soon after its characterisation, a role for RhoJ was described in adipocyte differentiation and glucose transport. Chiang *et al.* showed localisation of murine RhoJ (referred to as TC10 $\beta$ /TC10 $\beta$ L) to lipid rafts in differentiated 3T3L1 adipocytes, as well as a rapid and transient activation in response to insulin treatment (Chiang, Hou *et al.* 2002). Later, they also determined a nucleotide independent interaction between RhoJ and TCGAP, another protein involved in regulating glucose transport (via the GAP domain of TCGAP) (Chiang, Hwang *et al.* 2003). Others also investigated the role of RhoJ in adipogenesis, after expression was found to be high in the early stages of adipocyte differentiation. Knockdown of RhoJ prevented differentiation of mouse 3T3-L1 fibroblasts into adipocytes and led to reduced expression of adipogenic related genes whereas dominant active RhoJ induced differentiation of these cells (Nishizuka, Arimoto *et al.* 2003). More recent studies by Kawaji *et al.* have pinpointed the role of RhoJ in regulating mitotic clonal expansion (MCE) a process necessary for adipocyte differentiation, and in particular in mediating expression of C/EBP $\beta$  and C/EBP $\delta$ , two proteins required for MCE (Kawaji, Nishizuka *et al.* 2010).

#### **1.3.5 RhoJ in regulating endocytosis**

In 2003, de Toledo and colleagues identified a role for RhoJ in the regulation of the early endocytic pathway. Overexpressed wt-RhoJ localised to the plasma membrane and early/sorting endosomes in HeLa cells. Knockdown of endogenous protein impaired release of transferrin, while expression of dominant active RhoJ led to accumulation of transferrin to early/sorting endosomes and potentiated its release without use of perinuclear recycling endosomes (de Toledo, Senic-Matuglia *et al.* 2003).

Further work in endothelial cells failed to demonstrate a role for RhoJ in trafficking of transferrin or VEGFR2, however co-localisation of over-expressed RhoJ with the endosomal markers EEA1 and Rab11 and the lysosomal marker Lamp1 (lysosomal associated membrane protein 1) was observed (Katarzyna Leszczynska, PhD Thesis).

### **1.3.6 RhoJ *in vivo***

RhoJ is known to show a vascular expression pattern in the developing mouse embryo as well as the veins and capillaries of the retina. Expression has also been observed in the vasculature of a number of normal and cancer tissues including the lungs, liver, pancreas, ovarian cancer and bladder cancer (Fukushima, Okada *et al.* 2011, Kaur, Leszczynska *et al.* 2011, Yuan, Sacharidou *et al.* 2011).

The *in vivo* function of RhoJ has recently begun to be investigated, with knockdown of RhoJ inducing impaired vessel formation in Matrigel plugs, and reduced melanoma tumour growth and invasiveness into the lymphatic system (Yuan, Sacharidou *et al.* 2011, Ho, Soto Hopkin *et al.* 2013). Overexpression of RhoJ in the endothelial cells of mice led to embryonic lethality, with growth retardation and defective vascular development at E10.5. In accordance with the data gathered *in vitro*, membrane blebs were also found in retinal vessels of mice heterozygous for endothelial specific RhoJ overexpression (Fukushima, Okada *et al.* 2011).

Takase *et al.* have reported the generation of a RhoJ knockout mouse, which develops normally and is fertile. The retinal neovascularisation model however, showed that they



have delayed radial growth of vessels compared to wild-type controls, suggesting that RhoJ functions to stabilise these vessels normally (Takase, Matsumoto *et al.* 2012).

Recently, Kim *et al.* generated a RhoJ knockout mouse for extensive use in tumour angiogenesis studies. They first determined that RhoJ was highly and specifically expressed in the blood vessels of Lewis lung carcinomas and melanoma, as well as in tumours arising from a spontaneous breast tumour model. Expression was particularly high during early tumour formation and in the angiogenic peritumoral region. In the knockout mouse, tumour growth was inhibited, with reduced vessel sprouting, vascular density and metastasis. Additionally, increased vessel permeability was observed, along with reduced coverage by supporting pericytes and basement membrane.

An inducible endothelial-specific RhoJ knockout mouse echoed the phenotypes seen in the global knockout, although to a lesser extent (Kim, Yang *et al.* 2014). Interestingly, induction of the RhoJ knockout slowed growth of established tumours and increased the rate of survival, suggesting that RhoJ could be a target for anti-cancer therapies in the future. In addition, blockade of VEGF in the RhoJ knockout mouse enhanced the effect of RhoJ knockout alone, and this was phenocopied with simultaneous *in vivo* siRNA of RhoJ and VEGF blockade. Similarly, when RhoJ knockout mice were treated with the vascular disruption agent Combretastatin-A4-Phosphate (CA4P), the anti-tumour effect observed in either case was heightened (Kim, Yang *et al.* 2014).

In 2013, RhoJ was found to be part of a list of the 20 most highly upregulated genes in a range of cancers. Masiero *et al.* observed that in a panel of 121 head and neck squamous cell carcinomas, 959 breast cancers and 170 renal clear cell carcinomas, RhoJ was consistently

highly expressed, suggesting a role in mediating tumour angiogenesis (Masiero, Simoes *et al.* 2013). Additionally, RhoJ has been identified as a regulator of melanoma chemoresistance *in vitro*, and mediates the expression of Sox10, a known oncogene required for melanoma formation in both mice and humans (Ho, Aruri *et al.* 2012).

To conclude, RhoJ is an endothelial-expressed protein of the Cdc42 subfamily of Rho GTPases. It is known to regulate the actin cytoskeleton and focal adhesions, mediating cell migration and tube formation as a result. Linked to this, RhoJ is also known to regulate activity of Rac1, Cdc42 and RhoA, with its expression controlled by the transcription factor ERG. Recently, RhoJ has been implicated as having a role in melanoma invasion and chemoresistance, retinal vascularisation and tumour angiogenesis. Further understanding of the biochemical functions of RhoJ within endothelial cells and how it interacts with other proteins could give clues for further development as a therapeutic target in pathological angiogenesis.

## **1.4 The cytoskeleton and cell migration**

### **1.4.1 Overview**

Migration is a crucial part of numerous physiological and pathological processes, including development, angiogenesis and metastasis. A major factor in the regulation of cell migration is remodelling of the actin cytoskeleton and the formation and disassembly of lamellipodia, filopodia and focal adhesions. This process is a cyclical one, where external cues trigger actin polymerisation, membrane protrusion, adhesion to the extracellular matrix and retraction of the rear of the cell, ultimately enabling forward movement (Ridley, Schwartz *et al.* 2003).

### **1.4.2 Actin polymerisation, lamellipodia and filopodia**

Initially, cells must polarise in order to migrate, and this is aided by the inherent polarity of actin filaments which rapidly assemble at the barbed end (or the plus end), with slow, net disassembly at the pointed end (also called the minus end). This assembly/disassembly cycle is referred to as actin treadmilling. Filamentous actin is generated by the polymerisation of globular actin monomers, which are added at the barbed end of the filament. Actin monomers are bound by ATP, which is hydrolysed to ADP upon addition to the chain, and this energy release is crucial in mediating the polymerisation process (Disanza, Steffen *et al.* 2005, Lee and Dominguez 2010). Lamellipodia are broad membrane protrusions at the leading edge of the cell containing branched actin networks. Actin polymerisation is mediated by WASP and WAVE activation of the Arp2/3 complex in these regions, and is terminated by the addition of capping proteins to the barbed ends of the filament. Additionally, these structures are only weakly adhered to the extracellular matrix, enabling dynamic reorganisation and forward movement (Ridley, Schwartz *et al.* 2003, Chhabra and Higgs 2007). Filopodia meanwhile are finger-like protrusions arising from the front of the lamellipodia that serve to probe the environment, and contain long unbranched bundles of actin. In these projections, proteins which facilitate capping of filaments and branching are inhibited, thus allowing continuous elongation. There is a large amount of evidence to suggest that the Ena/VASP group of proteins act to promote actin polymerisation in an environment rich in capping proteins by antagonising the action of these proteins, although there has been some dispute about this (Mattila and Lappalainen 2008, Bear and Gertler 2009).

### 1.4.3 Adhesion to the extracellular matrix

In order to stabilise the membrane protrusions, adhesions form which connect the cell to the extracellular matrix (Parsons, Horwitz *et al.* 2010). These adhesions vary in type and composition, with nascent adhesions assembling initially and subsequently maturing into small focal complexes, larger focal adhesions and long, highly stable fibrillar adhesions (Zaidel-Bar, Cohen *et al.* 2004, Worth and Parsons 2008, Parsons, Horwitz *et al.* 2010). Not all cells display each type of adhesion though, with focal adhesions more apparent in adherent, contractile cells while nascent adhesions are commonly found in fast moving cells (Parsons, Horwitz *et al.* 2010). Figure 1.4 shows a diagram of a motile cell with the cytoskeletal structures that form and disassemble in order for the cell to migrate forwards.

One of the core features of adhesions between the extracellular matrix and intracellular cytoskeleton is the presence of integrins. These are heterodimeric receptors made up of  $\alpha$ - and  $\beta$ - chains which bind the extracellular matrix, and form the basis for the assembling focal adhesion. Binding of the extracellular domain of the integrin to a ligand in the ECM induces a conformational change in the  $\alpha$ - and  $\beta$ - chains, and enables interactions between the integrin cytoplasmic domain and intracellular proteins such as talin, filamin and  $\alpha$ -actinin (Zaidel-Bar and Geiger 2010). Such proteins enable indirect interactions between the integrin and filamentous actin; the head domain of talin, for example, binds the integrin while the tail domain is able to interact with actin either directly or indirectly via vinculin. Additionally, the interaction between the integrin and talin leads to inside-out activation of the receptor and allows downstream signalling events including integrin clustering and

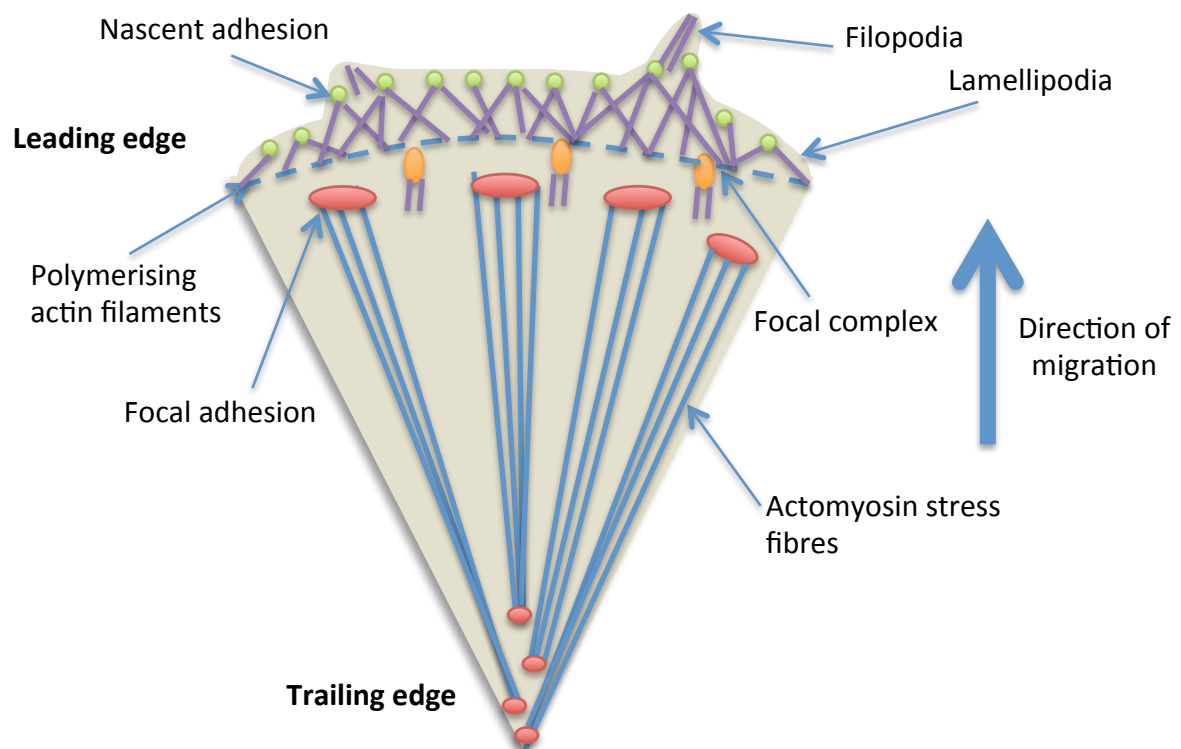


**Figure 1.4. The cytoskeleton in a migrating cell.** In the initial stages of migration, the cell polarises and forms a broad membrane protrusion called a lamellipodia, a site of much actin polymerisation. Finger-like protrusions called filopodia also form, serving to probe the environment. Nascent adhesions form at the front of the lamellipodia, helping to stabilise the protrusions and mature into focal complexes in a myosin-dependent manner. These focal complexes further mature into focal adhesions, which are found at the ends of stress fibres. Retraction of the stress fibres at the trailing edge of the cell and focal adhesion disassembly acts in balance with protrusion at the front, enabling forward migration.

adhesion formation (Ridley, Schwartz *et al.* 2003, Parsons, Horwitz *et al.* 2010, Schwartz 2010, Anthis and Campbell 2011). Figure 1.5 shows a diagram of a focal adhesion.

Both structural (or scaffolding) and signalling proteins are known to act as adaptors between the integrin receptor and actin, and it is also possible for proteins to act as both a scaffold and part of a signalling cascade. FAK is an example of such a protein, since it acts as a kinase and regulates Rho GTPase activities but also recruits Calpain 2 and p42 ERK/MAPK to adhesions (Carragher, Westhoff *et al.* 2003, Mitra, Hanson *et al.* 2005). Over 180 proteins have thus far been identified in the so-called 'integrin adhesome', forming a highly complex network of at least 742 interactions which may be switched on or off depending on the cellular environment (Zaidel-Bar and Geiger 2010). Moreover, the presence of signalling molecules enables crosstalk between different pathways, and the initiation of cascades important in processes including bacterial phagocytosis and thrombus formation (Huvener and Danen 2009).

#### **1.4.4 Adhesion formation and maturation**

Nascent adhesions are the initial class of adhesion that assembles in membrane protrusions, formed by integrin clustering. These adhesions are very small (less than 0.25  $\mu\text{m}$ ) and turn over rapidly, normally within 60 seconds (Parsons, Horwitz *et al.* 2010, Hanein and Horwitz 2012). The rate of assembly is proportional to the rate of membrane protrusion, and thus fast moving cells contain rapidly assembling and disassembling nascent adhesions (Vicente-Manzanares and Horwitz 2011). These adhesions are able to form in spite of myosin II inhibition, however, suggesting that while actin polymerisation appears to be important in

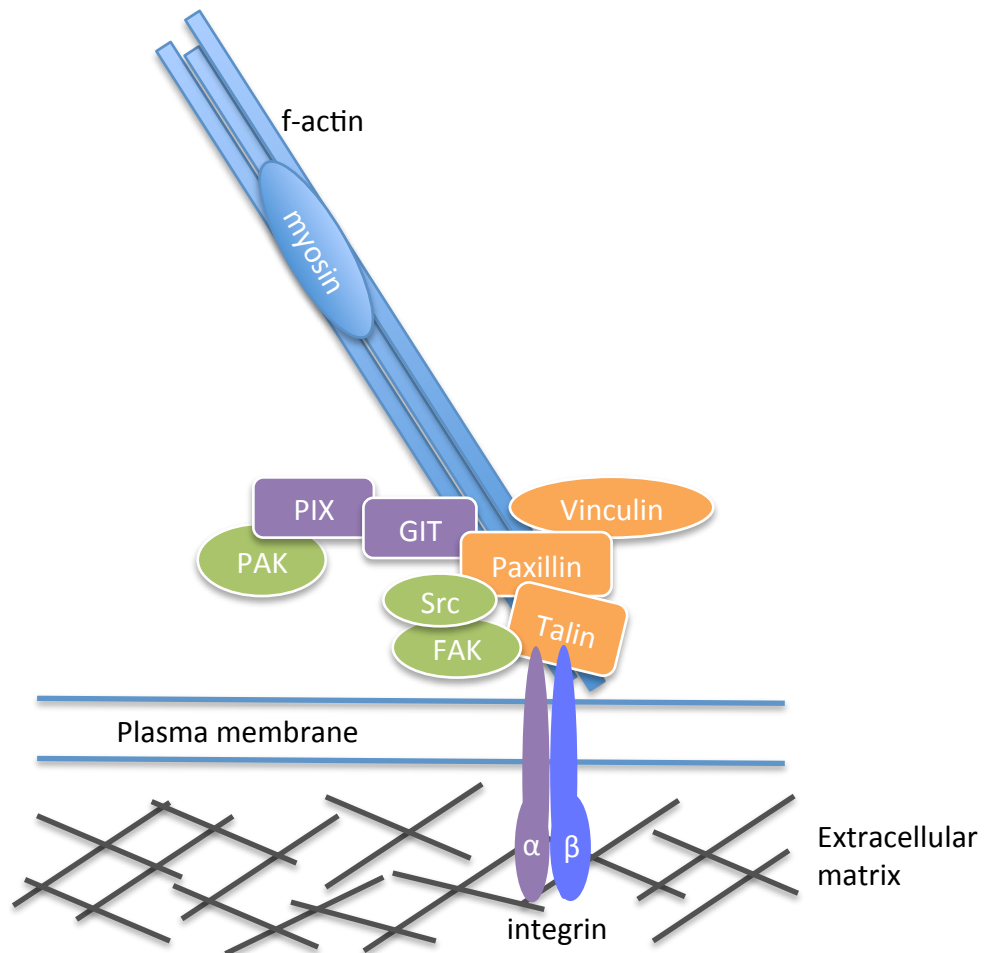


**Figure 1.5. The composition of a focal adhesion.** Transmembrane integrins (made up of  $\alpha$  and  $\beta$  chains) bind intracellular proteins including talin, which in turn interact with other proteins such as paxillin, forming a focal adhesion. A complex consisting of structural and signalling molecules is generated and this interacts with actomyosin stress fibres, connecting the intracellular cytoskeleton with the extracellular matrix.

their assembly, they are myosin-independent (Choi, Vicente-Manzanares *et al.* 2008, Vicente-Manzanares and Horwitz 2011). Choi and colleagues also determined that the components that make up the nascent adhesion, which include vinculin, FAK and GIT1, appear to recruit and disassemble at the same time, which may suggest that these proteins are already assembled into a complex when they form the adhesion (Choi, Vicente-Manzanares *et al.* 2008).

The proteins in the adhesion are mostly immobile, which indicates that they are more strongly associated with integrins than actin (Brown, Hebert *et al.* 2006). While the cell moves forwards, adhesions at the rear of the lamellipodia either disassemble, or mature into focal complexes. This maturation appears to be closely linked to contractility, and since contractility varies depending on the cell and its environment, not all cells display the full range of adhesion types (Parsons, Horwitz *et al.* 2010, Hanein and Horwitz 2012). More recently however, evidence has been put forward to suggest that adhesion maturation is independent of tension, but rather myosin II regulates this process by mediating retrograde flow and bundling of actin. Additionally, over-expression of  $\alpha$ -actinin or Dia1, two proteins that function in the formation of stress fibres, enable stabilisation of adhesions in low tension environments (Stricker, Beckham *et al.* 2013). This is in line, too, with the theory that adhesions require a stress fibre template in order to mature (Oakes, Beckham *et al.* 2012).

Nascent adhesions grow and mature into focal complexes, which are larger (approximately 1  $\mu\text{m}$  in diameter), and appear at the lamellipodia/lamellum transition zone (Parsons, Horwitz *et al.* 2010, Hanein and Horwitz 2012). Unlike nascent adhesions, focal complexes are dependent on myosin II activity (Vicente-Manzanares and Horwitz 2011). Most often, these



focal complexes are also fairly transient, with a lifetime that is longer than nascent adhesions, but still only several minutes (Parsons, Horwitz *et al.* 2010). These complexes tend to mature into focal adhesions due to retraction of the lamellipodium as the cell continues to migrate (Zaidel-Bar, Ballestrem *et al.* 2003).

Focal adhesions are larger still than focal complexes, measuring around 3-10  $\mu\text{m}$  in length, and grow from the site of the original focal complex towards the cell centre, generating a polarised structure (Wolfenson, Henis *et al.* 2009, Parsons, Horwitz *et al.* 2010). Rather than being found in one particular region of the cell as is seen with nascent adhesions, focal adhesions are spread across the base of the cell (Worth and Parsons 2008), and found at the ends of actin stress fibres. Additionally, the composition of the adhesion differs from less mature adhesions, zyxin in particular is observed in focal adhesions however this protein does not recruit to nascent adhesions or focal complexes (Zaidel-Bar, Ballestrem *et al.* 2003, Wolfenson, Lavelin *et al.* 2013).

Focal adhesions are more stable than early adhesive structures, with longer lifetimes. As the cell continues to migrate, these adhesions are drawn towards the rear of the cell where they are able to disassemble, allowing retraction of the cell and continued migration. They may also grow into fibrillar adhesions, which are long and highly stable with a much less complex composition than focal adhesions. Rather than a large array of scaffolding and signalling proteins, fibrillar adhesions are mainly composed of  $\alpha 5\beta 1$  integrins and tensin, and form parallel to fibronectin bundles (Le Clainche and Carlier 2008, Worth and Parsons 2008).

### **1.4.5 Adhesion disassembly**

Just as adhesion formation is crucial for formation of an anchor between the cell and the extracellular matrix, disassembly of these structures is equally important to enable release of the cell and recommencement of the migration cycle. While the formation of adhesions is largely understood, the disassembly of these adhesions is less well defined. Many different processes and proteins have been implicated in regulating this phase of adhesion dynamics, and while it would be impossible to cover all the potential mediators in this introduction, a summary of some of the key aspects are highlighted below, and depicted in Figure 1.6.

Firstly, targeting of adhesions by microtubules is known to be a method of adhesion disassembly, however it is not yet clear whether this is a mechanism common to all cell types. It is apparent that these targeting events are more frequently found at sites of adhesion disassembly, and that multiple microtubule targeting enables disassembly at both the leading and trailing edges (Efimov and Kaverina 2009, Stehbens and Wittmann 2012). There are several different theories regarding how microtubules are able to facilitate adhesion disassembly including the release of stress fibre-induced tension at the adhesion; triggering calpain-mediated proteolysis of adhesion components; and contraction of stress fibres by GEFs which are regulated by microtubule binding (Broussard, Webb *et al.* 2008).

As indicated in microtubule targeting of adhesions, calcium-dependent calpain proteolysis seems to be important in regulating focal adhesion dynamics. Knockdown of calpain 2 led to slower disassembly of adhesions and increased stability due to reduced calpain cleavage of a number of adhesion proteins. Talin, FAK and paxillin are all targets for this cleavage, and expression of calpain-resistant mutant proteins leads to changes in adhesion dynamics.

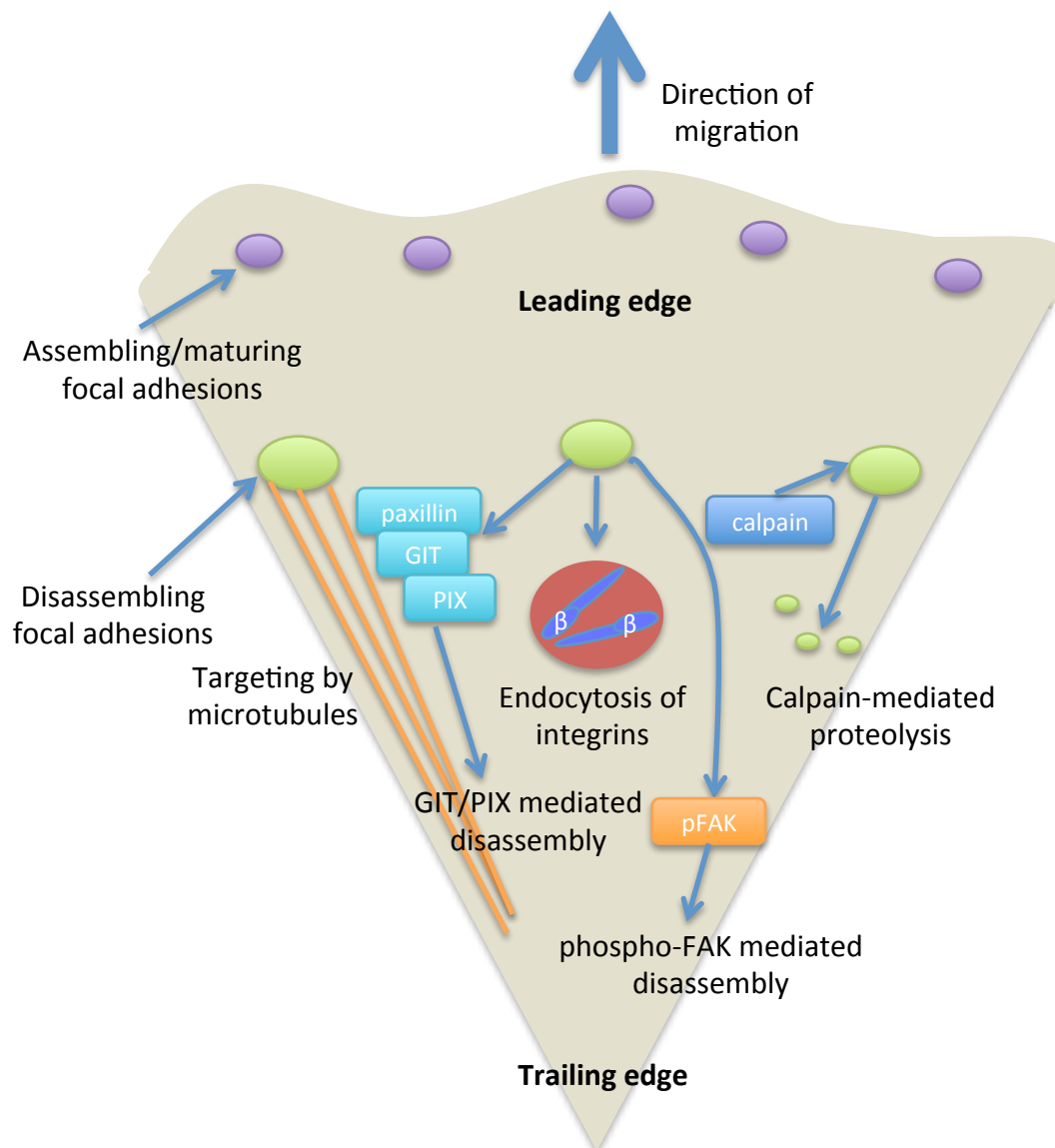


**Figure 1.6. Methods of focal adhesion disassembly.** Focal adhesions can be disassembled in a number of ways. Those depicted include targeting by microtubules; endocytosis of focal adhesion components, particularly integrins; proteolysis of adhesion components by calpain; and disassembly triggered by focal adhesion proteins including phosphorylated FAK and the GIT/PIX complex.

Proteolysis of talin in particular appears to be crucial for correct adhesion disassembly, with the turnover of paxillin, zyxin and vinculin at adhesions affected upon expression of the calpain-resistant form (Franco, Rodgers *et al.* 2004). In turn, FAK appears to regulate talin dynamics and its proteolysis is necessary for talin disassembly from (as well as recruitment to) adhesions (Chan, Bennin *et al.* 2010). Cleavage of paxillin, meanwhile, appears to have an inverse effect on adhesion disassembly. The resulting fragment appears to act as an antagonist to uncleaved paxillin, inducing slower disassembly of adhesions, while a resistant mutant results in faster turnover (Cortesio, Boateng *et al.* 2011). Together, these data suggest that calpain is able to both promote and inhibit adhesion disassembly, and it may be that the predominant function depends on the environment or cell type.

Both clathrin-mediated and caveolar endocytosis have also been shown to be involved in mediating focal adhesion disassembly, in particular in facilitating integrin uptake (Bass, Williamson *et al.* 2011, Brinas, Vassilopoulos *et al.* 2013). Phosphorylated dynamin interacts with FAK and Src in focal adhesions, and this complex potentiates the endocytosis of  $\beta$ 1-integrin and as such adhesion disassembly (Wang, Cao *et al.* 2011). Additionally, dynamin interacts with the phosphatase PTP-PEST, which itself plays a role in adhesion disassembly (Angers-Loustau, Cote *et al.* 1999, Eleniste, Du *et al.* 2012). The targeting of microtubules to adhesions is also important in mediating the uptake of adhesion components, with intracellular transport often taking place along microtubules, and disassembly being triggered by microtubule targeting but also requiring dynamin (Ezratty, Partridge *et al.* 2005, Stehbens and Wittmann 2012).

As well as external forces and structures regulating focal adhesion disassembly, proteins within the complex are known to regulate this process too. FAK in particular has been implicated in mediating adhesion disassembly, which is perhaps not surprising considering its role as both a scaffold and signalling protein. Phosphorylation of FAK is required for its activation, with six tyrosine residues in particular being identified as sites of phosphorylation. Of these, Tyr 397 is autophosphorylated, while other residues are phosphorylated by kinases like Src. Both Tyr 397 and Tyr 925 have been implicated in mediating focal adhesion disassembly. Expression of mutants of FAK that are unable to be phosphorylated induced heightened adhesion stability, with fewer disassembled adhesions and longer disassembly durations observed (Hamadi, Bouali *et al.* 2005, Deramaudt, Dujardin *et al.* 2011). Vinculin too has recently been shown to be necessary for recruitment and stabilisation of other focal adhesion proteins under tensile force (Carisey, Tsang *et al.* 2013).

The GIT/PIX complex meanwhile consists of the GIT proteins (GIT1 and GIT2) and PIX ( $\alpha$ -PIX and  $\beta$ -PIX) proteins and localises to focal adhesions via interactions between GIT and paxillin, while PIX binds the kinase PAK. Studies of expression of GIT1 in HeLa cells identified a role for the C-terminus of the protein, which binds paxillin, in mediating loss of focal adhesions and this was increased when full length GIT1 was expressed alongside  $\beta$ -PIX. One interpretation is that GIT1 is normally found in an autoinhibitory conformation, where the C-terminus is masked and affinity for paxillin reduced, and this inhibition is subsequently relaxed by interaction with  $\beta$ -PIX (Zhao, Manser *et al.* 2000).

Further investigation by Nayal *et al.* also distinguished that phosphorylation of paxillin at serine 273 strengthens the interaction with GIT1 and drives the localisation of the GIT/PIX/PAK complex to the leading edge where it triggers adhesion disassembly. Knockdown of GIT1 in Rat2 fibroblasts led to reduced turnover of adhesions, with lengthened durations of both assembly and disassembly. Expression of a GIT1 mutant lacking the PIX binding domain (SHD) along with a phosphomimetic paxillin Ser 273D mutant greatly impaired adhesion disassembly compared to cells expressing the paxillin mutant alone (Nayal, Webb *et al.* 2006). Together, these data suggest that localisation GIT1 and PIX to the leading edge is required for adhesion disassembly.

Phosphorylation of  $\beta$ -PIX at tyrosine 442 has also been implicated in mediating adhesion disassembly in NIH 3T3 cells. Treatment of cells with epidermal growth factor (EGF) is known to induce phosphorylation of  $\beta$ -PIX (via Src and FAK), and stimulated cells expressing a wild-type construct of  $\beta$ -PIX induced disassembly of adhesions. In contrast, cells expressing a mutant form of PIX that cannot be phosphorylated at Tyr 442 retained their adhesions (Feng, Baird *et al.* 2010). It appears that phosphorylation of  $\beta$ -PIX weakened the interaction with GIT, however this weakened interaction in turn strengthened the association between GIT and paxillin, which may explain why phosphorylated  $\beta$ -PIX enhances adhesion disassembly (Feng, Baird *et al.* 2010).

Additionally, Kuo *et al.* identified that myosin II activity suppressed the abundance of  $\beta$ -PIX in focal adhesions, which suggests an inverse role in adhesion maturation. The lifetime of adhesions in fibroblasts with diminished  $\beta$ -PIX expression was also increased, with slowed

adhesion disassembly rates. Consequently, it was concluded that  $\beta$ -PIX positively regulates nascent adhesion turnover, thus negatively regulating maturation (Kuo, Han *et al.* 2011).

#### **1.4.6 Rho GTPase involvement in focal adhesion turnover**

Several members of the Rho GTPase family of proteins are known to play roles in regulating the dynamics of focal adhesions and the related structures. Members of the Rho subfamily, for example, mediate adhesion formation and maturation. In particular, RhoA is known to mediate adhesion maturation via its effector ROCK, which regulates phosphorylation of myosin light chain, leading to activation of myosin and ultimately contractility (Parsons, Horwitz *et al.* 2010).

Rac, too, has been implicated in regulating the formation of focal complexes, by clustering integrins to stabilise newly formed membrane protrusions (Kiosses, Shattil *et al.* 2001). Additionally, PIX can act as a GEF towards Rac, and it appears that cycling of Rac is necessary for adhesion turnover, since expression of a dominant negative Rac mutant induced much slower disassembly of adhesions (Nayal, Webb *et al.* 2006).

The atypical Rho GTPase Wrch1 (a member of the Cdc42-like subfamily) meanwhile, is also thought to modulate focal adhesion dynamics. Early data identified a reduction in the number of focal adhesions seen in cells over-expressing Wrch1 (Saras, Wollberg *et al.* 2004), and more recent investigations have found that knockdown of Wrch1 induces the formation of focal adhesions while over-expression potentiates adhesion disassembly, potentially by regulating myosin light chain phosphorylation (Chuang, Valster *et al.* 2007).

## **1.5 The GIT/PIX complex**

### **1.5.1 Introduction to the GIT proteins**

The G-protein coupled receptor (GPCR)-kinase-interacting proteins 1 and 2 (GIT1 and GIT2) are known by numerous names, including Cool-associated tyrosine phosphorylated proteins 1 and 2 (Cat-1 and Cat-2) and ADP ribosylation factor (ARF)-GTPase activating protein, PIX-, paxillin-interacting proteins 1 and 2 (APP-1 and APP2), while GIT2 may also be referred to as p95 paxillin kinase linker (p95 PKL). These are multidomain proteins that have been shown to have far-reaching functions including regulation of the cytoskeleton, mediating receptor internalisation and catalytic activity towards Arf GTPases.

The GIT proteins are closely related, with 85% homology between GIT1 and GIT2, however GIT2 is subject to much alternative splicing and a truncated form of the protein, designated as GIT2 short also exists (Hoefen and Berk 2006). Additionally, the GIT proteins are found to be expressed in distinct regions within the mouse, for example, GIT2 is widely expressed in the lungs and liver while GIT1 is primarily restricted to the vasculature in these organs; conversely, only GIT2 is expressed in the granule cells of cerebellum (Schmalzigaug, Phee *et al.* 2007).

### **1.5.2 Domain structure of the GIT proteins**

Despite differences in expression, the domain structures of GIT1 and GIT2 are identical, as depicted in Figure 1.7. Essentially, these proteins consist of: an Arf GAP domain, containing a zinc finger-like motif necessary for catalytic activity (Vitale, Patton *et al.* 2000); 3 ankyrin repeats; a Spa homology domain (SHD), which acts as a binding domain for a number of



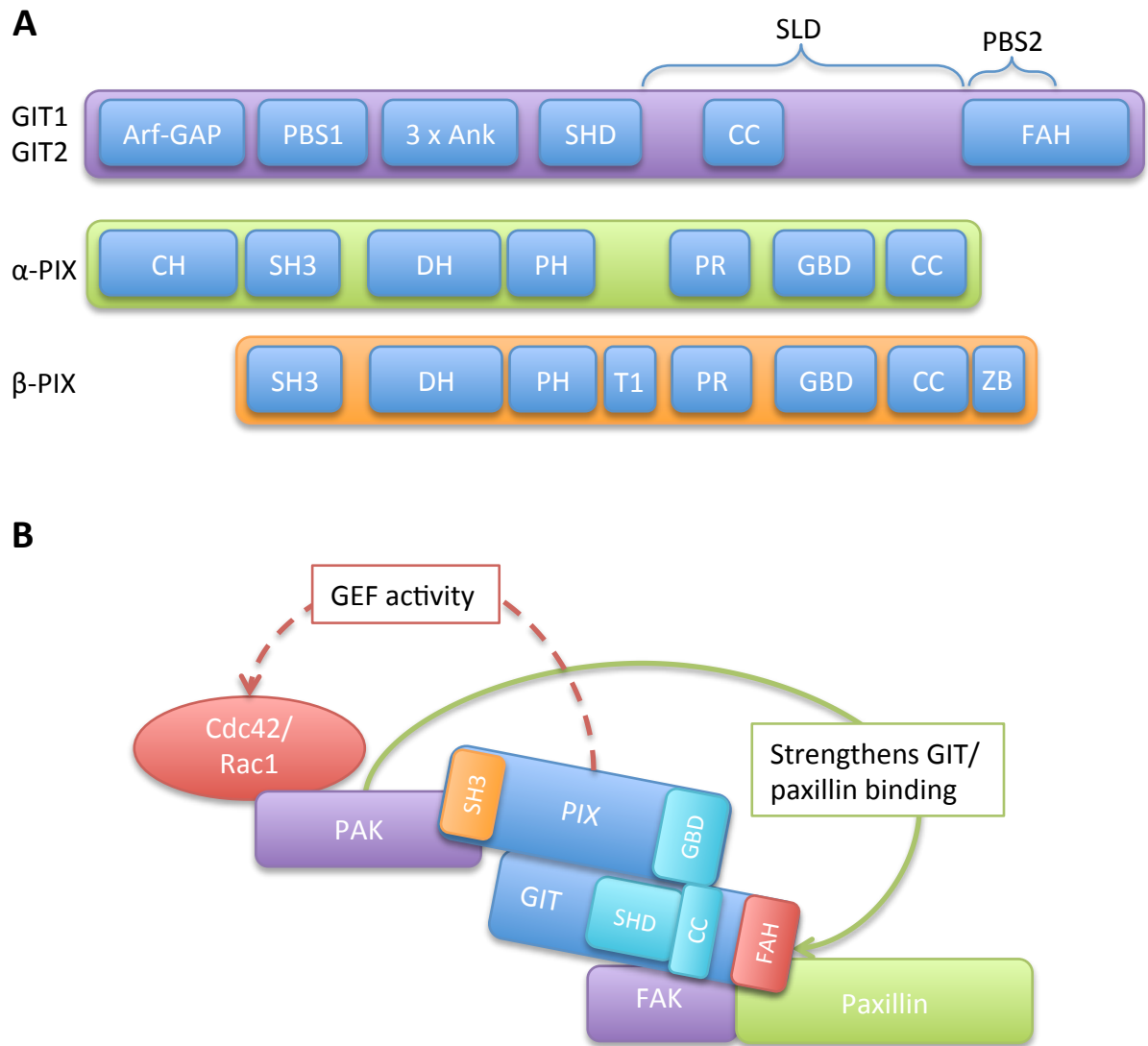


**Figure 1.7. The structure and interactions of the GIT/PIX proteins.** **A.** The domain structure of GIT1, GIT2, α-PIX and β-PIX. GAP: GTPase-activating protein; PBS: paxillin binding sequence; Ank: Ankyrin; SHD: Spa homology domain; CC: coiled-coil region; SLD: synapse localisation domain; FAH: focal adhesion targeting homology domain; CH: Calponin homology domain; SH3: Src homology 3 domain; DH: Dbl homology domain; PH: Pleckstrin homology domain; T1: T1 insert; PR: proline-rich region; GBD: GIT binding domain; ZB: PDZ domain binding motif. **B.** The interactions of the GIT/PIX complex in focal adhesions. GIT binds to PIX via its SHD and CC, and localises to adhesions by interacting with paxillin through its FAH domain. PIX in turn binds PAK via its SH3 domain, and small Rho GTPases are recruited to adhesions by binding the CRIB domain within PAK. PIX can also activate Rac1 and Cdc42, while PAK strengthens the interaction between GIT and paxillin.

other proteins including  $\beta$ -PIX (Zhao, Manser *et al.* 2000); a coiled coil containing a putative leucine zipper enabling dimerisation (Paris, Longhi *et al.* 2003) and finally a C-terminal focal adhesion targeting homology (FAH) domain which interacts with the LD4 motif within paxillin, promoting localisation to focal adhesions (Turner, Brown *et al.* 1999, Manabe, Kovalenko *et al.* 2002). In addition to the core domains of GIT, a region between the SHD and FAH domains is referred to as the synaptic localisation domain (SLD) (Zhang, Webb *et al.* 2003).

Many tyrosine, serine and threonine phosphorylation sites have also been identified in both GIT1 and GIT2, particularly between residues 300-600 (Webb, Mayhew *et al.* 2006). A number of these phosphorylation events are known to play roles in binding to proteins, intracellular localisation and function (Brown, Cary *et al.* 2005, Webb, Kovalenko *et al.* 2006).

### **1.5.3 Introduction to the PIX proteins**

The PAK-interacting exchange factors  $\alpha$  and  $\beta$  ( $\alpha$ -PIX and  $\beta$ -PIX) are also sometimes referred to as cloned-out-of-library 1 and 2 (Cool-1 and Cool-2), where Cool-1 (also sometimes called p85Cool-1) is  $\beta$ -PIX and Cool-2 is  $\alpha$ -PIX. Additionally,  $\beta$ -PIX has previously been designated as 85 kDa SH3 domain-containing proline-rich protein (p85SPR, (Oh, Yoo *et al.* 1997)). Much like GIT2, which may be expressed as a truncated GIT2-short protein,  $\beta$ -PIX has been found to be expressed as a smaller form, called p50Cool-1. Multiple splice variants of  $\beta$ -PIX have also been reported, in particular  $\beta$ -PIX-a (or  $\beta_1$ -PIX) and  $\beta$ -PIX-b (or  $\beta_2$ -PIX), which differ in that  $\beta_2$ -PIX contains a serine-rich region in place of the coiled-coil C-terminal domain (Koh, Manser *et al.* 2001). The PIX family of proteins has also been implicated in many cellular

functions, including cytoskeletal rearrangements, neurite outgrowth and cerebral vascular stability.

#### **1.5.4 Domain structure of the PIX proteins**

Both PIX proteins contain most of the same domains, and those features common to the  $\alpha$ - and  $\beta$ - isoforms include: a Src homology 3 (SH3) domain, which is able to interact with proline-rich regions of proteins including PAK (Oh, Yoo *et al.* 1997, Manser, Loo *et al.* 1998); the Dbl homology (DH) and Pleckstrin homology (PH) domains that are known to coordinate exchange activity in guanine nucleotide exchange factors (Bagrodia, Taylor *et al.* 1998, Cherfils and Zeghouf 2013); a proline-rich region that binds to the phosphatases POPX1 and POPX2, which inactivate PAK (Koh, Tan *et al.* 2002, Frank and Hansen 2008); a GIT-binding domain (GBD, also sometimes called Cat-binding domain or CBD) (Bagrodia, Bailey *et al.* 1999) and finally a coiled coil containing a leucine zipper motif, which mediates dimerisation much as it does in GIT (Kim, Lee *et al.* 2001, Koh, Manser *et al.* 2001).

In addition,  $\alpha$ -PIX contains a calponin-homology domain (Manser, Loo *et al.* 1998) while  $\beta$ -PIX includes an 18 amino acid T1 insert that regulates GEF activity (Feng, Albeck *et al.* 2002, Feng, Baird *et al.* 2006). A PDZ binding domain has also been identified in the C-terminus of  $\beta$ -PIX, which facilitates binding to proteins containing a PDZ domain such as Scribble (Audebert, Navarro *et al.* 2004).

It has been observed that multiple GIT and PIX proteins interact to form large oligomeric complexes. Both GIT and PIX proteins associate with themselves via their coiled coil domains, and it is thought that the 2 SHDs of a GIT dimer bind to 2 GBDs of a PIX trimer,

leaving one GBD unbound, forming a heteropentameric complex (Premont, Perry *et al.* 2004, Schlenker and Rittinger 2009).

## **1.5.5 General functions of the GIT and PIX proteins**

### **1.5.5.1 The GIT/PIX proteins as regulators of GTPase activity**

Both the GIT and PIX families have been identified as demonstrating catalytic activity towards other proteins. GIT1 and GIT2 act as GAPs towards members of the Arf family of GTPases, including Arf1, Arf3, Arf5 and Arf6 through their Arf GAP domain (Premont, Claing *et al.* 1998, Premont, Claing *et al.* 2000, Vitale, Patton *et al.* 2000, Turner, West *et al.* 2001, Hoefen and Berk 2006, Mazaki, Hashimoto *et al.* 2006). Since the Arf proteins are involved in regulating membrane dynamics and trafficking, it is thought that this activity contributes to several of the intracellular roles identified for the GIT proteins (Donaldson and Jackson 2000).

The PIX proteins, meanwhile, act as GEFs towards small Rho GTPases. There is some controversy surrounding the GEF activity of  $\beta$ -PIX, however it has been shown while dimerised,  $\alpha$ -PIX specifically displays exchange activity towards Rac1, monomeric  $\alpha$ -PIX functions as a GEF towards both Rac1 and Cdc42, and this activity is dependent on interaction with PAK or Cbl (Feng, Albeck *et al.* 2002, Feng, Baird *et al.* 2004). Additionally, active Cdc42 and Rac1 regulate the activity of dimeric  $\alpha$ -PIX towards Rac1; while active Cdc42 promotes GEF activity, GTP-bound Rac inhibits the Rac-specific GEF activity of  $\alpha$ -PIX (Baird, Feng *et al.* 2005).

Feng and colleagues also demonstrated that the full-length form of  $\beta$ -PIX facilitates

dissociation of GDP from Cdc42 when phosphorylated at tyrosine 442, which relieves the auto-inhibition imposed by the T1 domain; this was not, however, found in the case of Rac1 (Feng, Baird *et al.* 2006). Others have reported that  $\beta$ -PIX promotes activation of Rac1 (Manser, Loo *et al.* 1998, Koh, Manser *et al.* 2001, ten Klooster, Jaffer *et al.* 2006), however it is not clear whether it regulates the exchange activity of this GTPase. Additionally, there are multiple splice variants of  $\beta$ -PIX that differ in their C-terminii, the region where the coiled-coil is found (Koh, Manser *et al.* 2001). Since this domain is important for dimerisation, it is possible that as is the case for  $\alpha$ -PIX, different variants of  $\beta$ -PIX may display different exchange activities depending on their dimerisation state.

#### **1.5.5.2 Roles in trafficking**

It is via its Arf GAP activity that GIT1 is thought to regulate internalisation of the  $\beta_2$ -adrenergic receptor (Premont, Claing *et al.* 1998), and exocytosis in neuroendocrine cells (Meyer, Deliot *et al.* 2006). Further investigation has implicated GIT1 as having a more general role in clathrin-mediated endocytosis of G-protein coupled receptors, rather than the  $\beta_2$ AR alone (Claing, Perry *et al.* 2000), and both GIT proteins have been described as regulating ligand-stimulating trafficking of the receptor for the chemoattractant fMLP (Gavina, Za *et al.* 2010).

$\beta$ -PIX, meanwhile, has also been linked to trafficking, via its activity towards Rac. The regulation of Rac activation is thought to be important in mediating exocytosis in neuroendocrine cells (Momboisse, Lonchamp *et al.* 2009), membrane translocation of the infection-recognising receptor, NOD2, in monocytic cells (Eitel, Krull *et al.* 2008) and pinocytosis (Lee, Yang *et al.* 2011). Recently,  $\beta$ -PIX has also been identified as a regulator of

insulin-stimulated glucose secretion, by acting as a GEF for Cdc42 in pancreatic islet beta cells (Kepner, Yoder *et al.* 2011). Moreover, GIT1 and  $\beta$ -PIX appear to associate together with hScrib and Arf6 to regulate trafficking and recycling of the thyroid stimulating hormone receptor (Lahuna, Quellari *et al.* 2005).

#### **1.5.5.3 Roles in the cytoskeleton**

The GIT proteins have been implicated in mediating many aspects of the cytoskeleton, in particular focal adhesion dynamics, since they interact with the core adhesion protein paxillin (Turner, Brown *et al.* 1999, Zhao, Manser *et al.* 2000). GIT is recruited to focal adhesions via this interaction, however unlike GIT1, GIT2 must first be phosphorylated at 3 tyrosine residues (Tyr 286, 392 and 592) by Src or FAK before it can bind to paxillin and localise to adhesions (Brown, Cary *et al.* 2005). PIX in turn localises to these structures by interacting with the SHD and coiled coil of GIT (Premont, Perry *et al.* 2004), while PAK binds to the SH3 domain of PIX (Bagrodia, Taylor *et al.* 1998). PAK has been shown to strengthen the binding between paxillin and GIT by phosphorylating Ser 273 of paxillin. This potentiates the localisation of the GIT/PIX complex to the leading edge, and promotes membrane protrusion and adhesion turnover (Nayal, Webb *et al.* 2006). Additionally, PAK may be activated by GIT1 in association with PIX, independently of GTPases (Loo, Ng *et al.* 2004). Small GTPases such as Rac1 and Cdc42 are recruited to focal adhesions by interacting with the CRIB domain found in certain PAK proteins, or by directing binding to PIX. As described previously, the PIX proteins have been identified as GEFs for the Rho GTPases Rac1 and Cdc42, however it appears that they also act as scaffolds for these proteins at adhesions (Frank and Hansen 2008). GIT1 has also been identified as a scaffold for MEK1-ERK1/2 in

focal adhesions and promotes ERK activation, which is necessary for cell migration and spreading (Yin, Zheng *et al.* 2005, Zhang, Cai *et al.* 2010)

Phosphorylation of GIT1 appears to regulate many facets of its function in the cytoskeleton. Phosphorylation of serine 46 in GIT1 (which is a conserved residue in GIT2) for example, is thought to regulate cell spreading, protrusion and migration, and without this phosphorylation GIT1 is retained within stable focal adhesions (Huck, Kemkemer *et al.* 2012). PAK1 is also known to promote phosphorylation of GIT1 Ser709, a residue within the paxillin binding sequence, which induces increased interaction with paxillin and enhances membrane protrusion (Webb, Kovalenko *et al.* 2006), while phosphorylation of Tyr321 in the SHD is required for association with and activation of FAK, and regulates spreading and migration of osteoblasts (Ren, Yu *et al.* 2012). Meanwhile, phosphorylation of Ser273 in paxillin decreases its interaction with FAK and is postulated to cause a switch in binding partner preference to GIT thus triggering focal adhesion disassembly (Bertolucci, Guibao *et al.* 2008).

Together, the GIT/PIX complex is thought to regulate focal adhesion disassembly, which is outlined in Section 1.4.5. Briefly, it is understood that PIX promotes the interaction between GIT and paxillin by unmasking the C-terminal paxillin binding sequence of GIT, thus potentiating adhesion disassembly (Zhao, Manser *et al.* 2000). While Ser273 phosphorylation of paxillin decreases the interaction with FAK, it strengthens the binding to GIT and induces faster protrusion, focal adhesion turnover and cell migration. GIT1 knockdown meanwhile has been found to impair adhesion turnover, with cells forming more stable protrusions. Activation of Rac is necessary for adhesion disassembly, and it has been

proposed that the GIT/PIX complex targets active Rac to the leading edge (Nayal, Webb *et al.* 2006). Studies have also identified that knockdown of  $\beta$ -PIX specifically decreases adhesion disassembly, it appears that this protein accumulates at developing nascent adhesions and dissociates from maturing complexes and is negatively regulated by myosin II and contractility (Kuo, Han *et al.* 2011). Additionally,  $\alpha$ -PIX interacts with and acts downstream of the protease calpain-4 (Rosenberger, Gal *et al.* 2005); given that calpains are known to mediate adhesion disassembly by cleaving proteins within the complex it is possible that  $\alpha$ -PIX mediates this activity in some way.

It has also been reported that phosphorylation of Tyr 442 in  $\beta$ -PIX, which relieves auto-inhibition of GEF activity, weakens the interaction with GIT thus promoting the binding of GIT with paxillin. As a result, phosphorylation of  $\beta$ -PIX is thought to trigger adhesion disassembly, while the loss of this phosphorylation induces the formation of stable adhesions and potentiates association of paxillin with the plasma membrane (Feng, Baird *et al.* 2010).

Many studies have identified roles for the GIT and PIX proteins in regulating membrane protrusion, cell spreading and migration. In particular, knockdown of GIT2 has been found to induce the formation of unstable protrusions, along with a reduction in migration velocity and persistence, implicating the protein in mediating directional cell migration (Brown, Cary *et al.* 2005, Yu, Deakin *et al.* 2009). There is evidence to show that a GEF for Rac1/RhoA/Cdc42, Vav2, regulates the polarised localisation of GIT2 and  $\beta$ -PIX at the leading edge enabling directional migration (Jones, Machida *et al.* 2013). Others have demonstrated an interaction between  $\beta$ -PIX and myosin IIA that is released upon inhibition of myosin.



When associated with myosin,  $\beta$ -PIX is inactive as a GEF and thus its release leads to activation of Rac1 and subsequent lamellipodia and focal adhesion formation (Lee, Choi *et al.* 2010). The GIT/PIX complex is thought to regulate cell spreading after integrin engagement by mediating phosphorylation and activation of PLC $\gamma$  (Jones and Katan 2007).  $\alpha$ -PIX, too, is thought to function in a GEF independent manner to regulate integrin-mediated spreading (Rosenberger, Gal *et al.* 2005), while  $\beta$ -PIX has been found to target active Rac to focal adhesions and enhance spreading (Chang, Lemmon *et al.* 2007). A recently identified isoform of  $\beta$ -PIX,  $\beta$ -PIX-b<sub>L</sub> has also been implicated in enhancing microtubule induced cell spreading (Lee, Yang *et al.* 2011).

Interestingly, much like RhoJ (see Section 1.3.2), GIT1 has been identified in mediating podosome formation in vascular smooth muscle cells and endothelial cells. It appears that phosphorylation of Tyr392 (which is within the SHD) is important in this function by regulating the binding to and activation of PLC $\gamma$  (Haendeler, Yin *et al.* 2003, Wang, Taba *et al.* 2009, Wang, Yin *et al.* 2010).  $\alpha$ -PIX has also been found to regulate the formation and size of podosomes in macrophages (Gringel, Walz *et al.* 2006), while the hypoxia-induced formation of the related structures, invadopodia, requires  $\beta$ -PIX expression (Md Hashim, Nicholas *et al.* 2013).

#### **1.5.5.4 Roles in endothelial permeability**

The GIT proteins have also been described as regulating endothelial permeability and barrier function. In particular, treatment of endothelial cells with thrombin, which induces hyperpermeability via cell contraction and adhesion formation, was found to trigger reorganisation of GIT to adhesions in a RhoA/ROCK dependent manner. Knockdown of GIT1

enhanced the response of cells to thrombin, with cells more rounded and containing more adhesions, suggesting that GIT mediates the intracellular response to thrombin (Shikata, Birukov *et al.* 2003, van Nieuw Amerongen, Natarajan *et al.* 2004). Additionally, GIT1 and  $\beta$ -PIX are crucial in recruiting phospho-PAK to cell-cell junctions, and mediate activation of Erk and myosin light chain, thus controlling endothelial permeability (Stockton, Reutershan *et al.* 2007).

#### **1.5.6 GIT and PIX *in vivo***

Both GIT1 and  $\beta$ -PIX have been implicated in regulating vessel formation and angiogenesis *in vivo*. GIT1 in particular appears to be crucial in regulating the development of the pulmonary vasculature. Mice lacking GIT1 were found to have reduced numbers of microvessels, and increased pruning of arteriolar branches in the lungs. Additionally, hypoperfusion was observed in the capillaries of knockout mouse lungs compared to wild type. Closer inspection identified a reduced number of endothelial cells in GIT1 knockout lungs, and as a result this led to decreased expression of VEGFR2. Potentially linked to this, Pang and colleagues also demonstrated that GIT1 is required for normal endothelial proliferation *in vivo*, as well as identifying a role in mediating VEGF signalling, in particular in the activation of PLC $\gamma$  and ERK1/2 (Pang, Hoefen *et al.* 2009).

Phosphorylation of GIT1 Tyr 321 has also been identified as required for regulation of angiogenesis in the healing of bone fractures. Rats with fractured tibiae were injected with lentivirus containing either wild-type or Tyr 321-phosphorylation deficient (Tyr 321F GIT1) GIT1. Subsequently, VEGF expression was found to be reduced in those mice infected with

Tyr 321F GIT1 compared to wild-type controls, along with fewer vessels forming at the site of fracture, ultimately resulting in impaired healing (Rui, Li *et al.* 2012).

Recently, GIT1 has been found to mediate vessel remodelling after ligation of the carotid artery. In particular, it was observed that formation of the intima was significantly diminished in GIT1 knockout mice, while GIT1 expression greatly increased in the intima of wild-type mice after ligation. Further investigation demonstrated that GIT1 was involved in regulating the proliferation, apoptosis and migration of vascular smooth muscle cells. Moreover, echoing the findings of Pang *et al.*, the activation of ERK1/2 in the carotid artery after ligation observed in wild-type mice was impaired in GIT1 knockout animals (Pang, Xu *et al.* 2013).

$\beta$ -PIX meanwhile has been identified as a mediator of cerebral vascular stability and angiogenesis in the zebrafish. Zebrafish with a mutation in  $\beta$ -PIX have cerebral haemorrhages, which appear to be as a result of vessel instability. While blood vessel function is normal in these fish, the structure of the vessel network is highly abnormal and immature, and endothelial cells fail to establish contacts with underlying mesenchymal cells (Liu, Fraser *et al.* 2007). Further investigation has determined that the interaction with GIT1 is required for  $\beta$ -PIX to regulate stability of cerebral vessels, and loss of GIT1 phenocopies the haemorrhagic effect seen upon mutation of  $\beta$ -PIX. Additionally,  $\beta$ -PIX regulates cerebral angiogenesis specifically, in concert with integrins  $\alpha_v$  and  $\beta_8$  with GIT1 acting as the bridge between them. Furthermore, as was found in the lungs of GIT1 knockout mice, decreased proliferation of endothelial cells is observed in zebrafish with a mutation in  $\beta$ -PIX (Liu, Zeng *et al.* 2012). Other *in vivo* functions of the GIT and PIX proteins are outlined in Table 1.3.

**Table 1.3 *In vivo* functions of the GIT and PIX proteins**

<b>Protein</b>	<b>Functions <i>in vivo</i></b>	<b>References</b>
GIT1	Associated with ADHD and Huntington's disease; KO mice suffer impaired learning and fear responses; mediates osteoclast function, bone mass and resorption, regulates mitochondrial biogenesis and function in the heart	(Goehler, Lalowski <i>et al.</i> 2004, Schmalzigaug, Rodriguiz <i>et al.</i> 2009, Menon, Deane <i>et al.</i> 2010, Menon, Yin <i>et al.</i> 2010, Pang, Xu <i>et al.</i> 2011, Won, Mah <i>et al.</i> 2011, Salatino-Oliveira, Genro <i>et al.</i> 2012)
GIT2	Regulates anxiety responses in mice; mediates bone formation and resorption, and osteoblast differentiation; regulates cell migration and morphology in the developing zebrafish; modulates thymocyte selection and motility; mediates neutrophil chemotaxis and superoxide anion production	(Mazaki, Hashimoto <i>et al.</i> 2006, Schmalzigaug, Rodriguiz <i>et al.</i> 2009, Phee, Dzhagalov <i>et al.</i> 2010, Yu, Foley <i>et al.</i> 2011, Wang, Liao <i>et al.</i> 2012)
$\alpha$ -PIX	Gene mutation is associated with X-linked mental retardation and KO mice have impaired learning and behavioural control; implicated in lymphocyte maturation and migration, B cell proliferation and immune responses	(Kutsche, Yntema <i>et al.</i> 2000, Missy, Hu <i>et al.</i> 2008, Ramakers, Wolfer <i>et al.</i> 2012)
$\beta$ -PIX	Upregulated in breast cancer tissues; involved in tumourigenesis by interacting with and regulating the activity of PLC $\gamma$ ; phosphorylation of Tyr442 is involved in formation of v-Src induced tumours; recruited to the membrane in renal cell carcinoma to enhance metastatic potential; regulates kidney function	(Ahn, Chung <i>et al.</i> 2003, Bae, Ahn <i>et al.</i> 2005, Feng, Baird <i>et al.</i> 2006, Hsu, Lin <i>et al.</i> 2010, Pavlov, Chahdi <i>et al.</i> 2010, Staruschenko and Sorokin 2012)

## **1.6 Hypotheses and Aims**

Our group has previously shown that RhoJ localises to and regulates numbers of focal adhesions, as well as mediating migration and tube formation of endothelial cells. Additionally, RhoJ was found to interact with the focal adhesion proteins  $\beta$ -PIX and GIT1, which have previously been shown to regulate adhesion dynamics. At the beginning of these PhD studies, we postulated that RhoJ regulates cell migration and ultimately angiogenesis by

mediating focal adhesion turnover in concert with its interacting partners GIT and PIX. The aims of the studies outlined in the following chapters were to distinguish how RhoJ regulates focal adhesion dynamics, the physical and functional consequences of the interactions between RhoJ and the GIT/PIX complex, and finally to generate a RhoJ null mouse for use in *in vivo* angiogenesis assays.

**Hypothesis:** RhoJ regulates cell migration and ultimately angiogenesis by mediating focal adhesion turnover in concert with its interacting partners  $\beta$ -PIX and GIT1.

**Aims:**

**1. To determine how RhoJ regulates focal adhesion dynamics.**

Live cell imaging was used to track focal adhesions in cells with manipulated RhoJ expression and assess changes in dynamics i.e. overall lifetime, assembly and disassembly. The effect of RhoJ manipulation on focal adhesion size and microtubule targeting was also evaluated, and a RhoJ biosensor was created to determine the site of RhoJ activation.

**2. To characterise how RhoJ interacts with the GIT/PIX complex, and what the functional consequences of this interaction are.**

Yeast-two-hybrid and pulldowns were used to confirm binding of RhoJ to its partner proteins, and reciprocal recruitment to focal adhesions was studied. The effect of RhoJ/GIT/PIX knockdown on tube formation, and the role of  $\beta$ -PIX in mediating RhoJ activation were assessed to give insights into the functional effects of the interaction. Investigation of RhoJ regulation of GIT2 phosphorylation was also undertaken, and finally the role of RhoJ in phosphorylation of other kinases was probed.

### **3. To determine the role of RhoJ *in vivo*.**

Mice were generated using ES cells from the Knockout Mouse Project. The resulting colony of mice demonstrated germline transmission of a genetrap cassette that was designed to interrupt expression of RhoJ, however this genetrap did not function correctly. Subsequent investigation was carried out to determine the splicing that occurs in these mice, and further breeding performed to generate a complete knockout. This mouse was then used to investigate tumour growth.

## **CHAPTER 2**

### **Materials and Methods**

## 2.1 Buffers and solutions

The components of various buffers are listed in the table below, with their use described in later sections.

**Table 2.1 Common buffers**

Name	Components
Rho assay lysis buffer	1% (v/v) Igepal, 1% (w/v) N-octyl- $\beta$ -D-glucopyranoside, 150 mM NaCl, 30 mM MgCl <sub>2</sub> , 25 mM HEPES pH 7.5
2x SDS-PAGE sample buffer	100 mM Tris-HCl pH 6.8, 20% (v/v) glycerol, 20% (v/v) $\beta$ -mercaptoethanol, 4% (w/v) SDS, 0.2% (w/v) bromophenol blue
6x DNA loading buffer	30% (v/v) glycerol, 0.25% (w/v) bromophenol blue, 0.25% (w/v) xylene cyanol FF
Phosphate-buffered saline (PBS)	140 mM NaCl, 10 mM Na <sub>2</sub> HPO <sub>4</sub> , 2.7 mM KCl and 1.76 mM KH <sub>2</sub> PO <sub>4</sub> , pH 7.4
Phosphate-buffered saline Tween-20 (PBST)	140 mM NaCl, 10 mM Na <sub>2</sub> HPO <sub>4</sub> , 2.7 mM KCl and 1.76 mM KH <sub>2</sub> PO <sub>4</sub> , 0.1% (v/v) Tween-20, pH 7.4
Tris-buffered saline (TBS)	150 mM NaCl, 20 mM Tris-HCl pH 7.5
Tris-buffered saline Tween-20 (TBST)	150 mM NaCl, 20 mM Tris-HCl pH 7.5, 0.1% (v/v) Tween-20
High salt TBST	500 mM NaCl, 20 mM Tris-HCl pH 7.5, 0.1% (v/v) Tween-20
Tris acetate EDTA (TAE) buffer	40 mM Tris-base, 18 mM glacial acetic acid, 1 mM EDTA
Stacking gel buffer	125 mM Tris-HCl pH 6.8, 0.1% (w/v) SDS
Resolving gel buffer	375 mM Tris-HCl pH 8.8, 0.1% (w/v) SDS
SDS-PAGE running buffer	250 mM glycine, 25 mM Tris-base, 0.1% (w/v) SDS, pH 8.3
Western blotting transfer buffer	47.6 mM glycine, 6 mM Tris-base, 20% (v/v) methanol, pH 8.3



Western Blotting stripping buffer	62.5 mM Tris-HCl pH 6.8, 2% (w/v) SDS, 100 $\mu$ M $\beta$ -mercaptoethanol
Coomassie staining buffer	40% (v/v) methanol, 10% (v/v) glacial acetic acid, 0.2 g Coomassie Brilliant Blue dye
Coomassie destaining buffer	50% (v/v) methanol, 10% (v/v) glacial acetic acid
<i>E. coli</i> lysis buffer	50 mM Tris-HCl pH 7.5, 50 mM NaCl, 5 mM MgCl <sub>2</sub> , 1 mM dithiothreitol (DTT, added fresh), 1 mM phenylmethylsulphonyl fluoride (PMSF, added fresh)
<i>E. coli</i> wash buffer	50 mM Tris-HCl pH 7.5, 50 mM NaCl, 5 mM MgCl <sub>2</sub>
Nucleotide loading lysis buffer	1% (v/v) Igepal, 1% (w/v) N-octyl- $\beta$ -D-glucopyranoside, 150 mM NaCl, 25 mM HEPES pH 7.5, 10 mM MgCl <sub>2</sub>
Tail lysis buffer	50 mM Tris-HCl pH 8.5, 1 mM EDTA pH 8.0, 0.5% (v/v) Tween-20, 300 $\mu$ g/ml Proteinase K
1% (v/v) Triton X-100 lysis buffer	1% (v/v) Triton X-100, 150 mM NaCl, 10 mM Tris-HCl pH 7.5, 1 mM EDTA, 0.01% (w/v) NaN <sub>3</sub>
Immunofluorescence blocking buffer	10% (v/v) foetal bovine serum, 3% (w/v) bovine serum albumin, 0.1% (v/v) Tween-20, 0.01% (w/v) NaN <sub>3</sub>

## 2.2 siRNA duplexes

RhoJ siRNA duplexes were designed with dTdT overhangs on sense and antisense strands and purchased from Eurogentec, while those targeting GIT1, GIT2 and  $\beta$ -PIX were pre-designed and purchased from Life Technologies. Eurogentec negative control duplex was used in those experiments where RhoJ only was knocked down, otherwise Life Technologies negative control duplex was used (each referred to as siControl).

**Table 2.2 siRNA duplexes**

siRNA duplex	Target gene	Sequence
RhoJ siRNA 1	Human RhoJ (bases 155-174)	5'-ccacuguguuugaccacuau-3'
RhoJ siRNA 2	Human RhoJ (bases 455-474)	5'-agaaccucucacuuacgag-3'
$\beta$ PIX siRNA 1	Human $\beta$ PIX (bases 1830-1848)	5'-caacgacaggaatgacaattt-3'
$\beta$ PIX siRNA 2	Human $\beta$ PIX (bases 1536-1554)	5'-cagatagacaagatattcatt-3'
GIT1 siRNA 1	Human GIT1 (bases 345-363)	5'-acaucuccauugucaagcatt-3'
GIT1 siRNA 2	Human GIT1 (bases 945-963)	5'-ggcauuacaucauccacatt-3'
GIT2 siRNA 1	Human GIT2 (bases 1023-1041)	5'-cgaugaaguugacaggcgatt-3'
GIT2 siRNA 2	Human GIT2 (bases 774-792)	5'-cguugauuugcaaggcaatt-3'
Negative control duplex (siControl)	Non-specific to any known human gene sequences	Undisclosed by Eurogentec
Negative control duplex (siControl)	Non-specific to any known human gene sequences	Undisclosed by Life Technologies

## 2.3 Antibodies

### 2.3.1 Primary Antibodies

**Table 2.3.1 Primary antibodies**

Antibody	Clone Number/ Product code	Working Concentration	Supplier
Mouse monoclonal anti-human RhoJ	ab57584	1 µg/ml (WB)	Abcam
Mouse monoclonal anti-chicken tubulin (recognises human tubulin)	DM1A, Code T6199	0.1 µg/ml (WB)	Sigma
Rabbit polyclonal anti-human β-PIX SH3 domain	Code 07-1450	1 µg/ml (WB), 10 µg/ml (IF)	Millipore
Mouse monoclonal anti-human vinculin	hVIN-1, Code V9131	2 µg/ml (IF)	Sigma
Mouse monoclonal anti-human CD31	JC70A	1.29 µg/ml (IHC)	Dako Cytomation
Rabbit polyclonal anti-human GIT1	Code 2919	0.058 µg/ml (WB)	Cell Signaling Technology
Rabbit polyclonal anti-human GIT1	Code H-170	2 µg/ml (IF)	Santa Cruz
Rabbit monoclonal anti-human GIT2	D11B8, Code 8072	0.623 µg/ml (WB), 2.5 µg/ml (IF)	Cell Signaling Technology
Rabbit monoclonal anti-human α-PIX	C23D2, Code 4573	0.058 µg/ml (WB)	Cell Signaling Technology
Mouse monoclonal anti-GFP	3e1	Used 1/2000 (WB)	CRUK Central Services
Mouse monoclonal anti-chicken FAK (recognises human FAK)	77, Code 610088	0.25 µg/ml (WB)	Transduction Laboratories
Rabbit polyclonal anti-human phospho-FAK (Tyr397)	ab4803	0.786 µg/ml (WB)	Abcam
Rabbit monoclonal anti-human phospho-GIT2 (Tyr392)	D8N9A, Code 11873	0.324 µg/ml (WB)	Cell Signaling Technology
Rabbit polyclonal anti-human phospho-Src (Tyr416)	Code 2101	0.024 µg/ml (WB)	Cell Signaling Technology

Mouse monoclonal anti-human Src	L4A1, Code 2110	2.5 µg/ml (WB)	Cell Signaling Technology
Rabbit polyclonal anti-human phospho-Paxillin (Tyr118)	Code 2541	0.14 µg/ml (WB)	Cell Signaling Technology

Abbreviations: WB, Western blotting; IF, immunofluorescent staining; IHC, immunohistochemical staining

### 2.3.2 Secondary Antibodies

**Table 2.3.2 Secondary antibodies**

<b>Antibody</b>	<b>Working Concentration</b>	<b>Supplier</b>
Goat polyclonal anti-mouse conjugated to HRP	1 µg/ml (WB)	Dako Cytomation
Donkey polyclonal anti-rabbit conjugated to HRP	0.056 µg/ml (WB)	GE Healthcare
Goat polyclonal anti-mouse conjugated to Alexa Fluor488	4 µg/ml (IF)	Invitrogen
Donkey polyclonal anti-rabbit conjugated to Alexa Fluor488	4 µg/ml (IF)	Invitrogen
Goat polyclonal anti-mouse conjugated to Alexa Fluor546	4 µg/ml (IF)	Invitrogen
Goat polyclonal anti-mouse conjugated to Alexa Fluor647	4 µg/ml (IF)	Life Technologies
Goat polyclonal anti-mouse IgG (whole molecule) conjugated to Alkaline Phosphatase	Cat. Number A4656, used at 1:500 (IHC)	Sigma

Abbreviations: HRP, horseradish peroxidase; WB, Western blotting; IF, immunofluorescent staining; IHC, immuno-histochemical staining

## 2.4 Oligonucleotides

Oligonucleotides were purchased from Eurogentec with the exception of EW26-28, which were purchased from Alta Bioscience Ltd. Base numbers from the coding sequence of the appropriate genes are listed for those primers used for sequencing. Abbreviations: fwd, forward; rev, reverse; PCR, polymerase chain reaction

**Table 2.4 Oligonucleotide sequences**

Name	Sequence (5'-3')	Use
EW1	TAGTAGGAATTCGAATGTCCCGGAAGGG GCCGCG	Rat GIT1 fwd, cloning
EW2	CTACTAGAATTCTCACTGTTTCTTCTCTCG GGTGGTG	Rat GIT1 rev, cloning
EW3	TAGTAGCCCGGGGATGGCTGACAGATCTC GGCAAAGTGC	Rat GIT <sub>1251-500</sub> fwd, cloning
EW4	CTACTAGAATTCTCATGTGTGTTCTGCCCG TTCAGTGGG	Rat GIT <sub>1251-500</sub> rev, cloning
EW5	GGGCCGCGAGCGGAGGTGTG	Rat GIT1 fwd, sequencing (bases 65-86)
EW6	CTCCCAGATAGAGTTGGCCC	Rat GIT1 rev, sequencing (bases 264-283)
EW7	GGCACTACACCTCTACACGTG	Rat GIT1 fwd, sequencing (bases 551-571)
EW8	CGCAGTGCTGTGCCCTTCCTG	Rat GIT1 fwd, sequencing (bases 1004-1024)
EW9	GGGCTCCTGGTCTGTGTCTTC	Rat GIT1 rev, sequencing (bases 1247-1267)
EW10	CAGAGGGAGATCCACAAACTG	Rat GIT1 fwd, sequencing (bases 1451-1471)
EW11	GCTGAGCTGGAGAGCTTAGATG	Rat GIT1 fwd, sequencing (bases 1955-1976)
EW12	ACTGGGGACCCAAAGTCAAGTC	WT and knockout mouse RhoJ 5' arm fwd, genotyping

EW13	CCGGATCCAGACATGATAAGATAC	End of knockout cassette rev, genotyping
EW14	TGTTTCCCGAGTACTCTGTAG	WT mouse RhoJ allele rev, genotyping
EW15	TAGTAGGGATCCTCAGATAATTGAACAGC AGCTGTG	RhoJ rev, cloning
EW16	TAGTAGGAATTCGCCACCATGGTGAGCAA GGGC	Kozak-GFP fwd, cloning
EW18	CCATCTACCATAACATTGGCAG	Rac1 rev, sequencing (bases 122-143 of coding DNA sequence)
EW19	CACAGCGAGGCCTCAAGACAGTG	Rac1 fwd, sequencing (bases 482-504 of coding DNA sequence)
EW20	TAGTAGGGTACCATGAACTGCAAAGAGG GAACTGAC	Human RhoJ fwd, cloning
EW21	CTACTAGCGGCCGCGGCAGCTGTGACCCT CAGAACAGCG	Human RhoJ minus CAAX box rev, cloning
EW22	CTGTCCTGCAGTGTCTATAGTCC	Mouse RhoJ exon 2 rev, PCR
EW24	CCAGATCTTCCGGGTACCGAGC	Mouse construct splice acceptor rev, PCR
EW25	TCCAGCATGGTGAGCTGCGGG	Mouse exon 1 fwd, PCR
SK24	GATGAGCTACGCCAACGAC	Mouse exon 1 fwd, PCR
KB30	AATACCACTACAATGGATGATGTA	pACT2 Fwd, insert sequencing
Common en2	CCAACTGACCTTGGGCAAGAACAT	Front of knockout cassette rev, genotyping
Raf5	ACACCTCCCCCTGAACCTGAAC	End of knockout cassette fwd, genotyping
EW26	CCAGCTGAGCGCCGGTCGCTACC	Mouse Cre common fwd, genotyping
EW27	GGTTTGAAGTATGGCGAGC	Mouse Cre cleavage rev, genotyping
EW28	GGTTCTGTACGCTCCTGCAGAAGGC	Mouse Cre no cleavage rev, genotyping
Cre common	TCGTTGCATCGACCGGTAAT	Cre genotyping
PGK fwd	GCGCAGGTCTCCTCTTCCTC	Cre genotyping
PGK-wt rev	GACCAATGAAACGTGGGCG	Cre genotyping

## 2.5 qPCR primers

Primers for quantitative polymerase chain reaction (PCR) were designed using the web-based Universal ProbeLibrary Assay Design Centre (Roche) such that they covered exon boundaries, and purchased from Eurogentec. The appropriate probe as indicated was used for each reaction.

**Table 2.5 qPCR oligonucleotide primers**

Gene	Sequence (5'-3')	Probe required
$\alpha$ PIX (ARHGEF6)	Fwd: TCGCTGAAAAATGGGGTAGT Rev: TTTGGGGATCCAGACAAAAC	21
$\beta$ PIX (ARHGEF7)	Fwd: CAGCTGCTCTCTGCTACAAGG Rev: GAAGGCTTCCGTTCAAGTTT	44
GIT1	Fwd: CTGAGGATGTCCCGAAAGG Rev: CAGCACACCCCTGCTGAT	20
GIT2	Fwd: TCTCTGTGGCAGGAAACCA Rev: TGCCAATTCAGACAAATCCA	56
OAS1	Fwd: GGTGGAGTTCGATGTGCTG Rev: AGGTTTATAGCCGCCAGTCA	37
ISG20	Fwd: CACCCCTCAGCACATGGT Rev: TGGAAGTCGTGCTTCAGGT	17
RhoJ (Homo sapiens)	Fwd: AAACCCTGCCTCTTACCACA Rev: CATCACGGAGATCAATCTGG	79
Flotilin (Homo sapiens)	Fwd: GATCCTCAGCTTCACCATCAA Rev: TCAGCATCTCTCTGCACCAC	61



## 2.6 Plasmids

Cloning of plasmids listed in Table 2.6.1 was performed as described in Section 2.15. Those provided by collaborators are listed in Table 2.6.2; these were either used directly for transfections, or further manipulated according to Section 2.15.

**Table 2.6.1 Cloned plasmids**

Plasmid	Cloning details
pACT2-wtGIT1	Rat wtGIT1 was amplified using primers EW1 and EW2 and cloned into EcoRI restriction sites of pACT2.
pACT2-GIT1 $\Delta$ AB	Rat GIT1 $\Delta$ AB was amplified using primers EW1 and EW2 and cloned into EcoRI restriction sites of pACT2.
pACT2-GIT1 $\Delta$ SpaA	Rat GIT1 $\Delta$ SpaA was amplified using primers EW1 and EW2 and cloned into EcoRI restriction sites of pACT2.
pACT2-GIT1 $\Delta$ SpaB	Rat GIT1 $\Delta$ SpaB was amplified using primers EW1 and EW2 and cloned into EcoRI restriction sites of pACT2.
RhoJ biosensor	Human wtRhoJ was amplified using primers EW20 and EW21 and cloned into the KpnI-NotI restriction site of the Rac1 Raichu biosensor, replacing Rac1. The biosensor was then inserted into the pWPXL SmaI-PmeI restriction sites, replacing GFP.

**Table 2.6.2 Other plasmids**

Plasmid	Provided by
pWPXL-GFP-wtRhoJ pGBT9-wtRhoJ pGBT9-daRhoJ (Q79L) pGBT9-dnRhoJ (T35N) pWPXL-RFP-Paxillin	Dr. Katarzyna Lesczczynska University of Birmingham, UK (unpublished)
pWPXL-GFP-daRhoJ (Q79L)	Dr. Katarzyna Lesczczynska (Kaur, Lesczczynska <i>et al.</i> 2011)
pWPXL pWPI psPAX2 pMD2G	Addgene deposited by Prof. Didier Trono Swiss Institute of Technology (EPFL), Switzerland
pACT2	Dr. Victoria Heath University of Birmingham, UK (Heath, Shaw <i>et al.</i> 2004)
pBK( $\Delta$ )-rat GIT1-FLAG pBK( $\Delta$ )-rat $\Delta$ SpaAB GIT1-FLAG pBK( $\Delta$ )-rat $\Delta$ Spa2-A GIT1-FLAG pBK( $\Delta$ )-rat $\Delta$ Spa2-B GIT1-FLAG	Dr Richard Premont Duke University, USA (Premont, Perry <i>et al.</i> 2004)
pcDNA3-wtCool1-myc pcDNA3-Cool1DHm-myc	Prof. Richard Cerione Cornell University, USA (Feng, Baird <i>et al.</i> 2010)
Rac1 Raichu biosensor	Prof. Anne Ridley Kings College London, UK (Vega, Fruhwirth <i>et al.</i> 2011)

## 2.7 General tissue culture

Human umbilical vein endothelial cells (HUVEC) were isolated with collagenase from umbilical cords supplied by Birmingham Women's Hospital that had been obtained under informed consent (local ethics number: 11-063), and used in various assays. Cells from three separate isolates were used when performing replicates in order to ensure results were consistent across donors. HUVEC were cultured in HUVEC medium consisting of Medium 199 (Sigma) supplemented with 10% (v/v) foetal bovine serum (PAA Cell Culture Co.), 90 µg/ml heparin (Sigma), 4 mM L-glutamine (Sigma) and bovine brain extract, prepared as previously published (Maciag, Cerundolo *et al.* 1979), with 100 units/ml Penicillin and 100 µg/ml Streptomycin antibiotics (Invitrogen). This medium was filtered with 0.22 µm pore filters (Millipore), stored at 4°C and warmed to 37°C before use. Dishes were coated with sterile 0.1% (w/v) gelatin in sterile PBS before plating HUVEC. Immortalised human microvascular endothelial cell line-1 (HMEC-1) cells, which are transformed with the SV40 large T antigen (Ades, Candal *et al.* 1992), were cultured as per HUVEC.

Human embryonic kidney 293T cells (HEK293T, from Dr Mike Tomlinson, University of Birmingham), which are also transformed with the SV40 large T antigen (Abcouwer, Robinson *et al.* 1989) were cultured in Dulbecco's Modified Eagle's Medium (DMEM, Sigma) supplemented with 10% (v/v) foetal bovine serum, 4 mM L-glutamine and Penicillin/Streptomycin antibiotics. This medium was filtered and stored as per HUVEC medium and warmed before use. Normal human dermal fibroblasts (HDF, Promocell) were cultured as per HEK293T.

All cells were plated onto sterile 10 cm plates (Falcon) for routine tissue culture, and kept in a humidified incubator at 37°C, with 5% CO<sub>2</sub> (Sanyo).

HUVEC and HMEC-1 were passaged at a ratio 1:3 when they had reached confluence. To passage a 10 cm dish, cells were washed once with sterile PBS, and incubated for 5 min at 37°C with 3 ml 1% (v/v) trypsin-EDTA (Sigma) in PBS. Once cells had detached, HUVEC medium (containing FBS which inhibits the action of trypsin) was added. Cells were centrifuged at 195 x g, room temperature (25°C) for 5 min, and the pellet resuspended in HUVEC medium. This suspension was split equally into 3 gelatin coated 10 cm plates, in a total of 10 ml medium per plate. HDF were passaged 1:3 as per HUVEC, however complete DMEM was used to collect and resuspend cells, and this suspension split equally between 3 uncoated 10 cm plates in a total of 10 ml medium. HEK293T cells were passaged twice a week at a ratio of 1:10. Complete DMEM was used to collect detached cells and resuspend cells after centrifugation. This suspension was then split equally between 10 uncoated 10 cm plates, in 10 ml medium per plate.

## **2.8 Transfection**

### **2.8.1 RNAiMAX transfection**

Transfections were performed to introduce siRNA duplexes into cells. This enabled specific genes to be knocked down, and allowed assays to be performed to determine the *in vitro* effect of this knockdown. Table 2.8.1 outlines volumes required for various plate sizes. For a 10 cm plate, HUVEC were seeded at  $1 \times 10^6$  and the next day knockdowns were performed using siRNA duplexes at 10-50 nM and 0.3% (v/v) RNAiMAX lipofectamine (Invitrogen). Per

10 cm plate, 2 tubes were set up: one containing duplex diluted in 680  $\mu$ l OptiMEM (Invitrogen) and another containing a mixture of 12  $\mu$ l RNAiMAX lipofectamine diluted in 108  $\mu$ l OptiMEM. Mixtures were incubated at 25°C room temperature for 10 min before addition of the 120  $\mu$ l lipofectamine mix to duplexes. The combined mixes were then mixed gently and incubated for another 10 min at room temperature. During this incubation, cells were washed twice with 10 ml PBS and 3.2 ml OptiMEM added per plate. The transfection mix (800  $\mu$ l) was then added and plates gently rocked in a north-south east-west motion to mix before incubating at 37°C, 5% CO<sub>2</sub>. After 4 h, transfection mixtures were replaced with HUVEC medium lacking antibiotics and returned to the incubator. Experiments were performed 48 to 72 h after transfection, when knockdown was maximal. Efficiency of knockdown was checked by Western blot after each experiment.

**Table 2.7 Volumes of OptiMEM and lipofectamine required to transfect various densities of HUVEC**

Plate	Number of cells	Volume of duplex: OptiMEM mixture	Amount of lipofectamine	Volume of OptiMEM in plate
6 well plate	$2 \times 10^5$	170 $\mu$ l	3 $\mu$ l + 27 $\mu$ l OptiMEM	800 $\mu$ l
6 cm plate	$3.6 \times 10^6$	245 $\mu$ l	4.3 $\mu$ l + 38.7 $\mu$ l OptiMEM	1150 $\mu$ l
10 cm plate	$1 \times 10^6$	680 $\mu$ l	12 $\mu$ l + 108 $\mu$ l OptiMEM	3200 $\mu$ l

### **2.8.2 PEI transfection**

To introduce plasmid DNA into HEK293T cells, polyethylenimine (PEI) transfections were performed. The day before transfection,  $3 \times 10^6$  HEK293T cells were plated in complete

DMEM on sterile 10 cm dishes. To transfect one 10 cm plate of cells, 9 µg plasmid DNA was added to 1 ml OptiMEM, and mixed by flicking the tubes. Then, 36 µl 1 mg/ml PEI was added, mixed by gentle vortex and incubated for 10 min at room temperature. The DNA/PEI mix was added dropwise to cells, mixed by rocking in a north-south east-west motion and plates returned to 37°C, 5% CO<sub>2</sub>. After 48 h, experiments were performed.

## **2.9 Lentiviral transduction of HUVEC**

### **2.9.1 Production of lentivirus**

In order to transduce HUVEC to express proteins of interest, HEK293T cells were used to produce lentivirus which could be used to infect HUVEC. First,  $3 \times 10^6$  HEK293T cells were plated onto 10 cm plastic dishes in complete DMEM. The following day, PEI transfection was performed as described in Section 2.8.2, however the amount of plasmid DNA was changed as follows in order to reflect the fact that three different vectors were being transfected into cells: 4.4 µg transfer vector (containing the gene of interest), 3.3 µg packaging vector (psPAX2) and 1.3 µg envelope vector (pMD2G) were used per 10 cm plate transfected. The cells were incubated at 37°C, 5% CO<sub>2</sub> for 48 h, and the resulting virus used to infect HUVEC (as described in Section 2.9.2).

### **2.9.2 Infection of HUVEC with lentivirus**

To transduce HUVEC, cells were infected with lentivirus produced in HEK293T cells as follows:  $1 \times 10^6$  HUVEC were plated onto 10 cm plates coated with 0.1% (w/v) gelatin in PBS, in HUVEC medium. The next day virus was collected from HEK293T cells and centrifuged at 195 x g, 5 min. The virus was supplemented with 8 µg/ml polybrene (Sigma), 90 µg/ml heparin and bovine brain extract, filtered with a 0.45 µm<sup>2</sup> pore syringe filter (Corning) and

added to cells in place of HUVEC medium. Cells were incubated at 37°C, 5% CO<sub>2</sub> for 24 h, then virus was replaced with fresh HUVEC medium, and cells left to grow. Transduced cells were then cultured as per normal HUVEC.

## **2.10 Protein analysis**

### **2.10.1 Protein extraction**

To determine levels of protein expression, cells were lysed with Rho assay lysis buffer. First, cells were washed with PBS, scraped from wells with a cell scraper in a volume of 1 ml PBS and transferred to 1.5 ml tubes. Cells were centrifuged at 5000 x g for 2 min and the supernatant removed by aspiration. Then, an appropriate volume of Rho assay lysis buffer (supplemented with protease inhibitor cocktail (Sigma), 2 mM Na<sub>2</sub>VO<sub>3</sub> and 10 mM NaF) was added to the pellet (approximately 100 µl per 10 cm plate), mixed by vortexing and incubated on ice for 15 min to lyse cells. The lysates were then centrifuged for 10 min at 21910 x g at 4°C. Supernatants were added to an equal volume of 2 x SDS-PAGE sample buffer and stored at -20°C.

### **2.10.2 SDS Polyacrylamide gel electrophoresis**

Samples for electrophoresis were thawed (if frozen) and boiled for 5 min at 100°C. Approximately 10 µg samples (volumes calculated using the BioRad DC Protein Assay (BioRad) as per manufacturer's guidelines) were loaded onto a polyacrylamide gel (Sambrook and Russell 2001) alongside protein markers. Electrophoresis was performed at 100 mV in X Cell SureLock Mini Cell apparatus (Invitrogen) with running buffer until the dye front reached the bottom of the gel. For Western blotting of targets larger than 75 kDa, 8%

(w/v) gels were used, while samples were run on 10-12% (w/v) gels to blot for smaller proteins.

### **2.10.3 Western blotting**

After SDS-PAGE, proteins were transferred to a polyvinylidene difluoride (PVDF) membrane (Immobilon-P, Millipore) by wet transfer. The PVDF membrane was activated by wetting in methanol for 30 seconds, before soaking in transfer buffer. Whattmann filter paper, transfer pads and the SDS-polyacrylamide gel were also soaked in transfer buffer before setting up the transfer in XCell II Blot Module wet transfer apparatus (Invitrogen). The transfer was performed at 30 mV, for 1 h at 4°C and successful transfer confirmed by Ponceau S (Sigma) staining. The membrane was blocked in 5% (w/v) skimmed milk powder in TBST at room temperature, and then incubated with the appropriate primary antibody in TBST with 3% (w/v) BSA and 0.01% (w/v) sodium azide at 4°C overnight. The next day, the membrane was washed 5 times, each of 6 min with TBST and incubated with secondary antibody conjugated to horseradish peroxidase (HRP) diluted in 5% milk in TBST for 1 h at room temperature. It was then washed as before with TBST, incubated with enhanced chemiluminescent substrate (ECL) (GE Healthcare) and developed on Hyperfilm ECL (GE Healthcare) after exposure in the dark.

### **2.10.4 Stripping and reblotting membranes**

In order to reblot membranes using new or fresh aliquots of antibodies, membranes were incubated with 50 ml Western stripping buffer (with 350 µl β-mercaptoethanol added immediately prior to use) for 30 min at 60°C. The stripped membrane was then given six 5



min washes in TBST and blocked for 1 h in 5% (w/v) milk powder in TBST. The rest of the blotting procedure was performed as per Section 2.10.3.

## **2.11 RNA Analysis**

### **2.11.1 RNA extraction from HEK293T and HUVEC**

To assess levels of mRNA in different cell lines, total RNA was first extracted using the RNeasy mini kit (Qiagen). Initially, cells on 10 cm dishes were washed with PBS, scraped in 1 ml PBS and transferred to 1.5 ml tubes. Samples were then centrifuged at 5000 x g for 1 min and pellets stored at -80°C until RNA extraction was to be performed. Pellets were subsequently thawed, and the appropriate volume of buffer RLT added according to the manufacturer's instructions. Mixtures were thoroughly resuspended, then an equal volume of 70% (v/v) ethanol in Diethyl Pyrocarbonate (DEPC) treated-water added and mixed well. This water was prepared by adding 0.1% (v/v) DEPC (Sigma), which inhibits RNases, to ultrapure water and mixing thoroughly. The DEPC water solution was left at room temperature for approximately 16 h and then autoclaved before use. Up to 700 µl of the extraction mix was transferred to an RNeasy mini spin column and centrifuged at 12000 x g for 1 min, then any remaining mixtures added and centrifuged again. Flow through was discarded after each centrifuge step. Next, 700 µl buffer RW1 was added and centrifuged as before, followed by the addition of 500 µl buffer RPE and another centrifugation step. A final wash with 500 µl buffer RPE was performed, and tubes centrifuged for 2 min, 12000 x g. Any residual buffer was removed with a final centrifuge for 1 min, 12000 x g. Columns were transferred to fresh RNase-free 1.5 ml tubes and 50 µl RNase-free water added in order to elute RNA. Columns were centrifuged for 1 min 12000 x g, then 2 µl eluted RNA removed to

measure concentration and 2 µl removed to run on an agarose gel to check the quality of the RNA. RNA was snap frozen on dry ice and stored at -80°C until cDNA generation could be performed.

### **2.11.2 cDNA generation**

In order to perform analyses of gene expression, cDNA was generated from RNA (extracted as per Section 2.11.1) by reverse transcription, using the High Capacity cDNA Archive kit (Applied Biosystems, USA). RNA concentration was measured using the NanoDrop ND-1000 Spectrophotometer (LabTech, UK), and 1 µg used per 20 µl reaction. For each cDNA reaction performed a reaction mix was made up containing 2 µl 10x cDNA buffer, 0.8 µl dNTPs, 2 µl 10x random primers, 1 µl reverse transcriptase enzyme and 4.2 µl RNase free water. First, the appropriate volume of water required to dilute 1 µg RNA in 10 µl was added to RNase free tubes, then 10 µl of the reaction mix was added and finally 1 µg RNA. Mixes were incubated at 25°C for 10 min, then at 37°C for 2 h. The resulting cDNA was diluted 5-fold in RNase free water and subsequently used for both quantitative and traditional PCR.

### **2.11.3 qPCR**

In order to quantify relative gene transcription, quantitative PCR was performed using the Universal ProbeLibrary (Roche). Primers were designed using the web-based Universal ProbeLibrary Assay Design Centre (Roche) such that they covered exon boundaries. For each 25 µl reaction, a mix containing 12.5 µl 2x qPCR mix, 1 µl each primer, 0.25 µl probe and 0.25 µl water was combined with 10 µl cDNA (diluted 5-fold). qPCR was performed using the Rotor-Gene RG-3000 qPCR machine according to the following programme: an initial denaturation interval for 10 min at 95 °C, followed by 40 cycles of 95°C for 15 s and 60°C for

45 s. Standard curves were generated by the RotorGene 6 software from serial dilutions of cDNA assigned arbitrary units, giving calculated copies of cDNA for each sample. To assess gene knockdown, calculated copies of the gene of interest were divided by those of the housekeeping gene and expressed as a percentage, with siControl transfected cells representing 100% expression.

To determine relative abundance of gene expression across different cell lines, cycle threshold (CT) values were used. The CT value is the cycle at which the fluorescence signal of the gene is equal to the threshold set by the program, generated using a best fit to the curves generated by the serial dilutions. The CT value of the housekeeping gene (flotillin-2) was subtracted from the CT value of the gene of interest to generate  $\Delta CT$  values. The formula  $100/2^{\Delta CT}$  was subsequently used to calculate the expression of the gene of interest as a percentage of flotillin expression.

## **2.12 GFP trap pulldown**

In order to determine biochemical interactions between dominant active RhoJ and its partner proteins, HUVEC were lentivirally transduced to express GFP or GFP-daRhoJ as per Section 2.9. Per pulldown,  $20 \times 10^6$  GFP expressing HUVEC were used. Cells were lysed in 1 ml Rho assay lysis buffer as per Section 2.10.1, and 25  $\mu$ l of lysate was mixed with an equal volume of 2x SDS-PAGE sample buffer. The remaining 975  $\mu$ l was mixed with 20  $\mu$ l washed GFP-trap A beads (Chromotek), and pulldowns performed on a rotating wheel for 1 h at 4°C. Subsequently, beads were washed 3 times with Rho assay lysis buffer and bound proteins eluted with 50  $\mu$ l 2x SDS-PAGE sample buffer. Samples were then subjected to SDS-PAGE electrophoresis and Western blotting according to Sections 2.10.2 and 2.10.3.

## 2.13 Purification of GST fusion proteins

In order to produce and purify GST fusion proteins for use in pulldowns, BL21 (DE3) pLys S *E. coli* transformed with plasmids encoding GST-fusion proteins of interest were streaked onto Luria Bertani (LB) Agar plates containing antibiotics (100 µg/ml Ampicillin or 50 µg/ml Kanamycin with 20 µg/ml Chloramphenicol) and incubated at 37°C overnight. The following day, LB broth containing the appropriate antibiotics was inoculated with single bacterial colonies and left to grow overnight at 37°C with shaking. The next morning, starter cultures were diluted 1/100 in LB with antibiotics and bacteria allowed to grow at 30°C with shaking until they reached mid-log phase (approximately 0.5 OD at 600 nm). Expression was induced by adding 0.3 mM isopropyl β-D-1 thiogalactopyranoside (IPTG, Melford Laboratories) to the cultures, which were grown for 2.5 h at 30°C with shaking. Cultures were then centrifuged at 4435 x g for 10 min at 4 °C and pellets washed with *E. coli* wash buffer and centrifuged once more. Pellets were then frozen at -80°C before lysis.

Pellets were thawed on ice and resuspended with ice cold *E. coli* lysis buffer (2 ml used per 100 ml culture). Mixtures were sonicated for approximately 3 min (in a 20 s sonication, 10 s rest pattern), or until they could be pipetted smoothly. The resuspended bacteria were centrifuged in 1.5 ml tubes for 10 min at 21910 x g, 4 °C, and supernatants pooled and mixed with an equal volume of 100% glycerol. Lysates were stored at -20 °C.

In order to assess the concentration of bacterial lysates, fusion proteins were bound to glutathione agarose beads. Lyophilised glutathione agarose beads (Sigma) were swollen with *E. coli* lysis buffer and diluted to a 50% (v/v) slurry. For each volume of lysate to be checked, 25 µl bead slurry was used. Then, 50 µl, 100 µl and 200 µl bacterial lysate were added to

beads and made up to 1 ml with *E. coli* lysis buffer. Samples were incubated at 4°C for 1 h on a rotating wheel and washed 3 times with *E. coli* lysis buffer. Beads were then resuspended in an equal volume of 2x SDS-PAGE sample buffer and subjected to SDS-PAGE (as per Section 2.10.2) alongside BSA standards. Gels were stained overnight with Coomassie dye and destained with Coomassie destaining buffer.

## **2.14 RhoJ activation assay**

Glutathione agarose beads were swollen in *E. coli* lysis buffer, then resuspended to a 50% slurry. For each pulldown to be performed, 25 µl slurry was incubated with a volume of bacterial lysate containing approximately 5 µg GST-PBD protein (produced, purified and tested as per Section 2.13) in *E. coli* lysis buffer (supplemented with protease inhibitors) and left to bind for 1 h on a rotating wheel at 4 °C. Beads were then washed 3 times in 1 ml nucleotide loading lysis buffer (supplemented with protease inhibitors, 10 mM NaF and 2 mM Na<sub>2</sub>VO<sub>3</sub>) and resuspended to a 50% slurry in this buffer. Beads were left on ice until lysates were ready to be added.

Meanwhile, HUVEC were washed with PBS and starved for 1 h in Medium 199 + L-glutamine. Subsequently, cells were activated with 5 ml 10 ng/ml VEGF diluted in starving medium for appropriate lengths of time. After activation, medium was quickly removed from plates and cells placed on ice. Then, 200 µl 2x Rho assay lysis buffer (supplemented with 2x protease inhibitors, 20 mM NaF and 4 mM Na<sub>2</sub>VO<sub>3</sub>) was added to the plates and cells scraped into 1.5 ml tubes (approximated 400 µl lysate was removed from each plate). Cells were lysed for 10 min on ice, then lysates clarified by centrifugation at 4 °C, at 21910 x g for 5 min. To assess total RhoJ, 20 µl lysate was mixed with an equal volume of 2x sample buffer and stored at -

20 °C. The remaining lysate was mixed with the washed beads and incubated on a rotating wheel for 45 min at 4 °C. Beads were then washed 3x with Rho assay lysis buffer (supplemented with protease inhibitors, 10 mM NaF and 2 mM Na<sub>2</sub>VO<sub>3</sub>) and active RhoJ eluted with 30 µl 2x sample buffer.

## **2.15 DNA manipulation**

### **2.15.1 Production and purification of plasmid DNA**

Plasmids were purified from bacterial cultures on both large and small scale. The Qiagen plasmid maxi kit (Qiagen) was used according to the manufacturer's instructions for large-scale preps. For small-scale preps, the GeneJET plasmid miniprep kit (Fermentas) was used, also according to the manufacturer's instructions.

### **2.15.2 Amplification of DNA fragments by PCR**

In order to generate DNA fragments for insertion into plasmids, regions were amplified using the polymerase chain reaction (PCR). A high fidelity polymerase enzyme was used for these reactions in order to reduce errors. For each PCR, 100 µl mixes were set up containing 74 µl water, 20 µl 5 x Phusion HF buffer, 2 µl 10 mM dNTPs (Bioline), 1 µl each primer (at 100 µM, Eurogentec), 1 µl Phusion High-Fidelity DNA Polymerase (ThermoScientific) and 1 µl template DNA. PCR was performed as follows: an initial denaturation step of 30 s, 98°C followed by 30 cycles of denaturation (10 s, 98°C), annealing (30 s, 55°C) and elongation (30 s/500 bp DNA, 72°C) and a final elongation step of 10 min, 72°C. Following PCR reactions, products were purified using the QIAquick PCR purification kit (Qiagen).

### **2.15.3 Digestion of DNA with restriction enzymes**

To digest PCR products or plasmid DNA, reactions were carried out in a total volume of 50 µl. Either purified PCR products (generated as per Section 2.15.2) or 5 µg plasmid DNA were incubated with 5 µl 10 x enzyme buffer (New England Biolabs), 5 µl 10 x BSA (if required) and 2.5 µl restriction enzyme (20,000 U/ml) at the appropriate temperature for at least 1 h. Digestions were also scaled down to 10 µl volumes for diagnostic purposes.

### **2.15.4 DNA electrophoresis**

DNA was separated on gels containing 1-2% (w/v) agarose in TAE, with SYBR Safe DNA Gel Stain (Invitrogen). Samples were loaded in 6 x loading dye alongside 100 bp or 1 kb ladders (Fermentas) and gels visualised using the Gene Genius Bio Imaging System (Syngene).

### **2.15.5 Gel purification**

After electrophoresis, digested fragments and plasmids were cut from the gel and samples purified using the GeneJET gel extraction kit (Fermentas), according to the manufacturer's protocol.

### **2.15.6 DNA ligation**

To ligate DNA inserts and plasmids, T4 ligase was used. Reactions were performed in a volume of 20 µl, containing 2 µl 10 x T4 ligase buffer, 2 µl T4 ligase enzyme and DNA in a 3:1 ratio of insert: vector (approximately 150 ng: 50 ng DNA) in 16 µl. Samples were incubated at room temperature overnight, and stored at -20 °C.

### **2.15.7 Transformation of competent bacteria**

Chemically competent *E. coli* were transformed with ligation mixes by heat-shock. Bronze or gold efficiency  $\alpha$ -Select *E. coli* were used, with 5  $\mu$ l ligation reaction (generated as per Section 2.15.6) added to 50  $\mu$ l bacteria. Transformation mixes were incubated on ice for 30 min before 1 min heat shock at 42°C in a waterbath. Mixes were returned to ice for a further min, then 100  $\mu$ l LB was added and bacteria left to recover in a shaking incubator at 37°C for approximately 1 h. Bacteria were subsequently plated onto LB agar plates containing the appropriate antibiotics and left to grow overnight at 37 °C.

### **2.15.8 Storage of plasmids and sequencing of DNA**

Glycerol stocks were made from bacterial cultures grown in LB at 37°C overnight. Approximately 500  $\mu$ l cultures were mixed with equal volumes of sterile 30% (v/v) glycerol and stored at -80 °C. Plasmids were sequenced by the Functional Genomics, Proteomics and Metabolomics Facility (School of Biosciences, University of Birmingham, UK).

## **2.16 Yeast two-hybrid**

### **2.16.1 Yeast strain and media**

For the yeast two-hybrid experiments, PJ69.4A yeast with the genotype MATa trp1-901, leu2-3,112, ura3-52, his3-200, gal4 $\Delta$ , gal80 $\Delta$ , GAL2-ADE2, LYS2::GAL1-HIS3, met2::GAL7-lacZ (James, Halladay *et al.* 1996) was transformed with pGBT9 (fused to RhoJ) and pACT2 (fused to GIT1 mutants) constructs.



Transformed yeast was grown in synthetic complete dextrose (SCD) containing 0.67% (w/v) yeast nitrogen base without amino acids, 0.14% (w/v) yeast synthetic drop-out medium supplement without his, leu, trp, ura, 2% (w/v) dextrose, 20 mg/l uracil and 40 mg/l histidine. For growth on solid medium, 2% (w/v) bacto-agar was added. When necessary, 50 mg/l leucine or 100 mg/l tryptophan was also added.

Mutants fused to the activation domain of Gal4p in the pACT2 vector can be selected on SCD medium lacking leucine. Those fused to the DNA binding domain of Gal4p in the pGBT9 vector can be selected on SCD medium lacking tryptophan. Yeast transformed with both pACT2 and pGBT9 constructs can be selected on SCD medium lacking both leucine and tryptophan.

#### **2.16.2 Generation of yeast two-hybrid constructs**

Mutants of rat GIT1 were acquired from Richard Premont (as listed in Table 2.6.2) and fused with the activation domain of Gal4p in the pACT2 vector for use in yeast two-hybrid. Details of strategies used to subclone constructs are listed in Table 2.6.1. The original mutants (Premont, Perry *et al.* 2004) were first transformed into competent bacteria (as per Section 2.15.7), and subjected to miniprep as per the GeneJET Plasmid Miniprep kit (Fermentas). PCR was used to amplify the insert of interest and confirmed as successful by running on an agarose gel, then products were purified using the QIAquick PCR purification kit (Qiagen) and eluted in ultrapure ddH<sub>2</sub>O. Purified PCR products and the pACT2 vector were digested with restriction enzymes to generate sticky ends and the vector was treated with Antarctic phosphatase (NEB) to prevent relegation. Digested inserts (or vectors) were purified using the GeneJET Gel Extraction kit (Fermentas), and ligations performed overnight according to

Section 2.15.6. Ligation mixes were transformed into competent bacteria and resulting colonies subjected to miniprep and diagnostically digested before sequencing.

### **2.16.3 Transformation of yeast**

Single colonies of yeast were grown overnight in synthetic complete dextrose (SCD, lacking the appropriate amino acids) at 30°C with shaking. The following day, the optical density was measured at 600 nm and cultures diluted into a larger volume (40 ml) for further growth overnight (30 °C, with shaking).

The next day, the optical density was measured again at 600 nm and cultures diluted to 0.25 OD in 80 ml, then grown for 2 further generations until they reached an optical density of approximately 0.5. Yeast was centrifuged at 5000 x g, 2 min and pellets washed with sterile water before transferring to 1.5 ml tubes and centrifuging again at 5000 x g, 2 min. Then, 240 µl 50% (w/v) polyethylene glycol (PEG, MW 3350, Sigma), 36 µl 1 M lithium acetate pH 7.5, 10 µl single-stranded carrier DNA from salmon sperm (Invitrogen), which had been boiled for 5 min then chilled on ice, and 34 µl sterile water containing 0.1-0.5 µg plasmid DNA was added to the pellet, and yeast resuspended. This transformation mix was incubated at 30°C with shaking for 30 min before a 15 min heat shock at 42°C. Yeast were centrifuged at 5000 x g for 1 min, then the pellet was washed once with sterile water and centrifuged again for 2 min at 5000 x g. The resulting pellet was resuspended in 150 µl sterile water and plated onto solid SCD (lacking the appropriate amino acids). Plates were left at 30°C for yeast to grow and after 5 days colonies transformed with both pACT2 and pGBT9 fusions (and thus able to grow on Trp and Leu deficient medium) were restreaked.

#### **2.16.4 Yeast two-hybrid spot assay**

PJ69.4A yeast, which was transformed with constructs for yeast two-hybrid, contains a HIS3 reporter gene that is under the control of the Gal1 promoter (GAL1-HIS3). This promoter in turn is dependent on Gal4p, so in yeast where the proteins fused to Gal4p DBD and Gal4p AD come into contact, transcription of the HIS3 gene is activated allowing synthesis of histidine. Interactions can therefore be identified by plating yeast onto medium lacking histidine, since interacting proteins will stimulate the production of this amino acid and allow yeast growth. This reporter gene is however 'leaky' (James, Halladay *et al.* 1996) so test plates lacking His were supplemented with 3 mM 3-amino-1,2,4-triazole (3AT) to prevent false positives. 3AT competitively inhibits the enzyme imidazoleglycerol-phosphate dehydratase, the product of the HIS3 gene that contributes to the production of histidine.

Single colonies from plates of restreaked yeast transformed with pACT2 and pGBT9 constructs were grown overnight in SCD (lacking Trp and Leu) at 30°C in a shaking incubator. The next day, optical densities were measured at 600 nm and 4 five-fold dilutions of cultures prepared, starting at an OD<sub>600</sub> of 0.1. Dilutions were spotted onto solid SCD plates lacking Trp and Leu as a positive control, and solid SCD lacking Trp, Leu and His (+3AT) to test for interactions. Yeast were grown at 30°C for 3-5 days then pictures of spots were taken using the Gene Genius Bio Imaging System (Syngene).

#### **2.17 Immunofluorescent staining**

To visualise proteins of interest by confocal microscopy, cells were plated onto coverslips and subsequently fixed and stained. HUVEC were plated onto coverslips in a confluent

monolayer or sparsely depending on the experiment of choice (cell densities outlined in Table 2.8). Before use, coverslips were incubated with 1 M HCl for 10 min, washed 5 times with sterile ddH<sub>2</sub>O and stored in 70% (v/v) ethanol. Before seeding, coverslips were washed 6 times with PBS and coated with 0.1% (w/v) sterile gelatin in PBS.

To fix and stain all proteins except endogenous RhoJ, cells were first gently washed 3x with PBS and fixed with 4% (w/v) paraformaldehyde in PBS for 10 min. All subsequent washes were performed in plates. Cells were washed again 3x with PBS before neutralising with 50 mM NH<sub>4</sub>Cl in PBS for 10 min. Cells were washed 3x with PBS and then permeabilised with 0.1% (v/v) triton-X-100 for 4 min. After permeabilisation, cells were washed 3x with PBS and incubated with blocking buffer for 1 h. Coverslips were then removed from wells and placed face down onto 50 µl droplets of primary antibody diluted in blocking buffer for 30-60 min at room temperature. Coverslips were returned to wells and washed again 3 times with PBS and incubated with secondary antibody in blocking buffer for 30-60 min as per primary antibody. Coverslips were again returned to wells and washed twice with PBS and once with H<sub>2</sub>O, and mounted onto glass slides with 5.5 µl ProLong Gold Antifade reagent with DAPI (Invitrogen). Slides were left in the dark overnight and the following day edges of the coverslips were sealed with clear nail varnish and stored at -20°C.

To stain endogenous RhoJ, cells were washed twice with PBS then fixed and permeabilised in ice cold 100% methanol for 5 min. Cells were then washed 3x with PBS and blocked in 4% (w/v) BSA in PBS for 1 h at room temperature. Primary antibodies were diluted in 4% (w/v) BSA in PBS for 2 h at room temperature, then washed in PBST (2 x 5 min) at room temperature. Coverslips were subsequently incubated with secondary antibody in 4% (w/v)

BSA for 45 min at room temperature followed by 3 x 5 min washes with PBST and a single 5 min wash with water. Mounting was performed using ProLong Gold Antifade reagent as described above.

Staining was imaged using the Zeiss LSM 510-UV confocal microscope, and imported using the LSM Image Browser. Analysis was performed using ImageJ.

**Table 2.8 Cell densities used for immunofluorescent staining.**

Assay	Cell density per well
Sparse cells on coverslips in a 6 well plate	$5 \times 10^4$
Sparse cells on coverslips in a 12 well plate	$1.5 \times 10^4$
Confluent cells on coverslips in a 24 well plate	$1 \times 10^5$

## 2.18 Monitoring of focal adhesions in fluorescent HUVEC by TIRF microscopy

To monitor focal adhesion lifetime, HUVEC were transduced with fluorescent proteins as per Section 2.9. This allowed focal adhesions to be visualised under TIRF microscopy. Cells at a scratch edge were monitored by timelapse TIRF microscopy in order to analyse focal adhesion lifetime. Sparsely plated RFP-Paxillin HUVEC were also imaged by TIRF microscopy, in order to quantify numbers of focal adhesions per cell.

For cells in a scratch wound,  $3.5 \times 10^5$  RFP-Paxillin expressing HUVEC were seeded onto 6 well plates coated with 0.1% (w/v) gelatin, in HUVEC medium. The next day cells were transfected with siRNA as in Section 2.8.1, and 24 h later,  $2.5 \times 10^5$  cells were replated onto 35 mm diameter, 20 mm microwell MatTek plates (1.5 uncoated coverslip, MatTek Corporation). The next day, in order to ensure cells were migrating, the monolayer was

wounded with a sterile 20  $\mu$ l pipette tip. Complete DMEM lacking phenol red (Sigma), prepared as per HUVEC medium, was added to the cells and wounds left to heal at 37°C, 5% CO<sub>2</sub> for 2-4 h before imaging. Fluorescent cells along the wound edge were selected and monitored for 1.5 h using a Nikon TIRF system on a Nikon Eclipse Ti Inverted microscope (Nikon) at 37°C with CO<sub>2</sub> buffering. RFP-Paxillin expressing cells were imaged every 2 min using a Green Diode 561 nm laser (those expressing GFP constructs were also imaged with an Argon-Ion 457-514 nm laser) and a CFL Plan Apo 60x NA 1.49 objective. Images were captured on a 12-bit Ixon 1M EMCCD camera controlled by the Nikon NIS Elements software. Videos were converted to AVI files using NIS-Elements 3.2 and finally lifetime analysed using the cell counter plug-in on ImageJ.

To look at numbers of focal adhesions in sparsely plated cells, fluorescent HUVEC were plated at  $2 \times 10^5$  cells per well in a 6 well plate, and transfected with negative control or Rho1 specific siRNA as per Section 2.8.1. The next day, these cells were replated at a density of  $4 \times 10^4$  cells per well in 6 well, 20 mm diameter MatTek plates (1.5 uncoated coverslip, MatTek Corporation). Individual cells were imaged using TIRF as described above, and brightfield was used to confirm only one cell was being imaged at a time. Focal adhesions were counted using the cell counter plug-in on ImageJ.

## **2.19 Tube formation assay**

### **2.19.1 Co-culture tube formation assay**

The co-culture tube formation assay is an organotypic assay used to assess formation of tubules by HUVEC cultured on HDF. Tubules which form are more similar to those found *in*

*vivo* than other *in vitro* assays, as HDF secrete their own extracellular matrix on which HUVEC can grow, and these tubules are found to form lumens (Bishop, Bell *et al.* 1999, Kaur, Leszczynska *et al.* 2011). The protocol was carried out as per Figure 2.1. First,  $3 \times 10^4$  HDF were plated into 12 well plates in complete DMEM and incubated at 37°C, 5% CO<sub>2</sub>. HUVEC were plated at a density of  $2 \times 10^5$  cells per well in a 6 well plate on day 3 and transfected on day 4 as described in Section 2.8.1. HUVEC were harvested and  $3 \times 10^4$  replated onto HDF the day after transfection. Medium and treatments were then replaced every two days. Three days after transfection, HUVEC lysates were prepared for Western blotting as per Section 2.10 to confirm knockdown.

#### **2.19.2 Staining of co-culture tubules**

Six days after plating HUVEC, tubules were fixed and stained according to the following protocol. First, cells were washed once with PBS, then they were incubated for 30 min at room temperature with 70% (v/v) ethanol chilled to -20°C. Cells were washed twice with PBS before incubation with primary antibody (mouse anti-human CD31) in 1% (w/v) BSA in PBS for 1 h at 37°C. Then, wells were washed three times with PBS before adding secondary antibody conjugated to HRP (anti-mouse) in 1% (w/v) BSA in PBS, again for 1 h at 37°C. Cells were washed twice with PBS and three times with 1 ml ddH<sub>2</sub>O before adding 500 µl SigmaFAST BCIP/NBT (Sigma) substrate dissolved in ddH<sub>2</sub>O (1 tablet:10 ml water) for 25 min. Wells were washed with ddH<sub>2</sub>O and left to dry away from light, before imaging using a Leica DM IL microscope and a USB 2.0 2M Xli camera. The AngioSys Image Analysis software (TCS CellWorks) was used to assess mean tubule length and number of branches.

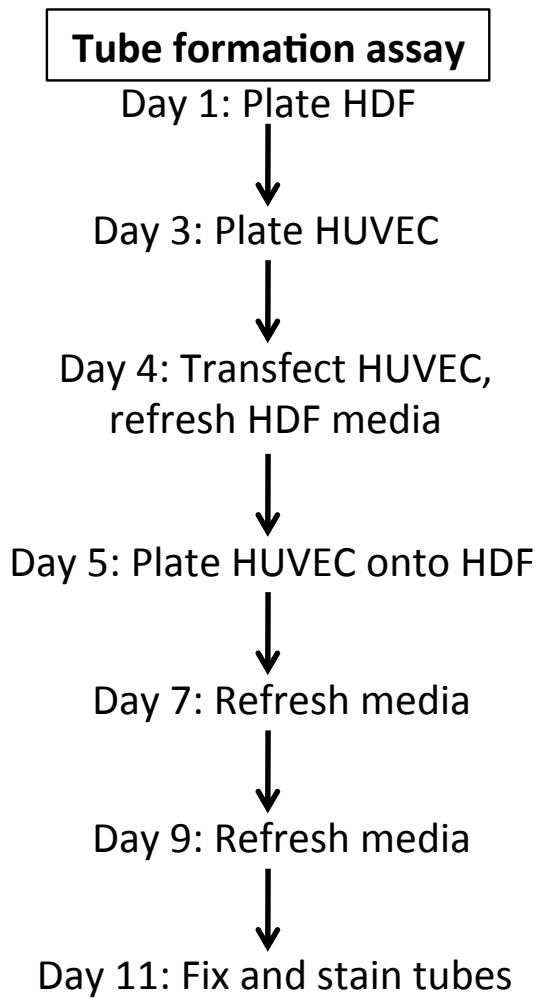


**Figure 2.1. Co-culture tube formation assay procedure.**



### **2.19.3 Matrigel tube formation assay**

In order to investigate tubulogenesis on the basement membrane extract Matrigel, natural Matrigel (VWR) was thawed on ice at 4 °C overnight. Wells in a 12-well plate were wetted with PBS before adding 70 µl Matrigel per well, which was left to solidify for 30 min at 37 °C. Cells were plated at  $1.4 \times 10^5$  per well in HUVEC medium, and incubated at 37 °C, 5% CO<sub>2</sub> for 24 h to allow tubes to form. Images were captured using a Leica DM IL microscope and a USB 2.0 2M Xli camera, with 5-6 images per condition. Analysis of tube formation was performed using the Angiogenesis Analyser plugin for ImageJ, with mean loop number calculated at 12 h.

### **2.20 Treatment of HUVEC with Src and FAK inhibitors**

To investigate further the phosphorylation of GIT2 in GFP-daRhoJ expressing HUVEC, and the role of Src and FAK in this phosphorylation, small molecule inhibitors were used to inhibit kinase activity. Dasatinib (SelleckChem) was used to reduce Src activity, and PF 573228 (SelleckChem) was used to reduce FAK activity.

HUVEC expressing GFP or GFP-daRhoJ were treated with 50 nM dasatinib for 30 min, or 1 µM PF 573228 for 1 h before lysis and Western blotting as per Section 2.10. Inhibitors were diluted in HUVEC medium. A combination of dasatinib and PF 573228 was also used, in this case cells were incubated with PF 573228 for 30 min, then medium was removed and replaced with that containing both PF 573228 and dasatinib for a further 30 min.

## **2.21 Phosphokinase array**

In order to assess the effect of dominant active RhoJ expression on phosphorylation of a panel of kinases, the human phospho-kinase array from R&D Systems was used. To perform the assay, HUVEC stably expressing GFP or GFP-daRhoJ were plated at  $2 \times 10^6$  on 10 cm dishes and the next day, cells were rinsed and scraped into 1 ml PBS. Cells were centrifuged at  $5000 \times g$  for 2 min, then lysed in 200  $\mu$ l lysis buffer 6 (supplemented with protease Inhibitors, 2 mM  $\text{Na}_2\text{VO}_3$  and 10 mM NaF) according to the manufacturer's instructions. Lysate concentrations were measured and approximately 500  $\mu$ g protein used per array. The assay was performed according to the manufacturer's protocol, and repeated with cells from a different isolate to account for individual cord variation.

Levels of phosphorylation was analysed using ImageJ. A single region of interest was used to measure the mean grey value of each spot, and background intensities (measured using the same region of interest at a blank space near the spot of interest) subtracted, then intensities compared between GFP and GFP-daRhoJ conditions.

## **2.22 Extraction and analysis of mouse protein and RNA**

### **2.22.1 Genomic DNA extraction from mouse samples**

Genomic DNA was extracted from ES cells or mouse ear clips to determine the presence or absence of the knockout cassette. To extract DNA from ES cells, they were first centrifuged at  $5000 \times g$  for 2 min, and incubated with 100  $\mu$ l tail lysis buffer (with Proteinase K added fresh) at  $55^\circ\text{C}$  overnight. Samples were vortexed the following morning and heated for 12

min at 100°C to inactivate the Proteinase K. Then, 400 µl sterile water was added, samples vortexed again and stored at 4°C for future genotyping.

For ear clips, extractions were performed as above, however 150 µl tail lysis buffer was used to lyse samples, and 600 µl sterile water added after Proteinase K inactivation.

### **2.22.2 Genotyping of mouse genomic DNA**

To determine whether mice were wild-type, heterozygous or knockouts, genotyping of genomic DNA was performed. PCR reactions (25 µl) were set up: 12.5 µl REDTaq ReadyMix (Sigma), 1 µl of each primer at 10 µM and 0.5 µl water were mixed with 10 µl template (genomic DNA extracted as per Section 2.22.1). The mixtures were then amplified by PCR as follows: a 5 min initial denaturation (96°C) was followed by 30 cycles of denaturation (96°C, 15 s), annealing (60°C, 30 s) and elongation (72°C, 30 s), and a final 5 min elongation (72°C). Afterwards, 10 µl samples were run on 2% (w/v) agarose gels and subjected to electrophoresis as per Section 2.15.4.

To check for the presence of Cre, a mix containing 12.5 µl REDTaq ReadyMix (Sigma) and 1 µl of each of 3 primers was mixed with 9.5 µl template. The samples were amplified by PCR as follows: a 2 min initial denaturation (94 °C) was followed by 30 cycles of denaturation (94 °C, 15 s), annealing (60 °C, 30 s) and elongation (72 °C, 30 s), and a final 5 min elongation (72 °C).

### **2.22.3 RNA extraction from mouse lung tissue**

Total RNA was extracted from lung tissue of mice of various genotypes for quantitative and standard PCR analysis of gene expression. First, mice were culled by CO<sub>2</sub> inhalation according

to Home Office guidelines, then lung tissue was quickly removed and snap frozen in liquid nitrogen. Approximately 30 mg tissue was used per RNA extraction. Tissue was placed in a chilled pestle and mortar, and ground into a fine powder under liquid nitrogen. After the nitrogen had evaporated, 700 µl QIAzol reagent (Qiagen) was added to the powder and once dissolved, the homogenate added to a QIAshredder (Qiagen) and centrifuged for 2 min. Then, 140 µl chloroform was added to the resulting samples and tubes shaken vigorously for 15 seconds. After 2-3 min, samples were centrifuged at 12000 x g for 15 min at 4 °C. At this point, the sample separates into 3 distinct phases and the RNA is contained in the upper, colourless phase. The RNA-containing phase was transferred to a fresh 1.5 ml tube (approximately 350 µl), and 1.5x volume of 100% (v/v) ethanol added and samples mixed thoroughly. Up to 700 µl sample was transferred to an RNeasy mini spin column (Qiagen) and centrifuged at 12000 x g for 15 seconds (subsequent centrifugation steps were carried out at the same speed), and repeated until all sample had passed through the column. The flow-through was discarded and 700 µl buffer RWT added to the column. This was centrifuged for 30 seconds, and again, flow-through discarded. Then, 500 µl buffer RPE was added to the column and centrifuged for 20s, then this step was repeated with a centrifuge of 1 min. The flow-through was again discarded and the column centrifuged for a further 1 min to remove any remaining buffer. The column was then transferred to a fresh 1.5 ml tube, 30 µl RNase free water added and column centrifuged for 1 min to elute RNA. To assess the concentration of the eluted RNA, 2 µl was removed for measurement with the NanoDrop. The remaining RNA was snap frozen on dry ice and stored at -80°C for future cDNA generation (performed as per Section 2.11.2).

#### **2.22.4 PCR of cDNA from mouse lung tissue**

In order to determine splicing in the RhoJ genetrapped mouse, cDNA generated from RNA extracted as per Section 2.22.4 was amplified by PCR. Primers spanning the exon boundaries were used in reactions made up as per Section 2.22.2, however genomic DNA was substituted for 10 µl cDNA. PCR was performed as follows: a 5 min initial denaturation (96°C) was followed by 30 cycles of denaturation (96°C, 15 s), annealing (55°C, 30 s) and elongation (72°C, 30 s), and a final 5 min elongation (72°C). Afterwards, 10 µl samples were run on 2% (w/v) agarose gels and subjected to electrophoresis.

#### **2.22.5 Tumour implantation in mice**

To perform preliminary tumour implantation experiments in wild-type and knockout mice,  $1 \times 10^6$  Lewis lung carcinoma cells were injected into the flank of mice in a volume of 200 µl complete DMEM. Mice were anaesthetised with isoflurane before injection, then weighed, shaved and sprayed with alcohol to sterilise the area to be injected into. After injection, mice were left to recover in clean cages. Once tumours were palpable, measurements were taken each day and mice culled according to Home Office guidelines when they reached the maximum tumour load of 1.2 cm<sup>3</sup>. Tumours were subsequently collected, weighed and images taken.

### **2.23 Image analyses**

All analysis of images was performed using ImageJ software. To assess lifetime, focal adhesions were manually tracked using the Cell Counter plug-in, lifetime was taken as the time from which the adhesion was first visible to the point where it could no longer be seen.

Assembly and disassembly durations were calculated by manually outlining tracked adhesions and measuring mean grey values across the lifetime of the adhesion. Assembly was taken as the time taken from when the adhesion was first visible to its highest mean grey value. Disassembly was taken as being from this brightest point to when the adhesion could no longer be seen. Focal adhesions were also manually counted using the Cell Counter plug-in.

To determine recruitment of partner proteins to adhesions, individual focal adhesions around the periphery of the cell were identified based on vinculin staining and manually outlined on the vinculin channel. Mean grey values of the protein of interest were measured on the corresponding channel using ImageJ. Imaging across conditions for each protein stained was performed using the same microscope settings in order to attempt to maintain similar intensities of background staining. For each of the recruitment replicates, data points from each experimental group were scaled to the mean of the siControl dataset for that experiment. Data were then pooled to determine relative recruitment across all the replicate experiments. Example images of adhesions that were outlined on the vinculin channel and measured on the respective partner protein channel are shown in Figure 2.2.

To determine adhesion size, individual focal adhesions around the periphery of the cell were manually outlined on the vinculin channel and area (in pixels<sup>2</sup>) measured using ImageJ.

## **2.24 Statistical analyses**

Experiments were performed 3 times unless otherwise stated, and the statistical significance of data was calculated using GraphPad Prism software. The specific tests used are outlined in

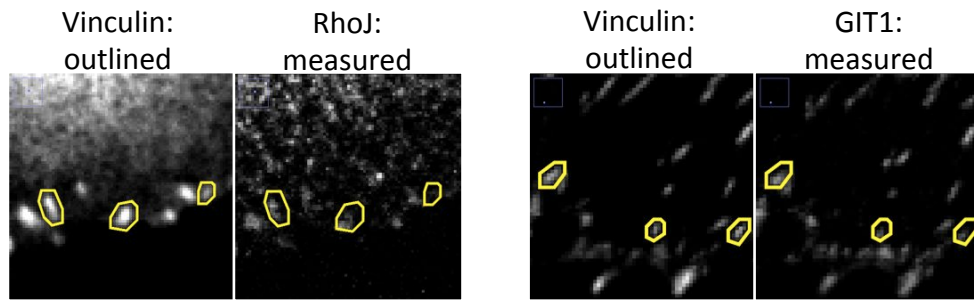


**Figure 2.2 Individual adhesions were outlined based on vinculin staining and the mean grey value of the partner protein measured on its corresponding channel. Yellow regions of interest were manually drawn on ImageJ using vinculin staining as a guide, and mean grey values of the partner protein measured to assess recruitment to adhesions.**

the results section, with the non-parametric Mann Whitney and Kruskal-Wallis tests used to analyse significance in most cases, as these tests do not assume a normal distribution of data. Paired t-tests were used to analyse tube formation and densitometry data. P values are as follows: \*\*\* for  $p \leq 0.001$ , \*\* for  $p \leq 0.01$ , \* for  $p \leq 0.05$  and ns for  $p > 0.05$ .

## **CHAPTER 3**

### **The role of RhoJ in regulating focal adhesion dynamics**



### 3.1 Introduction

Migration of cells is a key process in angiogenesis, and in order to migrate cells must remodel their cytoskeleton. Forward movement is facilitated by the formation of lamellipodia and focal adhesions at the leading edge of the plasma membrane, along with release and disassembly of adhesions at the rear (Raftopoulou and Hall 2004, Bryan and D'Amore 2007). Focal adhesions are multi-protein complexes made up of both scaffold and signalling constituents that connect the intracellular cytoskeleton with the extracellular matrix (Petit, Thiery 2000). They initially form as focal complexes, which either rapidly disassemble or mature into adhesions and disassemble as the cell moves forwards (Broussard, Webb *et al.* 2008).

Rho GTPases have long been described as regulators of cell migration, with members from the Rho, Rac, Cdc42 and Rnd subfamilies, as well as RhoD and RhoF being implicated in mediating aspects of cytoskeletal rearrangement. RhoA, Rac1 and Cdc42 in particular have been studied most often, and are all known to have roles in focal adhesion formation (Nobes and Hall 1995, Vega and Ridley 2007). Primarily, RhoA has been shown to regulate adhesion and stress fibre assembly (Ridley and Hall 1992) while Rac1 regulates lamellipodial protrusions and Cdc42 mediates filopodia formation. However in 1995, Nobes and Hall first identified RhoA-independent, Rac-induced focal complexes, as well as those formed by Cdc42. Additionally, Cdc42 was found to activate RhoA and Rac1 activity in confluent fibroblasts, proving a link between these Rho GTPases (Nobes and Hall 1995).

RhoJ is a member of the Cdc42 subfamily of Rho GTPases that is highly expressed in endothelial cells. Previous work by members of this laboratory and others has shown that it

localises to focal adhesions and regulates their numbers in HUVEC, as well as mediating aspects of the cytoskeleton in fibroblasts, PAEC and melanoma cells (Vignal, De Toledo *et al.* 2000, Aspenstrom, Fransson *et al.* 2004, Kaur, Leszczynska *et al.* 2011, Ho, Soto Hopkin *et al.* 2013). Recent work has also identified a role for RhoJ in regulating the activities of RhoA, Rac1 and Cdc42 (Yuan, Sacharidou *et al.* 2011), which in turn is likely to effect cytoskeletal rearrangement.

The aim of the work presented in this chapter was to determine how RhoJ regulates focal adhesion dynamics. In order to monitor adhesion dynamics by TIRF microscopy, HUVEC expressing a red fluorescent protein (RFP) tagged paxillin were generated and their behaviours confirmed as being comparable to untransduced cells. Their use in TIRF microscopy was optimised and subsequently RhoJ expression was manipulated using siRNA knockdown or expression of a dominant active mutant and lifetime, assembly and disassembly was assessed. The effect of RhoJ on microtubule targeting of focal adhesions was assessed, and investigations into focal adhesion size in knockdown and dominant active RhoJ expressing cells were performed. Finally, a RhoJ biosensor was generated and used in a pilot study to determine where RhoJ is active in the cell.

Experiments were primarily carried out on sparsely plated cells, since at this density stress fibre and focal adhesion number phenotypes had previously been observed. TIRF microscopy studies of focal adhesion dynamics were performed on cells at the edge of a scratch wound. While cells with manipulated RhoJ expression did not have increased numbers of adhesions when in a monolayer, those cells migrating to close a scratch did

(Kaur, Leszczynska *et al.* 2011). Presumably, this is because the scratch edge is the site of maximal motility and as a result, cytoskeletal rearrangement.

### **3.2 Manipulation of RhoJ expression by RNA interference and lentiviral transduction**

In order to assess the role of RhoJ *in vitro*, two methods were employed to manipulate its expression. RNA interference was used to diminish RhoJ protein expression in HUVEC while lentiviral transduction of cells allowed expression of GFP-tagged proteins, including a dominant active mutant of RhoJ.

For transfection of HUVEC with small interfering RNA (siRNA), two RhoJ specific duplex (RhoJ siRNA 1 and RhoJ siRNA 2) was used to knockdown RhoJ expression and a duplex with no known homology to human sequences used as a negative control (siControl). These duplexes have previously been validated by members of our laboratory, and are known not to induce the interferon response (Sukhbir Kaur, PhD thesis). As can be seen in Figure 3.1.A, HUVEC transfected with 10 nM of either RhoJ siRNA 1 or RhoJ siRNA 2 have minimal RhoJ protein expression compared to siControl HUVEC at 2 days after transfection. Densitometry performed also confirmed that on average, expression of RhoJ reduced by approximately 76% upon transfection with either RhoJ siRNA 1 or RhoJ siRNA 2. Levels of mRNA was also quantified in control and RhoJ knockdown cells, and data is shown in Figure 4.5, in Chapter 4. As expected, knockdown of RhoJ reduced levels of RhoJ mRNA in these cells compared to those transfected with siControl.

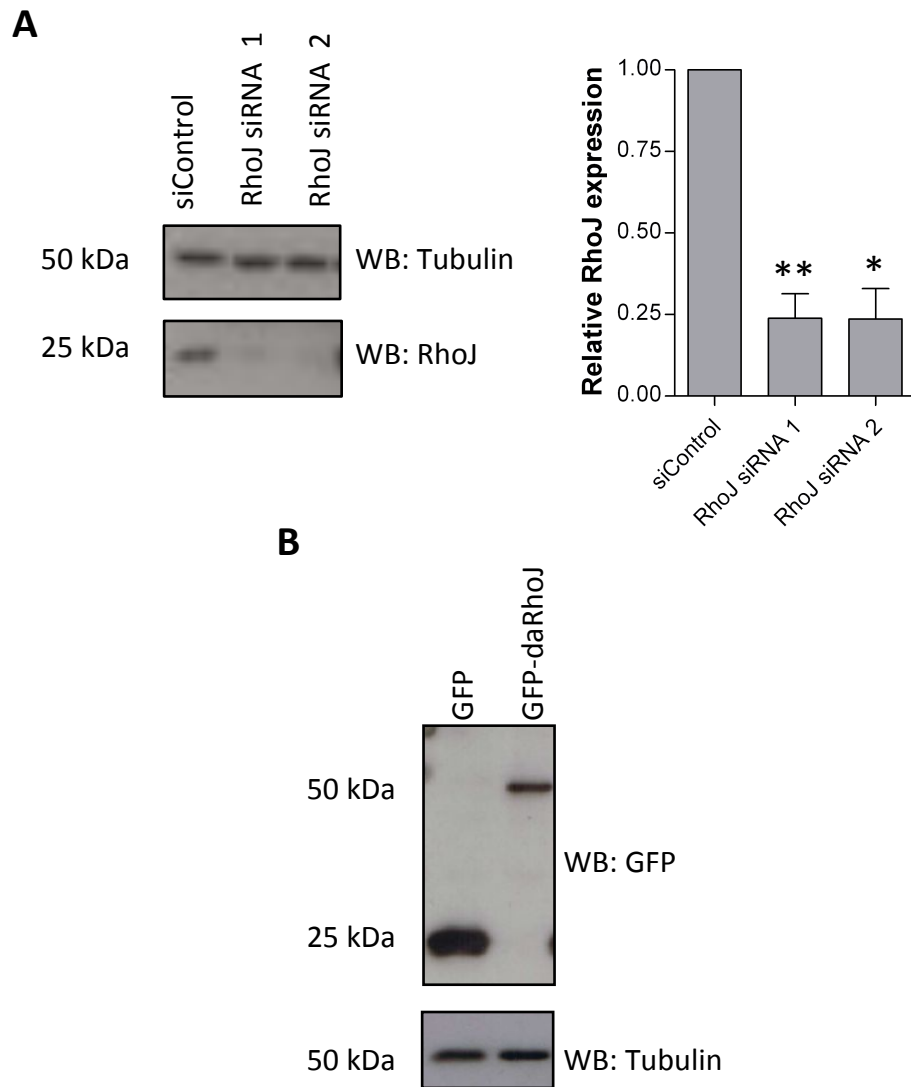


**Figure 3.1. Knockdown of endogenous RhoJ by siRNA transfection, and stable expression of GFP-dominant active RhoJ in HUVEC.** **A.** HUVEC were transfected with 10 nM control (siControl) or RhoJ specific (RhoJ siRNA 1 and RhoJ siRNA 2) siRNA duplexes. After 48 h cells were lysed, and samples Western blotted for RhoJ expression, with tubulin as a loading control. Densitometry was also performed to assess the expression of RhoJ (relative to tubulin) in each knockdown compared with controls, and data analysed using a paired t-test ( $n=3$  for each knockdown,  $*$  =  $p \leq 0.05$ ,  $**$  =  $p \leq 0.01$ ). **B.** HUVEC were infected with lentivirus to stably express GFP control or GFP-daRhoJ. Cells were lysed and samples Western blotted for GFP, with tubulin as a loading control.

To express GFP and a GFP-tagged dominant active mutant of RhoJ (GFP-daRhoJ), lentivirus was produced in HEK293T cells and used to infect HUVEC. These transduced HUVEC were capable of stably expressing the genes of interest, as the Western blot in Figure 3.1.B shows with expression of GFP and a GFP-daRhoJ fusion protein observed. The transduction efficiency of these cells was sufficiently high that cell sorting was not required and cells could be used in assays as a whole population. GFP transduction efficiency was consistently between 97-99% while GFP-daRhoJ transduction efficiency reached between 69-98%. These two methods of RhoJ protein manipulation were used to investigate the role of RhoJ in focal adhesion dynamics, in TIRF microscopy.

### **3.3 Optimisation of TIRF microscopy to monitor focal adhesion dynamics in HUVEC**

Previous work in our laboratory identified a role for RhoJ in regulating focal adhesion numbers, with more focal adhesions being observed in endothelial cells with reduced RhoJ expression and fewer in cells expressing a dominant active mutant of RhoJ (Kaur, Leszczynska *et al.* 2011). Since focal adhesions are dynamic complexes which assemble, mature and disassemble, experiments were designed to test the hypothesis that RhoJ may regulate this cycle in some way. Imaging by total internal reflection fluorescent (TIRF) microscopy is an ideal method of monitoring focal adhesion dynamics because only fluorophores approximately 100 nm or less from a coverslip can be visualised, reducing background noise (Mattheyses, Simon *et al.* 2010). As focal adhesions are found at the interface between the cell and the extracellular matrix, these complexes can be imaged by

introducing a fluorescently tagged focal adhesion protein. In these experiments a red fluorescent protein (RFP) tagged paxillin was introduced into HUVEC by lentiviral transduction in order to allow visualisation of adhesions. This work was done in collaboration with the Rappoport laboratory (School of Biosciences, University of Birmingham).

Initially, it was important to confirm that these RFP-paxillin expressing HUVEC demonstrated the same phenotype upon RhoJ knockdown as fixed, untransduced cells immunofluorescently stained and imaged by confocal microscopy. In order to do this, RFP-paxillin cells were transfected with control or RhoJ specific siRNA duplexes, then the following day plated sparsely onto MatTek dishes, and imaged by TIRF microscopy 48 h after transfection. Numbers of focal adhesions were counted using the cell counter plug-in for ImageJ, with at least 30 cells per condition imaged and analysed. Focal adhesion number per cell area was calculated by dividing numbers of focal adhesions by the total area of the cell, as measured on ImageJ, and was used to account for any differences in cell size.

As the data in Figure 3.2 show, focal adhesion number per cell area was significantly increased in RhoJ knockdown RFP-paxillin expressing HUVEC compared to control transfected cells. Furthermore, numbers of adhesions were significantly increased in RhoJ siRNA 2 transfected cells ( $p=0.0059$ , data not shown), however this was not the case for those transfected with RhoJ siRNA 1 ( $p=0.0581$ , data not shown), most likely due to subtle differences in cell size. From these experiments, it was concluded that RFP-paxillin expressing HUVEC display the same phenotype after transfection with RhoJ specific duplexes as untransduced fixed

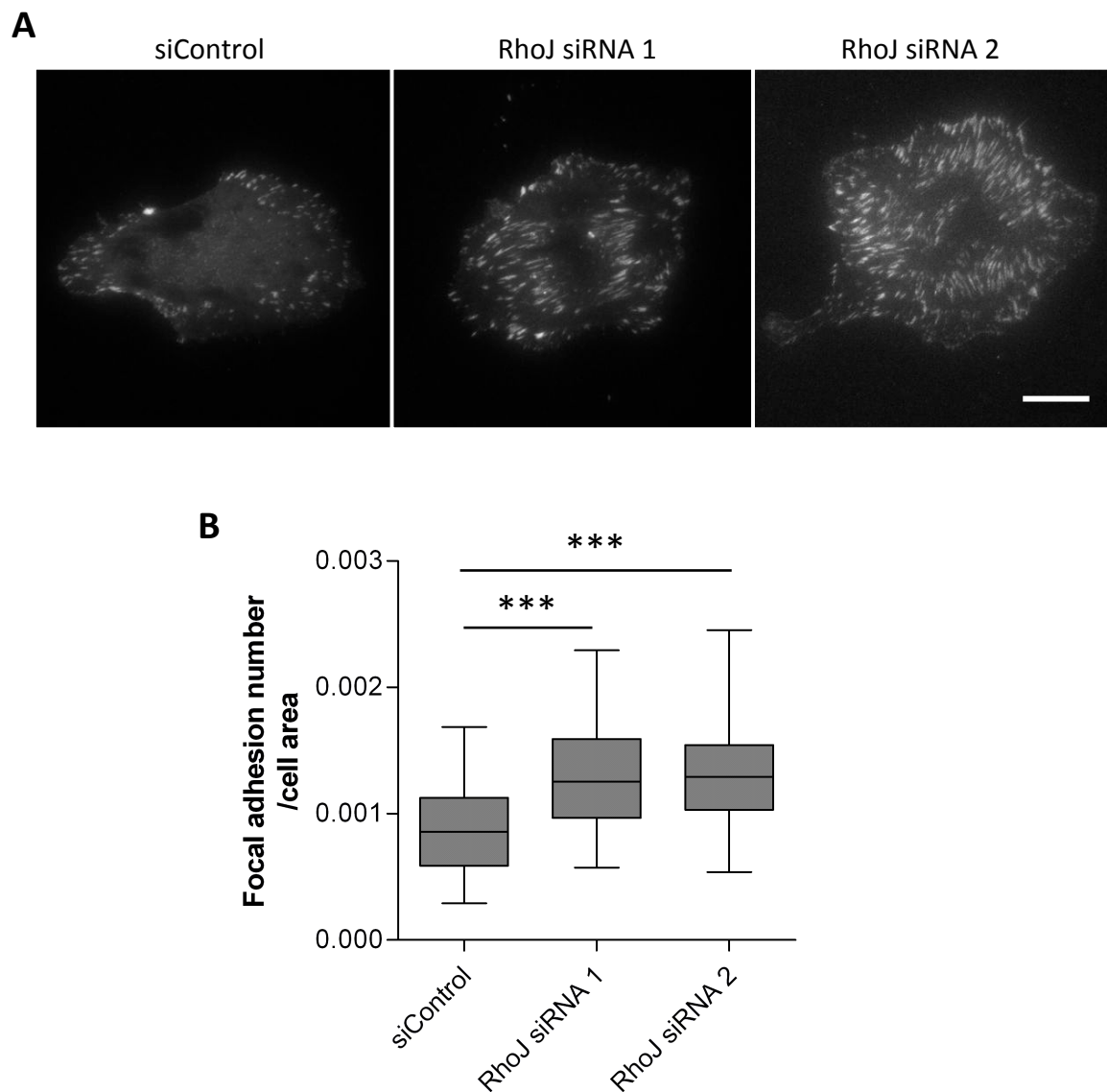


**Figure 3.2. RhoJ knockdown results in increased focal adhesion numbers per cell area in imaged by TIRF microscopy.** HUVEC stably expressing RFP-Paxillin were transfected with control or RhoJ specific siRNA, plated sparsely and imaged by TIRF microscopy. **A.** Representative images of single cells from each condition captured by TIRF microscopy. Scale bar: 20  $\mu$ m **B.** Focal adhesion numbers per cell area was calculated by dividing number of focal adhesions by cell area (counted and measured using ImageJ), in at least 30 cells from 3 independent experiments. Data are displayed as box and whisker plots. Error bars show minimum and maximum values, while the upper and lower edges of the box represent the 75th and 25th quartile respectively. The line within the box represents the median. The Mann Whitney test was used to analyse significance (\*\*\*=  $p < 0.001$ ).

HUVEC, and thus these cells and this method of transfection was used for all later investigations.

Upon analysis of focal adhesion number per cell area in RFP-paxillin HUVEC, there appeared to be more adhesions than normally found in untransduced HUVEC. It was therefore necessary to determine whether this was due to the imaging technique being more sensitive than the confocal microscopy used in the past (Kaur, Leszczynska et al. 2011), or whether expression of RFP-paxillin resulted in an increased number of adhesions. In order to investigate this, RFP-paxillin HUVEC were plated sparsely onto coverslips, as the increased focal adhesion numbers phenotype had previously been observed at this density (Kaur, Leszczynska *et al.* 2011), then fixed and stained with a different focal adhesion marker protein, vinculin. Single cells were then imaged by confocal microscopy, and focal adhesion number per cell area calculated as described above. Levels of RFP-paxillin expression were quantified by measuring the mean grey value of cells on the red channel. Cells were classified as low (<5000 units), medium (5000-10,000 units) or high (>10,000 units) expressers according to the intensity value generated. Focal adhesion densities were analysed in at least 10 cells per expression category from 3 independent experiments, each using different HUVEC isolates to eliminate cord variability. The Kruskal Wallis test was used to assess the statistical significance of differences in focal adhesion densities between different intensity categories.

The data in Figure 3.3.B show that the level of RFP-Paxillin expression did not lead to any changes in focal adhesion number per cell area, with the Kruskal Wallis test failing to show any significant differences across the three categories. Similarly, numbers of focal adhesions



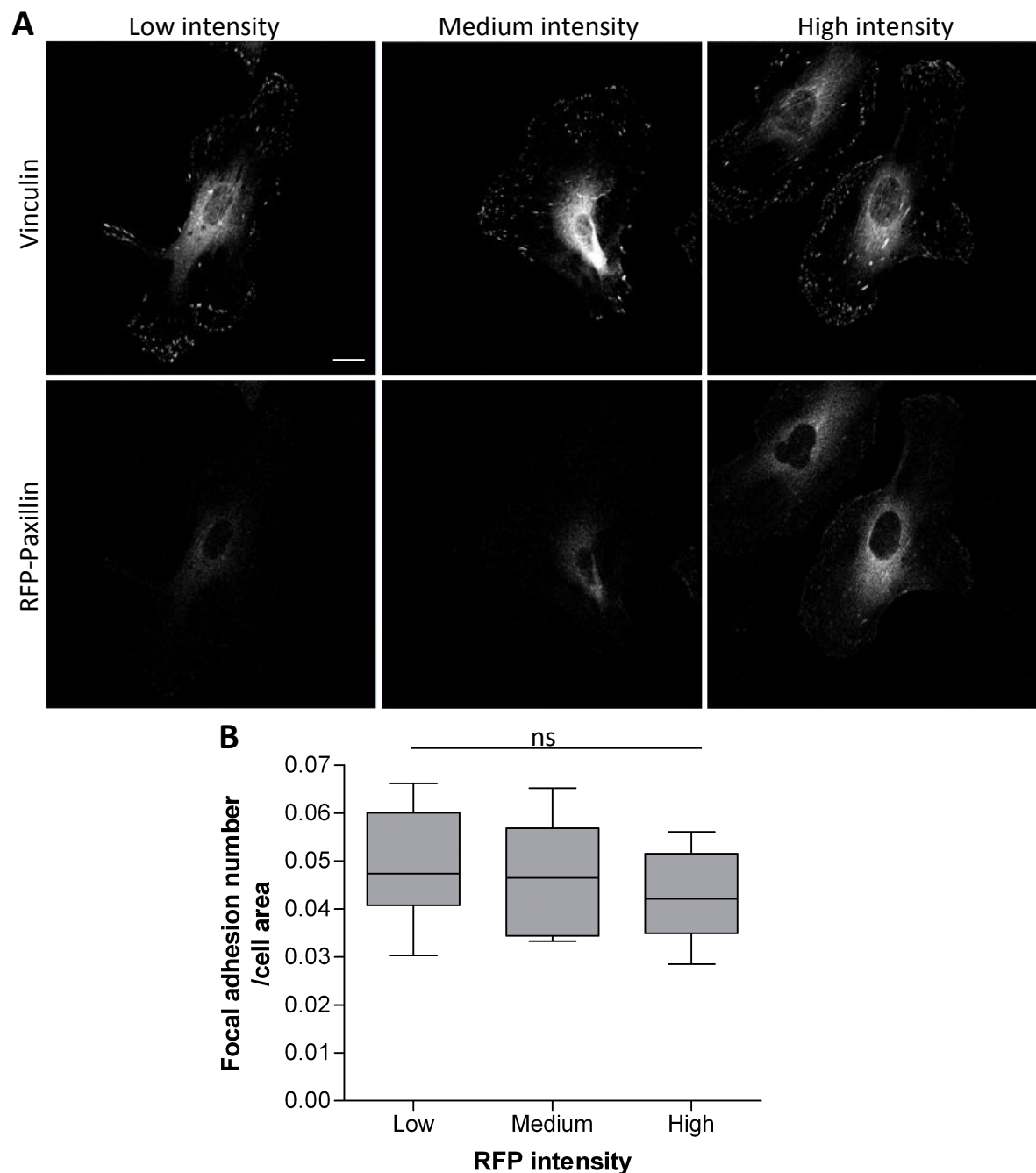


**Figure 3.3. Stable expression of RFP-Paxillin in HUVEC does not affect focal adhesion numbers per cell area.** HUVEC expressing RFP-Paxillin were plated sparsely onto coverslips, then fixed and stained for vinculin. Cells were imaged by confocal microscopy (**A**, scale bar: 20  $\mu$ m) and numbers of focal adhesions counted using the Cell Counter plug-in for ImageJ. Areas of cells and intensity of RFP were also measured using ImageJ. Focal adhesion numbers per cell area (number of focal adhesions divided by area of cell) were calculated and cells designated as low, medium or high RFP-Paxillin expressors according to the mean grey value (low: below 5000, medium: 5000-10,000 and high: above 10,000). **B**. Focal adhesion numbers per cell area were calculated and analysed for at least 10 cells per intensity band from 3 independent experiments. The data are presented in box and whisker plots. The Kruskal-Wallis test was used to analyse significance (ns= $p>0.05$ ).

did not vary significantly between groups (data not shown). These data confirmed that RFP-Paxillin is an appropriate marker for focal adhesions in these investigations. Additionally, co-localisation of RFP-Paxillin with vinculin was noted, showing that the construct localises correctly. It should however be noted that co-localisation was most obvious in those cells expressing high levels of RFP-Paxillin, although this is likely due to a sensitivity issue rather than incorrect localisation. An example of co-localisation is shown in Figure 3.4.

Since it had been confirmed that RFP-Paxillin HUVEC behave in the same manner as untransduced cells upon RhoJ knockdown, and the expression of RFP-Paxillin has no effect of focal adhesion numbers in itself, it was next important to optimise the imaging and analysis of focal adhesion lifetime in these cells. RFP-Paxillin cells were plated in a monolayer, then this monolayer was wounded and motile cells found at the scratch edge were imaged by TIRF microscopy. Cells were monitored for 2 hours by timelapse microscopy, with images taken every 2 minutes. Microscopy was performed on two separate occasions. A total of 5 cells were analysed and the lifetime time was assessed for 25 focal adhesions from each cell. The lifetime was defined as the time from when a focal adhesion first appeared to when it was no longer visible. The box plot (Figure 3.5.A) shows the range of lifetimes within cells. The variation between cells was analysed using the Kruskal Wallis test, with no significant differences seen between any of the 5 cells analysed. The line graph in Figure 3.5.B is a histogram showing the distribution of focal adhesion lifetime durations, with most adhesions present for between 20 to 40 minutes.

When analysing lifetime, focal adhesions were discounted if assembly had already begun when the timelapse was started, or if disassembly was incomplete by the end of the

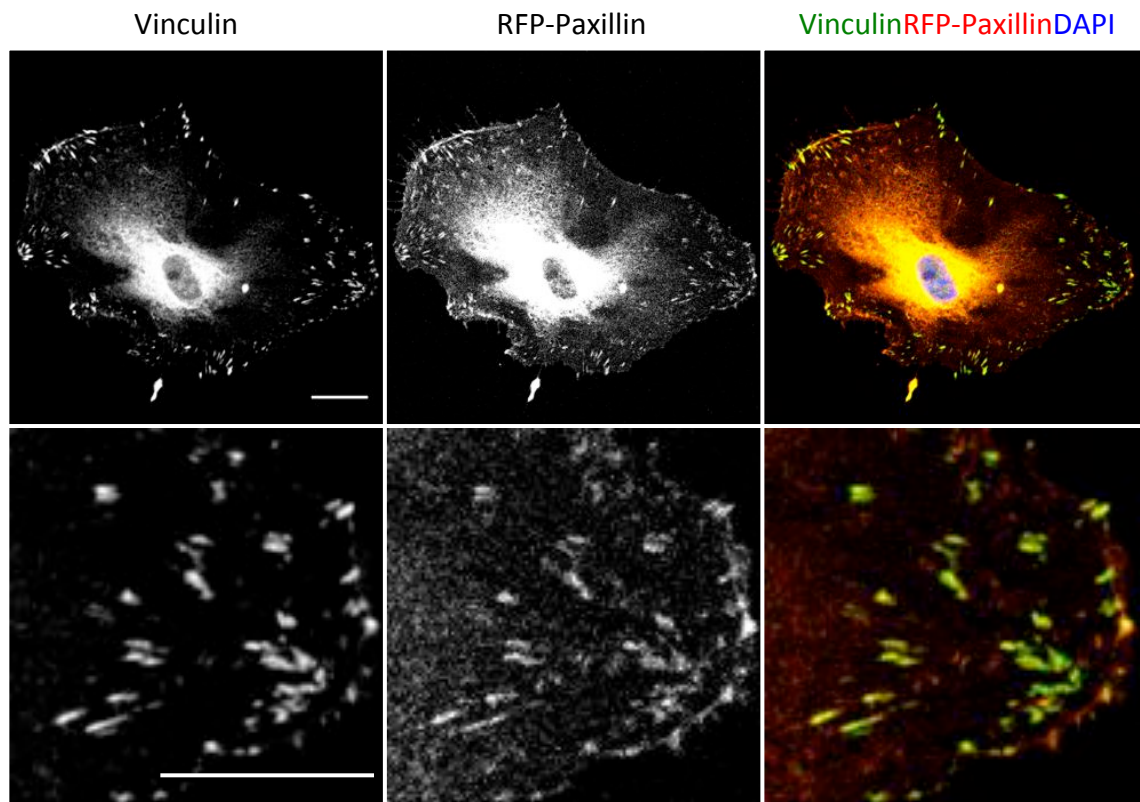


**Figure 3.4 RFP-Paxillin co-localises with vinculin at focal adhesions.** HUVEC stably expressing RFP-Paxillin were plated sparsely onto coverslips, then fixed and stained for vinculin. Cells were imaged by confocal microscopy (scale bar: 20  $\mu\text{m}$ ).

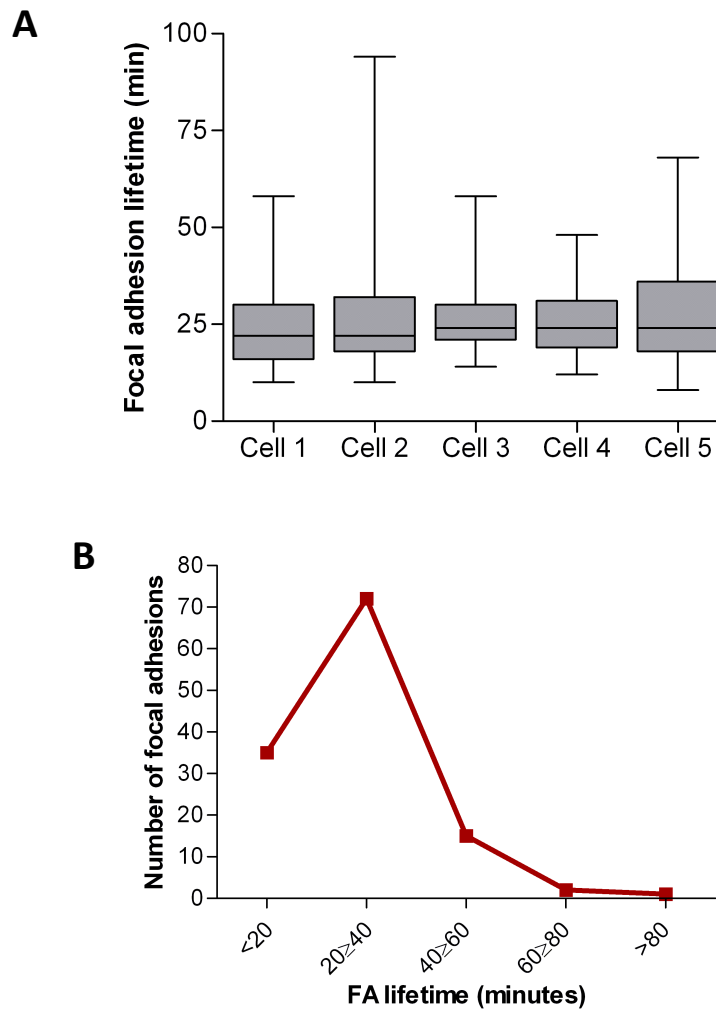


**Figure 3.5. Focal adhesion lifetime in transduced HUVEC is not significantly different between cells.** HUVEC expressing RFP-Paxillin were plated and the monolayer wounded before imaging with TIRF microscopy. Cells at the edge of the scratch were selected and monitored for 2 h, using timelapse imaging to take pictures every 2 min. **A.** 25 focal adhesions were tracked from 5 cells across 2 different imaging sessions using the cell counter plugin for ImageJ and displayed as a box and whisker plot. Duration of lifetime of focal adhesions were analysed by the Kruskal-Wallis test to assess statistical significance. **B.** Focal adhesion lifetime numbers were recorded and displayed as a line graph showing the spread of data.

timeframe. Adhesions were also not counted if they moved outside of the imaging field. Furthermore, cells were discounted if they appeared to be retracting, or if focus was insufficient to determine that only one focal adhesion was being monitored at a time. Efforts were made to discount focal adhesions that merged or split during their lifetime.

This initial data suggested that TIRF microscopy was an appropriate method by which to monitor the effect of RhoJ on focal adhesion lifetime, and gave an idea of the normal duration of lifetime in untreated cells. As such, investigation into the role RhoJ plays in focal adhesion lifetime could proceed and further TIRF microscopy was performed in cells with modified RhoJ expression or activity.

### **3.4 Investigating the effect of RhoJ knockdown on focal adhesion dynamics**

As the data in Section 3.3 demonstrate TIRF microscopy is an appropriate method to monitor focal adhesion dynamics, and show that the cells to be used (RFP-Paxillin expressing HUVEC) act in the same way as untransduced HUVEC, it was possible to investigate the effect of diminished RhoJ expression on focal adhesion dynamics. In order to do this, RFP-Paxillin expressing HUVEC were transfected with either control (siControl) or RhoJ specific siRNA (RhoJ siRNA). Two days later, the monolayer of transfected cells was wounded and TIRF microscopy performed. Images were taken every 2 minutes over a period of 90 minutes, and at least 10 focal adhesions tracked from 4 different cells per condition for each of the 3 independent replicates performed. In total, 165 focal adhesions were monitored for each condition.

The panels in Figure 3.6.B show representative focal adhesions (magnified regions of interest are highlighted with a white box in Figure 3.6.A) monitored from the siControl and RhoJ siRNA transfected cells, with arrows highlighting the adhesion monitored. Figure 3.6.C shows a box and whisker plot of the focal adhesion lifetime from control and RhoJ knockdown cells. When analysed using the Mann Whitney test, a significant difference was found between the lifetime durations of control and RhoJ knockdown focal adhesions, with RhoJ knockdown leading to an increased length of time taken for adhesions to assemble, mature and disassemble ( $p=0.0018$ ). The histogram in Figure 3.6.D shows the lifetime times separated into 10-minute groups. As can be seen, a rightwards shift is observed in the duration of the lifetime in RhoJ knockdown adhesions compared to control cells, with more adhesions taking between 40-50 minutes to assemble and disassemble in knockdown cells, and conversely more present for between 20-30 minutes in control cells.

These findings suggest that RhoJ promotes focal adhesion turnover, since reduced RhoJ expression leads to increased duration of focal adhesion lifetime. However, as has previously been mentioned, the lifetime of adhesions can be separated into assembly and disassembly phases and it was important to determine whether there were any differences between these two phases in the control and RhoJ knockdown conditions. In order to investigate this, focal adhesions already tracked in Figure 3.6 were re-analysed. Regions of interest were manually outlined around adhesions using ImageJ and mean grey values measured at each timepoint in which the adhesion was present. Assembly was taken as the point from which the adhesion was first visible until it reached its peak intensity (i.e. highest mean grey value), and disassembly was the length of time taken from the peak intensity of an adhesion to when it could no longer be seen.

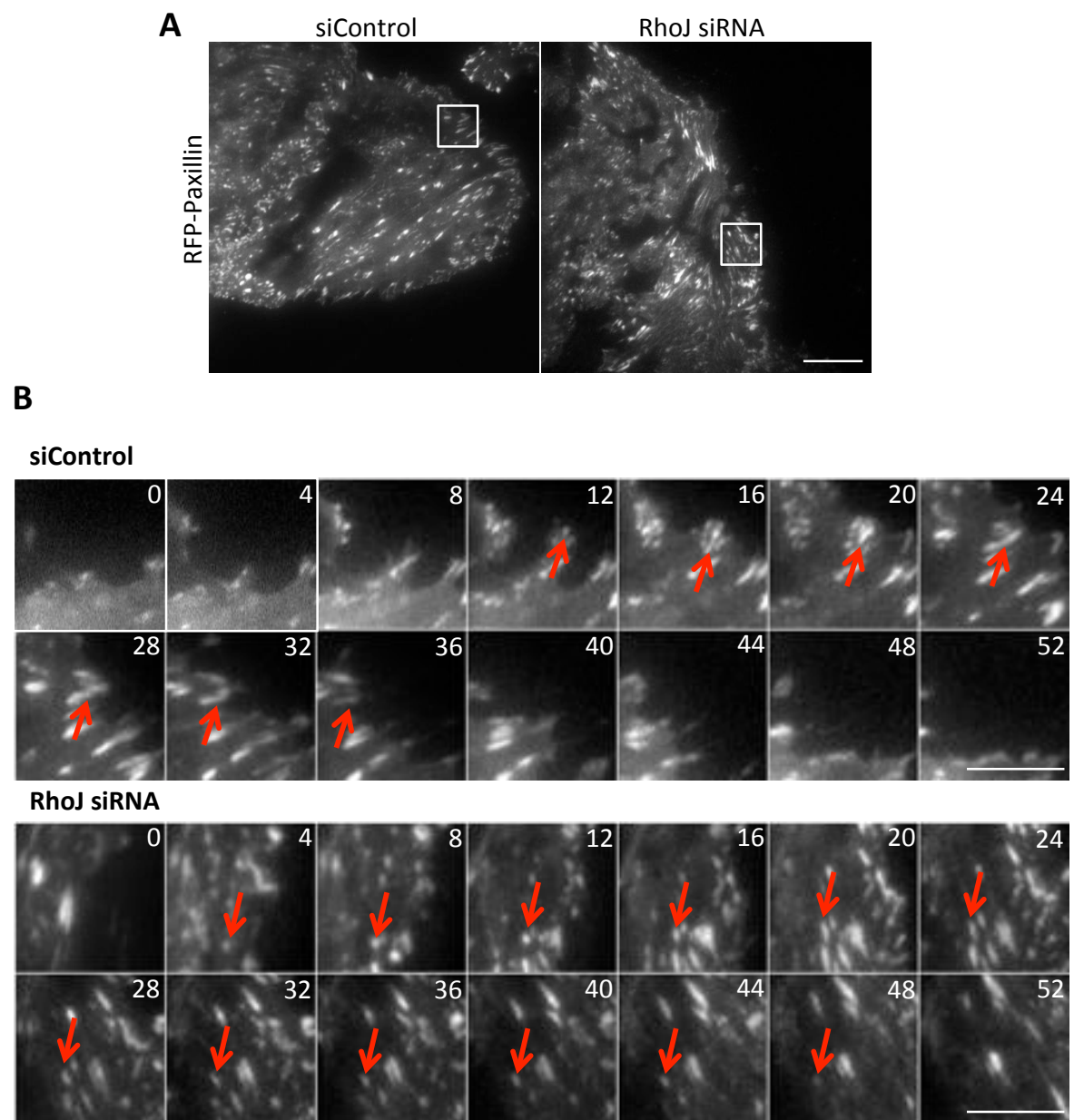


**Figure 3.6. Focal adhesion lifetime in HUVEC is prolonged upon knockdown of RhoJ expression.**

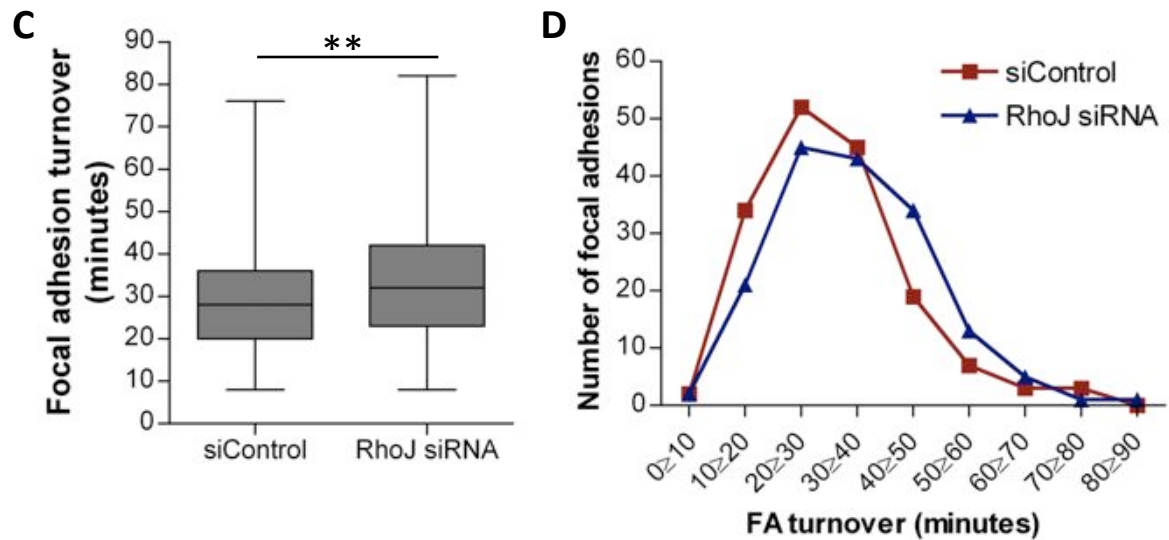


**Figure 3.6. Focal adhesion lifetime in HUVEC is prolonged upon knockdown of RhoJ expression.** HUVEC expressing RFP-Paxillin were plated, transfected with negative control duplex (siControl) or RhoJ specific siRNA 2 (RhoJ siRNA 2) and 2 days later, the monolayer wounded before imaging with TIRF microscopy. Cells at the edge of the scratch were monitored for 90 min, using timelapse imaging to take pictures every 2 min. **A-B.** At least 10 focal adhesions were tracked using the Cell Counter plug-in for ImageJ from 4 cells per condition, for 3 replicates using different HUVEC isolates (a total of 165 focal adhesions per condition). The whole of the cell analysed is shown in **A** (scale bar: 20  $\mu$ m) along with a close up region, indicated by a white box in **B** (scale bar: 10  $\mu$ m). **C.** Focal adhesion lifetime durations were recorded and data is presented as a box and whisker plot. The Mann Whitney test was used to test statistical significance (\*\*= $0.001 \leq p \leq 0.01$ ). **D.** Focal adhesion lifetime is displayed as a line graph to show the spread of data.



Durations of adhesion assembly and disassembly in both control and RhoJ knockdown cells were analysed using the Mann Whitney test, and this data is shown in the box plots in Figure 3.7.A and 3.7.B. While assembly rates (Figure 3.7.A) did not significantly alter between control and knockdown cells ( $p=0.8594$ ), there was a strong significance in the difference between the disassembly rates (Figure 3.7.B) in these two conditions ( $p=0.0001$ ).

Taken together, these data indicate that RhoJ mediates focal adhesion lifetime by specifically regulating disassembly. In order to confirm this role for RhoJ in focal adhesion disassembly, the next step was to investigate the effect of a dominant active RhoJ mutant on adhesion dynamics.

### **3.5 Investigating the effect of dominant active RhoJ expression on focal adhesion dynamics**

Given that the data gathered from cells with diminished RhoJ expression showed an increase in the duration of focal adhesion lifetime, it was crucial to investigate the effect of introducing a dominant active mutant of RhoJ (daRhoJ). Previous work to characterise the effect of daRhoJ showed that this mutant decreases focal adhesion numbers in HUVEC (Kaur, Leszczynska *et al.* 2011) and it was important to confirm whether it induced any change in focal adhesion dynamics.

In order to determine the effect of daRhoJ expression on focal adhesion lifetime, assembly and disassembly, HUVEC were doubly transduced with lentivirus encoding RFP-Paxillin and either GFP or GFP-daRhoJ. These cells were plated, and the following day the monolayer was wounded and migrating cells at the scratch edge imaged by TIRF microscopy. To ensure that

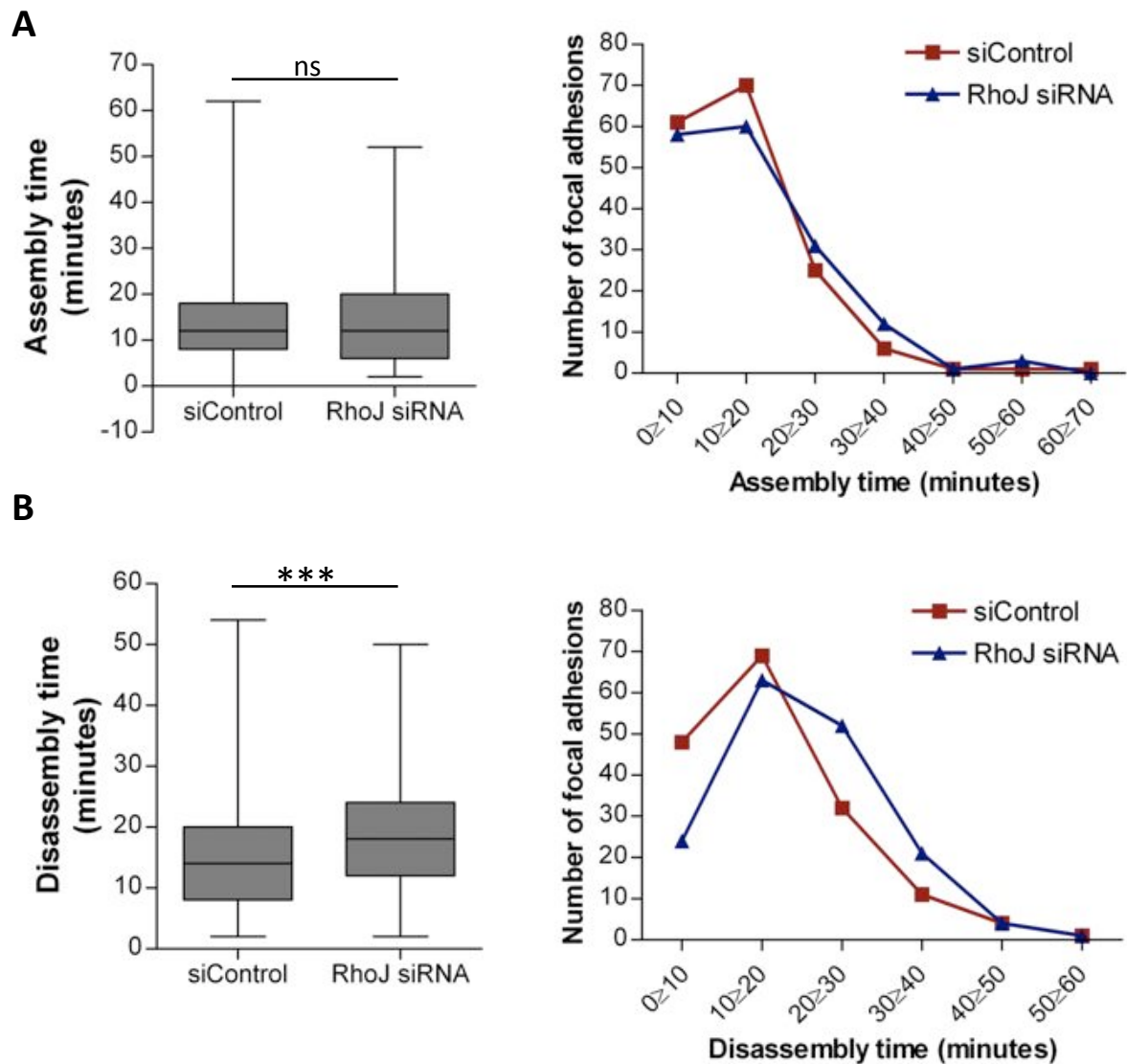


**Figure 3.7. Knockdown of RhoJ expression in HUVEC specifically prolongs focal adhesion disassembly.** Overall lifetime of focal adhesions in siControl and RhoJ siRNA 2 transfected RFP-Paxillin HUVEC (from Fig. 3.5) was separated into assembly and disassembly phases. The intensities of focal adhesions were measured throughout their duration using ImageJ. **A.** Assembly was characterised as the point from which focal adhesions were first visible to the point of highest intensity, and data displayed as a box and whisker plot and a line graph. No significant differences were found between assembly times of focal adhesions in siControl and RhoJ siRNA transfected cells, using the Mann Whitney test ( $ns=p>0.05$ ). **B.** Disassembly was characterised as being from the point of highest intensity to the point at which focal adhesions were no longer visible. Data are displayed as a box and whisker plot and a line graph. Analysis using the Mann Whitney test showed a significant difference between duration of focal adhesion disassembly in siControl and RhoJ siRNA transfected RFP-Paxillin expressing cells ( $***=p<0.001$ ).

any change in effect was due to the GFP-daRhoJ expression, cells were only examined if they expressed both RFP and GFP. These cells were monitored for 90 minutes (as in Section 3.4), with images taken every 2 minutes. Analysis was performed as per Section 3.4.

Figure 3.8.A shows colocalisation of GFP-daRhoJ and RFP-Paxillin. The panels in Figure 3.8.C show an example of focal adhesions that were monitored and analysed (magnified regions of interest are highlighted with a white box in Figure 3.8.B), the red arrows highlight these particular adhesions that appear and disappear in the time frame displayed. The box and whisker plot in Figure 3.8.D shows the absolute turnover times in GFP and GFP-daRhoJ expressing cells. When analysed using the Mann Whitney test a significant difference was found in overall turnover between these two conditions ( $p=0.001$ ), with GFP-daRhoJ expressing HUVEC displaying shorter focal adhesion lifetime durations compared to the GFP control. Figure 3.8.E shows the spread of data in 10 minute groups and demonstrates that in contrast to cells transduced with GFP only, GFP-daRhoJ expressing cells show a leftwards shift with a sharp peak in lifetime duration between 10-20 minutes, compared to a much broader spread between 10 and 40 minutes for adhesions in GFP control cells. These data are complimentary to those in Section 3.4, where RhoJ knockdown led to a rightwards shift and longer durations of focal adhesion lifetime, and together strongly indicate a role for RhoJ in regulating this process.

Since RhoJ knockdown led to an increase in focal adhesion disassembly times, adhesion lifetime durations in GFP/GFP-daRhoJ expressing cells were also separated into assembly and disassembly phases to determine whether there was similarly a specific effect on disassembly. Once again, individual adhesions already tracked in Figure 3.8 were outlined

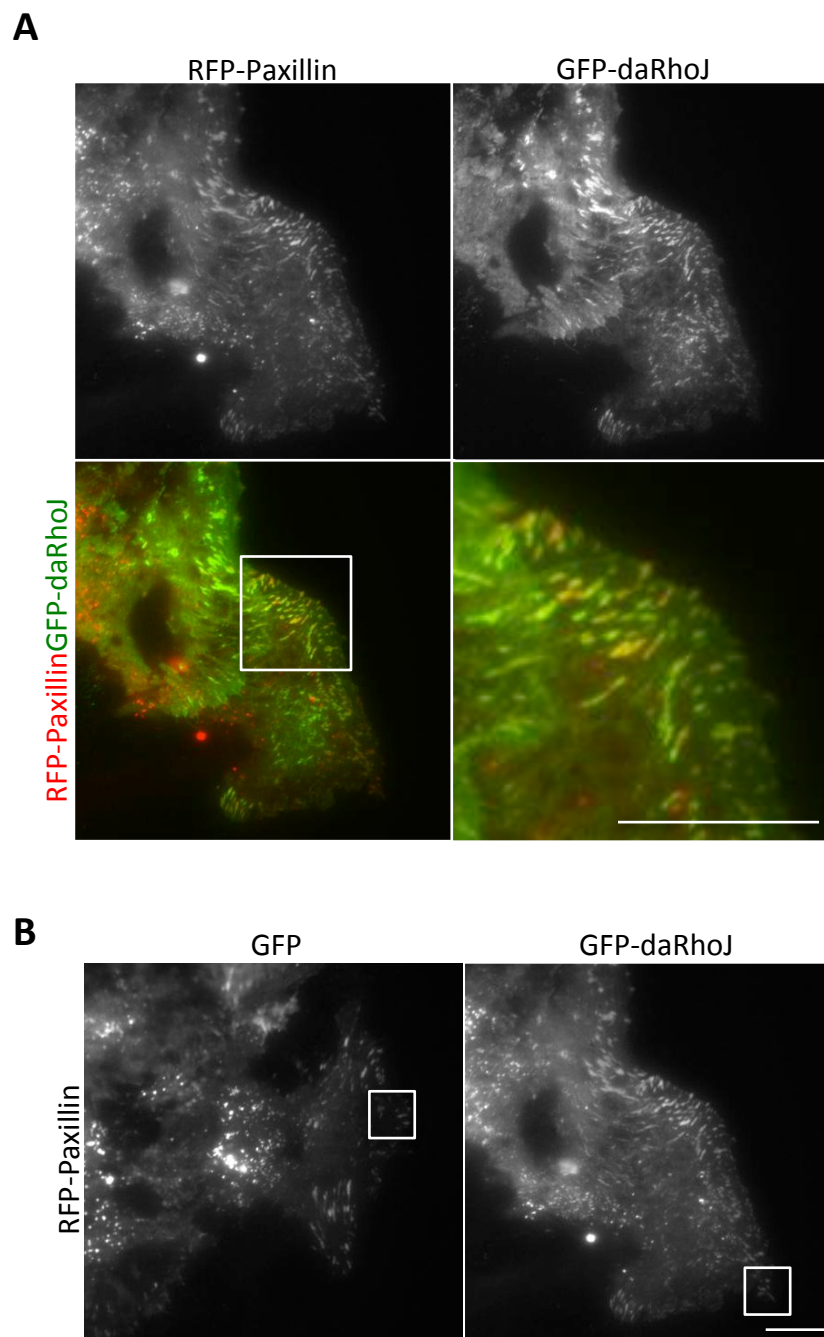
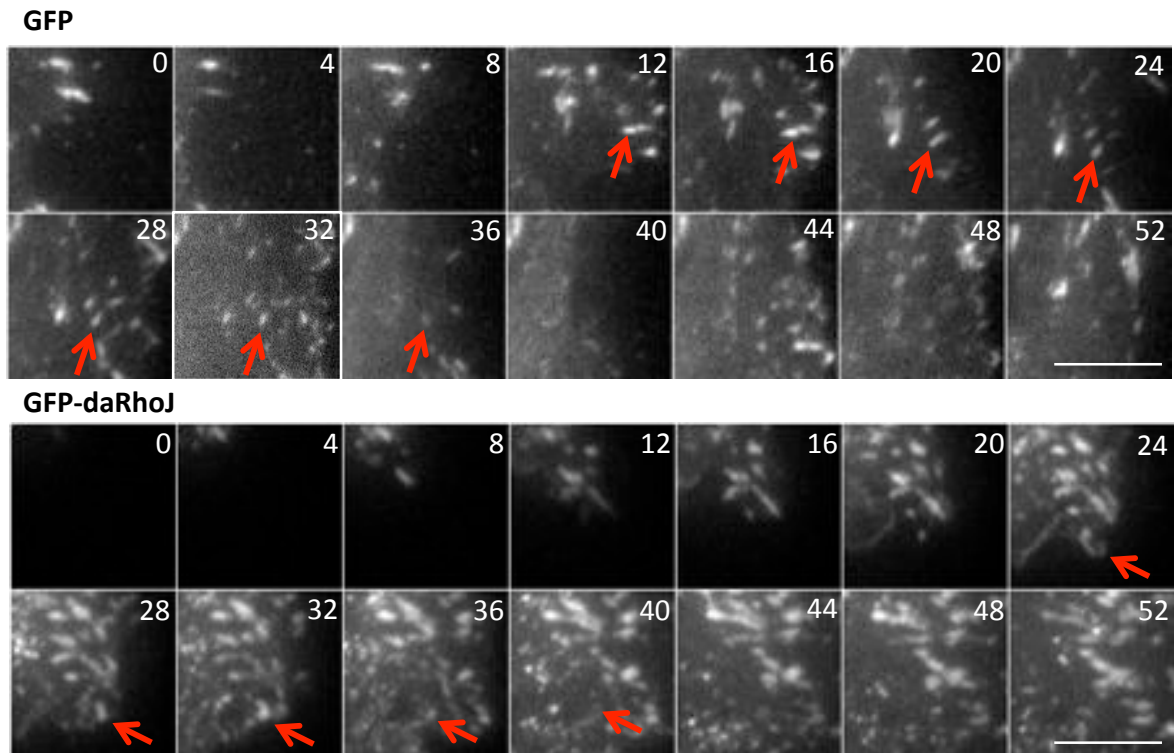
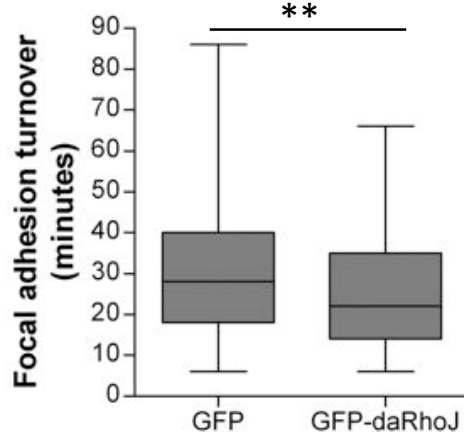


**Figure 3.8. Focal adhesion lifetime in HUVEC is shortened upon expression of a dominant active mutant of RhoJ.**

C



D



E

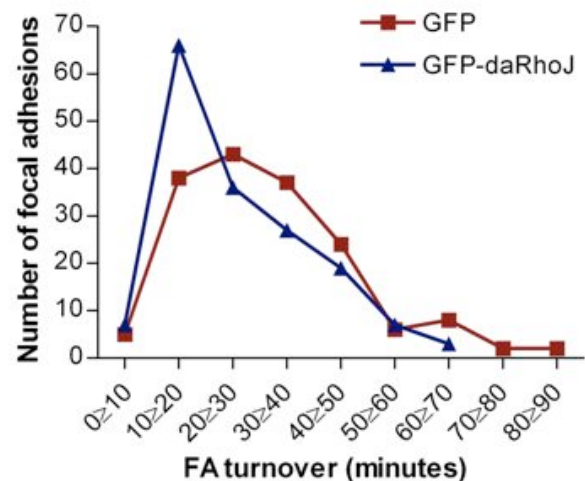


**Figure 3.8. Focal adhesion lifetime in HUVEC is shortened upon expression of a dominant active mutant of RhoJ.** HUVEC expressing RFP-Paxillin along with either GFP or GFP-dominant active RhoJ (daRhoJ) were plated and the following day the monolayer wounded before imaging with TIRF microscopy. Cells expressing GFP/GFP-daRhoJ at the edge of the scratch were monitored for 90 min, using timelapse imaging to take pictures every 2 min. **A.** GFP-daRhoJ co-localises with RFP-Paxillin at focal adhesions. **B-C.** At least 10 focal adhesions were tracked using the Cell Counter plug-in for ImageJ from 4 cells per condition, for 3 replicates using different HUVEC isolates (a total of 165 focal adhesions per condition). The whole of the cell analysed is shown in **B** (scale bar: 20  $\mu$ m) along with a close up region, indicated by a white box in **C** (scale bar: 10  $\mu$ m). **D.** Focal adhesion lifetime durations were recorded and data is presented as a box and whisker plot. The Mann Whitney test was used to test statistical significance (\*\*= $0.001 \leq p \leq 0.01$ ). **E.** Focal adhesion lifetime is displayed as a line graph to show the spread of data.

and mean grey values measured, with assembly and disassembly determined as described in Section 3.4. When analysed using the Mann Whitney test, assembly durations did not significantly alter between GFP and GFP-daRhoJ expressing cells, as shown in Figure 3.9.A ( $p=0.7075$ ). In contrast, however, disassembly was markedly shorter in GFP-daRhoJ expressing HUVEC compared to GFP controls ( $p<0.0001$ ). The box and whisker plot, along with the histogram in Figure 3.9.B show this decrease in adhesion disassembly durations, with more than double the number of GFP-daRhoJ adhesions disassembling in 10 minutes or less compared to those in GFP only expressing cells.

Cumulatively, these data suggest that when in its active state RhoJ enhances focal adhesion disassembly. When considered along with the data presented in Section 3.4, there appears to be strong evidence for the role of RhoJ in regulating focal adhesion disassembly. This is of particular interest since an interaction between RhoJ and the GIT/PIX complex was previously identified by our group (Katarzyna Leszczynska, PhD thesis). This complex has previously been shown to play a part in regulating focal adhesion disassembly (Zhao, Manser *et al.* 2000), and it may function in concert with RhoJ in this process.

### **3.6 Investigating the role of RhoJ in focal adhesion targeting by microtubules**

While the data described in Sections 3.4 and 3.5 demonstrate a clear role for RhoJ in regulating focal adhesion disassembly, there are a number of different mechanisms by which this can occur. One such mechanism is the targeting of focal adhesions by microtubules (Efimov and Kaverina 2009).

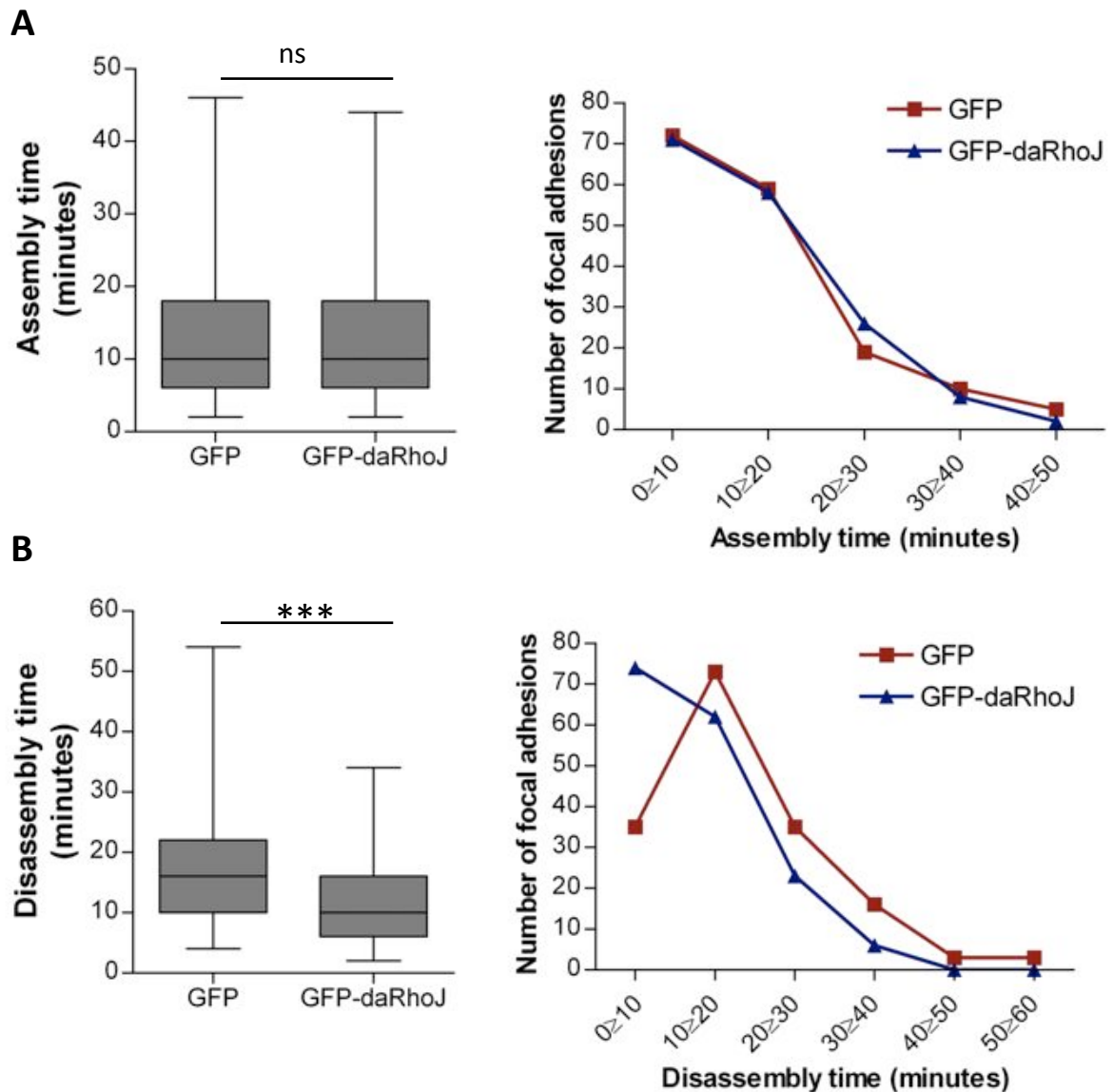


**Figure 3.9. Dominant active RhoJ expression in HUVEC leads to decreased focal adhesion disassembly time.** Overall lifetime of focal adhesions in GFP control and GFP-daRhoJ expressing RFP-Paxillin HUVEC (from Fig. 3.7) was separated into assembly and disassembly phases. The intensities of focal adhesions were measured throughout their duration using ImageJ. **A.** Assembly was characterised as the point from which focal adhesions were first visible to the point of highest intensity, and data displayed as a box and whisker plot and a line graph. No significant differences were found between assembly times of focal adhesions in GFP and GFP-daRhoJ expressing cells, using the Mann Whitney test ( $ns=p>0.05$ ). **B.** Disassembly was characterised as being from the point of highest intensity to the point at which focal adhesions were no longer visible. Data are displayed as a box and whisker plot and a line graph. Analysis using the Mann Whitney test showed a significant difference between duration of focal adhesion disassembly in GFP and GFP-daRhoJ expressing RFP-Paxillin cells ( $***=p<0.001$ ).

In order to determine whether RhoJ mediates focal adhesion disassembly via microtubule targeting, HUVEC were transfected with control (siControl) or RhoJ specific (RhoJ siRNA) siRNA duplexes. These cells were replated onto coverslips, then 48 h after transfection they were fixed and stained for the focal adhesion protein phospho-paxillin and the microtubule protein tubulin. Since RhoJ knockdown leads to slower disassembly of adhesions, our hypothesis was that microtubules may be less able to target focal adhesions and as such this may be reflected in the immunofluorescent staining seen in control and RhoJ knockdown cells.

The panels in Figure 3.10.A show representative cells stained for microtubules (tubulin) and focal adhesions (phospho-paxillin). Microtubule targeting was calculated by counting the number of adhesions positive for phospho-paxillin and calculating the percent also positive for tubulin. Five cells per condition were analysed from 3 independent experiments, and the percentage microtubule targeting shown in Figure 3.10.B. While there does appear to be a small decrease in the percentage of adhesions that co-localise with microtubule ends in RhoJ knockdown cells compared to controls, this was not statistically significant ( $p=0.0681$ ). Broadly, the microtubules in RhoJ knockdown cells are phenotypically normal, however there are some cases where the microtubules do not reach the sites of adhesions. It should, however, be noted that live cell imaging would be a more appropriate method of assessing focal adhesion targeting, and TIRF could be used in this instance to distinguish a role for RhoJ in this process. Based on the data shown in Figure 3.10, it is possible that a difference in the level of microtubule targeting in control and RhoJ knockdown cells would be found.



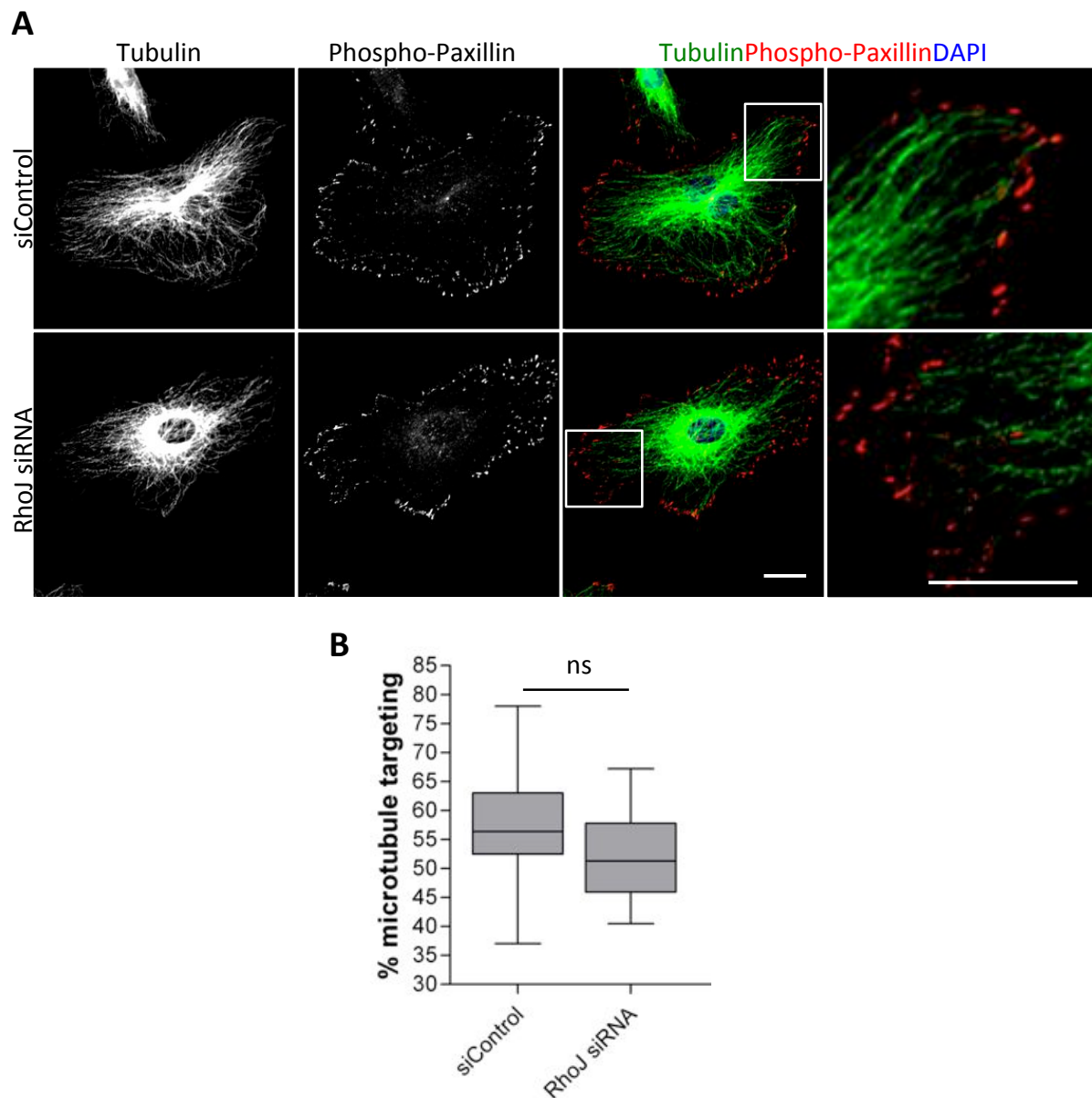


**Figure 3.10. Knockdown of RhoJ expression does not alter microtubule targeting of focal adhesions.** HUVEC were transfected with control (siControl) or RhoJ specific (RhoJ siRNA 2) siRNA duplexes. **A.** After 48 h, cells were fixed and stained with tubulin and phospho-paxillin, and confocal microscopy performed. Scale bar: 20  $\mu$ m. **B.** Focal adhesions were counted using the CellCounter plug-in on ImageJ and the percentage of adhesions exhibiting co-localisation with tubulin was calculated in 5 cells per condition, from 3 independent experiments. Data are presented as a box and whisker plot, the Mann Whitney test was used to test statistical significance, with no significant difference found between control and RhoJ knockdown cells (ns= $p>0.05$ ).

### 3.7 Investigating the effect of RhoJ on focal adhesion size

Upon imaging of GFP and GFP-daRhoJ expressing HUVEC by confocal microscopy, it was noted that there appeared to be differences in focal adhesion size between these conditions. In order to quantify this, HUVEC expressing GFP only, GFP wild-type RhoJ or GFP dominant-active RhoJ were plated sparsely and the following day, fixed and stained for vinculin. Cells were imaged by confocal microscopy and 15 focal adhesions outlined on ImageJ in 3 cells per condition from 3 independent experiments. Areas were measured and experimental groups were tested for statistically significant differences using the Mann Whitney test.

The images in Figure 3.11.A show representative cells stained for vinculin. When statistically analysed, as shown in the box and whisker plot in Figure 3.11.B, significant differences were found between focal adhesion areas of GFP only and GFP-wtRhoJ cells ( $p=0.0004$ ), GFP only and GFP-daRhoJ cells ( $p<0.0001$ ), and GFP-wtRhoJ and GFP-daRhoJ cells ( $p<0.0001$ ).

In order to investigate the effect reducing RhoJ expression, HUVEC were transfected with either control or RhoJ specific siRNA duplexes. After 24 h, cells were plated sparsely onto coverslips, then fixed and stained for vinculin the next day. Again, cells were imaged by confocal microscopy and at least 20 adhesions per cell for 3 cells in each condition for three independent experiments, were outlined and measured using ImageJ.

Images in Figure 3.12.A are representative of control and RhoJ knockdown cells stained for vinculin. The box and whisker plot in Figure 3.12.B shows the result of analysis of focal adhesion areas in these cells, with a significant decrease found in adhesion size of RhoJ knockdown cells compared to controls ( $p<0.0001$ ). These data together suggest that RhoJ

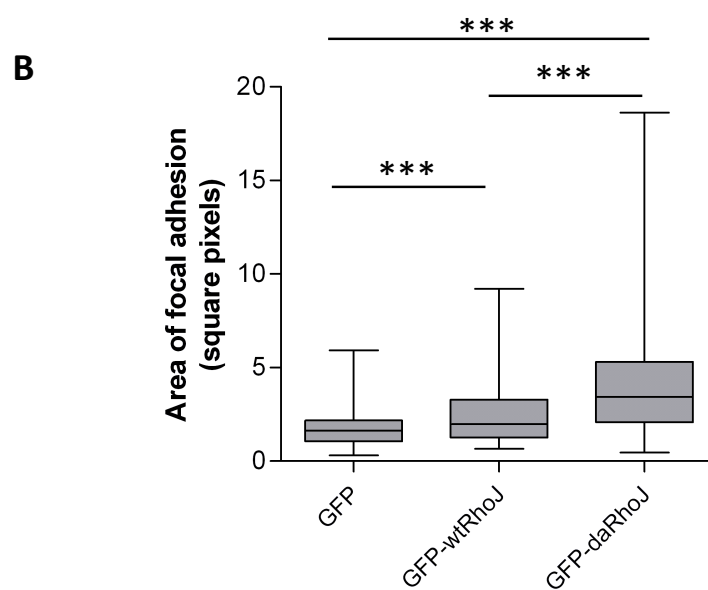
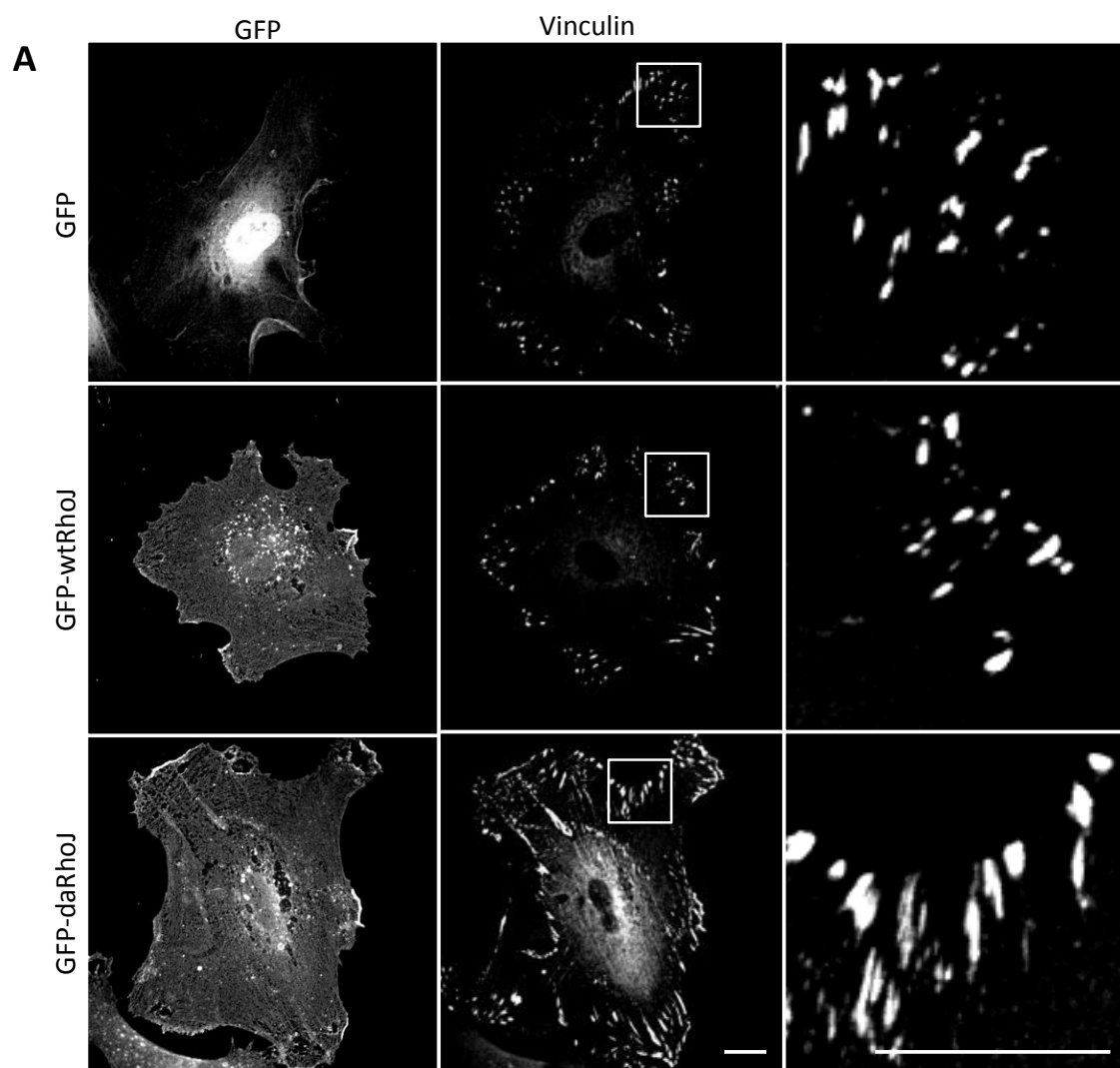


**Figure 3.11.** GFP-daRhoJ expression increases focal adhesion size in HUVEC, compared to GFP control expressing cells.

**Figure 3.11. GFP-daRhoJ expression increases focal adhesion size in HUVEC, compared to GFP control expressing cells.** HUVEC stably expressing GFP, GFP-wtRhoJ or GFP-daRhoJ were fixed and stained for vinculin. **A.** Cells were imaged by confocal microscopy. Scale bar: 20  $\mu\text{m}$  **B.** Focal adhesion size was measured using ImageJ, and data displayed as a box and whisker plot. The Mann Whitney test was used to assess statistical significance (\*\*=  $p < 0.01$ , \*\*\*=  $p < 0.001$ ).

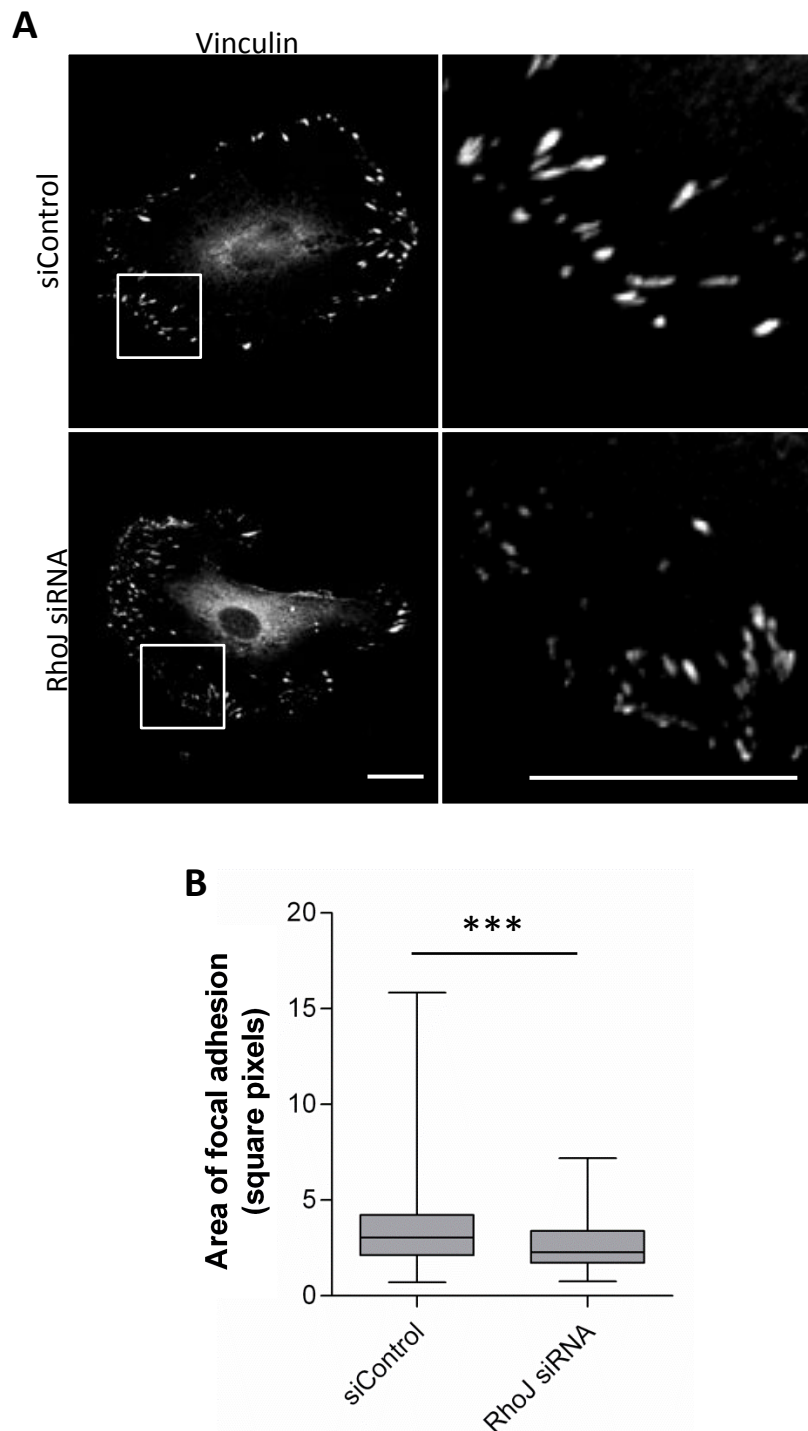


**Figure 3.12. RhoJ knockdown results in decreased focal adhesion size in HUVEC, compared to siControl transfected cells.** HUVEC were transfected with control (siControl) or RhoJ specific (RhoJ siRNA 2) siRNA were fixed and stained for vinculin. **A.** Cells were imaged by confocal microscopy. Scale bar: 20  $\mu$ m **B.** Focal adhesion size was measured using ImageJ, and data displayed as a box and whisker plot. The Mann Whitney test was used to assess statistical significance (\*\*\*=  $p < 0.001$ ).

positively regulates the size of adhesions in addition to regulating focal adhesion disassembly.

### **3.8 Generation of a RhoJ biosensor**

While previous data from our laboratory has shown that endogenous RhoJ and a dominant active mutant localise to focal adhesions, it has not yet been elucidated whether RhoJ is active at these sites. Biosensors to investigate activation of other Rho GTPases have been widely used, so a RhoJ biosensor was constructed. This was achieved by adapting a Rac1 biosensor, by replacing Rac1 with RhoJ. The biosensor construct contains both an RFP and GFP tag, along with a Pak binding domain (PBD). The PBD contains a CRIB domain, which is known to interact with active RhoJ (Vignal, De Toledo *et al.* 2000). As such, when RhoJ is active and interacts with the Pak-binding domain (PBD) the GFP and RFP tags come into close proximity, enabling energy transfer between the fluorescent proteins. This energy transfer can be measured as FRET, and thus wherever FRET occurs is identified as a site of RhoJ activation. Figure 3.13.A shows a diagram of the biosensor in its inactive and active states.

It was first important to establish where the newly generated RhoJ biosensor localised. HUVEC stably expressing the biosensor were imaged by TIRF microscopy and an example cell is shown in Figure 3.13.B. Initially, expression and localisation of the construct was confirmed by colocalisation of RFP and GFP, and was found to exhibit a pattern similar to that of the GFP-daRhoJ construct previously used for TIRF investigations.

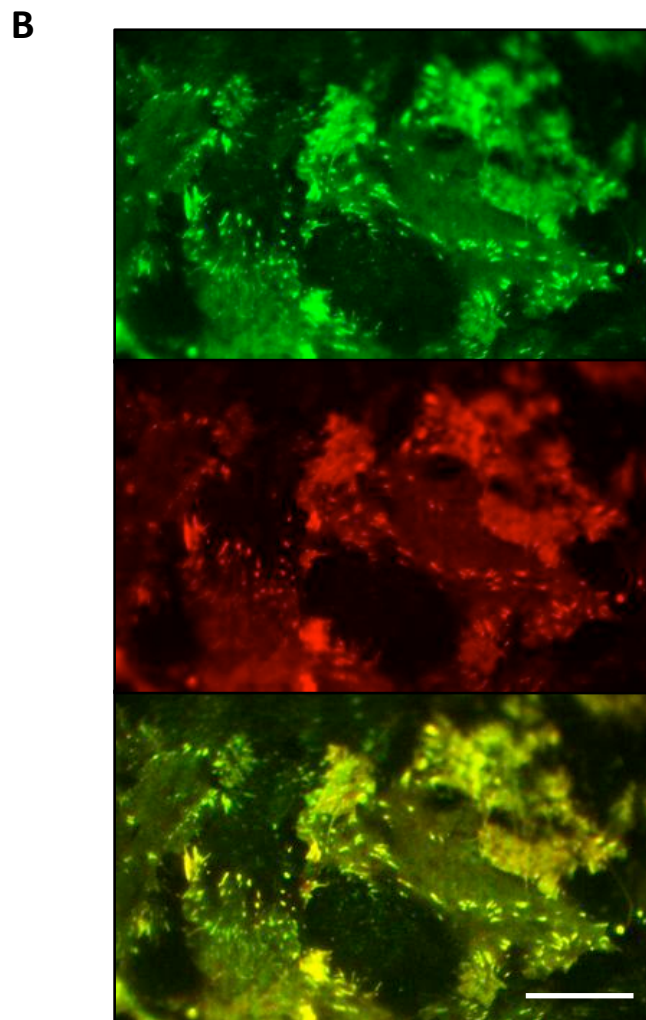
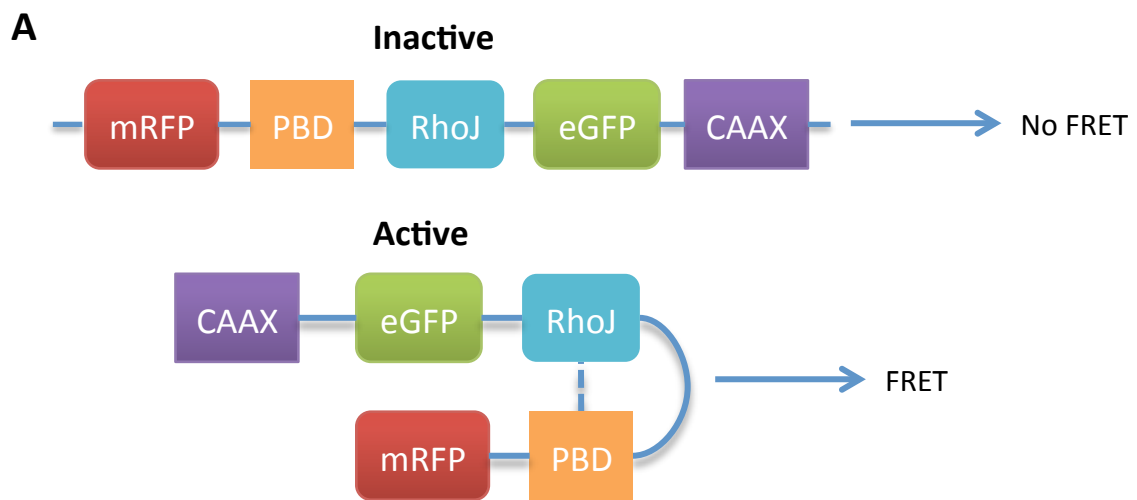


**Figure 3.13. Construction and expression of a RhoJ biosensor. A.** Structure of the RhoJ biosensor in inactive and active conformations. **B.** Representative TIRF microscopy image of the red and green channels and a merged image from HUVEC expressing the RhoJ biosensor. Scale bar: 10  $\mu\text{m}$ .

The time limitations of these PhD studies meant that only a small pilot study could be undertaken to assess whether RhoJ is active at focal adhesions. In order to do this, HUVEC expressing the RhoJ biosensor, and control cells co-expressing RFP-Paxillin and GFP-daRhoJ were imaged by TIRF microscopy. Images were taken of cells on both red and green channels and then samples bleached for 1 min using the red TIRF laser. Images were then taken again of both channels after bleaching. The GFP tag ordinarily acts as a donor of energy to the RFP tag if they are in close contact, however photobleaching destroys the RFP fluorophores, meaning that energy transfer no longer occurs since RFP cannot fluoresce. As a result, if energy is being transferred from the GFP tag to the RFP tag, the photobleaching process will lead to an increase in GFP fluorescence signal. In a scenario when the GFP and RFP tags are not interacting, the bleaching of the RFP fluorophores will also bleach the GFP fluorophores to some extent, and there will be a small decrease in green fluorescent signal post-bleach.

Representative images of control and biosensor expressing cells in the red and green channels both pre- and post-bleaching are shown in Figure 3.14. In an attempt to analyse these images, 5 focal adhesions were selected from each of 3 cells per condition (i.e. a total of 15 focal adhesions per condition). Adhesions were outlined on ImageJ and mean grey values measured pre- and post-bleaching, with the same regions of interest used for both the red and green channels. Analyses are presented as a scatter plot in Figure 3.15. As expected the red fluorescence is reduced to approximately 50% in control cells and 40% in biosensor cells after bleaching. In control cells, the green channel also shows a reduction in fluorescence, albeit to a lesser extent (around 90% of the original fluorescence). The biosensor cells however do not show a reduction in green fluorescence after bleaching of



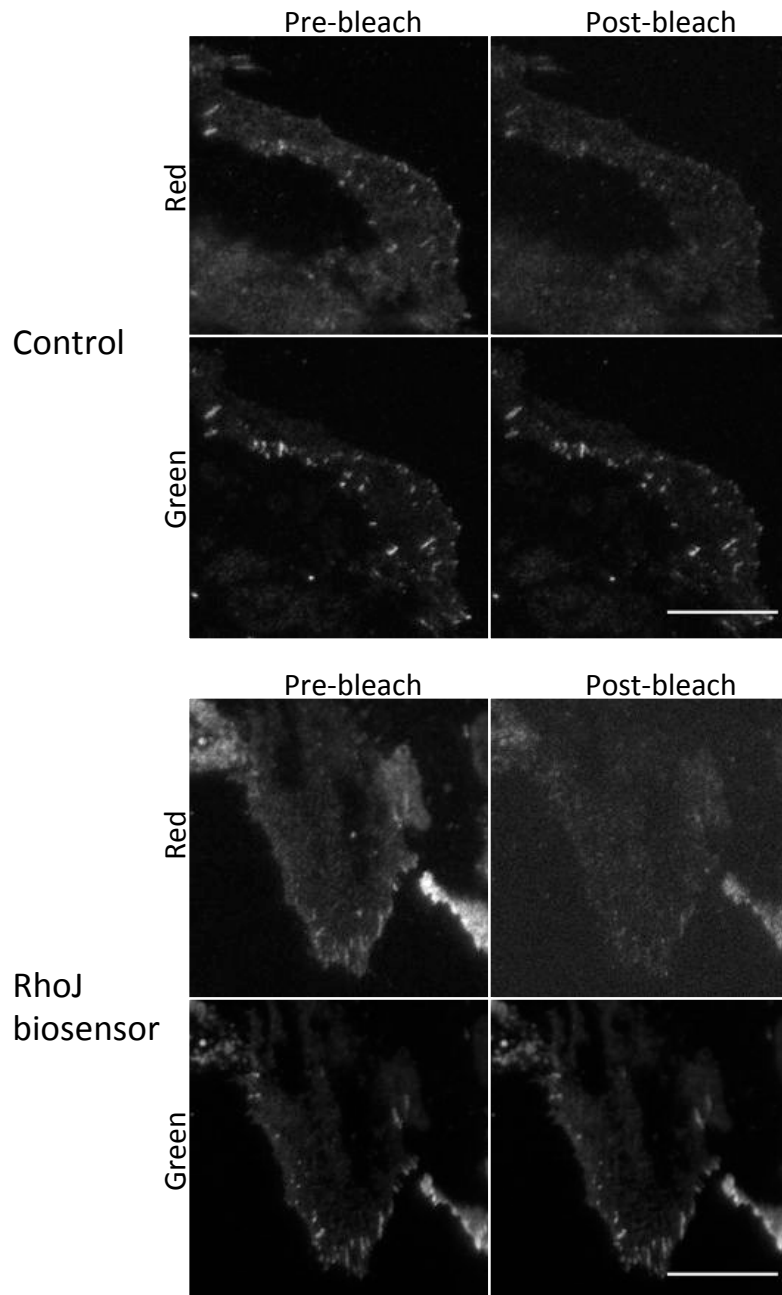


**Figure 3.14. Pre- and post-bleaching images of adhesions from control and RhoJ biosensor expressing cells in the red and green channels.** TIRF microscopy was performed using control RFP/GFP expressing cells and RhoJ biosensor cells. Images were taken on both the red and green channels before and after bleaching of the red channel . Scale bar: 10  $\mu$ m

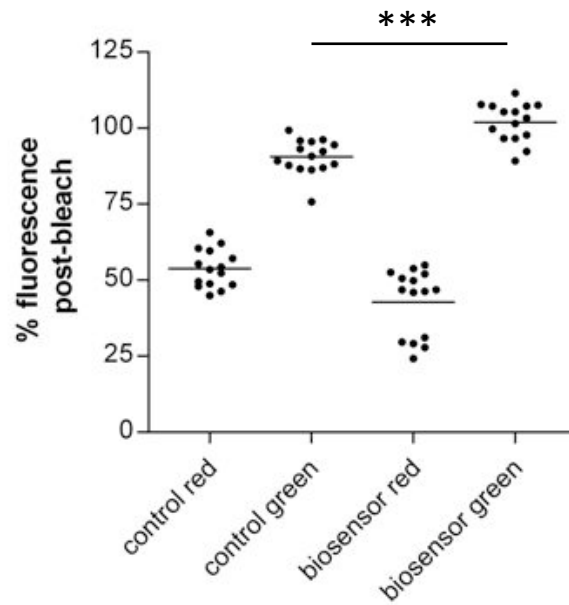


**Figure 3.15. Green fluorescence subtly increases in RhoJ biosensor expressing cells after red-bleaching.** HUVEC stably expressing control RFP and GFP constructs or the RhoJ biosensor were bleached on the red channel and fluorescence measured before and after bleaching. Percentage of fluorescence remaining after bleaching was calculated and displayed as a scatter plot, with lines indicating mean values. The Mann-Whitney test found a significant difference between green fluorescence in control and biosensor cells (\*\*=  $p < 0.01$ , \*\*\*=  $p < 0.001$ ).

the red channel, with a small average increase noted (around 105%). Analysis using the Mann Whitney test found the difference in green-bleaching to be significant ( $p=0.0001$ ).

It should however be noted that the system used for this pilot study is certainly not ideal and an automated system would be more accurate in terms of the duration of bleaching, and the focussing of the image after the photobleaching process. Furthermore, in order to determine the activation state of RhoJ at focal adhesions, ratiometric analysis must be performed. Nevertheless, the data presented above shows that the biosensor expresses correctly, and is a promising tools for future investigation into activation of RhoJ.

### **3.9 Discussion**

The results presented in this chapter demonstrate that RhoJ is a novel regulator of focal adhesion dynamics. Studies of RFP-Paxillin expressing cells with manipulated RhoJ expression suggest that this small GTPase promotes focal adhesion turnover, specifically focal adhesion disassembly. Additionally, the data show that RhoJ regulates focal adhesion size. Preliminary investigations using a GFP/RFP biosensor also indicate that RhoJ is active i.e. bound by GTP at focal adhesions, which is consistent with its functions in mediating adhesion disassembly. Given that RhoJ has previously been shown to regulate focal adhesion numbers, endothelial cell migration and tube formation, the data in this chapter suggest that these phenotypes are a consequence of its role in promoting adhesion disassembly.

The role of RhoJ in mediating focal adhesion disassembly is especially interesting considering the partner proteins that have been identified for this GTPase. Mass spectrometry and subsequent GST pulldowns, yeast-two-hybrid binding assays and immunofluorescent

staining has shown that RhoJ appears to form a complex with two other focal adhesion proteins, GIT1 and  $\beta$ -PIX (Katarzyna Leszczynska, PhD thesis). A number of studies have implicated the GIT/PIX complex in regulating adhesion turnover and disassembly in particular (Zhao, Manser *et al.* 2000, Nayal, Webb *et al.* 2006, Feng, Baird *et al.* 2010, Kuo, Han *et al.* 2011), and it seems likely that RhoJ acts in concert with these proteins to promote adhesion disassembly in endothelial cells. The interaction between GIT1 and paxillin is thought to induce changes to the conformation or phosphorylation state of paxillin, and drive its disassembly from adhesions. In turn, this interaction is potentiated by  $\beta$ -PIX (Zhao, Manser *et al.* 2000) and RhoJ may also play a role in this potentiation; certainly, expression of a dominant active mutant of RhoJ increased the loss of paxillin from adhesions.

Additionally, another Rho GTPase Wrch-1, which is part of the Cdc42-like subfamily along with RhoJ has been shown to play a role in adhesion disassembly. While Wrch-1 is an atypical Rho protein without intrinsic GTPase activity, multiple studies have demonstrated that manipulation of this protein affects focal adhesion numbers and dynamics (Saras, Wollberg *et al.* 2004, Chuang, Valster *et al.* 2007). Much like RhoJ, over-expression of Wrch-1 induced adhesion disassembly, however while Kaur *et al.* showed that knockdown of RhoJ increased levels of phospho-myosin light chain, Chuang and colleagues found the opposite upon knockdown of Wrch-1 (Chuang, Valster *et al.* 2007, Kaur, Leszczynska *et al.* 2011); thus it seems that RhoJ functions via a distinct pathway from Wrch-1 in promoting focal adhesion disassembly.

Contractility and focal adhesion dynamics are closely related and interdependent, and while increased tension and myosin II activity stimulates adhesion maturation and stability,

disassembling adhesions are subject to less force (Broussard, Webb *et al.* 2008, Parsons, Horwitz *et al.* 2010, Ciobanasu, Faivre *et al.* 2012). Knockdown of RhoJ increases levels of phospho-myosin light chain (pMLC) and contractility, suggesting that adhesions in these cells are under increased tension and therefore more stable, which may explain why disassembly is significantly prolonged. Additionally, given that dominant active RhoJ has previously been shown to reduce cell contraction (Kaur, Leszczynska *et al.* 2011), and here it has been demonstrated that active RhoJ promotes adhesion disassembly, it is possible that RhoJ modulates adhesion dynamics by negatively regulating contractility. This hypothesis is further supported by studies by Yuan and colleagues, who determined a role for RhoJ in regulating the activities of other Rho GTPases including RhoA, Rac1 and Cdc42 (Yuan, Sacharidou *et al.* 2011), since ROCK, a RhoA effector, phosphorylates MLC.

Components of focal adhesions are also able to regulate contractility. PAK, for example, phosphorylates and inhibits MLCK, therefore decreasing levels of pMLC and contractility (Sanders, Matsumura *et al.* 1999). FAK is also known to positively regulate focal adhesion disassembly, and in its absence, increased RhoA activity and pMLC levels are observed. Knockout of FAK in fibroblasts also impaired recruitment of PAK and GIT2 to adhesions (Schober, Raghavan *et al.* 2007). As described above, previous work in our laboratory has identified an interaction between RhoJ, GIT1 and  $\beta$ -PIX (Katarzyna Leszczynska, PhD thesis), and we postulate that RhoJ primarily regulates focal adhesion disassembly in complex with GIT and PIX. Therefore, it is possible that an effect on contractility is secondary to the effect on focal adhesion disassembly. Knockdown of RhoJ induces the formation of smaller focal adhesions that disassemble more slowly. These adhesions are likely to contain a lesser

abundance of components that negatively regulate contractility, meaning that RhoJ knockdown results in increased phosphorylation of MLC and tension as a result.

Another method by which adhesions can be disassembled is via endocytosis and early investigations into the function of RhoJ indicated a role in this process, with overexpressed protein localising to early and sorting endosomes in HeLa cells (de Toledo, Senic-Matuglia *et al.* 2003). Co-localisation was noted between RhoJ and Rab5, which has previously been shown to mediate internalisation and recycling of  $\beta$ 1 integrins (Pellinen, Arjonen *et al.* 2006). Activation of Rab5 is also crucial for focal adhesion disassembly in MDA-MB-231 tumour cells (Mendoza, Ortiz *et al.* 2013). Previous investigations in our laboratory failed to show co-localisation between RhoJ and Rab5-positive vesicles (Katarzyna Leszczynska, PhD thesis), however vesicular patterning is sometimes seen in cells with high expression of GFP-daRhoJ, so it is possible that RhoJ plays some role in the uptake and recycling of focal adhesion components from the leading edge. GIT, a partner protein of RhoJ also acts as a GAP for members of the Arf family of GTPases. One of these Arf GTPases is Arf6, which is involved in mediating clathrin dependent and independent internalisation of ligands from the plasma membrane; hydrolysis of Arf6-GTP by such GAPs is necessary for further trafficking into sorting and recycling endosomes (D'Souza-Schorey and Chavrier 2006). Given the indirect link between RhoJ and Arf6, and the role of endocytosis in focal adhesion disassembly, it cannot be ruled out that RhoJ regulates this process in some way.

Microtubules are known to mediate focal adhesion disassembly by targeting adhesions and facilitating processes such as calpain-mediated proteolysis of components of the adhesions (Broussard, Webb *et al.* 2008). While knockdown of RhoJ did decrease the percentage of

adhesions targeted by microtubules in HUVEC compared to controls, this was not significantly different with the numbers of cells analysed. For further study, live cell imaging could be used to visualise microtubule targeting of adhesions. This would be a more sensitive technique and could elucidate the true function of RhoJ in regulating microtubule dynamics. Additionally, it would be interesting to assess the role of RhoJ in the processes microtubules utilise to disassemble the adhesion complex, especially since certain GEFs are regulated by binding to microtubules, enabling contraction of stress fibres and destruction of the adhesion (Broussard, Webb *et al.* 2008).

Since RhoJ mediates focal adhesion dynamics it is not altogether surprising that it also regulates adhesion size, however the results are somewhat counterintuitive and the function of RhoJ in mediating RhoA activity would suggest the opposite should be true. RhoA has a well-defined role in regulating adhesion maturation, and it is thought that RhoJ inhibits RhoA activity (Yuan, Sacharidou *et al.* 2011). Thus it would be expected that active RhoJ would prevent this maturation and growth leading to the presence of small adhesions, however upon expression of GFP-daRhoJ significantly larger adhesions were observed compared to controls. Others have shown that knockdown of  $\beta$ -PIX led to the induction of larger adhesions (Kuo, Han *et al.* 2011) and since RhoJ interacts with this protein it may be expected that RhoJ knockdown would phenocopy that of  $\beta$ -PIX. However, active RhoJ may recruit a greater abundance of its partner proteins and other associated adhesion proteins, leading to the generation of larger focal adhesions. It is possible that these large adhesions are intrinsically unstable and rapidly disassemble as a result; or perhaps the increased recruitment of partner proteins such as GIT and PIX triggers faster disassembly.

The finding that RhoJ is activated at focal adhesions is logical given its function in mediating the dynamics of these complexes, however it also supports the theory that RhoJ is actively involved in regulating the adhesion assembly and disassembly cycle. Biosensors have previously been used to assess Rho GTPase activation *in vitro* and have shed light on the regions of the cell that these proteins are found to be active; RhoA, Rac1 and Cdc42 for example are all active at the leading edge (Machacek, Hodgson *et al.* 2009). Given that RhoJ regulates migration and tube formation of endothelial cells, it could be hypothesised that RhoJ is also likely to be active at the leading edge, and *in vivo* this may translate to activation in tip cells in newly-forming vessels.

In conclusion, the work presented thus far shows that RhoJ appears to be bound by GTP at adhesions and actively regulates focal adhesion disassembly, potentially via its interactions with GIT and PIX (which will be investigated further in Chapter 4). In addition to regulating adhesion dynamics, RhoJ mediates the size of these assemblies, potentially due to the recruitment of other partner proteins to the complex.



## **CHAPTER 4**

### **The physical and functional interaction of RhoJ with the GIT/PIX complex**

## 4.1 Introduction

Previous work by Katarzyna Leszczynska (PhD thesis, 2011) sought to identify interacting partners of RhoJ. Pulldowns from HUVEC lysates using RhoJ GST fusion proteins and subsequent mass spectrometry identified a list of candidate proteins which were later tested by yeast two-hybrid and pulldowns. Of the candidate proteins, the focal adhesion components GIT1 and  $\beta$ -PIX were confirmed as partner proteins, with a seemingly direct interaction observed between RhoJ and GIT1 and an indirect interaction between RhoJ and  $\beta$ -PIX.

GIT1 and  $\beta$ -PIX are proteins of the focal adhesion complex that interact with one another via the Spa homology domain (SHD) and coiled coil of GIT1 and the carboxyl terminal 200 amino acids of  $\beta$ -PIX (Premont, Perry *et al.* 2004). GIT1 interacts with paxillin via its focal adhesion targeting homology (FAH) domain in order to recruit to adhesions, while  $\beta$ -PIX localises to these structures by forming a complex with GIT (Rosenberger and Kutsche 2006, Frank and Hansen 2008).  $\beta$ -PIX also associates with PAK, and is known to be crucial for its recruitment to adhesions. PAK in turn phosphorylates paxillin, which strengthens its interaction with GIT. The GIT/PIX complex has previously been reported to have a role in focal adhesion disassembly (Zhao, Manser *et al.* 2000), which is particularly interesting given the data presented in Chapter 3.

Both GIT1 and  $\beta$ -PIX are also known to exert catalytic activity towards GTPases. GIT1 is a GAP for members of the ADP-ribosylation factor (Arf) family of Ras like G proteins including Arf6, which regulates membrane trafficking and actin remodelling (D'Souza-Schorey and Chavrier 2006). Full length  $\beta$ -PIX meanwhile acts as a GEF towards Cdc42, however this activity is

reliant on phosphorylation of Tyr442 by Src, which represses the auto-inhibition induced by the T1 insert (Feng, Albeck *et al.* 2002, Feng, Baird *et al.* 2006). Additionally, several groups have reported a role for  $\beta$ -PIX in regulating activation of Rac1, however it is unknown whether this is as a result of GEF activity (Manser, Loo *et al.* 1998, Koh, Manser *et al.* 2001, ten Klooster, Jaffer *et al.* 2006).

While GIT1 and  $\beta$ -PIX have frequently been studied in focal adhesions, the functions of their sister proteins GIT2 and  $\alpha$ -PIX have been investigated less. It is known that  $\alpha$ -PIX acts as a more potent GEF towards both Rac1 and Cdc42 than  $\beta$ -PIX, because it does not contain the T1 insert (Feng, Baird *et al.* 2004, Baird, Feng *et al.* 2005). GIT2 meanwhile also localises to focal adhesions and contains the same domains as GIT1, however it must be phosphorylated at 3 distinct tyrosine residues, Tyr 286, Tyr 392 and Tyr 592 by the kinases Src and FAK before it can recruit to adhesions (Brown, Cary *et al.* 2005).

The aims of the studies undertaken in this chapter were to further characterise the interactions between RhoJ and its partner proteins. Firstly, the binding site for RhoJ within GIT1 was mapped using a yeast two-hybrid method. The expression profiles of the GIT and PIX proteins were also characterised by qPCR and Western blot, and intracellular interactions determined by GFP-trap pulldown in HUVEC. Moreover, the functional effects of the interaction between RhoJ and its partner proteins were investigated in a number of ways. Firstly, the effect of expression of GFP-daRhoJ expression on partner protein recruitment to focal adhesions was assessed, and later siRNA knockdown was employed to diminish expression of each member of the RhoJ/GIT/PIX complex and study the effect on localisation to adhesions. Secondly, endothelial tube formation was studied in cells

transfected with siRNA duplexes specific for the partner proteins of RhoJ to determine whether these knockdowns show similar effects to RhoJ knockdown. Thirdly, since  $\beta$ -PIX acts as a GEF for other Rho GTPases, its role in regulating RhoJ activation was probed. Furthermore, given that GIT2 must be phosphorylated in order to recruit to focal adhesions, the effect of RhoJ manipulation on this phosphorylation was determined. Finally, the effect of GFP-daRhoJ expression on phosphorylation of kinases was investigated.

## **4.2 Mapping the interaction between RhoJ and GIT1**

Mass spectrometry and subsequent yeast two-hybrid experiments previously performed in our laboratory have shown a direct interaction between RhoJ and GIT1. Truncations of the GIT1 protein were cloned in order to map this interaction, and it was elucidated that the Spa homology domain is necessary for binding; interestingly it is this domain that also binds  $\beta$ -PIX. In the case of RhoJ however, a yeast two-hybrid screen performed using the Spa homology domain alone failed to bind, so it appears that this region is not sufficient for binding (Katarzyna Leszczynska, PhD thesis).

In order to more precisely define the RhoJ binding site of GIT1, mutants of the GIT1 protein were obtained from Richard Premont (Premont, Perry *et al.* 2004) and used in a yeast two-hybrid assay. The yeast two-hybrid system uses fusions of the proteins of interest, in this case RhoJ and GIT1 to the activation domain and DNA binding domain of Gal4 transcription factor respectively. The fusion proteins were transformed into pJ69.4A yeast, and when these two domains come into contact, Gal4 activates transcription of the HIS3 gene; thus enabling production of histidine and allowing yeast to grow on medium lacking histidine. The four mutants used were: wild-type GIT1 (wtGIT1), GIT1 with the Spa homology domain

deleted (GIT1  $\Delta$ AB), GIT1 lacking the first tandem repeat of the SHD (GIT1  $\Delta$ SpaA), and GIT1 lacking the second tandem repeat (GIT1  $\Delta$ SpaB). Given that the rest of the GIT1 protein is unchanged in these constructs, it was possible to investigate whether either or both of the tandem repeats are required for the GIT1/RhoJ interaction.

Example yeast two-hybrid spot assays are shown in Figure 4.1. As found previously, wild type GIT1 interacts with both wild type and dominant active RhoJ, and upon deletion of the Spa homology domain this binding is lost. However, deletion of the first tandem repeat (SpaA) of GIT1 still maintained some binding to dominant active RhoJ which was not evident when the second repeat (SpaB) was removed. In light of this, it appears that the SpaB domain of GIT1 is the most crucial region for binding to RhoJ, however given that the  $\Delta$ SpaA mutant seems to show weaker binding it is possible that there is a cumulative effect when both regions are present that allows complete binding.

It is also important to note that GIT1 only bound to RhoJ when there was some level of activation, i.e. in the wild type form (where GTP and GDP are both able to associate) and the dominant active form (which is GTPase deficient and thus constitutively GTP-bound). Dominant negative RhoJ yeast does not interact with GIT1. This may suggest that if RhoJ is regulating GIT1 it is only when in its active, GTP-bound form.

### **4.3 Profiling RhoJ, GIT and PIX expression in HUVEC, HMEC-1 and HEK293T**

In order to determine the relative expression of  $\alpha$ -PIX,  $\beta$ -PIX, GIT1 and GIT2 in endothelial cells and cell lines commonly used in the lab, both protein and mRNA levels were assessed.

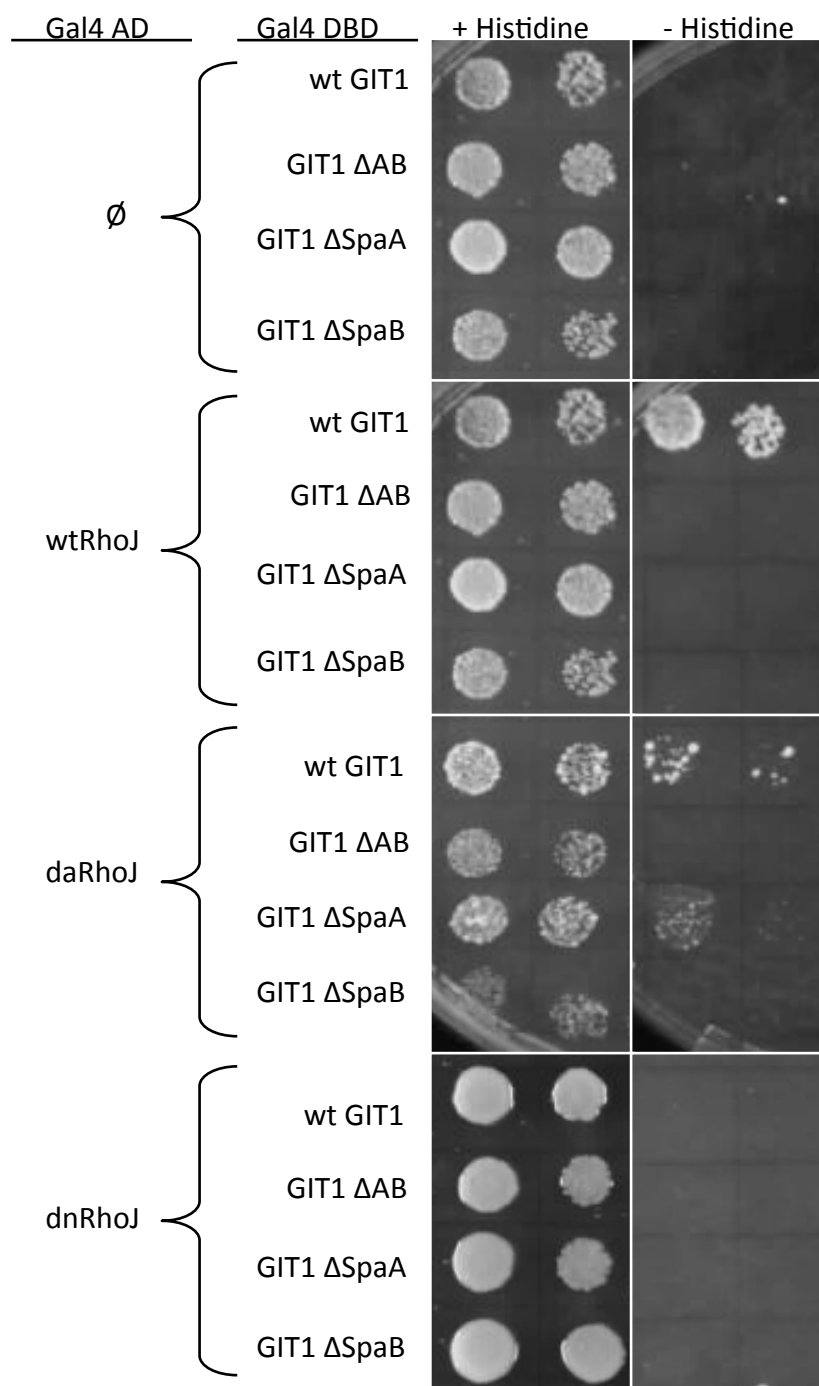


**Figure 4.1 wtRhoJ and daRhoJ interact with wtGIT1 in the yeast two-hybrid assay.**

PJ69.4A yeast were transformed with the pGBT9 vector containing DBD (DNA binding domain) fusions of wild-type (wt), dominant active (da) or dominant negative (dn) RhoJ, along with the pACT2 vector containing AD (activation domain) fusions of wt GIT1, GIT1 lacking the entire Spa homology domain (ΔSpaAB), or GIT1 lacking either the first or second tandem repeat of the Spa homology domain (ΔSpaA or ΔSpaB). Five-fold dilutions of yeast were prepared, starting from an OD600 of 0.1, and spotted onto control plates (+ histidine) or test plates (- histidine, + 3 mM 3AT). These were left to grow for 3-5 days at 30 °C before imaging. Growth of yeast on test plates indicates interaction between the RhoJ and GIT1 proteins.

To investigate protein levels, lysates were made from HMEC-1, HUVEC (3 different isolates to account for individual cord variation) and HEK293T cells. These lysates were probed by Western blot for RhoJ as well as both PIX proteins and both GIT proteins, as shown in Figure 4.2.A. The GIT and PIX proteins are expressed in all the cell types tested, whereas RhoJ is only expressed in endothelial cells as previously described by members of our laboratory (Kaur, Leszczynska *et al.* 2011).

However, since the levels detected are dependent on the efficiency of antibody binding it was important to also investigate mRNA expression. RNA was extracted from 3 HUVEC isolates, as well as HEK293T cells and cDNA generated before performing quantitative PCR for message levels of  $\alpha$ -PIX,  $\beta$ -PIX, GIT1 and GIT2. Relative message levels were calculated as outlined in Section 2.11.3. As can be seen in Figure 4.2.B,  $\beta$ -PIX is more highly expressed than  $\alpha$ -PIX in both HEK293T and HUVEC, while GIT2 is more highly expressed in both cell types than GIT1. Since GIT2 is expressed to a much greater level in HUVEC and GIT1 and GIT2 are highly homologous, RhoJ may primarily interact with GIT2 *in vivo*. However, since only  $\beta$ -PIX and GIT1 had been investigated thus far, it was necessary to confirm that GIT2 interacts with RhoJ.

#### **4.4 Pulldown of RhoJ partner proteins from GFP expressing HUVEC**

Previous work performed by Katarzyna Leszczynska elucidated an interaction between active RhoJ and the focal adhesion proteins GIT1 and  $\beta$ -PIX. The interaction with GIT1 was subsequently found to be direct (both in previous work and in Section 4.2), whereas the

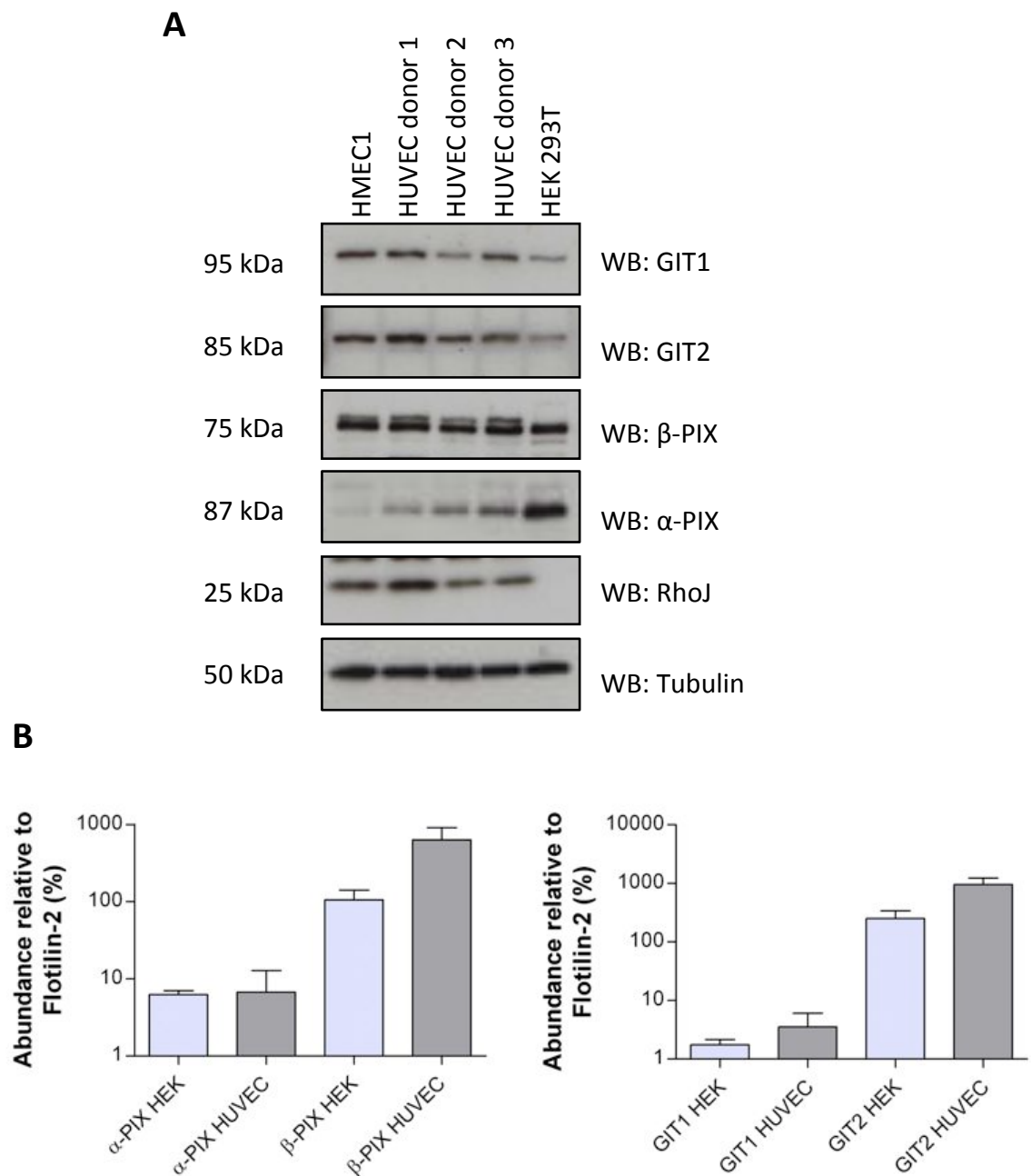


**Figure 4.2 Expression of RhoJ and its candidate partner proteins in endothelial and non-endothelial cells.** **A.** Lysates were prepared from HMEC-1, 3 HUVEC isolates and HEK 293T cells and Western blotted for RhoJ, its partner proteins β-PIX and GIT1 as well as the related proteins α-PIX and GIT2. **B.** RNA was extracted from HEK and 3 HUVEC isolates and cDNA generated. qPCR was performed for α-PIX, β-PIX, GIT1 and GIT2 and abundance relative to Flotilin-2 calculated as a percentage. The y-axis is shown as a log 10 scale.



association with  $\beta$ -PIX was not and most likely occurs via the interaction with GIT, as no interaction was detected using the yeast two-hybrid system (Katarzyna Leszczynska, PhD thesis). Following on from the data presented in Section 4.3, where GIT2 was found to be expressed at a higher level than GIT1 in both HEK293T and HUVEC, further pulldown experiments were performed to confirm the interactions with RhoJ and the GIT and PIX proteins in HUVEC transduced to express GFP or GFP-daRhoJ.

Lysates of HUVEC stably expressing GFP or GFP-daRhoJ, introduced via lentiviral transduction, were incubated with GFP-trap beads and pulldowns performed. Samples were probed for GIT1, GIT2 and  $\beta$ -PIX, with representative blots shown in Figure 4.3. Samples were also blotted for  $\alpha$ -PIX, however no interaction was found (data not shown), most likely because expression is low. These experiments confirmed that active RhoJ interacts with both GIT1 and GIT2, as well as  $\beta$ -PIX. The absence of bands in GFP control lanes also suggests that this is a specific interaction.

## **4.5 Knockdown of RhoJ and its partner proteins in HUVEC**

While data presented in the sections above confirm a physical interaction between RhoJ, GIT1, GIT2 and  $\beta$ -PIX, further work was required to investigate the functional consequence of these interactions. It was therefore important to be able to manipulate expression of the members of this complex using transfection with siRNA duplexes.

Two duplexes per gene (RhoJ,  $\beta$ -PIX, GIT1 and GIT2) were acquired from Life Technologies. Subsequently, single knockdowns of RhoJ using the Eurogentec original duplex previously published (Kaur, Leszczynska *et al.* 2011) and  $\beta$ -PIX were performed, along with double

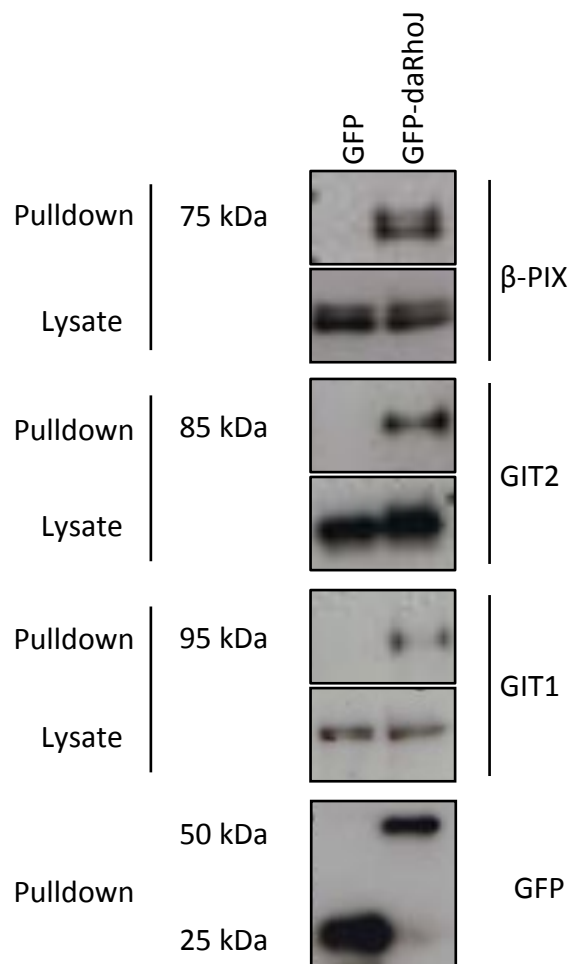


**Figure 4.3 GFP-daRhoJ interacts with  $\beta$ -PIX, GIT1 and GIT2 in the GFP trap pulldown assay.** HUVEC stably expressing GFP or GFP-daRhoJ were lysed and incubated with GFP-trap beads. After pulldown, beads were washed and bound proteins eluted with 2x SDS sample buffer. Western blots were carried out on samples to determine the interacting partners of RhoJ, and the level of GFP or GFP-daRhoJ bound to beads.

knockdowns for GIT1 and GIT2. The first set of duplexes were RhoJ siRNA2,  $\beta$ -PIX siRNA2, GIT1 siRNA2 and GIT2 siRNA1. Lysates were made after 48 and 72 h and protein knockdown assessed by Western blot, as shown in Figure 4.4.A. A second set of duplexes was also used, these were RhoJ siRNA1,  $\beta$ -PIX siRNA1, GIT1 siRNA1 and GIT2 siRNA2. Representative blots of lysates made 48 h after transfection are shown in Figure 4.4.B.

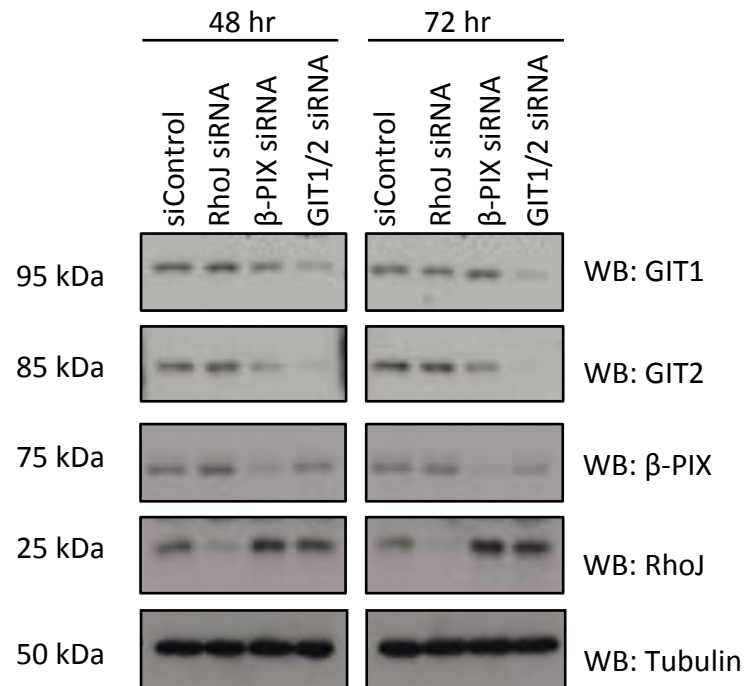
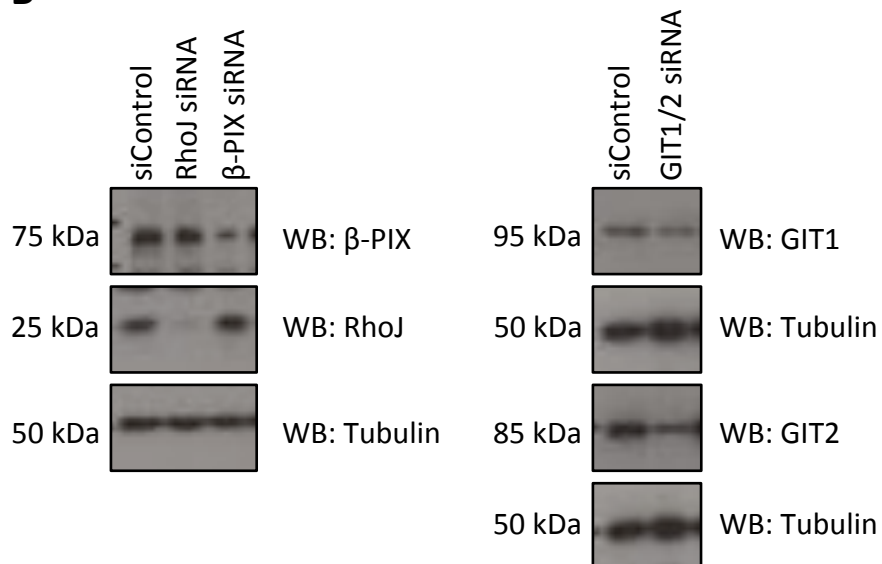
RNA was also extracted from HUVEC transfected with the first set of duplexes after 48 h and qPCR performed to determine the level of knockdown achieved. There was at least a 68% reduction in mRNA levels for each gene tested, as shown in Figure 4.5.A-D.

The interferon response of cells was also assessed, since siRNA duplexes are able to induce this response and cause off-target effects. To do this, levels of the interferon response genes OAS1 and ISG20 (Espert, Rey *et al.* 2004, Clemens 2005) were measured by qPCR (Figure 4.5.E-F). Increased expression of these genes suggest an induction of the interferon response, however the duplexes used in these transfections at 10 nM led to no major increases in their levels.

Taken together, these data suggest that the duplexes tested are capable of diminishing protein and mRNA levels of the relevant genes in HUVEC, and do not induce off-target effects via the interferon response. They were used for all future studies on the functional interactions between RhoJ and its partner proteins.

## **4.6 Determining co-localisation of RhoJ with GIT1, GIT2 and $\beta$ -PIX**

In order to investigate the functional interaction between RhoJ and  $\beta$ -PIX, GIT1 and GIT2, it was first necessary to determine whether these proteins localise to the same cellular

**A****B**

**Figure 4.4 Knockdown of RhoJ,  $\beta$ -PIX and GIT1/2 with siRNA.** **A.** HUVEC were transfected with 10 nM control (siControl), RhoJ specific (RhoJ siRNA),  $\beta$ -PIX specific ( $\beta$ -PIX siRNA) or a combination of GIT1 and GIT2 specific (GIT1/2 siRNA) siRNA duplexes. After 48 h and 72 h cells were lysed, and samples Western blotted for protein expression, with tubulin as a loading control. **B.** HUVEC were transfected with a second set of duplexes at 10 nM. Cells were lysed after 48 h and samples Western blotted for protein expression, with tubulin as a loading control.

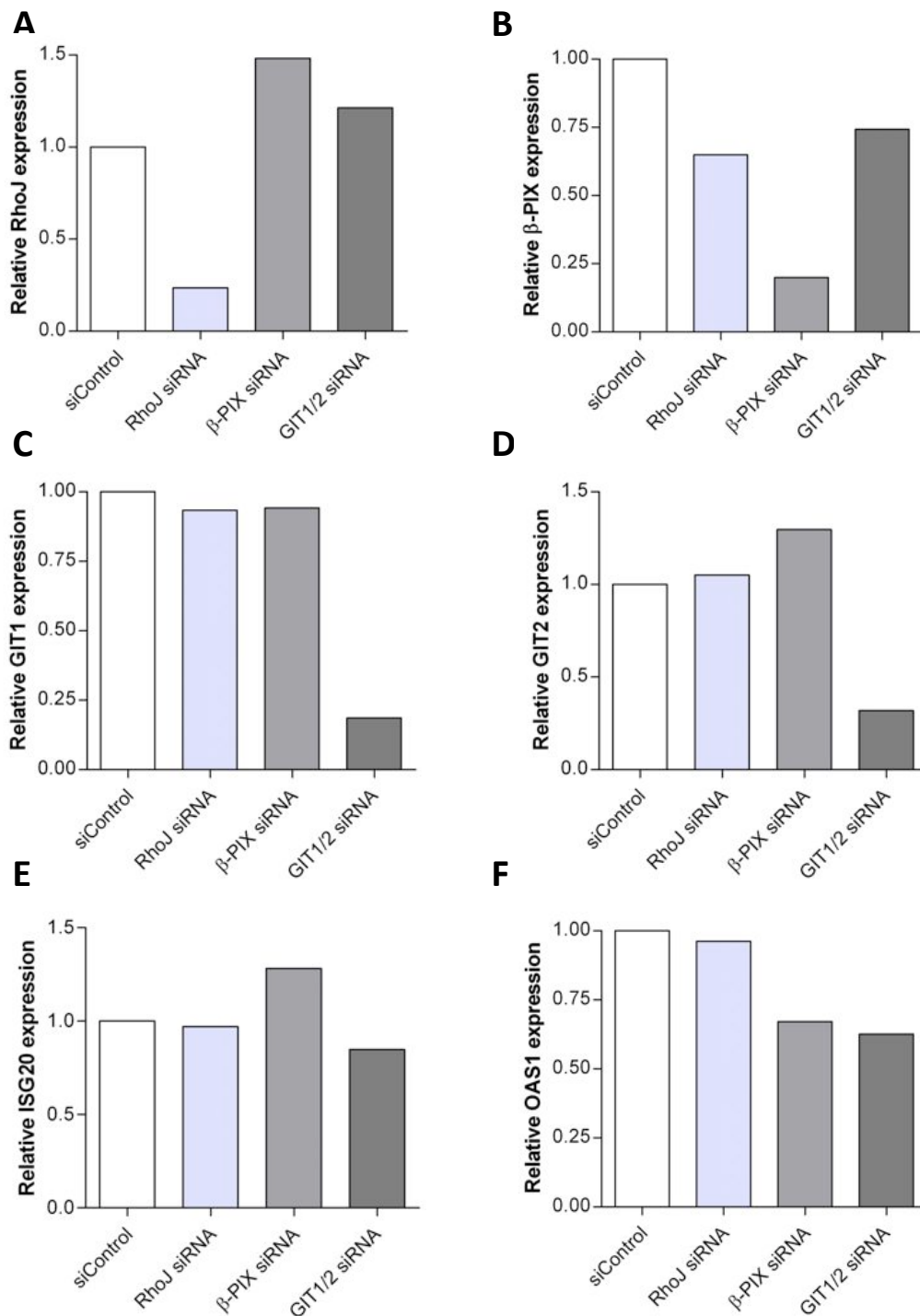


**Figure 4.5 Knockdown of RhoJ, β-PIX and GIT1/2 with siRNA.** HUVEC were transfected with 10 nM control (siControl), RhoJ specific (RhoJ siRNA), β-PIX specific (β-PIX siRNA) or a combination of GIT1 and GIT2 specific (GIT1/2 siRNA) siRNA duplexes. After 48 h RNA was extracted from cells and cDNA generated before performing qPCR. **A-D.** Calculated copies of RhoJ, β-PIX, GIT1 and GIT2 for each condition were normalised to Flotillin-2 and relative expression levels plotted. **E-F.** Transcription of the interferon response genes ISG20 and OAS1 was also assessed, with no obvious differences in calculated copies of siControl transfected cells compared to knockdown conditions. This was performed once.

compartments. It was not possible to co-stain endogenous RhoJ with GIT1, GIT2 and  $\beta$ -PIX, because the antisera were from the same species (rabbit). Instead, GFP tagged constructs of RhoJ were introduced into HUVEC by lentiviral transduction, and cells stained for GIT1, GIT2 and  $\beta$ -PIX.

HUVEC expressing GFP, GFP-wtRhoJ or GFP-daRhoJ were stained for  $\beta$ -PIX, GIT1 and GIT2 and colocalisation of RhoJ with its partner proteins assessed using confocal microscopy. While there is diffuse GFP expression at the membrane, particularly in GFP-wtRhoJ expressing cells, Figures 4.6, 4.7 and 4.8 demonstrate that there is partial co-localisation between RhoJ and  $\beta$ -PIX, GIT1 and GIT2 at focal adhesions. Co-localisation appears more pronounced in GFP-daRhoJ expressing cells compared to GFP-wtRhoJ, as GFP-wtRhoJ localises to the plasma membrane in general and it is difficult to distinguish its presence at individual adhesions. The finding that GFP-daRhoJ co-localises with  $\beta$ -PIX, GIT1 and GIT2 is consistent with the observation that the constitutively GTP bound daRhoJ interacts with GIT1 in the yeast two-hybrid assay, while GDP-locked dnRhoJ does not.

## **4.7 Investigating the effect of GFP-daRhoJ expression on GIT and PIX localisation to focal adhesions**

Since RhoJ co-localises with  $\beta$ -PIX, GIT1 and GIT2 in focal adhesions, the effect of daRhoJ expression on the recruitment of the GIT/PIX complex to adhesions was studied. Once again, GFP, GFP-wtRhoJ and GFP-daRhoJ expressing HUVEC were stained with antibodies against  $\beta$ -PIX, GIT1 and GIT2, as well as vinculin to act as a focal adhesion marker protein.

The panels in Figures 4.9, 4.10 and 4.11 show that in addition to increasing focal adhesion

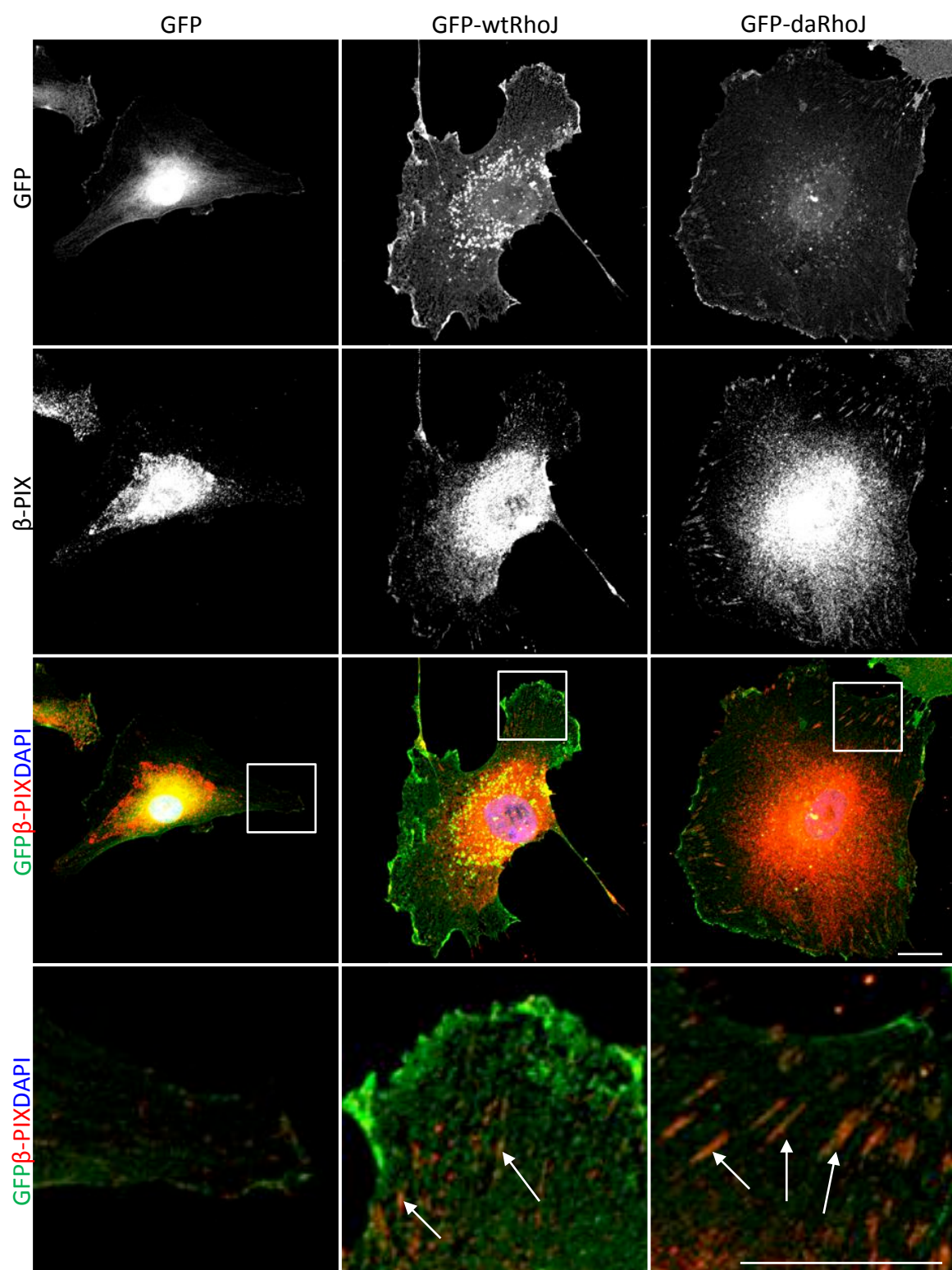


**Figure 4.6  $\beta$ -PIX primarily co-localises with GFP-daRhoJ at focal adhesions.** HUVEC stably expressing GFP, GFP-wtRhoJ or GFP-daRhoJ were plated onto gelatin-coated coverslips, and the following day fixed and immunofluorescently stained for  $\beta$ -PIX. White arrows indicate co-localisation between RhoJ and  $\beta$ -PIX. Scale bar: 20  $\mu$ m.



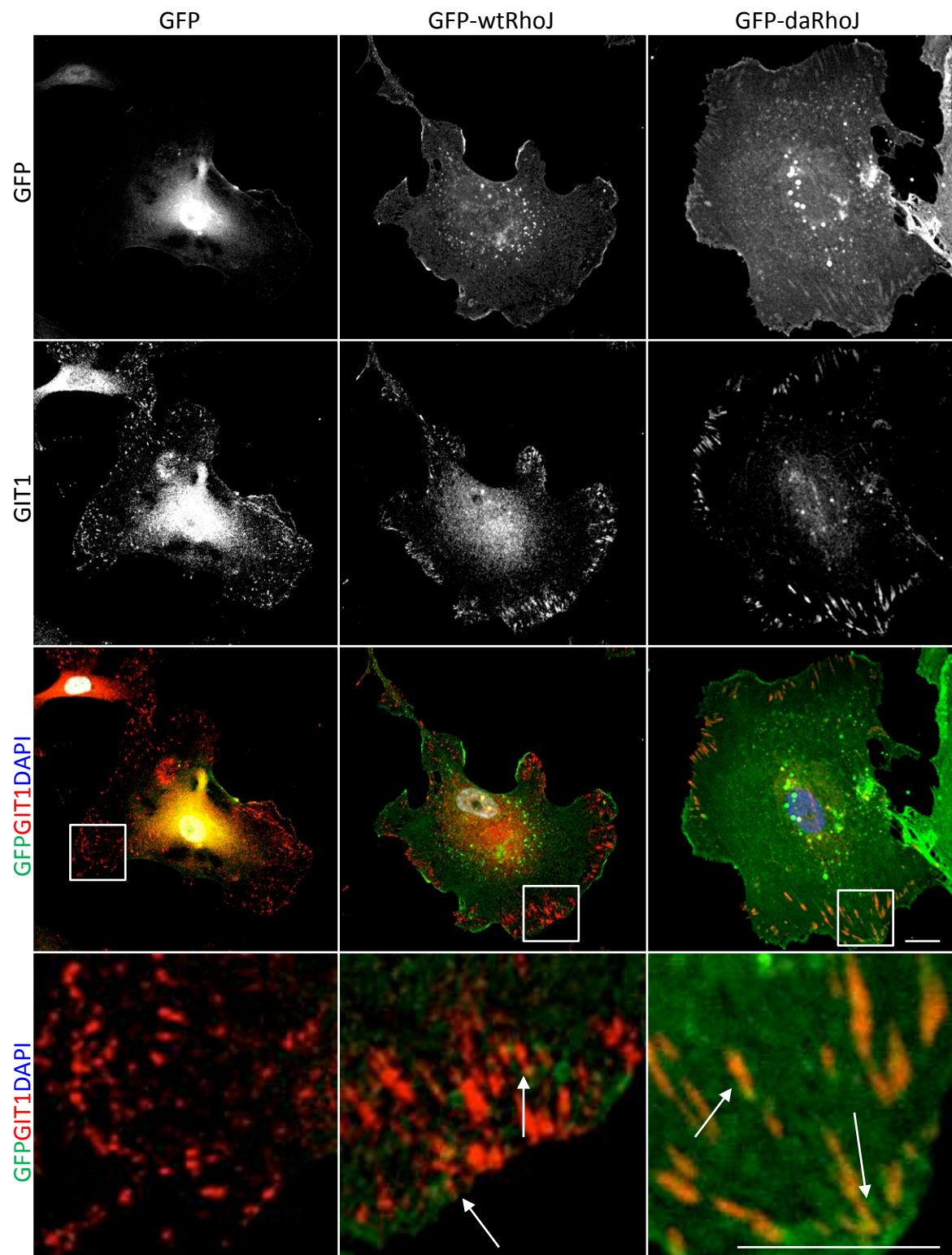


**Figure 4.7 GIT1 primarily co-localises with GFP-daRhoJ at focal adhesions.** HUVEC stably expressing GFP, GFP-wtRhoJ or GFP-daRhoJ were plated onto gelatin-coated coverslips, and the following day fixed and immunofluorescently stained for GIT1. White arrows indicate co-localisation between RhoJ and GIT1. Scale bar: 20  $\mu$ m.



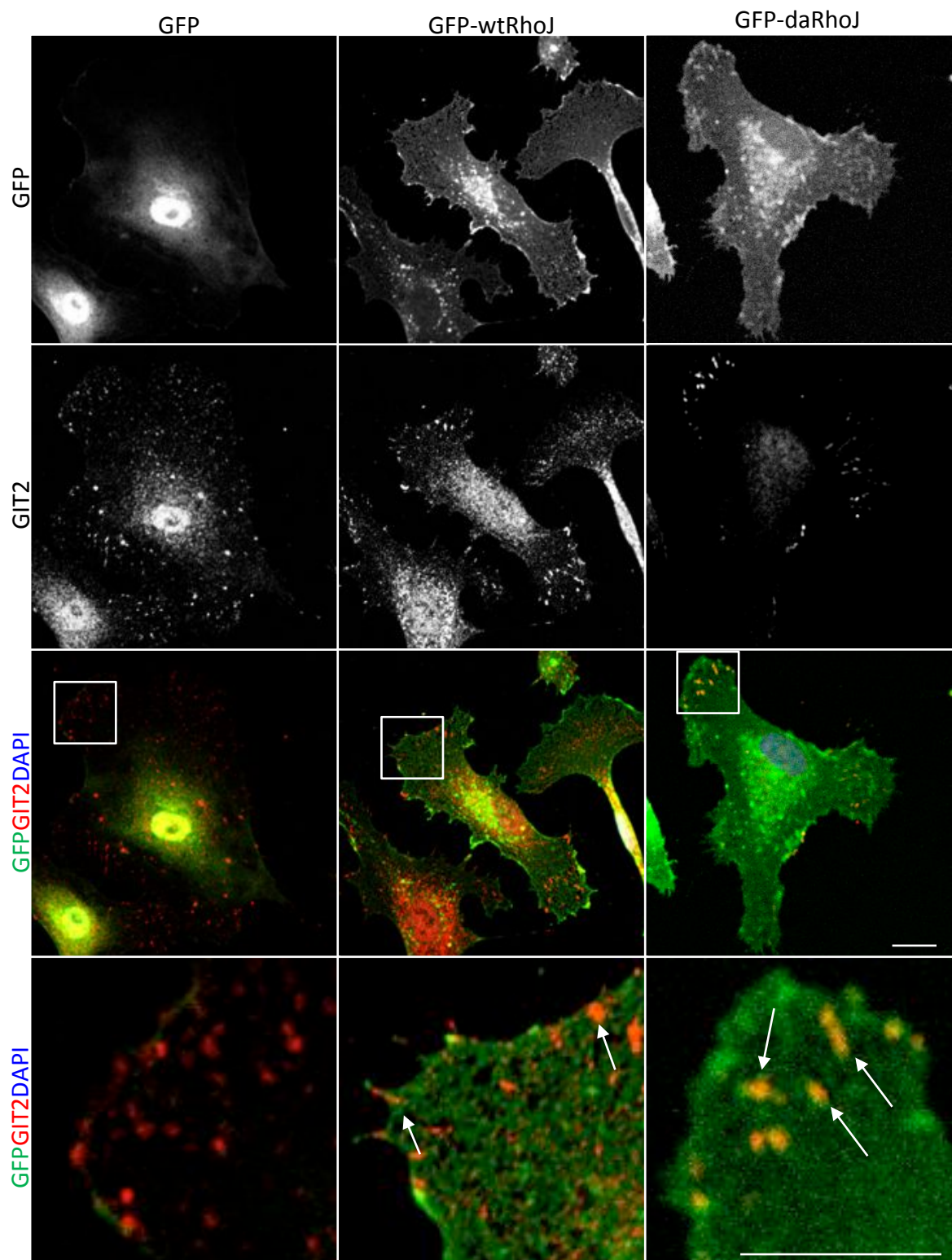


**Figure 4.8 GIT2 co-localises with GFP-daRhoJ at focal adhesions, and with GFP-wtRhoJ to a lesser extent.** HUVEC stably expressing GFP, GFP-wtRhoJ or GFP-daRhoJ were plated onto gelatin-coated coverslips, and the following day fixed and immunofluorescently stained for GIT2. White arrows indicate co-localisation between RhoJ and GIT2. Scale bar: 20  $\mu$ m.

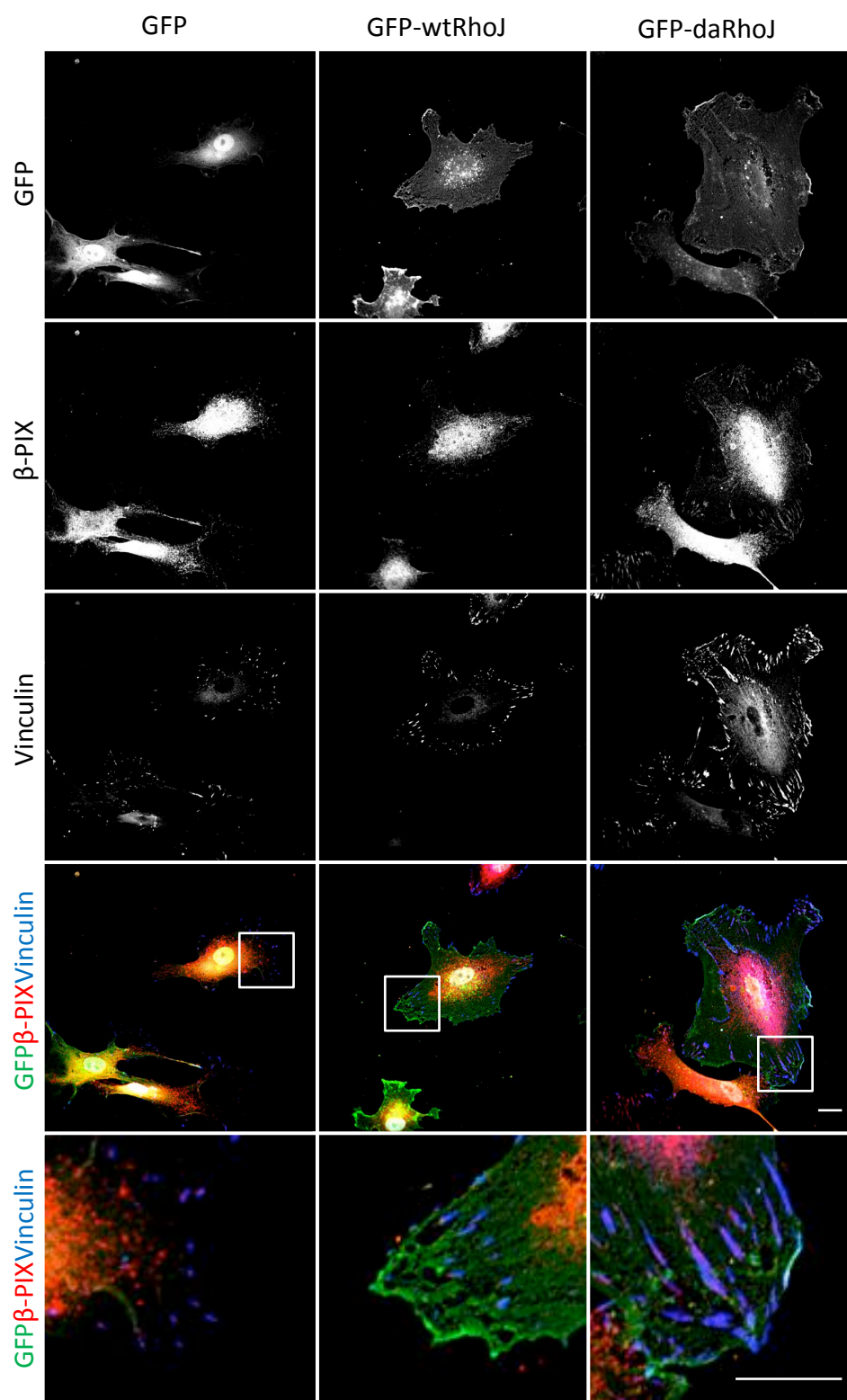


**Figure 4.9 Expression of GFP-daRhoJ increases recruitment of  $\beta$ -PIX to focal adhesions.** HUVEC stably expressing GFP, GFP-wtRhoJ or GFP-daRhoJ were plated onto gelatin-coated coverslips and the following day fixed and immunofluorescently stained for vinculin and  $\beta$ -PIX. Scale bar: 20  $\mu$ m.

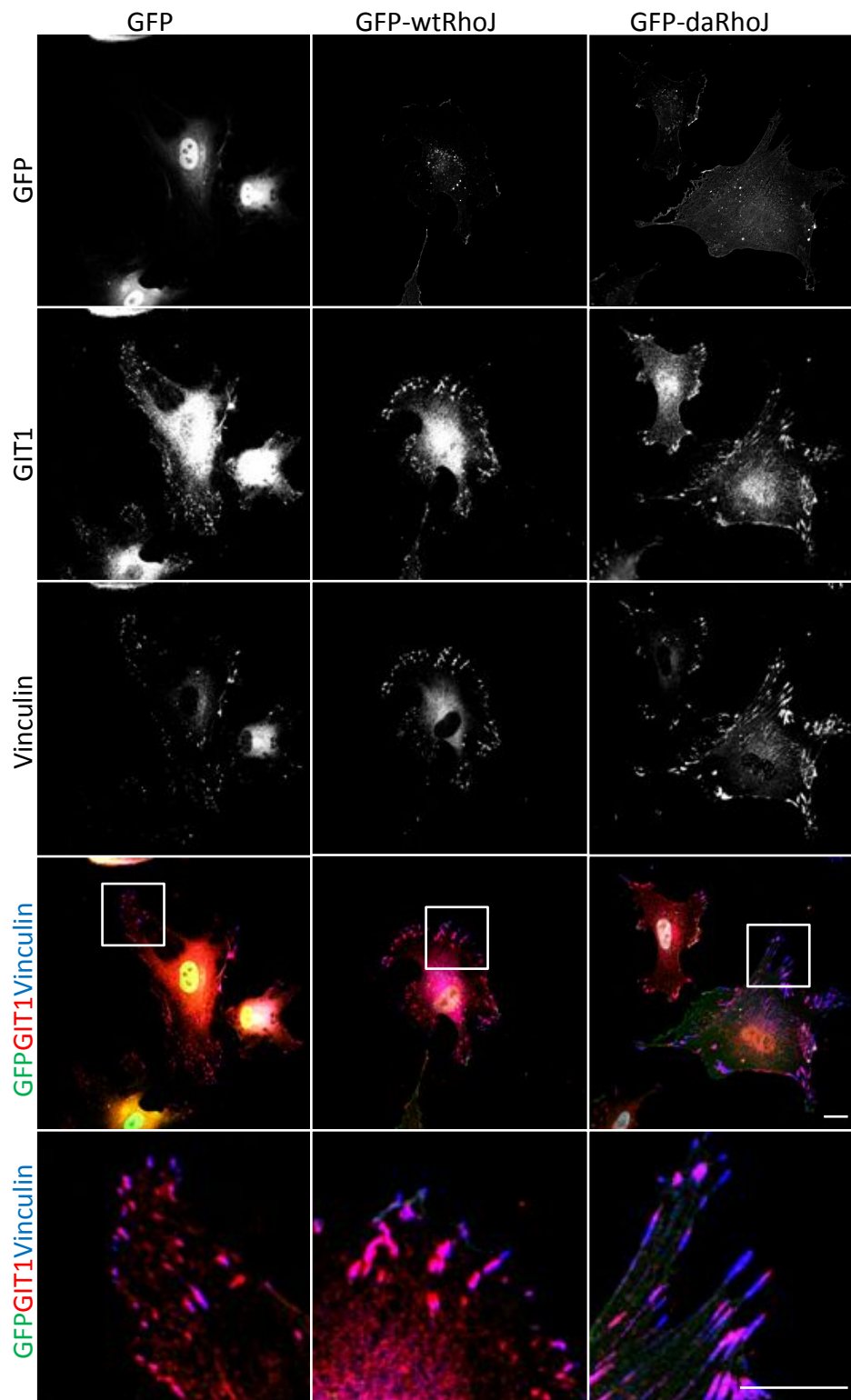


**Figure 4.10 Expression of both GFP-wtRhoJ and GFP-daRhoJ increases recruitment of GIT1 to focal adhesions.** HUVEC stably expressing GFP, GFP-wtRhoJ or GFP-daRhoJ were plated onto gelatin-coated coverslips and the following day fixed and immunofluorescently stained for vinculin and GIT1. Scale bar: 20  $\mu$ m.

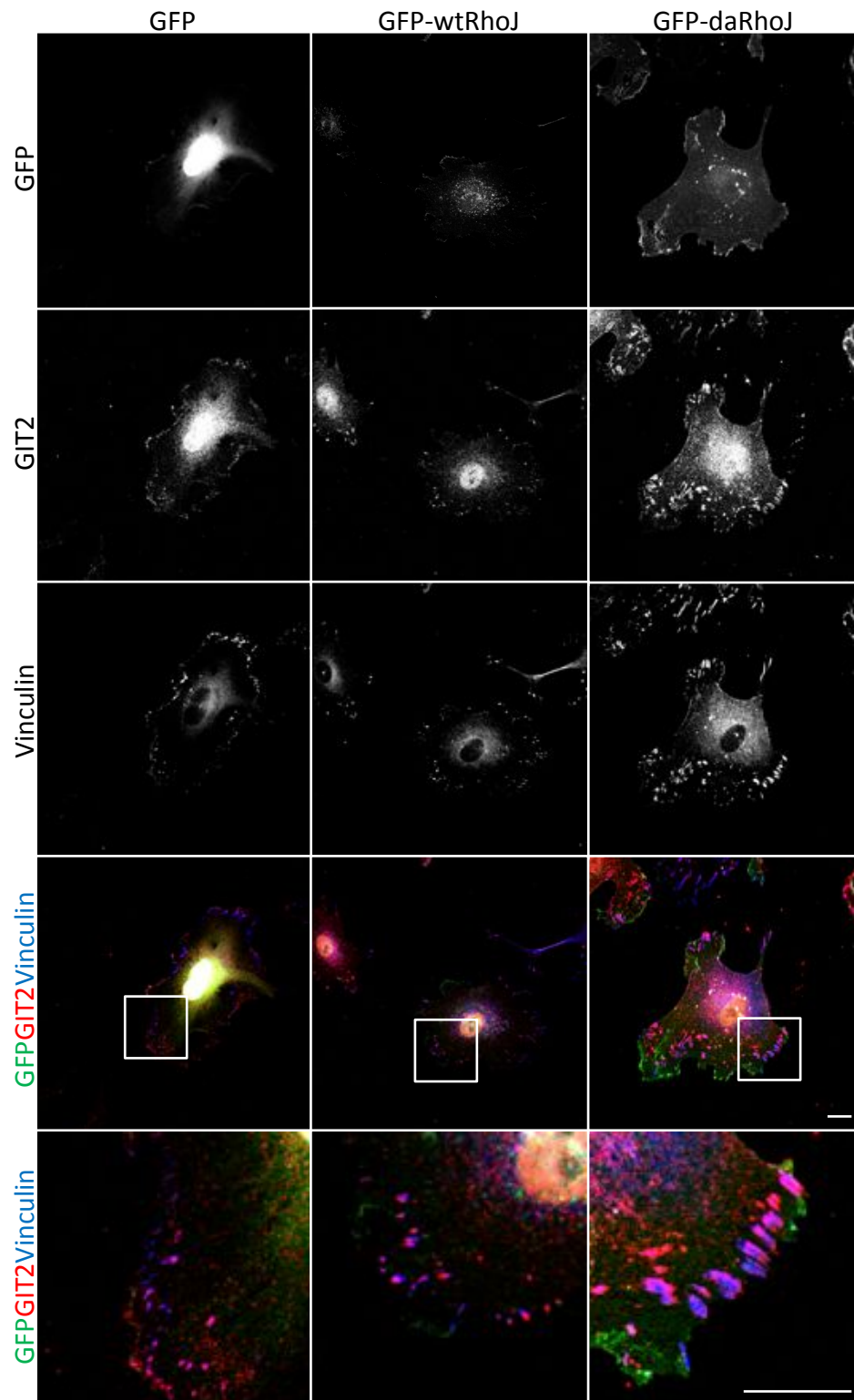


**Figure 4.11 Expression of GFP-daRhoJ increases recruitment of GIT2 to focal adhesions.** HUVEC stably expressing GFP, GFP-wtRhoJ or GFP-daRhoJ were plated onto gelatin-coated coverslips and the following day fixed and immunofluorescently stained for vinculin and GIT2. Scale bar: 20  $\mu$ m.

size (as shown in Figure 3.10), expression of GFP-daRhoJ increases recruitment of  $\beta$ -PIX, GIT1 and GIT2 to adhesions compared to those in cells expressing GFP only and GFP-wtRhoJ.

Figure 4.9 demonstrates that there is little difference in  $\beta$ -PIX recruitment to adhesions between GFP and GFP-wtRhoJ expressing cells, with an increase in recruitment only apparent in GFP-daRhoJ expressing cells. Similarly, GIT2 localisation (Figure 4.11) seems to be especially increased in GFP-daRhoJ expressing cells, with a much greater level of co-localisation seen with vinculin in these cells as demonstrated by pink/purple regions. Like  $\beta$ -PIX, there is little difference in recruitment of GIT2 to focal adhesions between GFP and GFP-wtRhoJ expressing cells. GIT1 (Figure 4.10) is also most obvious at adhesions in GFP-daRhoJ expressing cells. Unlike  $\beta$ -PIX and GIT2, however, GIT1 does appear to be recruited to focal adhesions more readily in GFP-wtRhoJ expressing cells compared to those expressing GFP only. GIT2 must be phosphorylated at 3 tyrosine residues before it is able to recruit to focal adhesions, whereas this is not necessary for GIT1 recruitment (Brown, Cary *et al.* 2005). Since the change in GIT1 focal adhesion localisation in response to GFP-daRhoJ expression is more subtle, compared to a striking difference in GIT2 localisation, this may suggest an additional role for RhoJ in regulating GIT2 phosphorylation and hence recruitment.

## **4.8 Investigating the effect of knockdown of members of the RhoJ/GIT/PIX complex on recruitment to focal adhesions**

While the data presented in Section 4.7 suggests that dominant active RhoJ potentiates recruitment of its partner proteins  $\beta$ -PIX, GIT1 and GIT2 to focal adhesions, it was also important to determine whether these proteins reciprocally regulate one another's

localisation.

In order to assess the role of each member of the complex in recruitment to adhesions, HUVEC were transfected with siRNA duplexes specific for each gene of interest and subsequently fixed and stained for vinculin and RhoJ,  $\beta$ -PIX, GIT1 or GIT2. Cells were imaged by confocal microscopy and the amount of staining at focal adhesions assessed using ImageJ. The panels in Figures 4.12-4.15 show immunofluorescent staining of RhoJ,  $\beta$ -PIX, GIT1 and GIT2 respectively in control cells, or those with diminished expression of RhoJ,  $\beta$ -PIX or GIT1/2. Two duplexes were used for each gene, with the first set of duplexes shown in the first panel (A) and the second set in the second panel (B).

To quantify recruitment, adhesions around the periphery of the cell were outlined on the vinculin channel in ImageJ, and mean grey values measured for the protein of interest. Example images to demonstrate recruitment of each partner protein to individual adhesions in each condition are shown as inset images in each panel. Figures 4.12.C-4.15.C show the raw recruitment data for a single representative replicate presented as a box and whisker plot, with statistical significance analysed using the Mann Whitney test.

In order to compare recruitment across experiments, data points were scaled to enable the mean for each datapoint across all experiments to be calculated. For each replicate experiment, all data points from each of the experimental groups were scaled to the mean of the siControl dataset for that experiment by dividing the mean grey value of each focal adhesion measured in the knockdown datasets by the mean of the appropriate siControl dataset. The scaled data points from three independent experiments were then pooled. The bar charts in Figures 4.12.D/E-4.15.D/E display relative recruitment for each protein upon



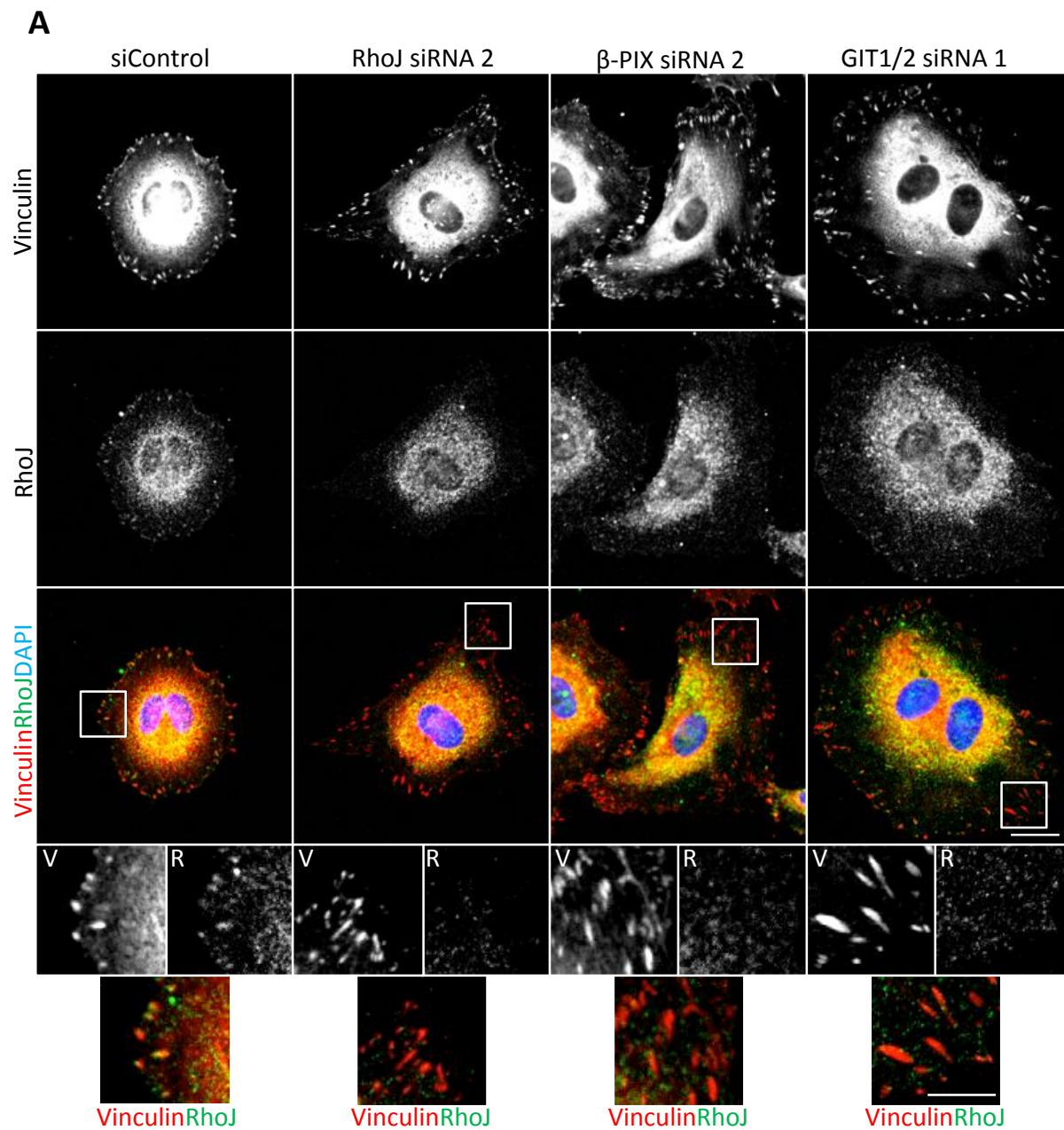


**Figure 4.12 Knockdown of  $\beta$ -PIX or GIT1/2 reduces recruitment of RhoJ to focal adhesions. A.** HUVEC transfected with control, RhoJ specific,  $\beta$ -PIX specific or GIT1/2 specific siRNA duplexes were fixed and stained for RhoJ after 48 h and imaged by confocal microscopy. Scale bar: 20  $\mu$ m. Inset scale bar: 10  $\mu$ m. V: vinculin; R: RhoJ.

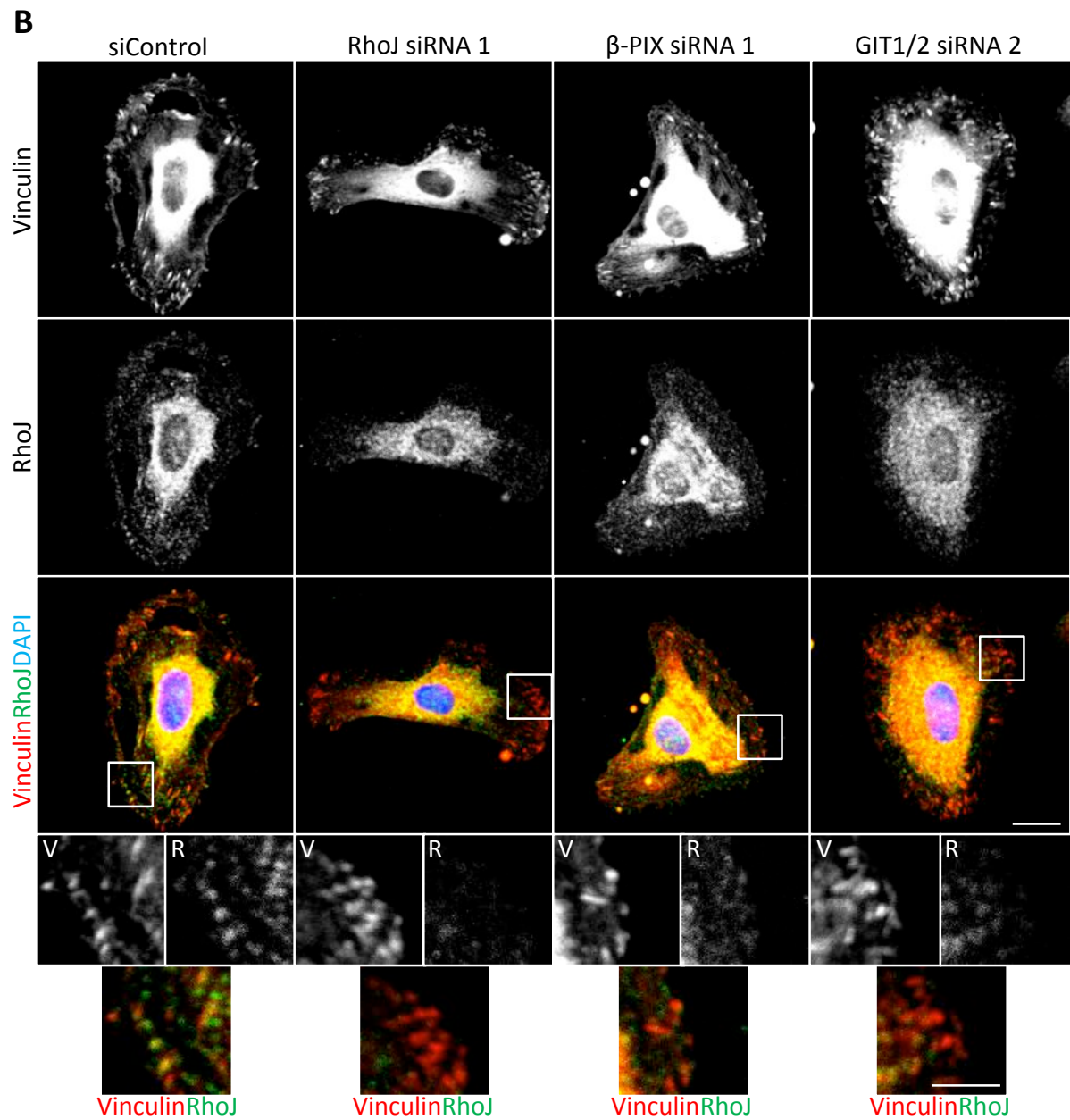


**Figure 4.12 Knockdown of  $\beta$ -PIX or GIT1/2 reduces recruitment of RhoJ to focal adhesions. B.** HUVEC were transfected with a second independent set of duplexes. After 48 h, cells transfected with control, RhoJ specific,  $\beta$ -PIX specific or GIT1/2 specific siRNA duplexes were fixed and stained for RhoJ and imaged by confocal microscopy. Scale bar: 20  $\mu$ m.



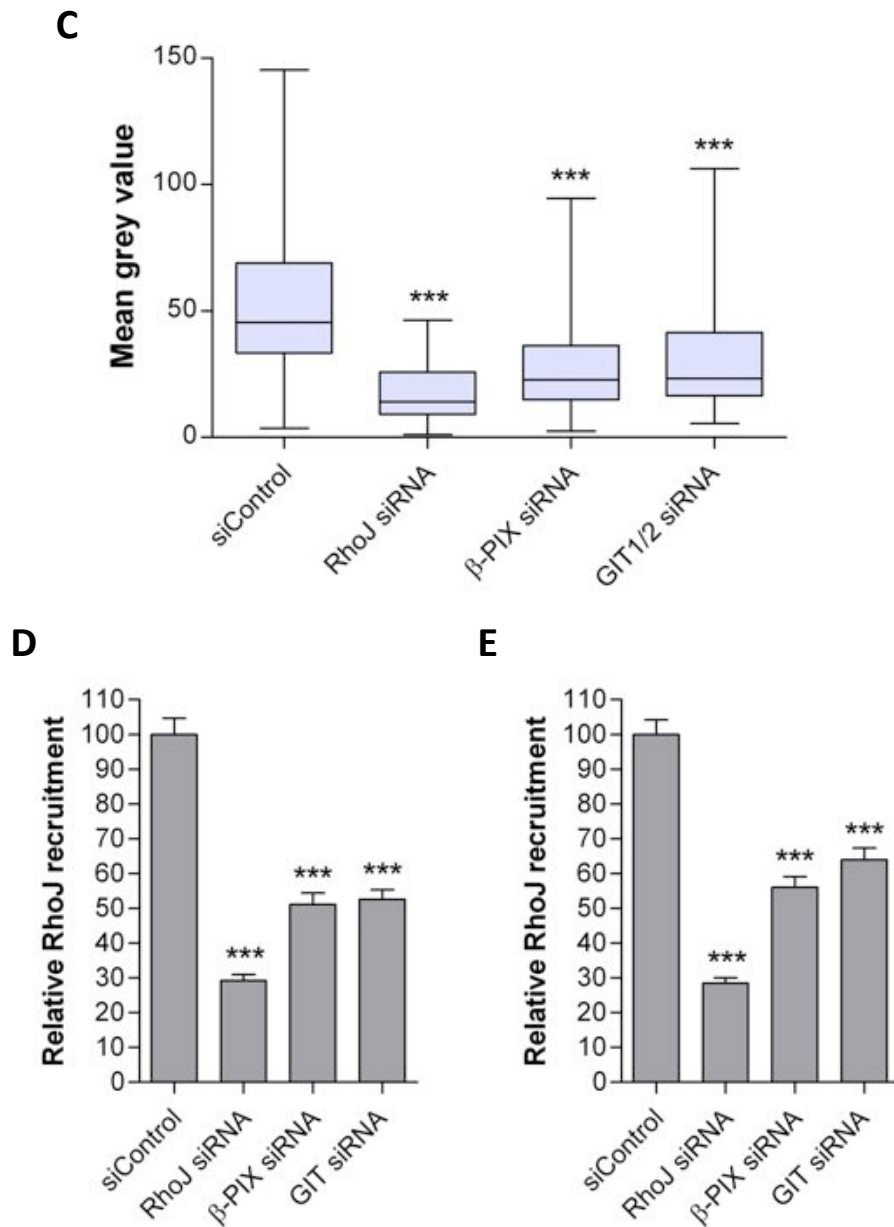


**Figure 4.12 Knockdown of  $\beta$ -PIX or GIT1/2 reduces recruitment of RhoJ to focal adhesions.** **C.** Vinculin positive adhesions in cells transfected with siRNA duplexes were outlined and mean grey values of RhoJ staining were measured using ImageJ. Knockdown cells were compared to controls, and one experiment using the first set of duplexes presented as a box and whisker plot. The Mann Whitney test was used to assess statistical differences. **D-E.** Relative recruitment of RhoJ to adhesions was calculated and presented as a bar chart for the first (D) and second (E) set of duplexes. The Mann Whitney test was used to assess statistical significance.

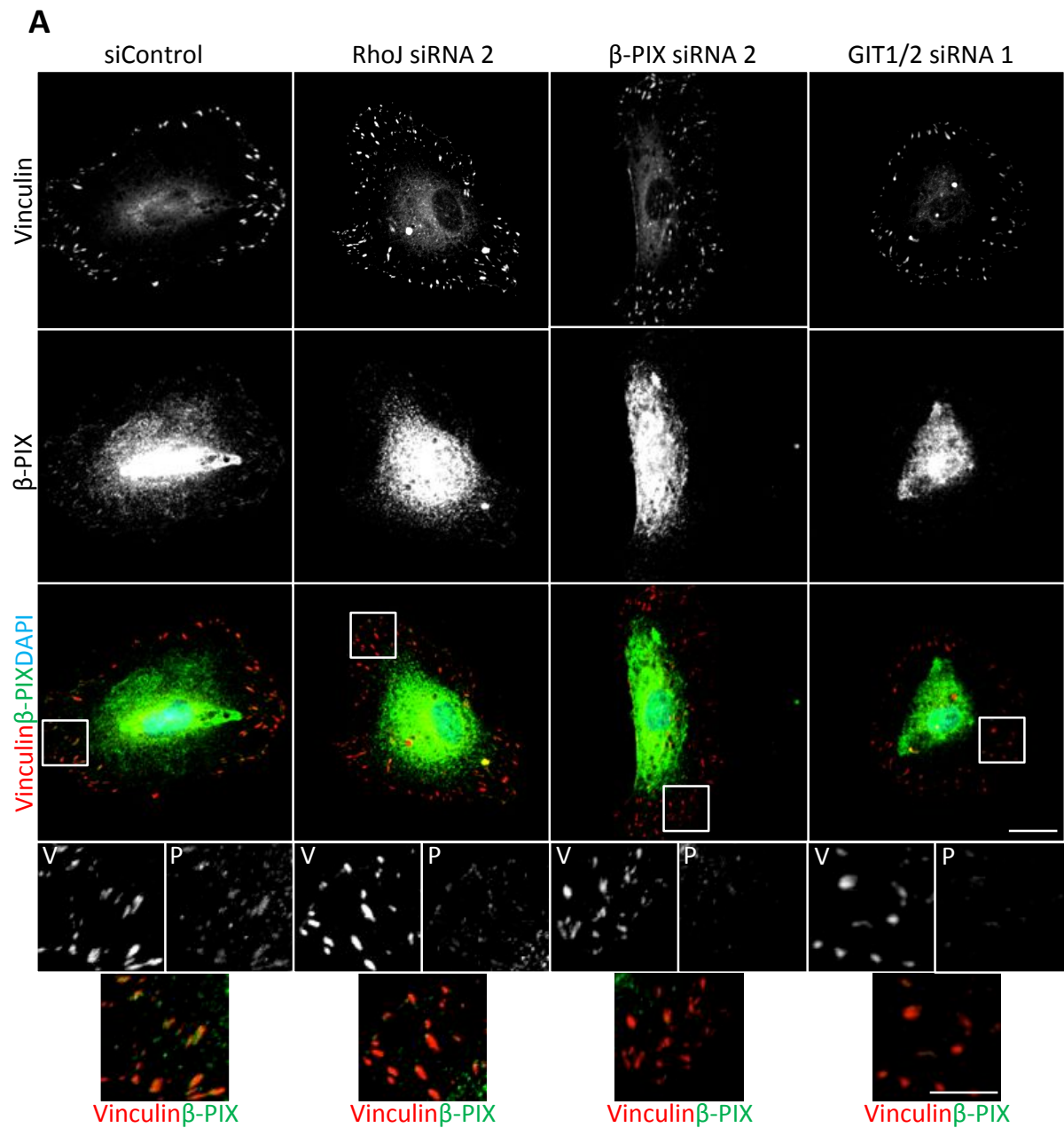


**Figure 4.13 Knockdown of RhoJ or GIT1/2 reduces recruitment of  $\beta$ -PIX to focal adhesions.** **A.** HUVEC transfected with control, RhoJ specific,  $\beta$ -PIX specific or GIT1/2 specific siRNA duplexes were fixed and stained for  $\beta$ -PIX after 48 h and imaged by confocal microscopy. Scale bar: 20  $\mu$ m. Inset scale bar: 10  $\mu$ m. V: vinculin; P:  $\beta$ -PIX.

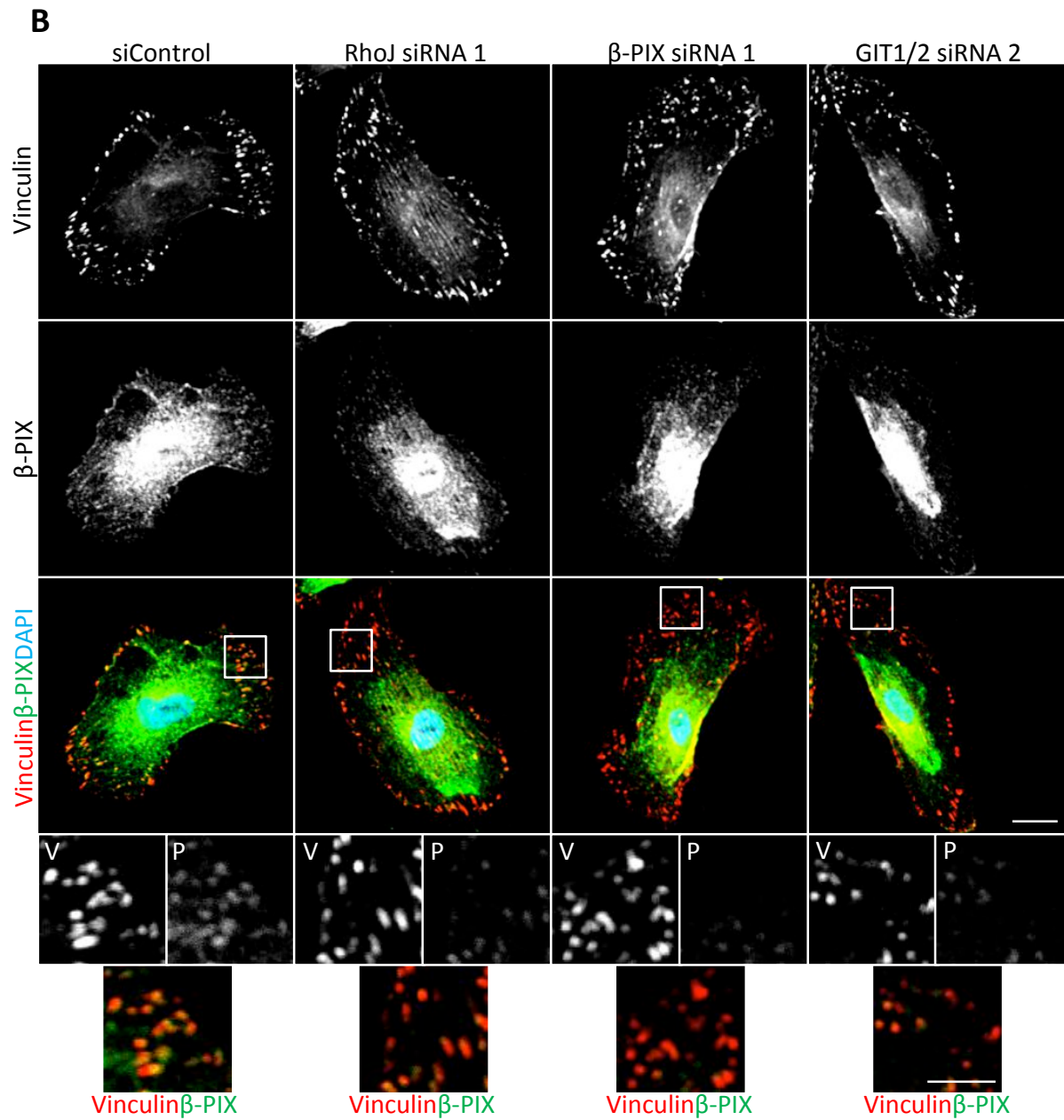


**Figure 4.13 Knockdown of RhoJ or GIT1/2 reduces recruitment of  $\beta$ -PIX to focal adhesions. B.** HUVEC were transfected with a second independent set of duplexes. After 48 h, cells transfected with control, RhoJ specific,  $\beta$ -PIX specific or GIT1/2 specific siRNA duplexes were fixed and stained for  $\beta$ -PIX and imaged by confocal microscopy. Scale bar: 20  $\mu$ m. Inset scale bar: 10  $\mu$ m. V: vinculin; P:  $\beta$ -PIX.

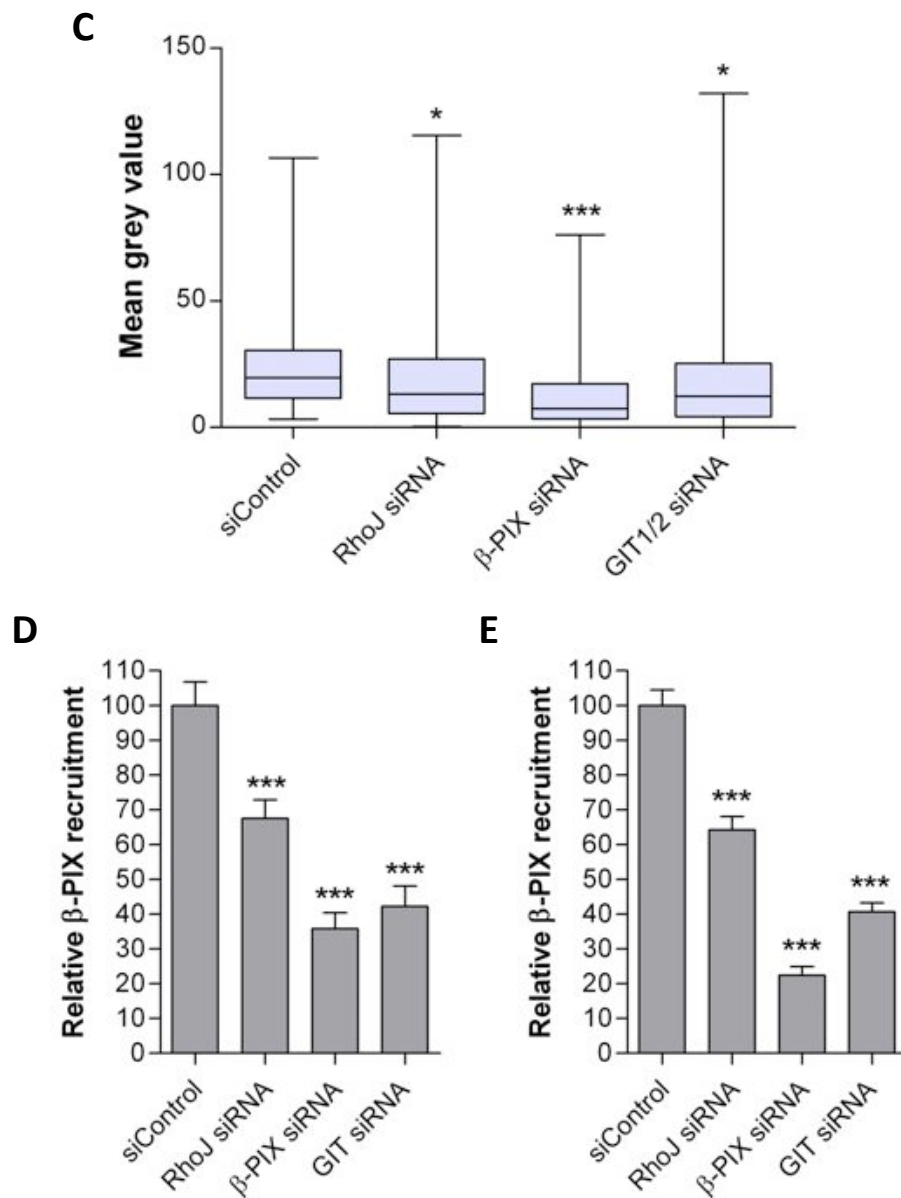


**Figure 4.13 Knockdown of RhoJ or GIT1/2 reduces recruitment of  $\beta$ -PIX to focal adhesions.** **C.** Vinculin positive adhesions in cells transfected with siRNA duplexes were outlined and mean grey values of  $\beta$ -PIX staining were measured using ImageJ. Knockdown cells were compared to controls, and one experiment using the first set of duplexes presented as a box and whisker plot. The Mann Whitney test was used to assess statistical differences. **D-E.** Relative recruitment of  $\beta$ -PIX to adhesions was calculated and presented as a bar chart for the first (D) and second (E) set of duplexes. The Mann Whitney test was used to assess statistical significance.

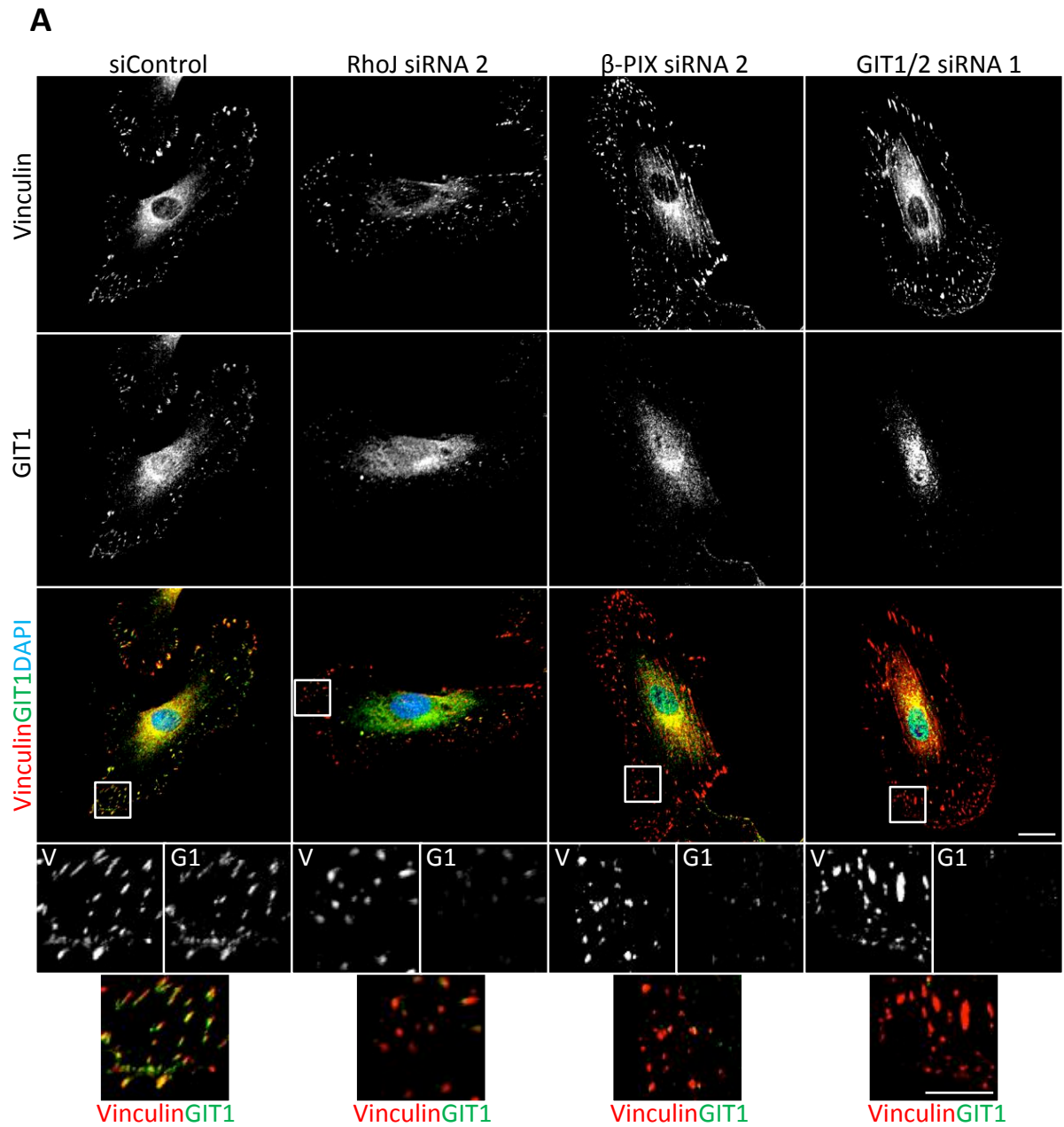


**Figure 4.14 Knockdown of RhoJ or  $\beta$ -PIX reduces recruitment of GIT1 to focal adhesions.**  
**A.** HUVEC transfected with control, RhoJ specific,  $\beta$ -PIX specific or GIT1/2 specific siRNA duplexes were fixed and stained for GIT1 after 48 h and imaged by confocal microscopy. Scale bar: 20  $\mu$ m. Inset scale bar: 10  $\mu$ m. V: vinculin; G1: GIT1.

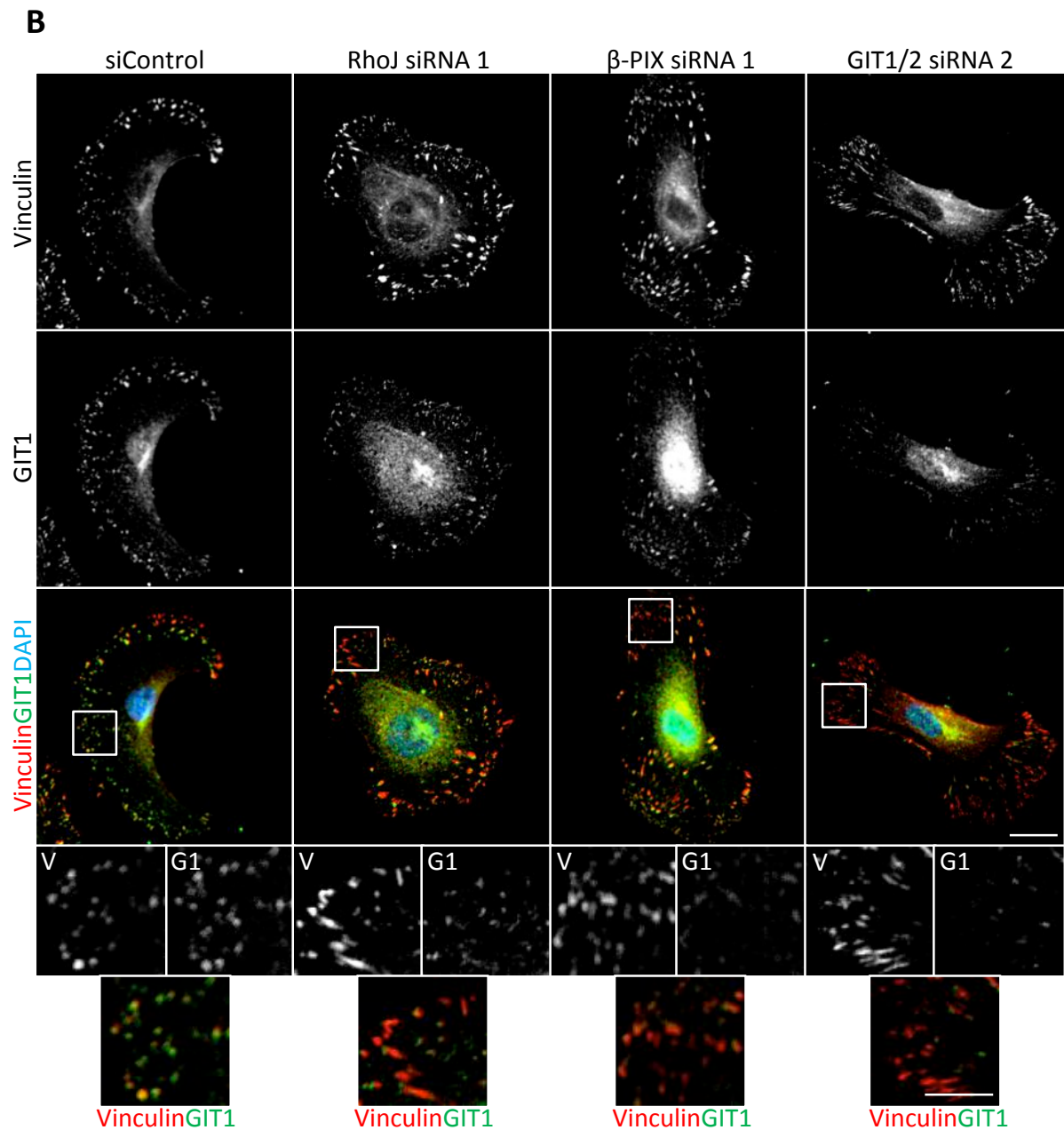


**Figure 4.14 Knockdown of RhoJ or  $\beta$ -PIX reduces recruitment of GIT1 to focal adhesions.**  
**B.** HUVEC were transfected with a second independent set of duplexes. After 48 h, cells transfected with control, RhoJ specific,  $\beta$ -PIX specific or GIT1/2 specific siRNA duplexes were fixed and stained for GIT1 and imaged by confocal microscopy. Scale bar: 20  $\mu$ m. Inset scale bar: 10  $\mu$ m. V: vinculin; G1: GIT1.

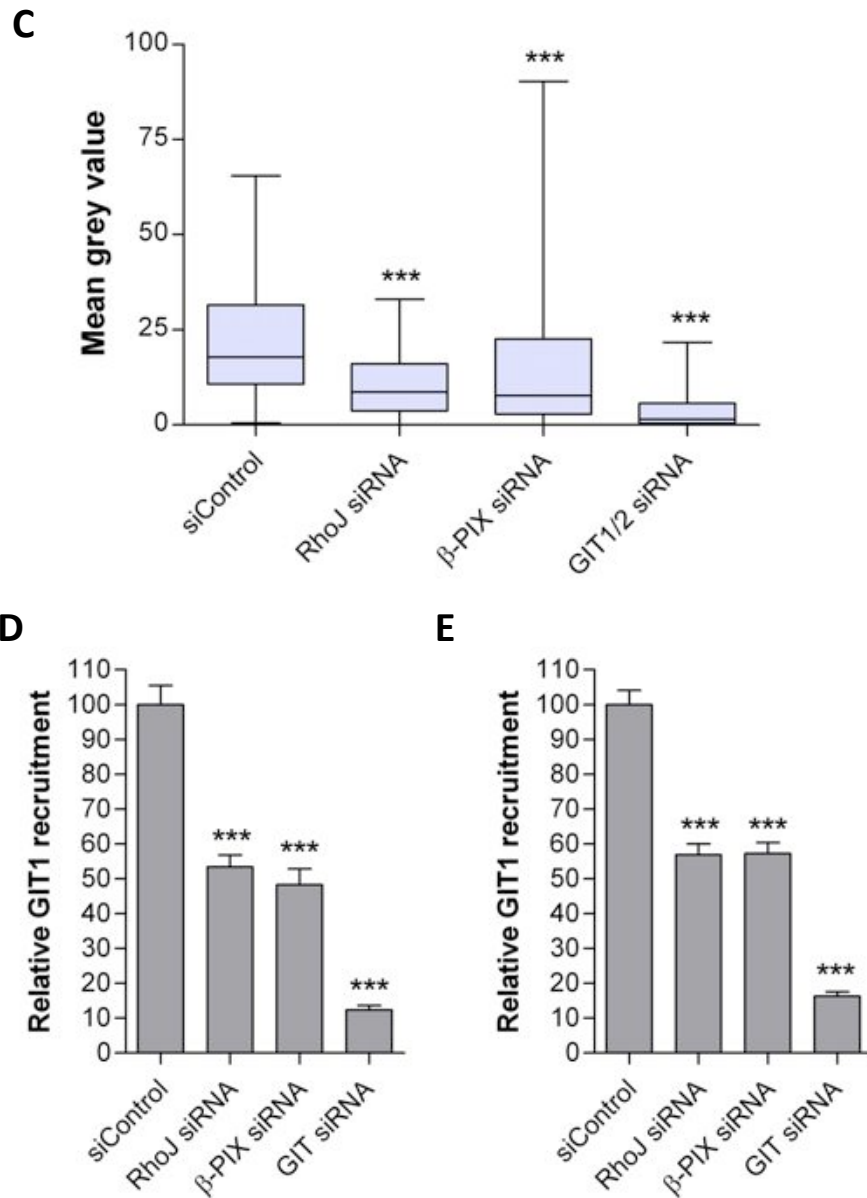


**Figure 4.14 Knockdown of RhoJ or β-PIX reduces recruitment of GIT1 to focal adhesions.**

**C.** Vinculin positive adhesions in cells transfected with siRNA duplexes were outlined and mean grey values of GIT1 staining were measured using ImageJ. Knockdown cells were compared to controls, and one experiment using the first set of duplexes presented as a box and whisker plot. The Mann Whitney test was used to assess statistical differences. **D-E.** Relative recruitment of GIT1 to adhesions was calculated and presented as a bar chart for the first (D) and second (E) set of duplexes. The Mann Whitney test was used to assess statistical significance.



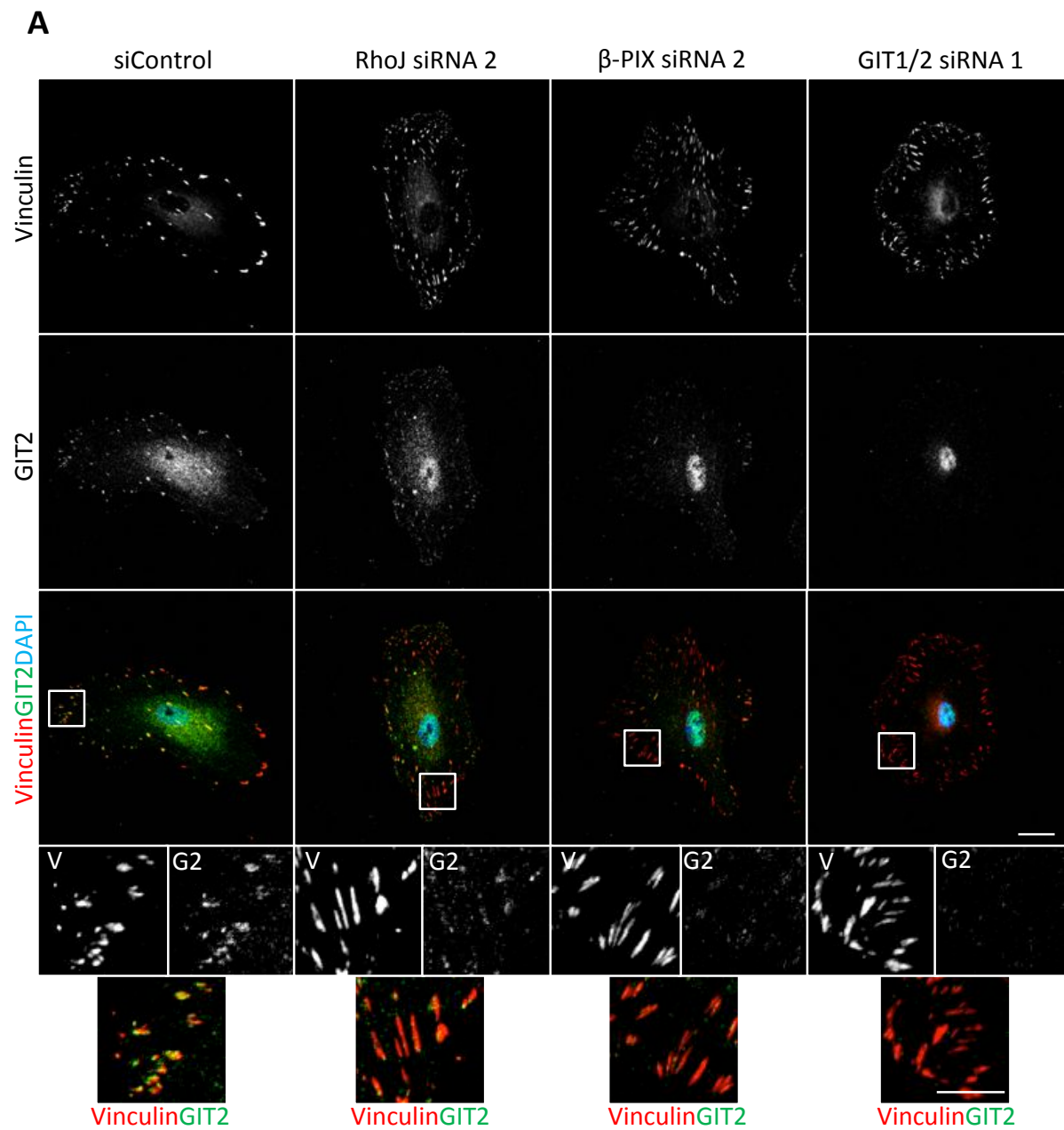


**Figure 4.15 Knockdown of RhoJ or  $\beta$ -PIX reduces recruitment of GIT2 to focal adhesions.**  
**A.** HUVEC transfected with control, RhoJ specific,  $\beta$ -PIX specific or GIT1/2 specific siRNA duplexes were fixed and stained for GIT2 after 48 h and imaged by confocal microscopy. Scale bar: 20  $\mu$ m. Inset scale bar: 10  $\mu$ m. V: vinculin; G2: GIT2.



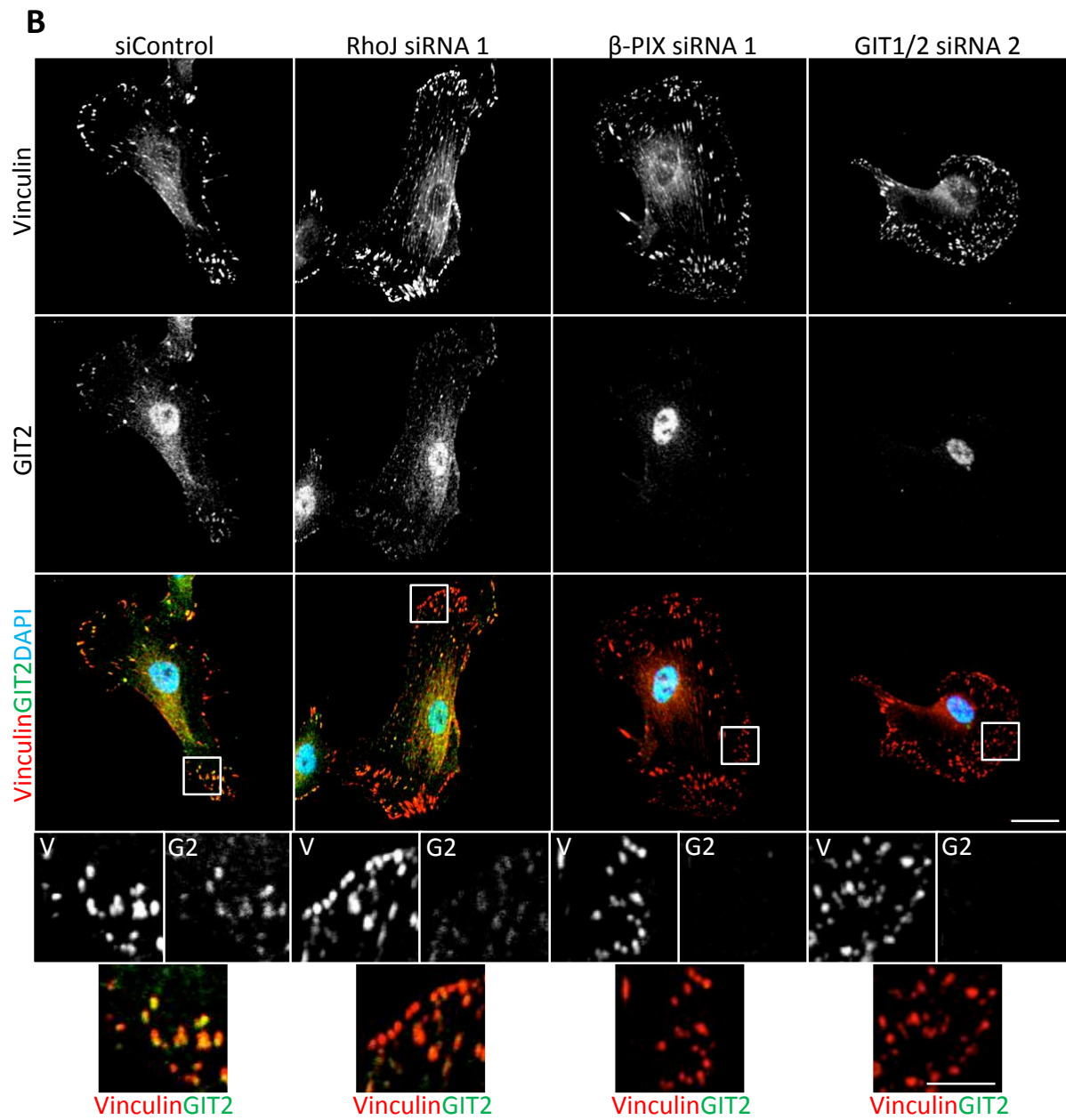


**Figure 4.15 Knockdown of RhoJ or  $\beta$ -PIX reduces recruitment of GIT2 to focal adhesions.**

**B.** HUVEC were transfected with a second independent set of duplexes. After 48 h, cells transfected with control, RhoJ specific,  $\beta$ -PIX specific or GIT1/2 specific siRNA duplexes were fixed and stained for GIT1 and imaged by confocal microscopy. Scale bar: 20  $\mu$ m. Inset scale bar: 10  $\mu$ m. V: vinculin; G2: GIT2.

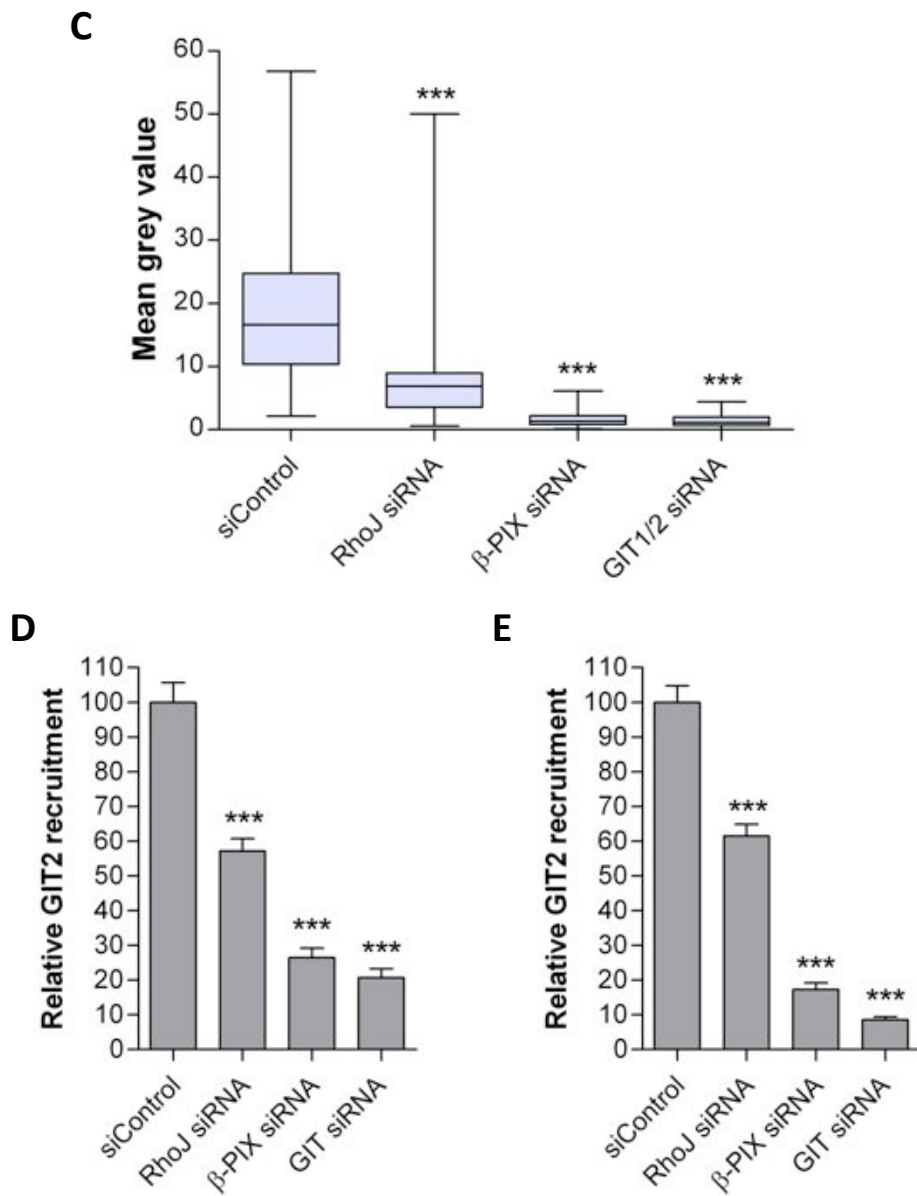


**Figure 4.15 Knockdown of RhoJ or β-PIX reduces recruitment of GIT2 to focal adhesions.** **C.** Vinculin positive adhesions in cells transfected with siRNA duplexes were outlined and mean grey values of GIT2 staining were measured using ImageJ. Knockdown cells were compared to controls, and one experiment using the first set of duplexes presented as a box and whisker plot. The Mann Whitney test was used to assess statistical differences. **D-E.** Relative recruitment of GIT2 to adhesions was calculated and presented as a bar chart for the first (D) and second (E) set of duplexes. The Mann Whitney test was used to assess statistical significance.

knockdown of RhoJ,  $\beta$ -PIX or GIT1/2. Significance was again analysed with a Mann Whitney test.

As expected, and echoing the data in Figures 4.12.C-4.15.C, each protein was least recruited to adhesions in cells transfected with siRNAs specific to that gene, e.g. RhoJ was mostly absent from focal adhesions in cells transfected with RhoJ specific duplexes.

RhoJ recruitment seemed to be similarly affected by knockdown of  $\beta$ -PIX and GIT1/2. The localisation of  $\beta$ -PIX to focal adhesions was also impaired in cells transfected with siRNA duplexes specific to RhoJ and GIT1/2. While the double knockdowns of GIT1 and GIT2 had the greatest effect on  $\beta$ -PIX recruitment, RhoJ knockdown also led to a modest, but still significant, reduction in  $\beta$ -PIX localisation.

Additionally, levels of GIT1 and GIT2 at focal adhesions were significantly reduced in cells transfected with RhoJ and  $\beta$ -PIX specific siRNA. GIT1 localisation was similarly affected in both conditions, GIT2 meanwhile was strikingly reduced in vinculin positive adhesions in  $\beta$ -PIX knockdown cells. RhoJ knockdown had a lesser but still significant effect on GIT2 recruitment.

In summary, the recruitment of each protein was found to be impaired upon knockdown of any of the other proteins in the complex, suggesting that their localisation to adhesions is interdependent. Given that each protein is required for proper recruitment of the RhoJ/GIT/PIX complex to focal adhesions, these data suggest that they function in concert to regulate focal adhesion dynamics.

## 4.9 Determining the effect of GIT and $\beta$ -PIX knockdown on endothelial tube formation

Previous data published by our laboratory (Kaur, Leszczynska *et al.* 2011) has shown a role for RhoJ in regulating endothelial tube formation. Knockdown of RhoJ leads to impaired tube formation in both Matrigel and co-culture assays, while expression of dominant active RhoJ induces enhanced branching of tubes. The data presented in the previous sections of this chapter suggest that RhoJ acts in a complex together with  $\beta$ -PIX, GIT1 and GIT2. If this is the case, it is logical to assume that the phenotype of  $\beta$ -PIX and GIT knockdown in these tube formation assays should be similar to that seen upon knockdown of RhoJ.

To investigate this hypothesis, HUVEC transfected with siRNA duplexes specific to RhoJ,  $\beta$ -PIX and GIT1/2 were cultured on HDF and allowed to form tubes for 6 days. Tubes were then fixed and stained for CD31. The panels in Figure 4.16.A show representative images of tubes formed by cells transfected with control or test siRNA duplexes. As expected diminished RhoJ expression leads to impaired tube formation, and this is also true of  $\beta$ -PIX and GIT1/2 knockdowns although perhaps to a slightly lower level. Numbers of tubules and junctions were analysed using AngioSys software (Figure 4.16.C), and while a decrease in these data was observed across all conditions, only RhoJ showed a significant difference compared to the control.

Tube formation on Matrigel was also investigated by Dr. Victoria Heath. HUVEC transfected with RhoJ,  $\beta$ -PIX and GIT1/2 siRNA duplexes were allowed to form tube-like networks on Matrigel, a solubilised basement membrane extract (Passaniti 1992). The panels in Figure

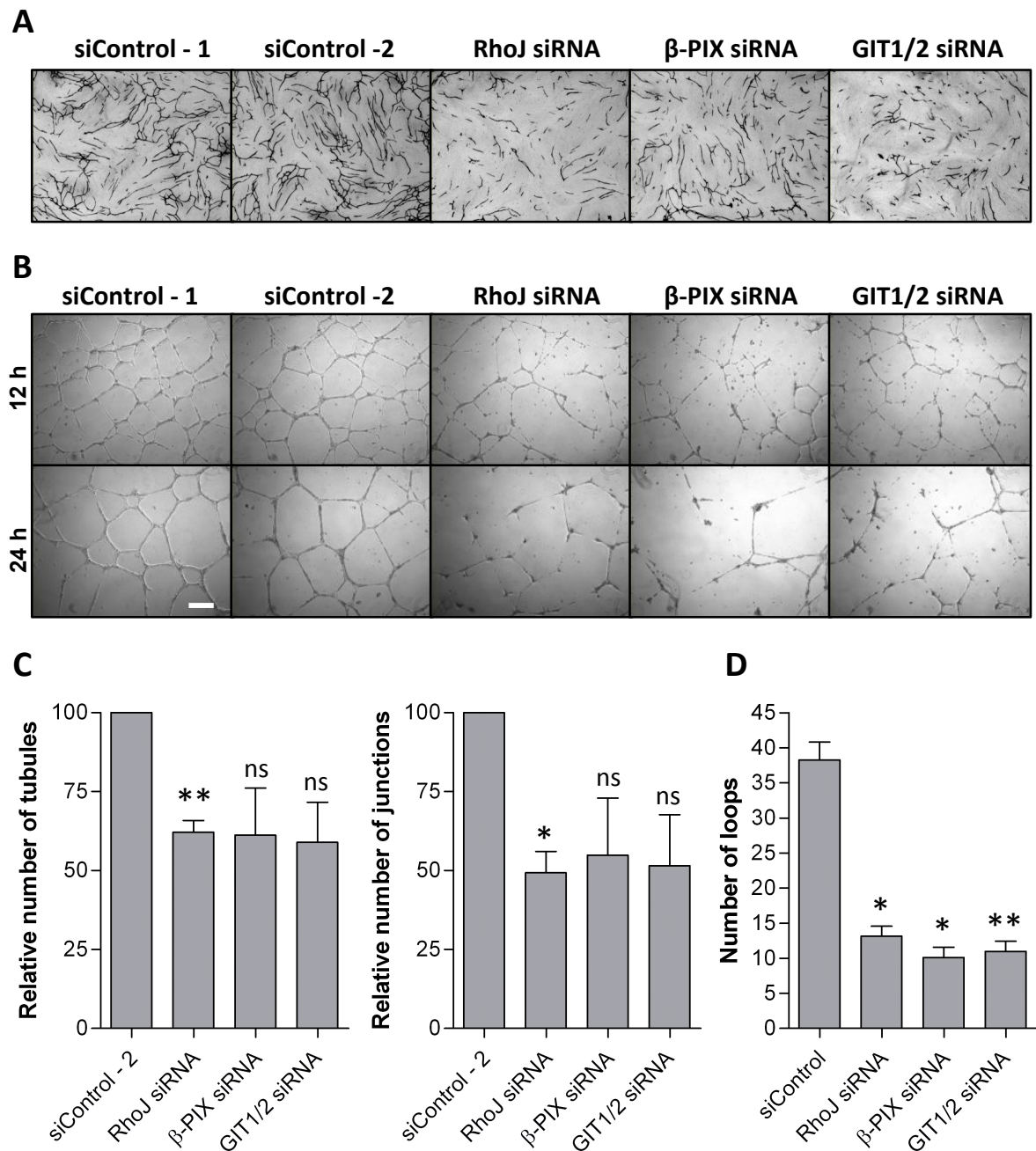


**Figure 4.16 Knockdown of  $\beta$ -PIX or GIT1/2 impairs tube formation.** **A.** HUVEC transfected with control (siControl-1 at 25 nM and siControl-2 at 50 nM), RhoJ specific (RhoJ siRNA 2),  $\beta$ -PIX specific ( $\beta$ -PIX siRNA 2, each at 25 nM) or GIT1/2 (a combination of GIT1 siRNA 2/ GIT2 siRNA 1 at 25 nM each) specific siRNA duplexes were plated onto fibroblasts one day after transfection. Endothelial tubes were stained after a further 6 days. These data are representative of 3 experiments. Tube assays were primarily carried out by Dr. Victoria Heath, however staining and transfections were performed by EW. **B.** HUVEC were transfected as above and 48 h after transfection, the cells were replated on matrigel and imaged after 12 and 24 h. Scale bar: 200 mm. **C.** Numbers of tubules and junctions, relative to controls, in the co-culture assay were analysed using the AngioSys software, and data displayed as a bar chart. A paired t-test was used to test significance. **D.** Tube formation in the Matrigel assay was analysed using the angiogenesis analyser for Image J to calculate numbers of loops formed after 12 h, and data displayed as a bar chart. A paired t-test was used to test significance.

4.16.B show example images of these tubes, with knockdowns leading to less connected networks. When these data were analysed using ImageJ, the numbers of loops formed in each of the knockdown conditions was found to be statistically significant (Figure 4.16.D).

Taken together, these data suggest that at a higher level the RhoJ/GIT/PIX complex functionally regulates tube formation in endothelial cells.

#### **4.10 Assessing the role of $\beta$ -PIX in regulating RhoJ activation**

Currently, no regulatory GAP and GEF proteins have been described for RhoJ, however  $\beta$ -PIX is a well-characterised GEF for Rac1 and Cdc42 (Manser, Loo *et al.* 1998, Koh, Manser *et al.* 2001, Feng, Albeck *et al.* 2002, ten Klooster, Jaffer *et al.* 2006). Since RhoJ interacts with  $\beta$ -PIX, the role of  $\beta$ -PIX in regulating RhoJ activation was explored.

Previous work by Katarzyna Leszczynska demonstrated that VEGF stimulation can activate RhoJ, as measured by pulldown of RhoJ bound to GST-CRIB beads. RhoJ is only capable of interacting with the CRIB domain (which is found in many effector proteins including PAK1-3) when bound by GTP and thus this is a suitable method of determining the levels of active RhoJ within the cell.

To assess the role of  $\beta$ -PIX in RhoJ activation, HUVEC were transfected with a  $\beta$ -PIX specific siRNA duplex. After 48 h, cells were starved for 1 h, activated with 10 ng/ml VEGF for 15-30 min, lysed and incubated with GST-CRIB bound glutathione agarose beads. After pulldown, samples were subjected to SDS-PAGE and levels of active RhoJ compared to total levels.

Western blots from two independent replicates are shown in Figure 4.17. While an increase in levels of active RhoJ can be seen after 30 min stimulation of control cells with VEGF, there

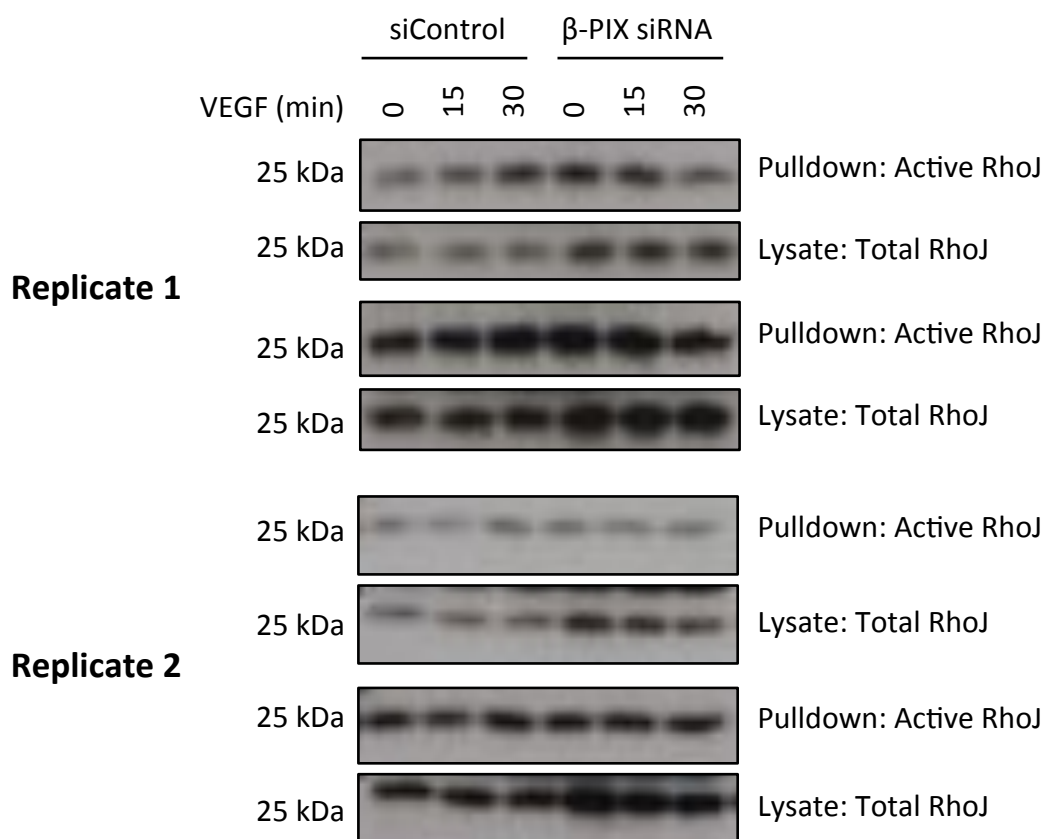


**Figure 4.17 Knockdown of  $\beta$ -PIX may partially impair VEGF-stimulated RhoJ activation.** HUVEC were transfected with either siControl or  $\beta$ -PIX ( $\beta$ -PIX siRNA 2) specific duplexes at 10 nM. After 48 h cells were rested for 1 h and stimulated with VEGF for the indicated time periods. Cells were then lysed and active RhoJ-GTP was pulled down. Both pull downs and lysates were subjected to SDS-PAGE and Western blotting for RhoJ. Blots from two independent replicates are shown (each with two different exposures).

is no induction of RhoJ activation in  $\beta$ -PIX knockdown cells. These data suggest that  $\beta$ -PIX expression is required for proper RhoJ activation and as such may be involved in the regulation of its activity, however further replicates must be performed in order to draw firm conclusions.

#### **4.11 The effect of dominant active RhoJ expression on GIT2 phosphorylation**

Previous data presented in this chapter has shown that RhoJ interacts with the focal adhesion protein GIT2, however GIT2 itself must be phosphorylated by Src or FAK at 3 tyrosine residues (Tyr 286, 392 and 592) before it can recruit to focal adhesions. Since expression of GFP-daRhoJ led to increased recruitment of GIT2 to adhesions (as seen by immunofluorescence in Section 4.6), the effect of this protein on total and phospho-GIT2 was assessed by Western blotting.

Whole cell lysates were made from GFP only and GFP-daRhoJ expressing HUVEC and probed for expression of total GIT2 and phospho-GIT2 (Tyr 392). Representative blots of lysates from each condition are shown Figure 4.18, with GFP blotted to confirm expression of constructs and tubulin to act as a loading control. As can be seen, expression of GFP-daRhoJ leads to increased levels of GIT2, which is phosphorylated at Tyr 392. Densitometry was also performed, which confirmed that the increase in levels of both GIT2 and phospho-GIT2 were approximately five-fold. The increase in GIT2 was not statistically significant ( $p=0.0539$ ), while the increase in levels of phospho-GIT2 was significant ( $p=0.0176$ ), and this difference is likely due to variation between experimental replicates.



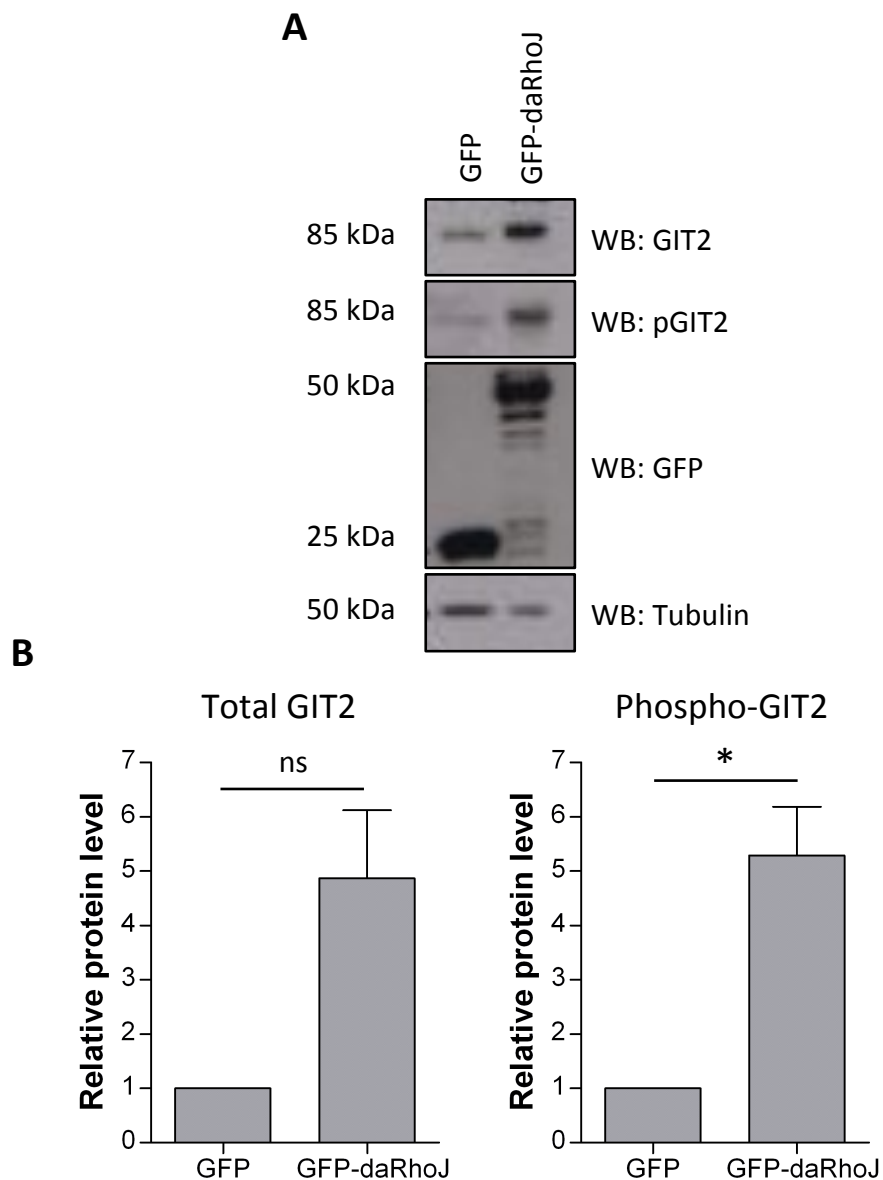


**Figure 4.18 GFP-daRhoJ expression increases levels of GIT2, which is phosphorylated at Tyr 392. A.** HUVEC stably expressing GFP or GFP-daRhoJ were lysed and samples Western blotted for total and phospho-GIT2 (Tyr 392, pGIT2), with tubulin and GFP acting as controls for loading and plasmid expression respectively (representative of 4 experiments). **B.** Relative levels of total and phospho-GIT2 (Tyr 392) were measured using densitometry, and corrected to the tubulin loading control. Data are presented as a bar chart, with a paired t-test used to test significance (\* =  $p \leq 0.05$ ).

There is also a small increase in size of the GIT2 band in the GFP-daRhoJ which is possibly due to increased levels of phosphorylation on serine and threonine residues. Many sites of tyrosine, threonine and serine phosphorylation have been identified in GIT1, and these residues are frequently conserved in the GIT2 protein (Webb, Mayhew *et al.* 2006). These data suggest that dominant active RhoJ potentiates GIT2 expression (or stabilises the protein), and that this increased level of protein is also more phosphorylated than in GFP controls.

#### **4.12 The effect of RhoJ knockdown on GIT2 expression**

While the data in Section 4.11 show that expression of a dominant active mutant of RhoJ induces an increase in levels of total GIT2, knockdown of RhoJ expression did not lead to a noticeable decrease in total GIT2 protein. To determine whether there was any effect on phosphorylation, lysates from were blotted with antibodies against total and phosphorylated (Tyr 392) GIT2.

Example Western blots of lysates from HUVEC transfected with control or RhoJ specific siRNA duplexes are shown in Figure 4.19. While total levels of GIT2 do not appear to be altered in RhoJ knockdown cells, which is confirmed by the results from densitometry ( $p=0.5628$ ), there is a small but consistent decrease in phospho-GIT2 (Tyr 392) in these cells compared to control HUVEC, suggesting that RhoJ is involved in the regulation of GIT2 phosphorylation. Densitometry of levels of phospho-GIT2 in control and RhoJ knockdown lysates demonstrate that this decrease is statistically significant ( $p=0.0424$ ).

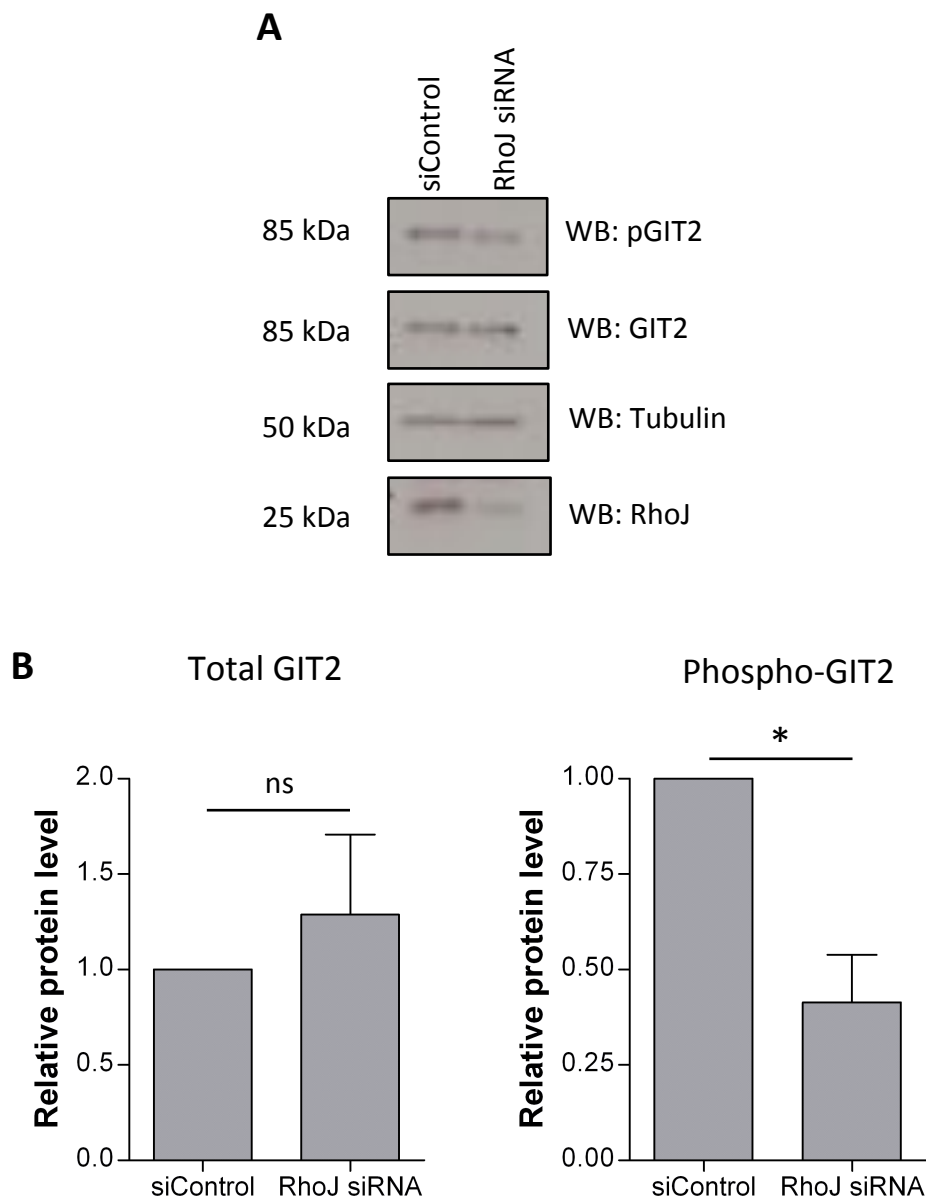


**Figure 4.19 Knockdown of RhoJ reduces phosphorylation of GIT2 on Tyr 392 but has no effect on the level of total GIT2. A.** HUVEC were transfected with 10 nM control (siControl) or RhoJ specific (RhoJ siRNA 2) siRNA duplexes and 48 h later cells were lysed and samples Western blotted for levels of total and phospho-GIT2 (Tyr 392, pGIT2). Tubulin was used as a loading control and RhoJ to confirm knockdown (representative of 3 experiments). **B.** Relative levels of total and phospho-GIT2 (Tyr 392) were measured using densitometry, and corrected to the tubulin loading control. Data are presented as a bar chart, with a paired t-test used to test significance (\* =  $p \leq 0.05$ ).

## 4.13 Investigating the effect of Src and FAK inhibitors on GIT2 phosphorylation

It has been established by others (Brown, Cary *et al.* 2005) that Src and FAK phosphorylate GIT2 at 3 tyrosine residues, and this phosphorylation enables binding to paxillin and localisation to focal adhesions. The work in the previous sections demonstrate that RhoJ has some function in regulating GIT2 phosphorylation, so inhibitors of Src and FAK were used to determine whether inhibiting their action would abolish the increase in total and phospho-GIT2 (Tyr 392) seen in GFP-daRhoJ expressing cells.

HUVEC expressing GFP or GFP-daRhoJ were treated with dasatinib to reduce Src activity (Lombardo, Lee *et al.* 2004), and PF573228 to inhibit FAK activity (Slack-Davis, Martin *et al.* 2007). Lysates were made and samples blotted for total and phospho-GIT2, as well as the total and phospho- forms of FAK (Tyr397) and Src (Tyr416).

The blots in Figure 4.20 show samples from untreated cells alongside those treated with dasatinib only, PF573228 only or dasatinib and PF573228 together. While there is little to no effect on total GIT2, phospho-GIT2 (Tyr 392) levels are reduced in all cells treated with inhibitors. Both Src and FAK inhibition appear to reduce phosphorylation of GIT2 Tyr 392 to a similar extent, with a small additive effect when the inhibitors are combined. There is not, however, a complete abolishment of phosphorylation in GFP-daRhoJ expressing cells treated with both inhibitors. This may partly be due to increased FAK activity induced by Src inhibition, as shown by increased levels of FAK autophosphorylation. Taken together, these data confirm that the increased phosphorylation of GIT2 in GFP-daRhoJ cells is due to Src

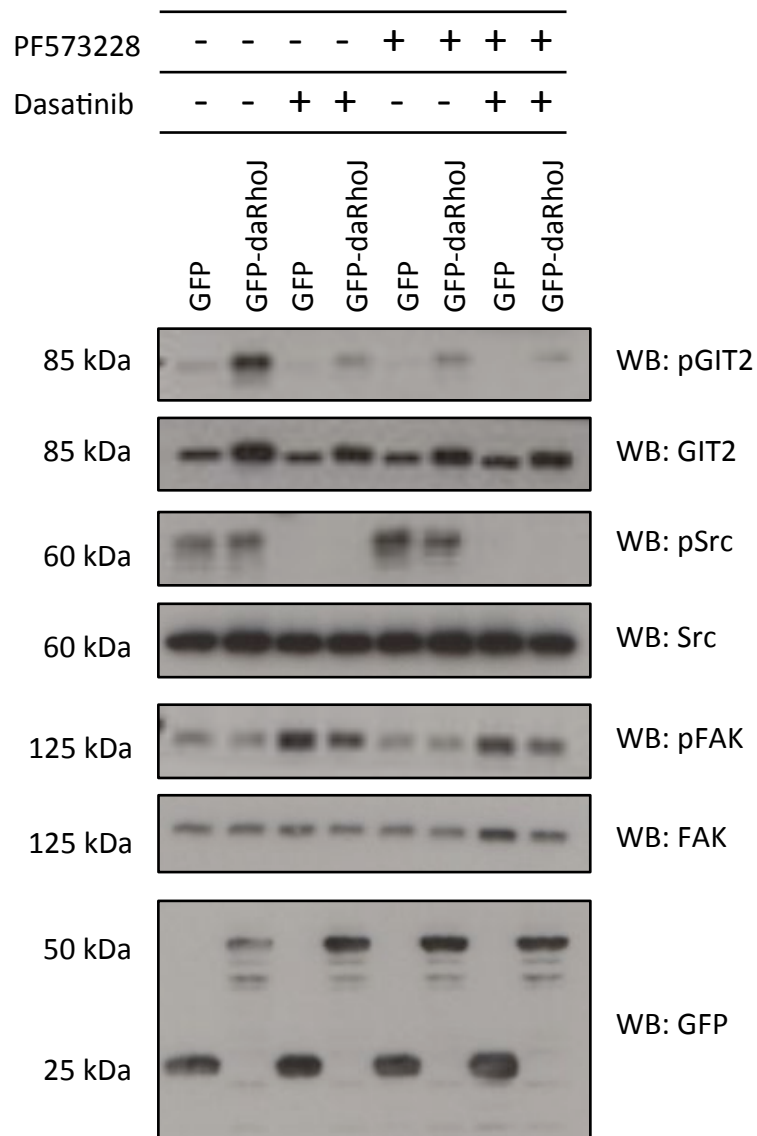


**Figure 4.20 Inhibitors of Src and FAK inhibit the GFP-daRhoJ induced increase in GIT2 phosphorylation on Tyr 392 but do not reduce the increase observed in total GIT2 levels.** HUVEC stably expressing GFP or GFP-daRhoJ were treated with the FAK inhibitor PF573228 (1  $\mu$ M), Src inhibitor Dasatinib (50 nM) or a combination of both and subsequently lysed. Samples were Western blotted for total and phospho-GIT2 (Tyr 392), as well as total and phosphorylated Src and FAK. GFP was used as a control to confirm expression of plasmids (representative of 3 experiments).

and FAK activity. However, it should be noted that while the FAK inhibitor PF573228 appears to be inhibiting phosphorylation of GIT2, it does not appear to completely inhibit FAK auto-phosphorylation (at Tyr 397). This inhibitor should be very specific, and its effect on GIT2 phosphorylation must be carefully considered and investigated further in order to conclusively say that FAK inhibition impairs phosphorylation of GIT2.

One point of note from these experiments is that the shift in size observed in total GIT2 in GFP-daRhoJ expressing HUVEC is not lost upon treatment with inhibitors. This indicates that the change in molecular weight is not due to phosphorylation of Tyr392, and is not dependent on Src or FAK activity, however this must be further investigated since the increased level of protein could also have an impact on the apparent molecular weight.

#### **4.14 Screening the effect of dominant active RhoJ expression on kinase phosphorylation**

RhoJ plays a role in regulating GIT2 phosphorylation, so a screen was performed to determine if daRhoJ affected phosphorylation of other proteins. The human phospho-kinase array kit (R&D Systems) was used to characterise lysates from GFP and GFP-daRhoJ expressing cells. It utilises immobilised antibodies against phosphorylated forms of a wide range of kinases. Membranes spotted with capture antibodies against specific protein phosphorylation sites were incubated with lysates from each condition. Subsequently, these membranes were probed with pre-prepared cocktails of biotinylated detection antibodies, and finally Streptavidin-HRP was used to detect the relative phosphorylation levels of each protein in the screen.

A representative blot of membranes incubated with lysates from GFP or GFP-daRhoJ expressing cells is shown in Figure 4.21. The histograms in Figure 4.22 show the relative phosphorylation of each protein in the array in GFP control and GFP-daRhoJ cells. Proteins have been separated into graphs of similar phosphorylation levels. As expected, reference spots gave almost identical levels of intensity in both conditions (A1,A2, A17, A18 and G1,G2) and negative control spots (PBS) showed minimal intensities (G9, G10 and G17,G18).

When statistically analysed (2 spots per experiment, performed on 2 different HUVEC isolates), several proteins were found to be more phosphorylated in GFP-daRhoJ expressing cells compared to GFP only controls. These proteins were c-Jun N-terminal kinase (JNK), EGF receptor (EGFR), AMP-activated protein kinase  $\alpha 2$  (AMPK $\alpha 2$ ), Signal Transducer and Activator of Transcription 5 a/b (STAT5a/b), haemopoietic cell kinase (Hck) and  $\beta$ -catenin. Data are presented as a scatter plot in Figure 4.23.A, and as individual histograms in Figures 4.23.B.

A further 4 proteins, Mitogen and Stress-activated protein kinase 1 and 2 (MSK1/2), endothelial nitric oxide synthase (eNOS), heat shock protein 27 (HSP27) and proline-rich Akt substrate of 40 kDa (PRAS40), were found to have a significance of below 0.1, these are presented in Figure 4.24.A with the individual histograms in Figures 4.24.B. Of these proteins, only eNOS (S1177) was more phosphorylated in GFP cells compared to GFP-daRhoJ cells. Finally, 5 more proteins, STAT5b, P38 $\alpha$ , Fyn, Lyn and cAMP-response element-binding protein (CREB), showed a trend towards increased phosphorylation in GFP-daRhoJ expressing cells in both replicates as shown in Figure 4.25, however variation between levels

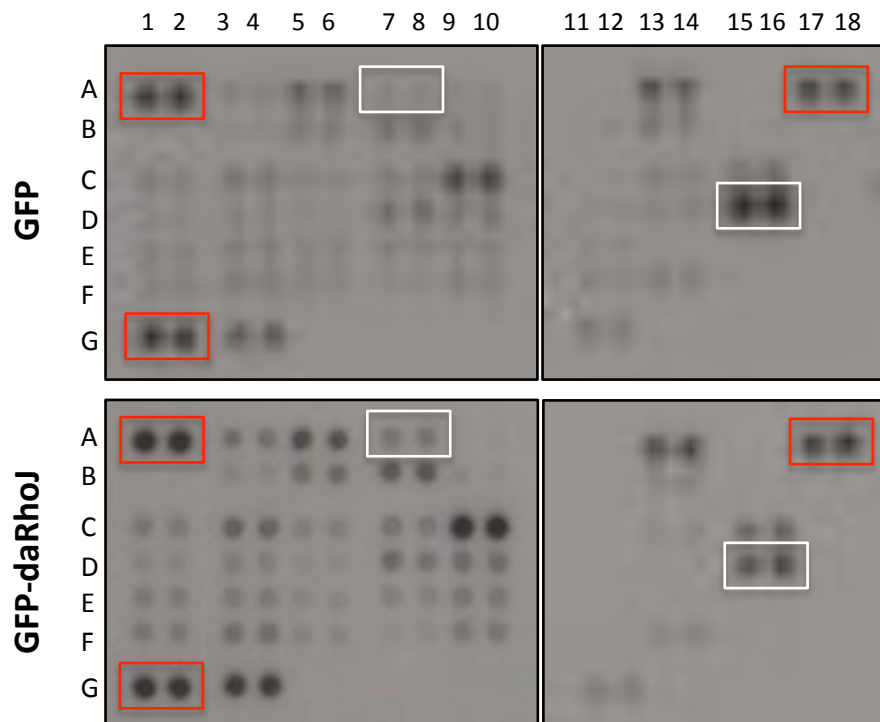


**Figure 4.21. GFP-daRhoJ expression induces changes in phosphorylation of a panel of human kinases.** GFP or GFP-daRhoJ expressing cells were probed using the Proteome Profiler human phospho-kinase array, with representative blots of membranes incubated with lysates from GFP and GFP-daRhoJ expressing cells. Relative levels of phosphorylation were calculated for each kinase by measuring mean grey values of each spot in each condition. Red boxes highlight reference spots (A1-2, A17-18 and G1-2). White boxes highlight spots for eNOS Ser 1177 (D15-16) and JNK Thr 183/Tyr 185, Thr 185/Tyr 187 (A7-8).



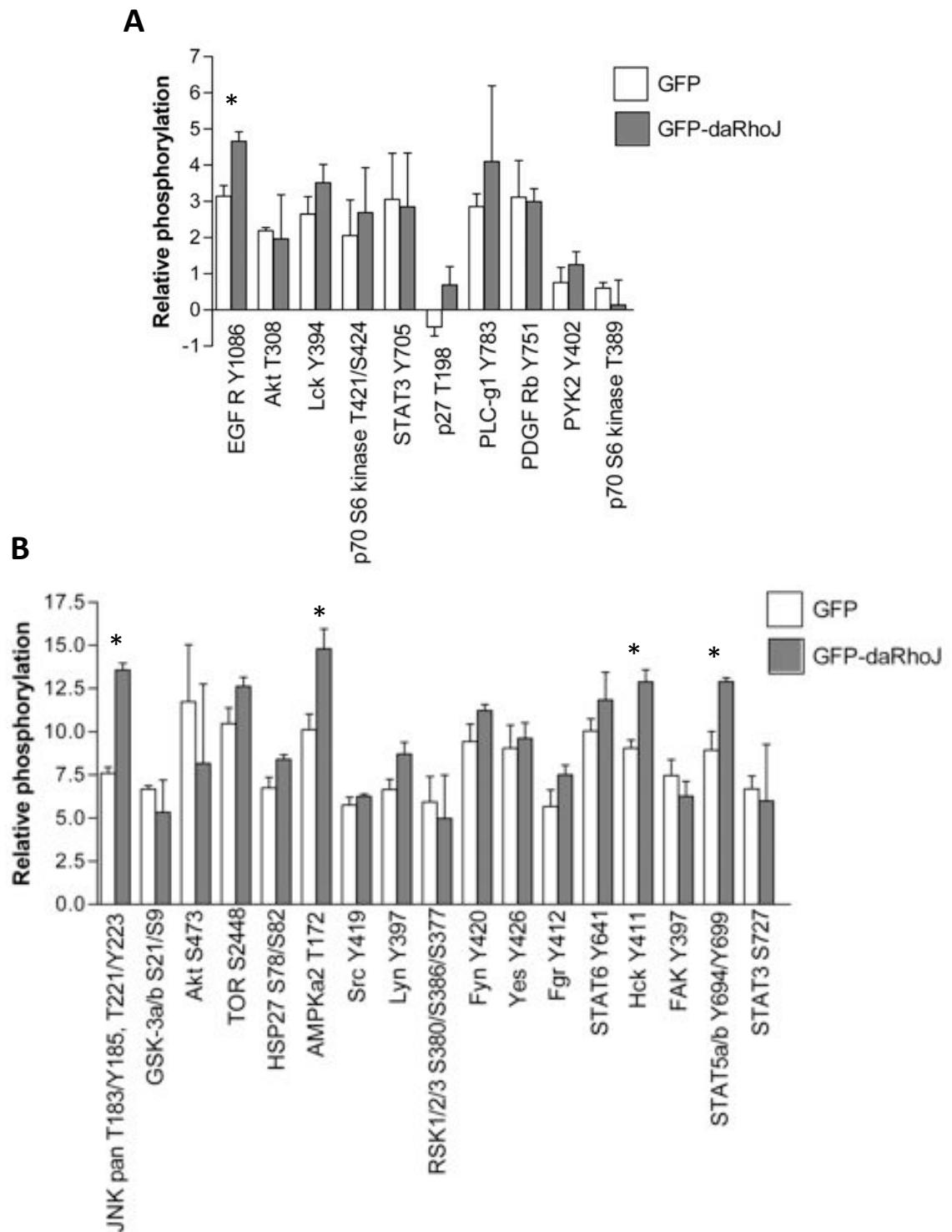


**Figure 4.22. GFP-daRhoJ expression induces changes in phosphorylation of a panel of human kinases.** GFP or GFP-daRhoJ expressing cells were probed using the Proteome Profiler human phospho-kinase array and relative levels of phosphorylation calculated for each kinase. **A-D.** Proteins have been separated into graphs of similar relative phosphorylation values, with **A** showing the lowest levels and **D** the highest (\*= $p \leq 0.05$ ).

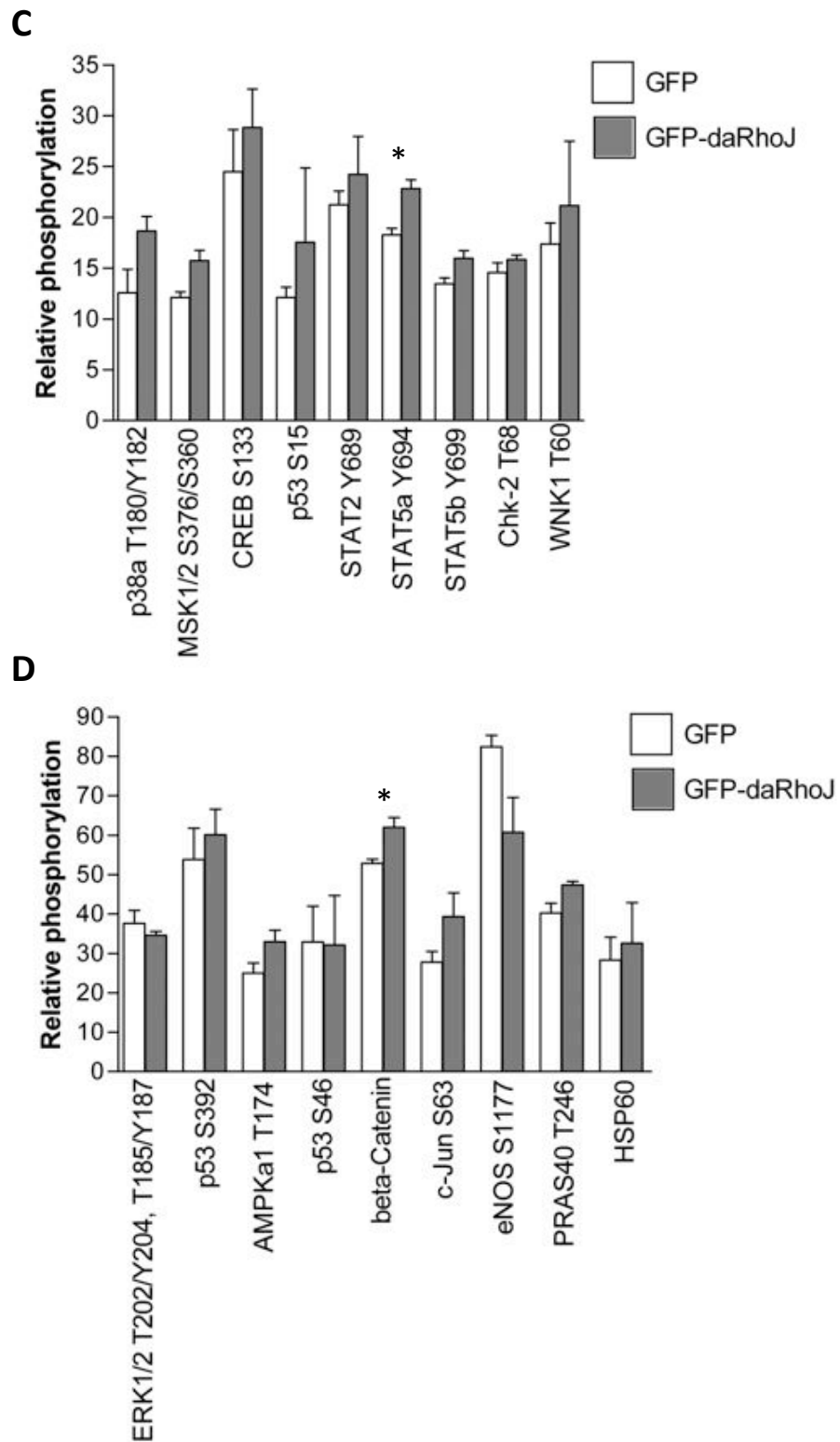


**Figure 4.22. GFP-daRhoJ expression induces changes in phosphorylation of a panel of human kinases.**

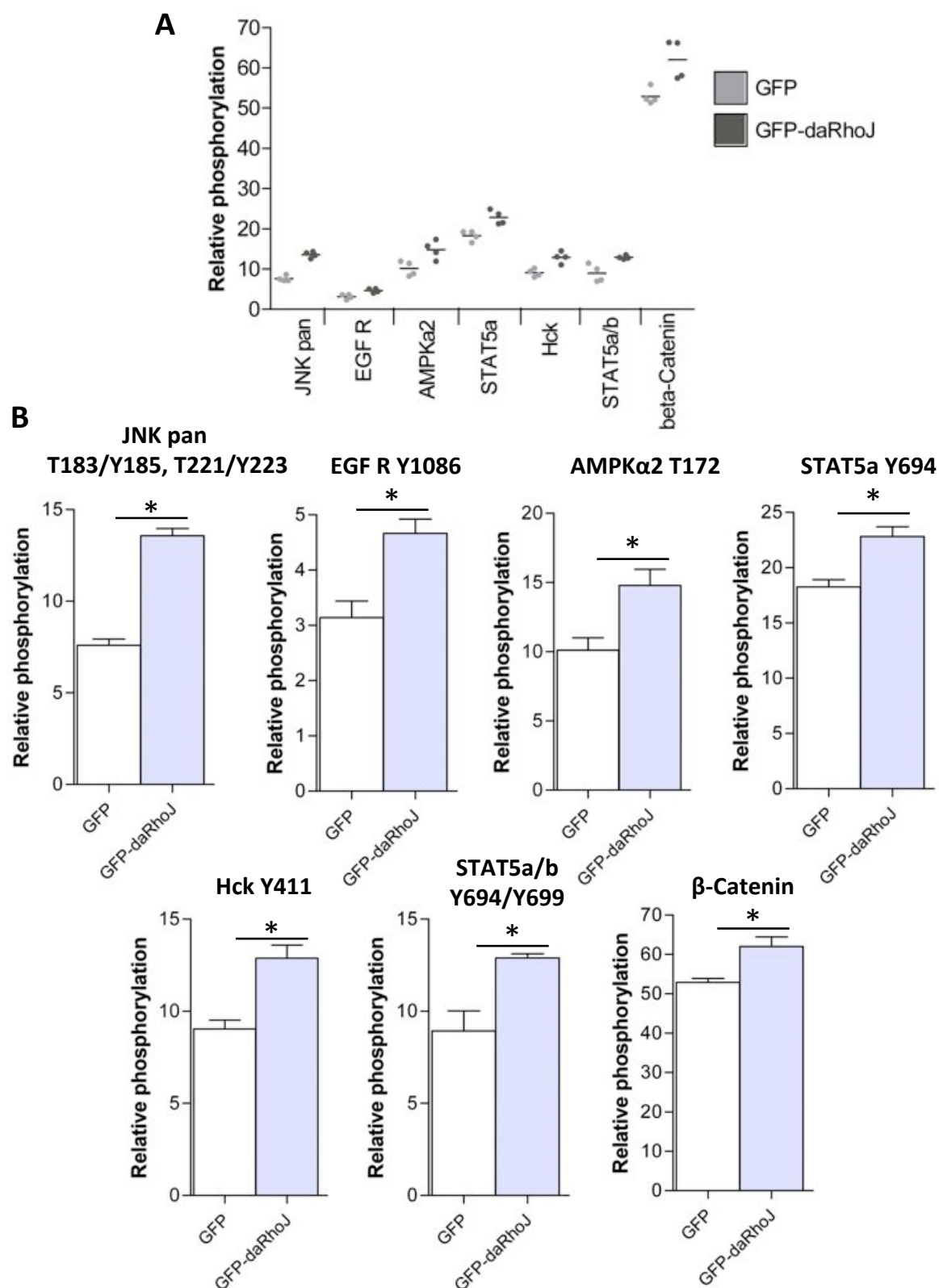


**Figure 4.23** GFP-daRhoJ expression increases phosphorylation of JNK, EGF receptor, AMPKa2, STAT5a and b, Hck and  $\beta$ -Catenin. Data from human phospho-kinase array were analysed and 7 proteins were found to be significantly more phosphorylated in GFP-daRhoJ expressing cells compared to GFP only cells when analysed with the Mann Whitney test. **A.** Data are presented as a scatter plot. **B.** Data are presented as histograms for each protein (\*= $p \leq 0.05$ ).

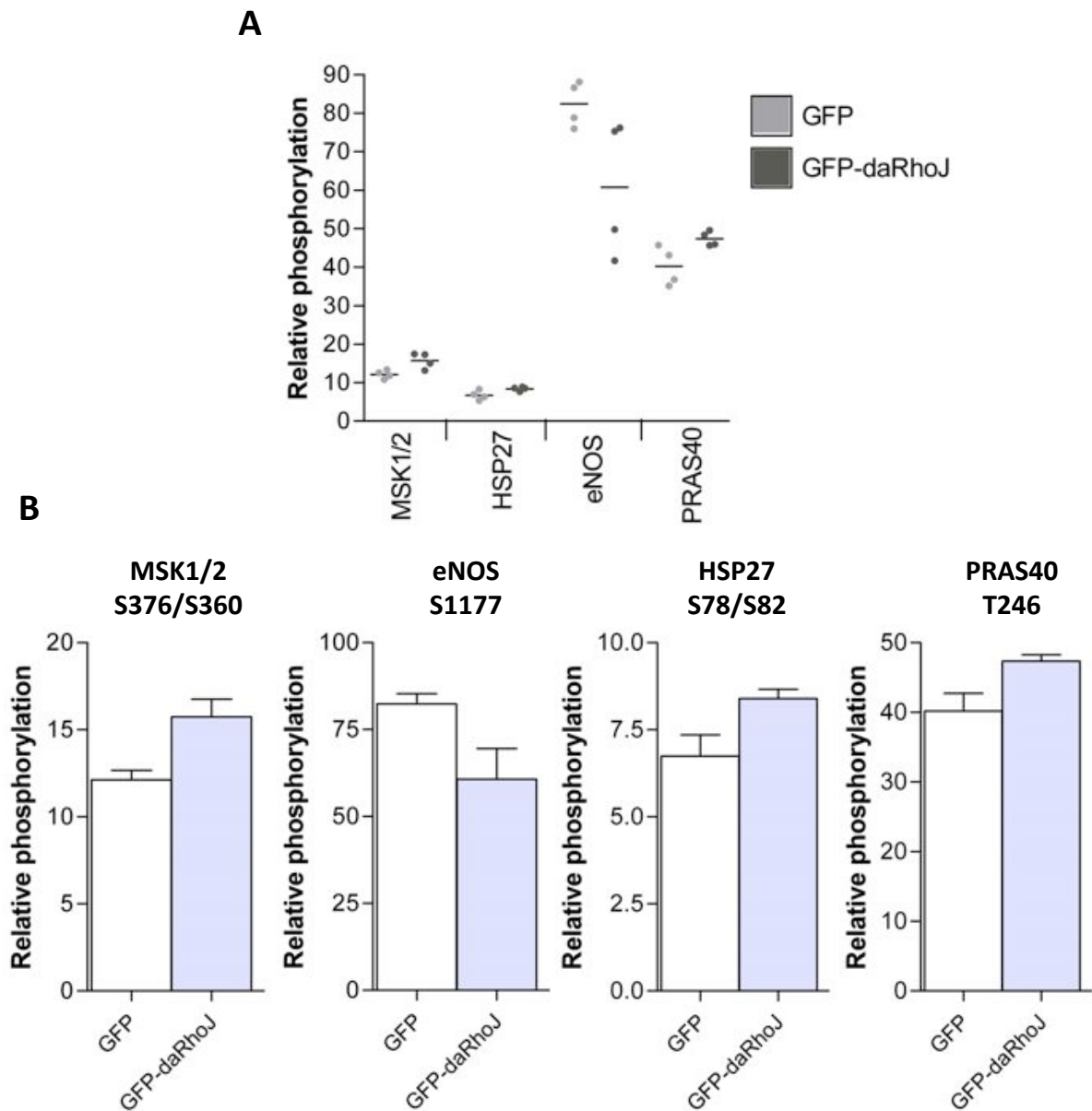


**Figure 4.24 GFP-daRhoJ expression affects phosphorylation of MSK1/2, eNOS, HSP27 and PRAS40.** Data from human phospho-kinase array were analysed and the 4 proteins listed were all found to have significance values close to 0.05 when analysed using the Mann Whitney test, however they were not statistically significant. **A.** Data are presented as a scatter plot of relative phosphorylation. **B.** Data are shown as histograms for each protein.

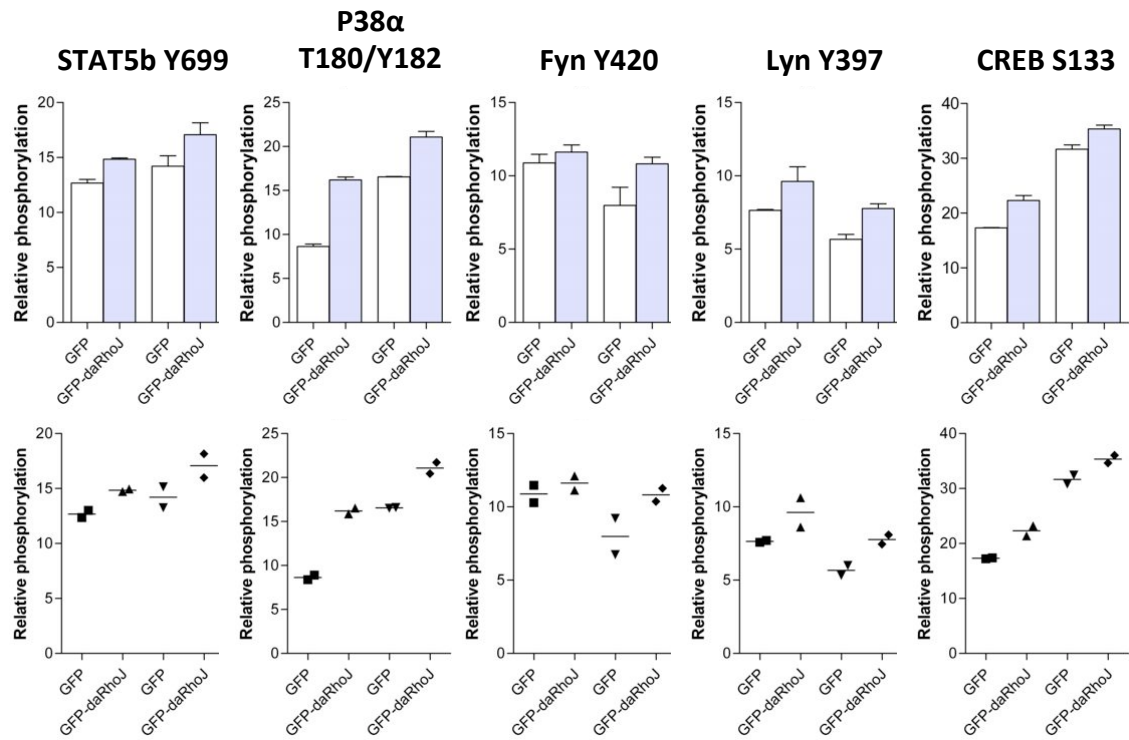


**Figure 4.25 GFP-daRhoJ expression led to a trend in increased phosphorylation of STAT5b, P38α, Fyn, Lyn and CREB.** Data from the human phospho-kinase array were analysed and it was found the proteins listed showed a trend towards an increase in phosphorylation in both the isolates used. The variability of individual HUVEC isolates was such that they were not statistically significant when using the Mann Whitney test. Relative phosphorylation values of the indicated residues are presented as histograms and scatter plots, with replicates separated for each protein.

of phosphorylation between isolates meant that statistical analysis did not detect any differences.

These data suggest that RhoJ may be involved in regulating phosphorylation of other proteins, primarily when in its active form. Further validation and investigation is however required to confirm these results and draw conclusions.

## 4.15 Discussion

The results presented in this chapter demonstrate interactions between RhoJ and the focal adhesion proteins GIT1, GIT2 and  $\beta$ -PIX. RhoJ directly interacts with the SHD domain of GIT1, as shown by yeast two-hybrid, while GFP-trap assays have demonstrated that daRhoJ is also capable of pulling down GIT2 and  $\beta$ -PIX. Immunofluorescent staining also indicates that these proteins co-localise at and regulate one another's recruitment to focal adhesions, while multiple *in vitro* assays have shown a function in endothelial tube formation. Additionally, it appears that  $\beta$ -PIX regulates RhoJ activation, and RhoJ activity modulates GIT2 phosphorylation. Finally, a kinase array has suggested that expression of daRhoJ affects phosphorylation of multiple other proteins, including JNK and eNOS. Taken together, the data presented strongly suggests that RhoJ interacts both functionally and physically with the GIT/PIX complex in order to regulate endothelial cell biology.

Previous experiments performed in our laboratory identified  $\beta$ -PIX and GIT1 as interacting partners for RhoJ, with a model proposed whereby RhoJ interacts directly with the SHD of GIT1 and associates with  $\beta$ -PIX as a result of this interaction (Katarzyna Leszczynska, PhD thesis).  $\beta$ -PIX binds to the SHD and coiled coil domains of GIT1 (Premont, Perry *et al.* 2004),

and the interaction between RhoJ and GIT1 had previously been mapped to the Spa homology domain using GIT truncation mutants (Katarzyna Leszczynska, PhD thesis). It did not, however, appear that the SHD was sufficient for binding RhoJ (Katarzyna Leszczynska, PhD thesis), so the binding site for RhoJ within GIT1 was assessed further using deletion mutants previously employed to map the interaction between  $\beta$ -PIX and GIT1 (Premont, Perry *et al.* 2004).

Deletion of the entire SHD region but preservation of all other GIT1 domains eliminated binding of RhoJ to GIT1, a result also seen upon deletion of the second tandem repeat (SpaB). Deletion of the first tandem repeat of the GIT1 SHD did not completely prevent the interaction with RhoJ, however less yeast growth was observed. These data suggest that both SpaA and SpaB are required for full binding of RhoJ to GIT1, but that RhoJ interacts more strongly with SpaB than SpaA. Additionally, these data demonstrate that both RhoJ and  $\beta$ -PIX interact with the same region of GIT1, although since a RhoJ/GIT/PIX complex recruits to focal adhesions together, RhoJ and  $\beta$ -PIX do not appear to compete for this domain. A number of other proteins also bind GIT at the SHD, including phospholipase C- $\gamma$ , Piccolo and MEK (Haendeler, Yin *et al.* 2003, Kim, Ko *et al.* 2003, Yin, Haendeler *et al.* 2004), and others have shown previously that GIT1 is capable of simultaneously binding to  $\beta$ -PIX and FAK, rather than binding of one protein displacing another (Zhao, Manser *et al.* 2000). Kim *et al.* also determined that Piccolo, FAK and  $\beta$ -PIX bind to distinct regions within the SHD (Kim, Ko *et al.* 2003). Thus it seems that this is also the case for RhoJ and  $\beta$ -PIX, although since the individual residues that are responsible for binding these proteins within the SHD have yet to be identified, it cannot be concluded precisely where each protein binds. While direct binding has not been established between RhoJ and GIT2, the GIT proteins are highly

homologous (Hoefen and Berk 2006) and given that GIT2 is pulled down with GFP-daRhoJ it is likely that these proteins also interact in a similar fashion to RhoJ and GIT1.

Functionally, RhoJ, GIT and  $\beta$ -PIX appear to work in a complex. While co-localisation within cells is not complete, some overlap can be seen between GFP-daRhoJ and GIT/PIX at focal adhesions, and moreover the recruitment of each protein is reciprocally regulated by the others in the complex. GIT localises to focal adhesions by binding to paxillin, and  $\beta$ -PIX in turn localises to these complexes by binding GIT (Turner, Brown *et al.* 1999, Zhao, Manser *et al.* 2000, Premont, Perry *et al.* 2004). It has been demonstrated that RhoJ binds to GIT, and indirectly associates with  $\beta$ -PIX (Katarzyna Leszczynska, PhD thesis). The observation that silencing of any member of the RhoJ/GIT/PIX complex affects recruitment of the other proteins in the complex demonstrates that there is some interplay between this localisation, however there are still questions remaining regarding the order of recruitment, and how each protein regulates the others. For example, it is known that GIT binds to both RhoJ and paxillin, and it is thought that the interaction with GIT enables localisation of RhoJ to focal adhesions, however it is unclear why RhoJ knockdown should affect recruitment of GIT to focal adhesions. GIT2 must be phosphorylated at 3 tyrosine residues (Tyr 286, 392 and 592) before it is able to interact with paxillin and be recruited to focal adhesions (Brown, Cary *et al.* 2005), and the results in this chapter show that RhoJ activation modulates GIT2 phosphorylation. It is therefore possible that the loss of RhoJ weakens the interaction between GIT and paxillin, and impairs recruitment to adhesions as a result.

The data presented in Chapter 3 show that RhoJ regulates focal adhesion dynamics, and in particular adhesion disassembly. GIT1 and  $\beta$ -PIX have previously been implicated in



regulating focal adhesion disassembly, and knockdown of either protein has been found to impair the disassembly phase of adhesion dynamics (Nayal, Webb *et al.* 2006, Kuo, Han *et al.* 2011), phenocopying the effect of RhoJ knockdown and further suggesting that these proteins function in concert with one another. Given that knockdown of  $\beta$ -PIX or GIT1/2 also phenocopies the effect of RhoJ silencing on tube formation, these data strongly suggest that RhoJ, GIT and  $\beta$ -PIX function together in order to regulate adhesion disassembly and migration and tube formation.

As mentioned previously, the data presented in this chapter suggests that RhoJ regulates tyrosine phosphorylation of GIT2. While it does not appear that RhoJ modulates the activities of Src or FAK, since there was no change in auto-phosphorylation of FAK Tyr 397 or Src Tyr 416 in GFP-daRhoJ expressing cells, the role of RhoJ in regulating activity of a phosphatase cannot be ruled out. GIT2 has been identified as a substrate for the phosphatase PTP-PEST, which is also involved in regulating adhesion disassembly (Angers-Loustau, Cote *et al.* 1999, Jamieson, Tumbarello *et al.* 2005, Brinas, Vassilopoulos *et al.* 2013), and it would be interesting to investigate whether the activity of this phosphatase is altered upon expression of daRhoJ. Alternatively, it is possible that since active RhoJ increases recruitment of GIT2 to adhesions, there is more protein available for phosphorylation by Src and FAK at these adhesions. Expression of daRhoJ also increased total GIT2 levels, and it is not yet clear whether RhoJ affects the stability of GIT2, thereby increasing the levels *in vitro*, or whether it regulates transcription or translation of the protein, which could in part be investigated by qPCR of GIT2 in GFP and GFP-daRhoJ expressing cells.

The electrophoretic mobility of GIT2 was altered upon expression of daRhoJ, and this shift in size was not diminished after treatment with Src and FAK inhibitors. Given that multiple sites of serine and threonine phosphorylation have been identified in GIT1, and many of the affected residues are conserved in GIT2 (Webb, Mayhew *et al.* 2006) it is likely that active RhoJ regulates a Ser/Thr kinase. The PAK proteins are a family of Ser/Thr kinases and are known to phosphorylate myosin II (Zhang, Webb *et al.* 2005), a process that RhoJ is also known to mediate (Kaur, Leszczynska *et al.* 2011).  $\beta$ -PIX recruits PAK to focal adhesions via its SH3 domain (Bagrodia, Taylor *et al.* 1998), and thus it is possible that active RhoJ induces increased PAK recruitment to adhesions and as such increased phosphorylation of serine and threonine residues in GIT.

The results gathered in this chapter indicate that  $\beta$ -PIX may act as a GEF for RhoJ, since knockdown of  $\beta$ -PIX resulted in reduced RhoJ activation. However, further work would be required to confirm this hypothesis, since it is also possible that  $\beta$ -PIX indirectly activates RhoJ. GEF exchange assays have been developed, and recombinant RhoJ and  $\beta$ -PIX proteins could be generated for use in this assay to conclude whether  $\beta$ -PIX is in fact a GEF for RhoJ.

Phosphorylation of Tyr 442 is required for relaxation of  $\beta$ -PIX auto-inhibition and its activity as a GEF (Feng, Baird *et al.* 2006), however this phosphorylation has also been identified as weakening the interaction between  $\beta$ -PIX and GIT1, thus promoting binding of GIT to paxillin and as a result adhesion disassembly (Feng, Baird *et al.* 2010). Given that active RhoJ also promotes adhesion disassembly, it would be interesting to determine whether phosphorylation of  $\beta$ -PIX is also necessary for its activation of RhoJ. In the context of the results gathered in this chapter, it is certainly possible that phosphorylated  $\beta$ -PIX activates

RhoJ and stimulates adhesion disassembly via GIT1 and active RhoJ. Additionally, since RhoJ has been found to regulate phosphorylation of GIT2, it would be useful to determine whether there is also an effect on phosphorylation of  $\beta$ -PIX, which would suggest a positive feedback loop on RhoJ activity. Alternatively, as daRhoJ enhances  $\beta$ -PIX recruitment to adhesions, and  $\beta$ -PIX regulates RhoJ activation, this may function as a feedback loop to promote adhesion disassembly.

In terms of the effect of GFP-daRhoJ expression on phosphorylation of other kinases, several of the proteins highlighted as being differentially phosphorylated in GFP-daRhoJ expressing cells have interesting roles related to Rho GTPases, the GIT/PIX complex and cell migration. For example, JNK was phosphorylated at T183/Y185, T221/Y223 to a greater extent in GFP-daRhoJ cells compared to GFP only cells, and it is known that this protein is found downstream of Rac1 and Cdc42 (Strath, Georgopoulos *et al.* 2009). Since RhoJ is thought to regulate Rac1 and Cdc42 activity in some way (Yuan, Sacharidou *et al.* 2011), it is possible that RhoJ is also upstream of JNK and regulates its phosphorylation and activity.

Endothelial nitric oxide synthase (eNOS) too has been shown to interact directly with GIT1 in sinusoidal endothelial cells. Moreover, Liu *et al.* demonstrated in 2012 that manipulation of GIT1 expression was associated with a change in phosphorylation of eNOS at serine 1177 which is representative of eNOS activation; for example overexpression of GIT1 led to increased phosphorylation (Liu, Premont *et al.* 2012). The data from the phosphokinase array suggested that expression of active RhoJ decreased eNOS phosphorylation, so it is possible that RhoJ acts to balance the GIT1 induced activation of eNOS in endothelial cells. However, GIT1 and eNOS were primarily found to associate in the perinuclear region of

sinusoidal endothelial cells, rather than the plasma membrane or focal adhesions where RhoJ is located. If RhoJ decreases eNOS phosphorylation *in vivo*, this would lead to reduced enzyme activation and as such reduced NO production and release. Nitric oxide levels in HUVEC could therefore be measured using methods previously described, including the Griess reaction which measures basal NO production (Privat, Lantoiné *et al.* 1997). Given that NO is important for normal endothelial function and pulmonary angiogenesis, a role for RhoJ in reducing its production would indicate a negative effect on vascular remodelling *in vivo* (Klinger, Abman *et al.* 2013). In *in vitro* tube formation assays, GFP-daRhoJ expression induced increased branching (Kaur, Leszczynska *et al.* 2011), which potentially suggests a reduction in pruning during remodelling.

In summary, the data presented in this chapter show that RhoJ interacts with the focal adhesion proteins GIT1, GIT2 and  $\beta$ -PIX and this complex regulates one another's recruitment to adhesions. It seems likely that these proteins work in concert to regulate focal adhesion disassembly and ultimately cell migration and tube formation, certainly knockdown of each protein in the complex impaired tubule formation in both the Matrigel and co-culture assays. Functionally, it appears that  $\beta$ -PIX plays a role in mediating RhoJ activation, while RhoJ activity regulates GIT2 levels and phosphorylation. Furthermore, expression of GFP-daRhoJ affects phosphorylation of a number of kinases including JNK, STAT5 and eNOS, which may indicate a wider role for RhoJ in multiple signalling pathways, however much more investigation and validation must be performed before these results can be fully understood.

## **CHAPTER 5**

### **Generation of a RhoJ knockout mouse**

## 5.1 Introduction

The use of transgenic mice is a well-described method to investigate the role of genes *in vivo*. Often mice are generated which lack the gene of interest (knockout mice), either by direct deletion of the gene or gene-trap technology. Knock out mice are frequently used to describe the function of genes in normal physiological development, as well as in pathological conditions. Conversely, it is possible to overexpress particular proteins *in vivo*, to assess the inverse effect of gene knockout. It is also possible to 'knock-in' a gene of interest, often a mutant version of the gene is inserted into the genome, replacing the endogenous form. For example, VEGFR2 contains two tyrosine residues that are auto-phosphorylated in response to VEGF stimulation, triggering signalling cascades relating to endothelial cell proliferation, focal adhesion turnover and migration (Takahashi, Yamaguchi *et al.* 2001, Cross, Dixelius *et al.* 2003). Mice have been generated whereby mutant forms of the VEGFR2 gene with these tyrosine residues substituted for phenylalanine, have been knocked-in, demonstrating that phosphorylation of one tyrosine in particular is required for blood vessel development (Sakurai, Ohgimoto *et al.* 2005).

It is also possible to induce recombination in a tissue specific manner and in a tissue specific inducible manner. Soluble VEGFR1 for example has been specifically deleted in the endocardium to investigate its role in coronary angiogenesis (Zhang and Zhou 2013). Induction of gene deletion after birth is particularly useful when a deletion is lethal. For example, bacteriophage Cre recombinase may be fused to mutated domains of the estrogen receptor, which is activated after mice are treated with tamoxifen (Feil, Valtcheva *et al.* 2009). Cre recombinase cleaves loxP sites within the genome, enabling recombination at

these sites and deletion of the exon of choice. This allows for temporal control of gene manipulation, for example deletion of VEGFR1, which is ordinarily embryonic lethal, in adult mice (Fong, Rossant *et al.* 1995, Ho, Duan *et al.* 2012).

While RhoJ has been subject to much investigation *in vitro*, there has been little *in vivo* data to describe its function in a mammalian organism. The use of endothelial cells *in vitro* has indicated a role for RhoJ in cell migration and tube formation, which are both vital for the process of angiogenesis (Kaur, Leszczynska *et al.* 2011, Yuan, Sacharidou *et al.* 2011). Recent publications have also shown that RhoJ plays a role in mediating melanoma invasion and chemoresistance (Ho, Aruri *et al.* 2012, Ho, Soto Hopkin *et al.* 2013) as well as being highly upregulated in a number of different cancers (Masiero, Simoes *et al.* 2013). Together, these data suggest that RhoJ could have interesting functions *in vivo* which have yet to be fully studied.

Yuan *et al.* previously used *in vivo* siRNA knockdown to demonstrate a role for RhoJ in vessel formation in Matrigel plugs (Yuan, Sacharidou *et al.* 2011), while Fukushima and colleagues generated a line of RhoJ overexpressing mice (Fukushima, Okada *et al.* 2011). Homozygous endothelial RhoJ overexpression led to embryonic lethality, with impaired vessel growth and vascular development in embryos 10.5 dpc. In neonatal heterozygous endothelial-specific overexpressing mice, dysfunctional retinal vascular development was also observed, with membrane blebs found in the sprouting vessels. A RhoJ knockout mouse was also reported in 2012 by Takase *et al.* Little was presented, however a small but significant decrease in radial growth of the neonatal retinal vascularisation was found, with increased numbers of

empty sleeves i.e. basement membrane sleeves which lacked the endothelial marker isolectin B4 (Takase, Matsumoto *et al.* 2012).

Recently, Kim *et al.* presented the use of a RhoJ knockout mouse in various tumour assays. They determined that loss of RhoJ expression impaired tumour growth due to decreased vessel density and stability. Additionally, decreased metastasis was observed in these mice. Furthermore, it was suggested that RhoJ could be a target for future therapies, as inducible knockout reduced growth of established tumours, and its knockout in combination with other anti-angiogenic therapies enhanced anti-tumour effects (Kim, Yang *et al.* 2014).

The aim of this chapter was to generate a line of RhoJ knockout mice for use in *in vivo* angiogenesis assays. Mice classified as knockout from their genomic DNA were produced and splicing was characterised in these mice. The genetrap system employed by the cassette relies on interrupting splicing from the endogenous exon 1 to exon 2, however this splicing was still present in the mice generated. Thus, since the genetrap did not function correctly, generation of a true knockout involved removal of exon 2 using Cre recombinase cleavage of and recombination at the loxP sites. Further crossings were performed to ultimately generate a full RhoJ knockout mouse. Preliminary experiments to assess the role of RhoJ in tumour growth and angiogenesis were also performed.

## **5.2 Generation of chimeras with germline transmission**

In order to ultimately breed a RhoJ knockout mouse colony, mice which transmit the knockout cassette first needed to be produced. C57 black 6 (C57BL/6N) JM8.N4 feeder-independent embryonic stem (ES) cells containing the RhoJ knockout first promoter driven

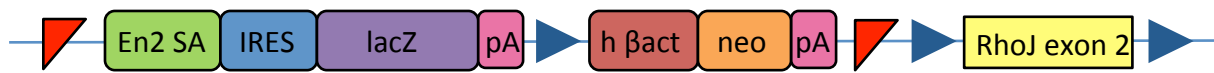


cassette (RhoJ<sup>tm1a(KOMP)Wtsi</sup> project ID CSD25401) were procured from the Knockout Mouse Project (University of California, Davis). A diagram of the construct is shown in Figure 5.1.A. Culturing of ES cells, injection into albino C57BL/6 blastocysts and subsequent implantation into pseudo-pregnant albino C57BL/6 females was performed by Dr. Andrea Bacon (Transgenic Facilities Manager, University of Birmingham).

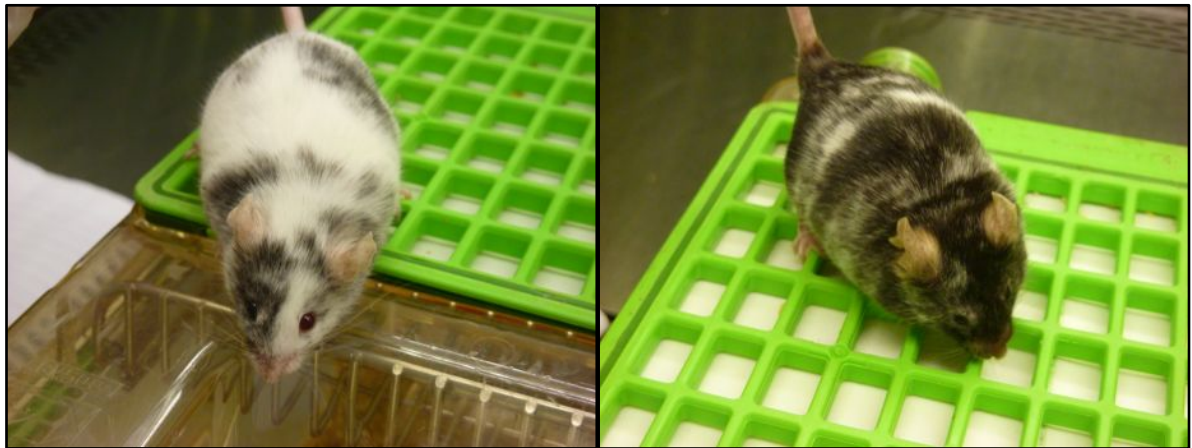
Initially, pseudo-pregnant FVBN females were used for implantations, and the resulting chimeras bred with FVBN mice. Five chimeras were generated, 3 males and 2 females. All 3 males and 1 female were bred to assess germline transmission, however the female chimera did not become pregnant, and no germline transmission was observed from the male chimeras after a total of 296 pups were born (98 from 1 chimera, 99 from each of the remaining 2 chimeras). As a result, albino C57 black 6 females were used for implantations. Using the same strain of mice to inject into as the ES cell background eliminates any differences that might be found between strains, and is the ideal method for generating chimeras.



Two male pups resulting from these injection sessions were classified as chimeras based on coat colour, since regions of black fur suggest successful transmission of the knockout ES cells (which are derived from C57 black 6 mice) into the albino C57 black 6 blastocysts. As can be seen in the images in Figure 5.1.B, both chimeras have reasonable levels of black in their coats and as such were bred to C57 albino black 6 females to determine whether either showed germline transmission. Black offspring act as an indication of germline transmission of the knockout cassette, resulting in a mixture of wild-type and heterozygous mice may be produced. Only one of the chimeras showed germline transmission, and interestingly it was

**A**



**B**



**Figure 5.1 ES cells containing the RhoJ knockout cassette were injected into blastocysts and implanted into pseudo-pregnant female mice, resulting in two good chimeras. A.** Map of the RhoJ knockout cassette contained within ES cells acquired from the Knockout Mouse Project.  : FRT sites  : LoxP sites, En2 SA: mouse en2 splice acceptor, IRES: internal ribosomal entry site, lacZ: lacZ gene, pA: SV40 polyadenylation, h  $\beta$ act: human  $\beta$ -actin promoter, neo: neomycin resistance gene. **B.** Two male chimeras based on percentage of black in the coat resulted from the injection sessions.

the less chimeric male (left-hand panel, Figure 5.1.B). The numbers and genotypes of the litters are outlined in Table 5.1. From 10 litters, there were a total of 27 black pups born of which 16 were male (59%) and 11 female (41%). Of these 16 males, 12 were heterozygous (75%) and 4 wild-type (25%). Of the 11 females, 5 were heterozygous (45%) and 6 were wild-type (55%).

**Table 5.1. Genotypes of black pups born from the germline-transmitting RhoJ chimera**

Litter Number	Number of black pups	Number of males	Number of females	Male genotype	Female genotype
LN1	2	1	1	Het	Het
LN2	2	2	0	2 Het	
LN3	5	4	1	3 Het, 1 WT	WT
LN4	1	1	0	Het	
LN5	4	2	2	1 Het, 1 WT	1 Het, 1 WT
LN6	3	3	0	2 Het, 1 WT	
LN7	1	0	1		Het
LN8	3	2	1	1 Het, 1 WT	WT
LN9	2	1	1	Het	WT
LN10	4	0	4		2 Het, 2 WT

### **5.3 Optimisation of a genotyping strategy to distinguish between the wild-type allele and knockout cassette**

Genotyping of offspring from the chimera matings was necessary to determine whether pups were wild-type or heterozygous for the RhoJ knockout allele. In order to optimise the genotyping strategy, a pair of primers to amplify a region of the wild-type allele and 2 pairs

of primers to amplify regions from the knockout cassette were tested. The products were designed to be 200-400 bp in length, with both the beginning and end of the knockout cassette covered. Figures 5.2.A and 5.2.B show the locations of the primers in the wild-type and knockout alleles, with the expected sizes of the PCR products.

To ascertain whether the primer pairs were suitable, a wild-type albino C57 black 6 mouse genomic DNA sample extracted from an ear clip, the original ES cells and a water control were tested with each set. Figure 5.2.C shows the products from each PCR. As expected, the water control shows no amplified product in any of the three reactions. The wild-type control mouse sample meanwhile only gives a product using the pair of primers designed to amplify a region of mouse DNA lacking the cassette. While this region could theoretically be amplified in a knockout mouse, the knockout cassette interrupts it, meaning that a very large product would be generated. The possibility of this scenario was eliminated by allowing a short length of time for elongation, meaning that only a small product could be amplified. This wild-type product is also amplified from the ES cell sample, which is heterozygous for the knockout allele.

Both primer pairs designed to amplify regions from the knockout cassette give a product of the expected size in the ES cells only. The intensity of the band generated by the pair at the start of the cassette is greater than that of the pair at the end and was therefore selected as being most optimal. Going forwards, the wild-type pair was used in combination with the pair designed to amplify the start of the cassette in order to genotype litters from the chimera and subsequent het/het pairings.

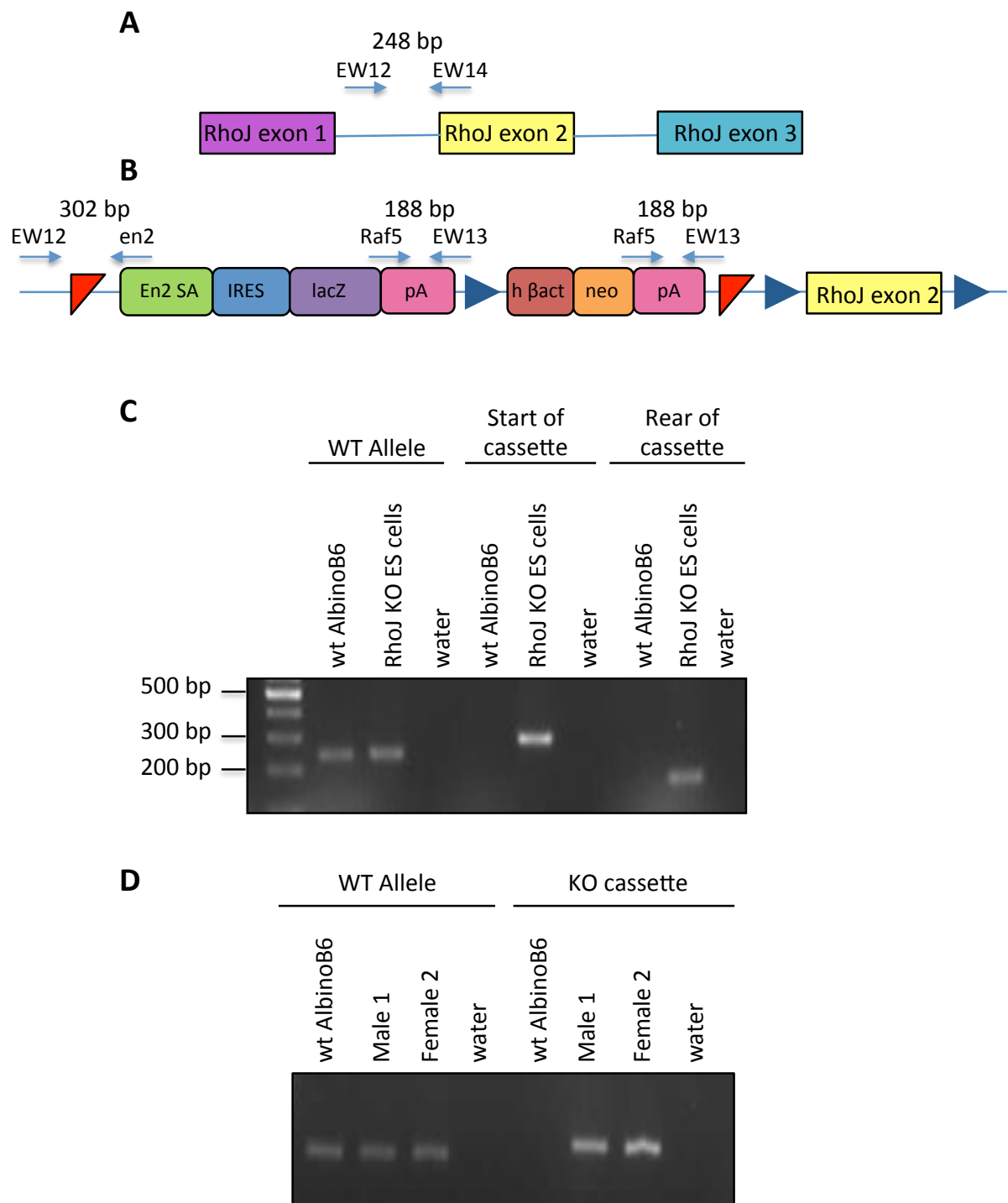


**Figure 5.2 Optimisation of genotyping strategy.** **A.** Primers used to amplify a region in the wild-type RhoJ allele near exon 2 (EW12 and EW14). **B.** Primers used to amplify regions at the start (EW12 and common en2) and rear (EW13 and Raf5) of the cassette. **C.** Genomic DNA from a wild-type albino black 6 mouse was genotyped along with the RhoJ ES cells using the primers shown in A and B. **D.** The primers for the wild-type allele were used in combination with those for the start of the cassette (EW12 and common en2) to genotype offspring from the chimera.

The panel in Figure 5.2.D shows the genotyping of litter 1 from the chimera mating, products for both the wild-type allele and knockout cassette show that both male 1 and female 2 are heterozygous (as noted in Table 5.1). Along with the water negative control and wild-type control, this demonstrates that these primers are suitable for genotyping ear clips and characterising mice as wild-type, heterozygous or knockouts.

## **5.4 Confirmation of splicing in wild-type, heterozygous and knockout mice**

The RhoJ knockout cassette contains a lacZ gene, which is translated into  $\beta$ -galactosidase protein in place of RhoJ and should be able to be stained for with Xgal. Initial attempts to stain for  $\beta$ -galactosidase failed, and it was not possible to discriminate RhoJ protein from a non-specific band of similar size by Western blotting (data not shown). It was therefore important to confirm the splicing events that occurred *in vivo*.

RNA was extracted from mouse lung tissue and cDNA generated, which was subsequently used for traditional PCR. Primers that spanned the RhoJ exon 1-exon 2 boundary were used in addition to those spanning the RhoJ exon 1-KO cassette splice acceptor boundary. A diagram of the 2 splicing events probed for, along with the primers used is shown in Figure 5.3. The results of the cDNA PCR are shown in Figure 5.4.

As can be seen in the wild-type mouse, only the RhoJ exon 1-exon 2 boundary primers have amplified a product, while primers have amplified the exon 1-exon 2 boundary as well as the exon 1-KO splice acceptor boundary in the heterozygous mouse. The presence of the splice acceptor in the knockout mouse cassette should mean that RhoJ exon 1 in those mice that

**A**

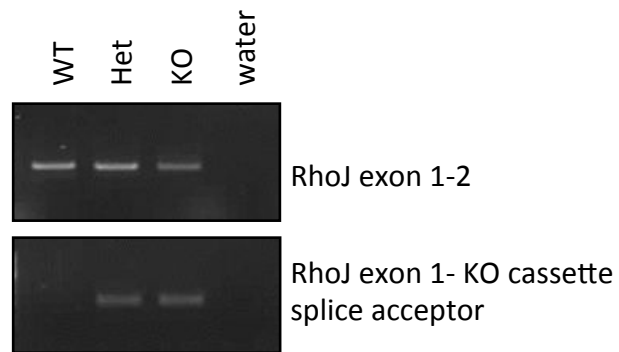
atggaatgcagcaggaaaccacgatttcctgacactcggcaagctggaggaagcaggggggggaaactccgtttaaaagc  
 ccttctctcctcatattagttgtgtggtggaaaaccgggcaggagttatccaaatcccacgtgtcattagccaggctggggatg  
 gggagggtagagtgagattctacgggctgctgatattttagactgccaggaagtcccgggaagtctatggacatgagagtctc  
 ttaactccagctctaccccaactccacttctcgttgggattgggagaaaggacagaccctttcatccctctcccaagagtgc  
 cttccttctccagcatggtgagctgctgggctgagtggtgtgtctgggctgtgcctgggagagcccggccagccagagtccaggccgc  
 ctgagctccagcctggggccggtgccaccgctccatgcactgcagaagcccagcagctgctgcgggagccgccaacatgagc  
 tgcagagagaggaccgacagcagctgctggctgcaatggacatgaggagaacaggatcctgaagtgcgtggtggtcggggacg  
 gcgcggtggggaagacctgcttgctgatgagctacgcaacgacgccttcccagaggaatacgtgccactgtgtttgaccacta  
 cgagttaccgtgacgggtgggaggcaagcagcacttgcctggactatacgacactgcaggacaggaggattacaaccagctgc  
 ggccactctcttaccacaacagatgtgtttctcatctgcttctctgtctaaaccagcctcttaccacaacgttcaggaggagt  
 ggggtccggaactgaaggactgcatgcctcatgtgccttatgtgctcatcggaaccag

**B**

gagagaggaccgacagcagctgcggctgcaatggacatgaggagaacaggatcctgaagtgcgtggtggtcggggacggcgc  
 ggtggggaagacctgctgctgatgagctacgccaacgacgccttcccagaggaatacgtgccactgtgtttgaccactacgc  
 agcaggtcccaggtcccgaataacaaagaagaagaacccatacaaaaggaggaacagcggtcgcacagccttactgctgag  
 cagctccagaggctcaaggctgagtttcagaccaacaggtacctgacagagcagcggtccagaggtctggcacaggagctcggg  
 taccggaagatctggactctagagaattccgcc cctctccctc cccccccc

**Figure 5.3. Strategy to determine splicing events in the wild-type and RhoJ genetrapped mice. A.** In a wild-type scenario, RhoJ exon 1 splices to exon 2. Sequence shows RhoJ exons 1-3. Blue: exon 1; purple: exon 2; green: exon 3. Boxes outline primers used to amplify the exon 1-exon 2 boundary (fwd: EW25 and rev: EW22). **B.** Upon insertion of the knockout (KO) cassette, RhoJ exon 1 should splice to the cassette splice acceptor. The sequence shows the end of RhoJ exon 1 and the start of the KO cassette after the splice acceptor. Blue: exon 1; red: KO cassette after splice acceptor. Boxes outline primers used to amplify the exon 1-splice acceptor boundary (fwd: SK24 and rev: EW24).

**A**



**B**

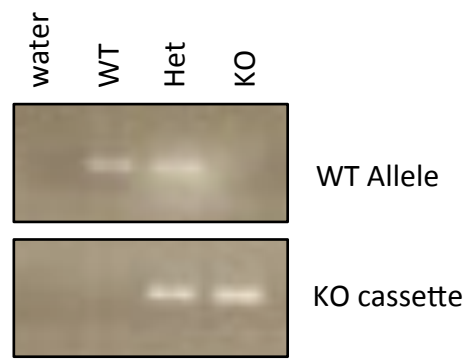


**Figure 5.4 RhoJ exon 1 is still splicing to exon 2 in the RhoJ genetrapped mouse. A.** PCR of cDNA generated from mouse lung tissue shows splicing from RhoJ exon 1 to RhoJ exon 2 or exon 1 to the splice acceptor in the knockout cassette. **B.** Mice used to characterise splicing were re-genotyped to confirm the presence of the wild-type (WT) allele or knockout (KO) cassette.



have the cassette in both alleles only splices to the knockout cassette rather than exon 2, however there is a clear product from the primers spanning the exon 1-exon 2 boundary. This suggests that while there is some splicing to the knockout cassette, it is not complete, and not sufficient to inhibit production of wild-type RhoJ mRNA and subsequent translation of the RhoJ protein. These data confirm that the genetrap cassette was not resulting in elimination of RhoJ mRNA despite the indications of the genotyping, which was repeated, as shown in Figure 5.4.B.

## **5.5 Breeding of RhoJ genetrap mice with PGK-Cre mice**

The PCR of RhoJ genetrap mouse cDNA showed that the en2 splice acceptor at the start of the knockout cassette was not working as it was designed. RhoJ exon 1 was still splicing to RhoJ exon 2 rather than just the cassette splice acceptor, so to combat this issue and generate a true RhoJ knockout mouse, exon 2 was removed using Cre mediated recombination at the loxP sites flanking this exon. This was achieved by crossing homozygous genetrap mice with female PGK-Cre mice.

Expression of the enzyme Cre recombinase is under control of the phosphoglycerate kinase (PGK-1) promoter in PGK-Cre mice. This enzyme cleaves loxP sites and enables DNA recombination at these sites, leading to deletion of the floxed exon. RhoJ exon 2 is flanked by loxP sites in the knockout cassette, so breeding the RhoJ genetrap mice with PGK-Cre mice enables generation of offspring with exon 2 removed, meaning that the problems with splicing identified in Section 5.4 are no longer relevant. The PGK-Cre females give rise to offspring that all have the loxP-flanked region cleaved by Cre recombinase, regardless of whether those offspring inherit the PGK-Cre gene (Lallemand, Luria *et al.* 1998). As such, all

the litters born from this pairing should lack the RhoJ exon 2 in the knockout allele and can be used to generate a line of full RhoJ knockout mice.

PGK-Cre mice were acquired from Prof. Steve Watson (University of Birmingham), and were otherwise wild-type. Primers were designed to amplify regions that would indicate cleavage with Cre recombinase (and as such remove the region spanned by the loxP sites), or no cleavage.

The genotyping in Figure 5.5.A shows that in all offspring, Cre recombinase has cleaved the region spanned by the loxP sites since products are found in the samples subjected to PCR using primers that would be sufficiently far apart in a non-cleaved cassette that no product could be amplified in the time given for elongation.

The presence of Cre recombinase was also probed in mice from this pairing, with the results shown in Figure 5.5.B. The lower band indicates a Cre positive mouse, while the upper band acts a control. Approximately half the mice genotyped were found to be Cre positive, which is the expected Mendelian ratio for a pairing of a homozygous positive mouse with a homozygous negative mouse.

The PCR products generated as described above were also sequenced with the forwards primer used to determine whether there had been loxP cleavage, with the product shown in Figure 5.6. As can be seen, the sequencing product aligns with the reference sequence of the RhoJ cassette where loxP-Cre recombination has occurred.

These data show that crossing the RhoJ genetrap mice with PGK-Cre mice generated offspring that lack the loxP flanked region of the knockout cassette, and thus lack RhoJ exon

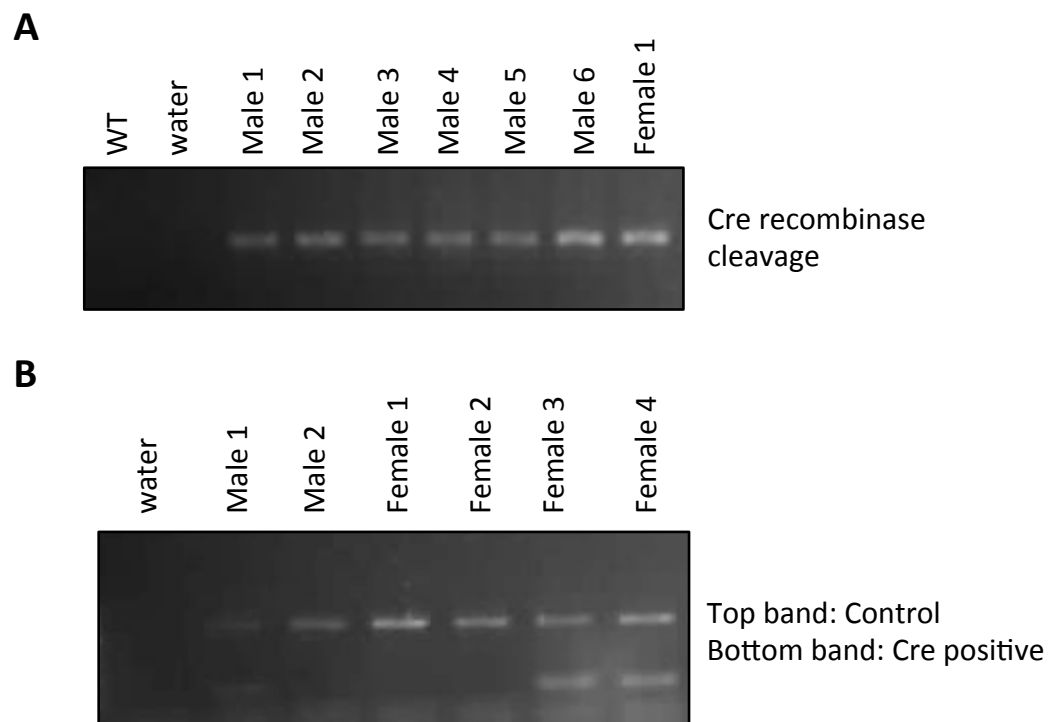
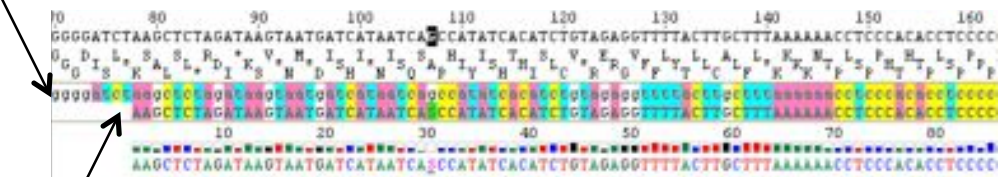


**Figure 5.5. Breeding of RhoJ genetrapp mice with PGK-Cre mice produced a line of mice with RhoJ exon 2 removed by Cre recombinase. A.** Mice from the RhoJ genetrapp x PGK-Cre pairings were genotyped for a region of the genomic DNA only amplified in those mice with the loxP sites cleaved. **B.** Offspring from these pairings were genotyped for the presence Cre.

LoxP-Cre recombination  
sequence



Sequencing

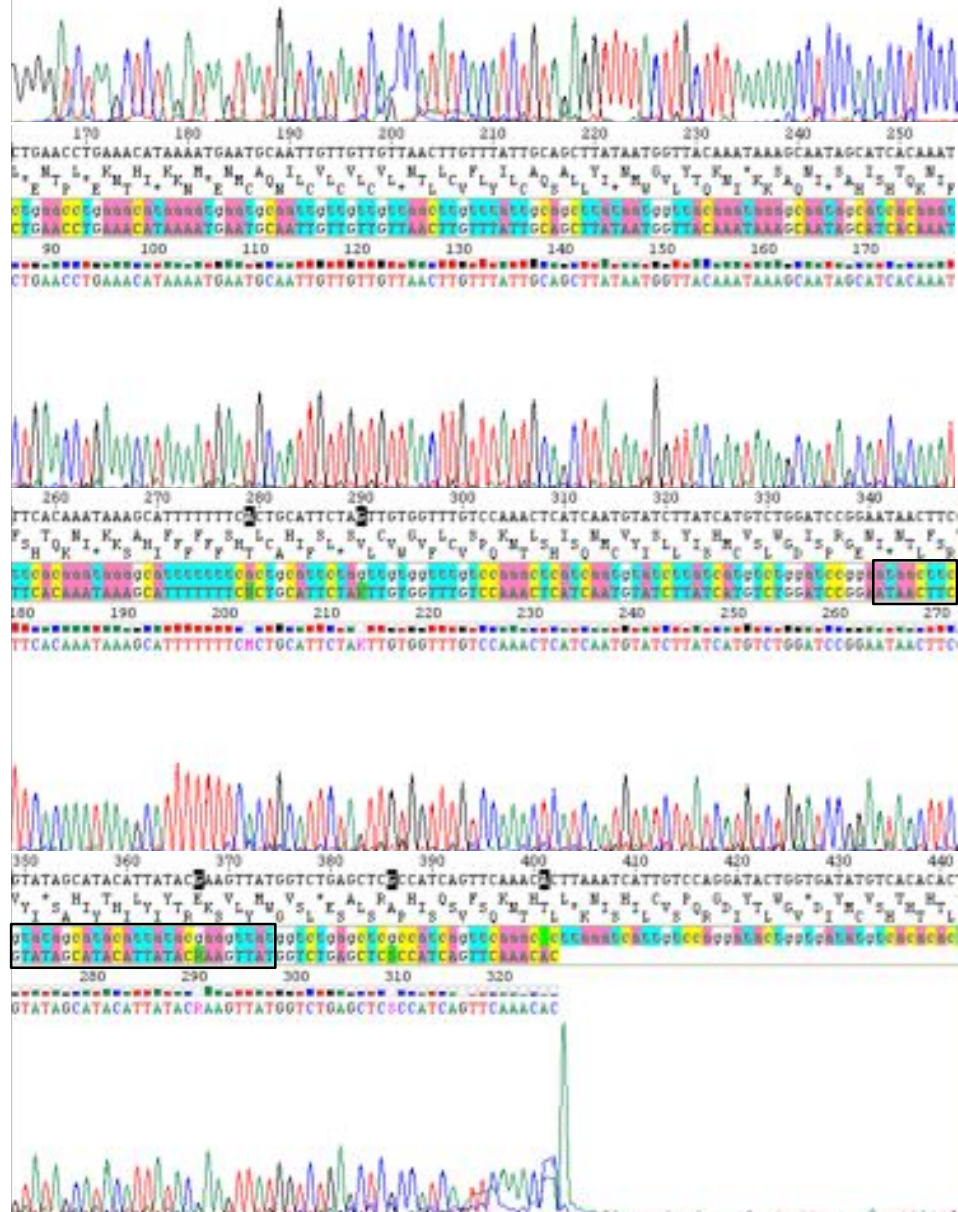


**Figure 5.6 Sequencing of the PCR product from PGK-Cre x RhoJ genetrapp offspring.** The primer EW26 was used to sequence the genotyping PCR product of the offspring of PGK-Cre x RhoJ genetrapp pairings. The sequencing product is the lower band of sequence, along with the chromatogram of the sequencing reaction, while the top band is the reference sequence of the cassette with loxP-Cre recombination. The loxP site where recombination occurred is highlighted with a black box.

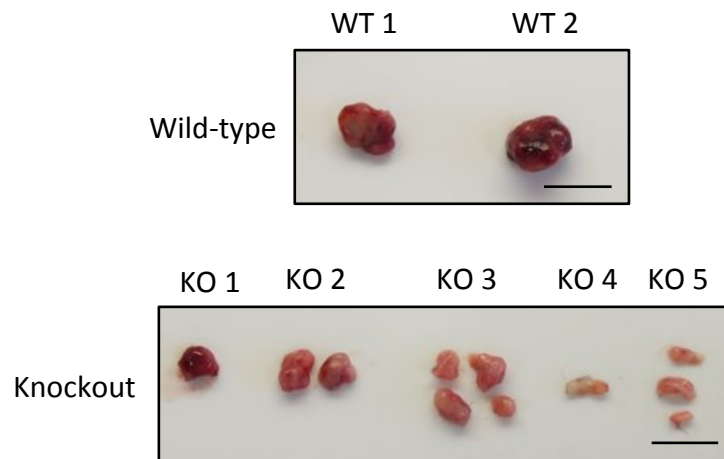
2. At this stage, all offspring were heterozygous for the cleaved cassette because the homozygous RhoJ genetrapped mice were bred with wild-type PGK-Cre mice. In order to produce full RhoJ knockout mice, the Cre negative offspring were bred together giving a mixture of wild-type, heterozygous and RhoJ knockout homozygous mice, enabling further investigation into the function of RhoJ *in vivo*.

## 5.6 Tumour growth in RhoJ knockout mice

In order to assess the effect of *in vivo* RhoJ knockout on growth and vascularisation of tumours, Lewis lung carcinoma cells were injected into the flank of wild-type and knockout mice (resulting from the breeding in Section 5.5). Mice were culled after 2 weeks, by which point the maximum tumour burden ( $1.2\text{ cm}^3$ ) had been reached in one of the mice used. Due to the time limits of this PhD, these preliminary experiments were performed by Dr. Victoria Heath, and data is presented with permission.

As can be seen in the images in Figure 5.7.A, tumours from wild-type mice were highly vascularised and large whereas those from RhoJ knockout mice were much smaller, with fewer vessels. In some of the knockout mice, multiple small tumours formed, while only single tumours were found in wild-type mice. Cumulative masses of tumours were plotted as a bar chart in Figure 5.7.B. Despite the presence of multiple tumours in RhoJ knockout mice, the masses of these tumours were smaller than those of wild-type mice; when analysed with a Mann Whitney test, the difference between the masses was statistically significant ( $p=0.0041$ ).

**A**



**B**

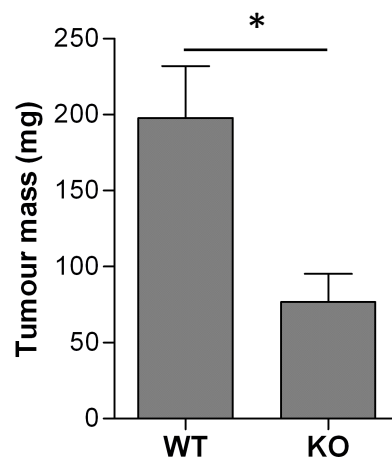


**Figure 5.7. Preliminary data from *in vivo* tumour growth assays.** Lewis lung carcinoma cells were injected into the flank of wild-type and RhoJ knockout mice and tumours left to grow. **A.** Mice were culled, tumours removed and images taken. Scale bar: 1 cm. **B.** Tumours from each mouse were weighed, and total masses displayed as a bar chart of the mean and SEM. Data was analysed using the Mann Whitney test. WT: n=5; KO: n=7.

While only preliminary, these data support the findings of Kim *et al.*, and suggest that RhoJ has a role in regulating growth and angiogenesis of tumours, and could be a useful target for future therapies.

## 5.7 Discussion

The original aim of this chapter was to generate a RhoJ knockout mouse for use in *in vivo* angiogenesis assays, to identify a role for RhoJ in either physiological or pathological angiogenesis. The data presented above demonstrates that while mice carrying the genetrap cassette were successfully created, further investigation into splicing showed that the cassette did not result in the generation of a knockout mouse. Despite mice being homozygous for the knockout cassette, RhoJ exon 1 continued to splice to RhoJ exon 2, in addition to the splice acceptor within the cassette. As a result, RhoJ was not properly knocked out, so further breeding was required in order to generate a full knockout. PGK-Cre mice, which produce the enzyme Cre recombinase, were mated with the RhoJ genetrap mice. Cre recombinase cleaves loxP sites, which span RhoJ exon 2 in the knockout cassette, so offspring from these pairings should have the RhoJ exon 2 removed in one allele. Cre negative offspring were subsequently bred together, in order to generate a mixture of wild-type, heterozygous and homozygous mice which can ultimately be used for *in vivo* assays. An initial experiment to assess tumour growth in wild-type and RhoJ knockout mice was also performed, with small, unvascularised tumours forming in knockouts.

While several papers have been published regarding the *in vitro* function of RhoJ in endothelial cells in recent years, at the start of these PhD studies the role of RhoJ *in vivo* had yet to be investigated. In the interim, Takase *et al.* published the use of a RhoJ knockout

mouse created from the same ES cell clone as used in these studies (Takase, Matsumoto *et al.* 2012). They reported that RhoJ knockout mice had impaired retinal neovascularisation, with slightly delayed radial outgrowth and an increase in the number of empty sleeves. The paper did not include any examples of staining for lacZ gene expression or blots for protein expression though, so it is unclear whether any method other than genotyping was used to confirm knockout status. We did note that the PCR of cDNA (shown in Figure 5.4.A) showed a small decrease in the amount of splicing between RhoJ exon 1 and RhoJ exon 2 in the genetrap knockout mouse, which may explain why a minimal phenotype was reported by Takase and colleagues.

Kim and colleagues subsequently generated a RhoJ knockout mouse whereby exon 1 was replaced with GFP. As a result, GFP expression could be used as a reporter gene to determine where RhoJ would normally be expressed. They determined that RhoJ is expressed in tumour vessels, and knockout leads to a reduction in tumour growth associated with vessel impairment (Kim, Yang *et al.* 2014). Preliminary data in Section 5.6 echo the findings of Kim and colleagues, with small, unvascularised tumours forming in RhoJ knockout mice. Taken together, these data support our hypothesis that RhoJ is an important mediator of angiogenesis, and provides a basis for further investigation with our knockout mouse.

While extensive tumour data has already been published, and it has been shown that the knockout mouse is fertile and develops normally, there are other avenues yet to be explored. In particular, the sponge implantation assay is an established protocol in our laboratory and enables assessment of vessel growth into a subcutaneously implanted sponge in response to VEGF. Additionally, models of sprouting and splitting angiogenesis



have been developed which could be performed in the RhoJ knockout mice. Sprouting angiogenesis is modelled by removal of the *tibialis anterior* muscle, which induces overload on the *extensor digitorum longus* (EDL) muscle, resulting in hyperplasia and hypertrophy and ultimately increased angiogenesis. Splitting angiogenesis meanwhile is modelled by treatment of mice with prazosin, a vasodilator that induces increased blood flow, also measured in the EDL (Egginton, Zhou *et al.* 2001, Hussain, Steimle *et al.* 2012). Given that data previously published (Kaur, Leszczynska *et al.* 2011) and in Chapter 3 of this thesis demonstrate that RhoJ promotes focal adhesion disassembly, cell migration and tube formation, it could be hypothesised that the RhoJ regulates sprouting angiogenesis, and a phenotype would be seen in this model *in vivo*.

It is also possible that while the RhoJ knockout mouse appears to develop normally, there may be some changes during development of vascular beds that do not affect viability. To more closely assess the role of RhoJ in vascular development, timed matings could be performed and mice studied at stages throughout gestation, which would determine whether angiogenesis is abnormal at any stage *in utero*.

Additionally, RhoJ is expressed in thymus and B cells, as well as platelets (Sukhbir Kaur, PhD thesis, 2011). It would therefore be interesting to assess whether RhoJ has any effect in regulating platelet function or the development of thymocytes. Platelets for example are important regulators of angiogenesis, by stimulating the release of both pro- and anti-angiogenic factors and supporting proliferation and survival of endothelial cells (Lakka Klement, Shai *et al.* 2013). Meanwhile, given that the thymus is involved in producing T cells, the role of RhoJ in immunity and protection against infection could be investigated (Pearse

2006). GIT2 has also been identified as regulating thymocyte selection and motility (Phee, Dzhalalov *et al.* 2010), and since RhoJ functionally interacts with this protein, it is possible that RhoJ may also influence these processes.

In conclusion, work performed during these PhD studies has resulted in the generation of a knockout mouse, which will enable further study of the role of RhoJ *in vivo*, both in the vasculature and elsewhere.

## **CHAPTER 6**

### **General Discussion**

RhoJ is an endothelial expressed Rho GTPase that had previously been found to have wide-ranging functions in regulating the cytoskeleton including modulating focal adhesion numbers and stress fibres, mediating cell migration and regulating tube formation. Given that these are crucial processes in angiogenesis, the formation of new blood vessels from the existing vasculature, it was hypothesised that RhoJ is a novel regulator of angiogenesis as a result of its effects on the cytoskeleton. The data presented in this thesis sought to further characterise the role of RhoJ in focal adhesion dynamics, as well as investigating its physical and functional interaction with its partner proteins GIT and PIX.

Initially, the role of RhoJ in regulating focal adhesions was studied using TIRF microscopy. It was found that RhoJ specifically promotes focal adhesion disassembly, and this is likely the reason for increased numbers of adhesions upon RhoJ silencing previously observed in our laboratory (Kaur, Leszczynska *et al.* 2011). RhoJ had previously been identified as an interacting partner of the GIT/PIX complex (Katarzyna Leszczynska, PhD thesis). These focal adhesion proteins have been implicated in regulating adhesion disassembly (Zhao, Manser *et al.* 2000, Nayal, Webb *et al.* 2006, Kuo, Han *et al.* 2011), which is particularly interesting given that it has been shown in this thesis that RhoJ also specifically modulates focal adhesion disassembly. Interactions between RhoJ and GIT1, GIT2 and  $\beta$ -PIX have been demonstrated, and these interactions appear to be functionally relevant, as the recruitment of any member of the complex to adhesions is dependent on the expression of the others. Dominant active RhoJ enhances focal adhesion disassembly as well as increasing the recruitment of the GIT/PIX complex to adhesions, suggesting that RhoJ functions in concert with GIT and PIX in order to promote adhesion disassembly. This is further supported by the finding that individual knockdowns of RhoJ, GIT and PIX phenocopy one another in *in vitro*

tube formation assays, which are dependent on migration and as a result, adhesion disassembly. Additionally, knockdown of the entire complex does not have an additive effect on tube formation impairment, suggesting that their functions are not independent.

Figure 6.1 depicts the interactions formed by the RhoJ/GIT/PIX complex, and the functional consequences of these interactions. While on one hand, it seems likely that RhoJ predominantly influences adhesion disassembly via the GIT/PIX proteins, it is possible that there are multiple pathways that converge to enable RhoJ to promote disassembly and in turn migration and tube formation. Firstly, focal adhesion disassembly is closely related to contractility. Loss of tensile strength is associated with adhesion disassembly, since RhoA/ROCK enhance both contractility and adhesion maturation (Broussard, Webb *et al.* 2008, Parsons, Horwitz *et al.* 2010, Ciobanasu, Faivre *et al.* 2012). Active RhoJ is known to downregulate RhoA activity, and a ROCK inhibitor has been shown to rescue the effect of RhoJ knockdown on focal adhesion numbers, demonstrating that RhoJ regulates contractility via the RhoA/ROCK pathway (Kaur, Leszczynska *et al.* 2011, Yuan, Sacharidou *et al.* 2011, Kim, Yang *et al.* 2014). The observation that RhoJ knockdown impairs adhesion disassembly is consistent with its increase of cell contraction, while the inverse is seen with expression of active RhoJ. Together these data suggest that RhoJ may modulate disassembly by inhibiting RhoA and ROCK activity, thereby reducing intracellular tension and switching from maturation to disassembly of adhesions.

RhoJ has also previously been implicated in regulating early endocytosis (de Toledo, Senic-Matuglia *et al.* 2003), and the interaction with the Arf GAP GIT proteins may be important for this function. Endocytosis is also important in regulating the uptake of focal

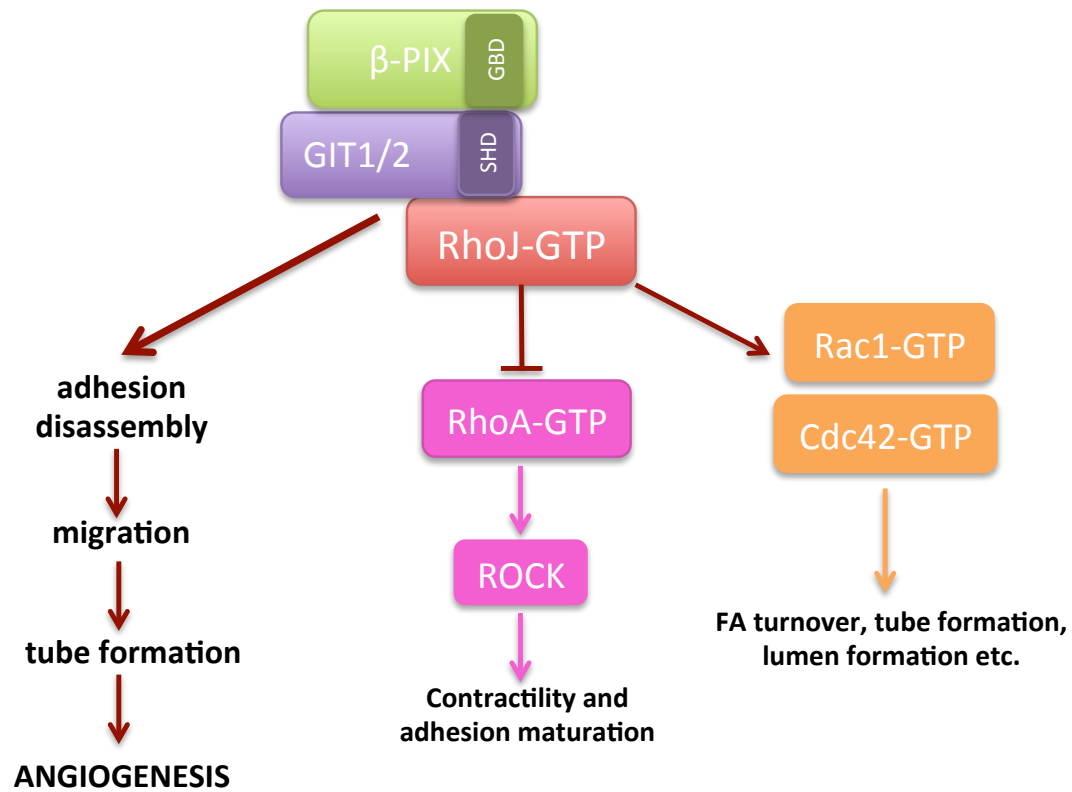


**Figure 6.1. RhoJ regulates angiogenesis by promoting focal adhesion disassembly in complex with GIT and PIX.** The data presented in this thesis suggests that RhoJ directly interacts with GIT1 and GIT2, and associates with  $\beta$ -PIX as a result. Together, we hypothesise that the RhoJ/GIT/PIX complex modulates focal adhesion disassembly, which in turn mediates endothelial cell migration, tube formation and potentially, angiogenesis. Additionally, RhoJ may regulate adhesion dynamics by negatively regulating the RhoA/ROCK pathway, reducing contractility and adhesion maturation, and promoting disassembly. Finally, RhoJ has previously been identified as a positive regulator of Rac1 and Cdc42 activation. Since these proteins have roles in endothelial cell biology, RhoJ may promote these functions, ultimately regulating angiogenesis.

adhesion components, and as such adhesion disassembly, so it is possible that RhoJ plays a role in regulating this mechanism.

Initial data assessing the role of RhoJ in mediating focal adhesion targeting by microtubules, another method of adhesion disassembly, showed a small, but not statistically significant, decrease upon RhoJ silencing. This could be investigated further using a more sensitive imaging technique that could study individual targeting events more readily, for example TIRF microscopy of GFP-tubulin, RFP-paxillin expressing cells could be employed. Others have previously visualised microtubule plus-end targeting of adhesions in endothelial cells by TIRF microscopy, using GFP-tubulin and DsRed-paxillin (Rovini, Gauthier *et al.* 2013). Focal adhesion targeting and subsequent adhesion disassembly is itself regulated by a number of processes, including calpain mediated proteolysis and regulation of Rho GTPase activity (Stehbens and Wittmann 2012). Polymerisation of microtubules is known to induce rapid disassembly of adhesions, and is thought to induce activation of Rac1 (Rooney, White *et al.* 2010, Stehbens and Wittmann 2012). Treatment of endothelial cells with the microtubule-depolymerisation drug nocodazole could be performed, and levels of active RhoJ measured before and after washout and subsequent microtubule polymerisation (Ezratty, Partridge *et al.* 2005). The effect of silencing of RhoJ and expression of the dominant active mutant could also be studied, to determine whether silencing of RhoJ would impair the rapid disassembly of adhesions normally seen after nocodazole washout, potentially due to a decrease in active Rac.

In addition, the GIT/PIX proteins have been implicated in regulating aspects of microtubule dynamics, including reorientation of the microtubule organising centre (MTOC); bundling of

microtubules to stabilise membrane protrusions and regulating microtubule assembly and disassembly via Calmodulin (Brown and Turner 2004, Yu, Deakin *et al.* 2009, Lee, Yang *et al.* 2011, Singh, Munro *et al.* 2012). Since RhoJ interacts with these proteins, it is possible that it contributes to their functions in modulating microtubule dynamics.

Since angiogenesis, and in particular sprouting angiogenesis, is so dependent on cell migration, the data gathered in this thesis support the hypothesis that RhoJ is involved in mediating vessel formation ultimately by regulating focal adhesion disassembly in endothelial cells, which in turn affects cell migration and tube formation. Others have also found that RhoJ upregulates Rac1 and Cdc42 activity (Yuan, Sacharidou *et al.* 2011), which are both known to regulate tube formation and lumen formation *in vivo* (Bayless and Davis 2002, Connolly, Simpson *et al.* 2002, Davis, Bayless *et al.* 2002), meaning that RhoJ may mediate these processes via Cdc42 and Rac1, in addition to its own intrinsic functions. RhoA activity is associated with the collapse of lumen (Bayless and Davis 2004), and RhoJ's role in regulating RhoA activity may additionally be related to its function in tube and lumen formation. It should however be noted that others have reported pro-angiogenic functions for RhoA, for example in positively mediating VEGF-stimulated cell migration and endothelial cell organisation (Hoang, Whelan *et al.* 2004, Bryan, Dennstedt *et al.* 2010), which is somewhat contradictory to the hypothesis that RhoJ mediates angiogenesis in part by downregulating RhoA activity.

RhoJ has recently been implicated in regulating pathological angiogenesis in tumours, with decreased growth and impaired vascular development in tumours from knockout mice (Kim, Yang *et al.* 2014). Preliminary tumour growth experiments performed by Dr. Victoria Heath



also found that RhoJ knockout mice develop smaller, multiple, poorly vascularised tumours. In addition to the *in vivo* data already gathered from the RhoJ knockout mouse, it would be useful to determine how loss of RhoJ affects splitting and sprouting angiogenesis. Assays to model these forms of angiogenesis have been published (Egginton, Zhou *et al.* 2001), and the RhoJ knockout mouse could be studied in these. It would also be interesting to assess whether expression of GIT and PIX are altered in the RhoJ knockout mice. Both GIT1 and  $\beta$ -PIX have been identified as regulating vessel formation and stability in rodents and zebrafish (Liu, Fraser *et al.* 2007, Pang, Hoefen *et al.* 2009, Liu, Zeng *et al.* 2012, Rui, Li *et al.* 2012), and given the recent evidence that RhoJ regulates tumour vessel formation and permeability (Kim, Yang *et al.* 2014), it would be useful to assess whether RhoJ knockout phenotypes could be rescued by treatment with GIT or PIX. Additionally, double knockouts could be generated, to determine whether RhoJ functions in a complex with GIT and PIX to regulate angiogenesis, and whether there is any additive effect on the phenotypes observed in the GIT and PIX knockout mice (see Section 1.5.6).

In addition, a role for RhoJ in regulating signalling has been identified. Figure 6.2 outlines how RhoJ is thought to regulate and be regulated by other proteins. It is known that GIT2 must be phosphorylated by the kinases Src and FAK at Tyr 286, 392 and 592 in order to localise to adhesions (Brown, Cary *et al.* 2005). Additionally, many threonine and serine phosphorylation events have been identified in GIT1, with residues conserved in GIT2 (Webb, Mayhew *et al.* 2006). It was observed that GIT2 in GFP-daRhoJ expressing cells was shifted in size compared to GIT2 in those cells expressing GFP only, suggesting that active RhoJ potentiates the level of Ser/Thr phosphorylation within these cells. It is known that  $\beta$ -PIX interacts with both GIT and the Ser/Thr kinase PAK, and given that active RhoJ interacts

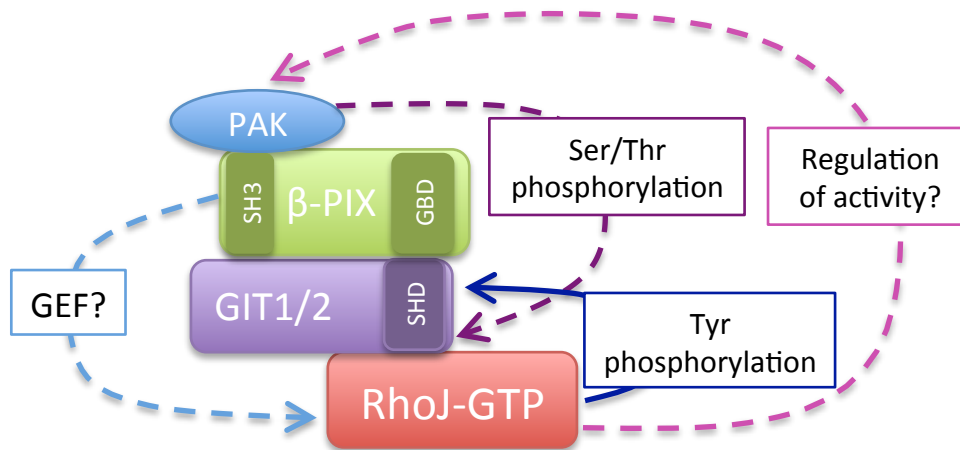


**Figure 6.2. The RhoJ/GIT/PIX interactions are functionally relevant to signalling and phosphorylation.** Data presented in this thesis has identified that active RhoJ regulates phosphorylation of GIT2 at Y392 by Src and FAK. RhoJ also appears to promote Ser/Thr phosphorylation, potentially by regulating the activity of the Ser/Thr kinase PAK. Finally,  $\beta$ -PIX has been found to regulate the activation of RhoJ, and thus may act as a GEF.

with GIT and, as a result, PIX, these data may indicate that RhoJ regulates the activity of PAK *in vivo*. Yuan and colleagues previously found that knockdown of RhoJ led to a decrease in levels of phospho-PAK2 and phospho-PAK4 during lumen formation (Yuan, Sacharidou *et al.* 2011). Various phosphorylation sites in the GIT proteins have been found to be relevant to their functions in the cytoskeleton (Webb, Kovalenko *et al.* 2006, Huck, Kemkemer *et al.* 2012, Ren, Yu *et al.* 2012), and it would be interesting to determine whether RhoJ has any effect on the phosphorylation of particular residues, since this may fine-tune its influence in regulating the cytoskeleton.

We have not identified an effect of RhoJ manipulation on  $\beta$ -PIX phosphorylation, however given that RhoJ regulates phosphorylation of GIT2, it is entirely possible that there would also be a role for RhoJ in modulating phosphorylation of  $\beta$ -PIX. It has previously been shown that phosphorylation of  $\beta$ -PIX Tyr 442 influences its GEF activity, as well as its interaction with GIT (Feng, Baird *et al.* 2006, Feng, Baird *et al.* 2010). It would be particularly interesting to investigate the level of phosphorylation at this residue in cells with manipulated RhoJ expression given that we believe  $\beta$ -PIX may act as a GEF towards RhoJ, however a phospho-specific antibody is not readily available. There is, however, the ability to perform mass spectrometry on samples prepared from cells expressing GFP or GFP-daRhoJ. Phosphorylation sites could therefore be mapped and analysed to determine whether levels of phosphorylation at Tyr 442 changes upon expression of dominant active RhoJ.

Given that a RhoJ biosensor has now been generated, it could be utilised to investigate the localisation of RhoJ activation. While we envisage that RhoJ would be activated at focal adhesions, and preliminary data supports this theory, this has yet to be confirmed. Others

have used biosensors to visualise sites of Rac, Rho and Cdc42 activation (Kraynov, Chamberlain *et al.* 2000, Nalbant, Hodgson *et al.* 2004, Pertz, Hodgson *et al.* 2006), giving insights into spatiotemporal activity, as well as gradients of activation. Additionally, regulation of RhoJ activation could be investigated further, in order to identify how a wider range of growth factors and endogenous angiogenesis inhibitors affect its activity *in vitro*. The biosensor could also be used to determine how RhoJ is activated during tubulogenesis. Our laboratory routinely uses both Matrigel and co-culture assays to model endothelial tube formation, and live cell imaging could be performed on the growing tubes expressing the RhoJ biosensor. Information gathered would be invaluable in determining how active RhoJ is regulated during physiological processes.

While the original aims of the project have largely been fulfilled, there are still mechanistic questions that remain unanswered. In particular, how does the RhoJ/GIT/PIX complex form *in vivo*? We do not believe that RhoJ and  $\beta$ -PIX compete for GIT, however it would be informative to determine the specific residues that are required for the individual interactions. Also, both GIT and PIX proteins are known to form homo- and heterodimers, as well as forming a heteropentameric structure (Premont, Perry *et al.* 2004, Schlenker and Rittinger 2009), however we do not know the stoichiometry of the RhoJ/GIT/PIX interactions. We have also hypothesised that RhoJ primarily interacts with GIT2 *in vivo*, however this is based on expression levels of GIT2 compared to GIT1 rather than biochemical data, which would need to be gathered in order to eliminate ambiguity. Additionally, we cannot unequivocally conclude that  $\beta$ -PIX acts as a GEF for RhoJ without performing exchange assays, and no GAPs have yet been reported for RhoJ. Identifying the regulatory proteins for RhoJ would be useful, as would determining how RhoJ regulates the

activities of other Rho GTPases *in vivo*. Finally, while others have reported the use of a RhoJ knockout mouse in angiogenesis assays, there are many avenues yet to be explored, not least the effect on GIT and PIX *in vivo*.

The ability to understand how RhoJ functions *in vivo*, in combination with knowledge of its *in vitro* biology is crucial if RhoJ is to be pursued as a potential target in therapies that modulate angiogenesis. The data presented in this thesis, along with that which has previously been published suggests that RhoJ promotes angiogenesis, and its inhibition *in vivo* could prove useful in treating cancer. In particular, RhoJ could be targeted in combination with anti-VEGF therapies, which are frequently used yet often give little long-term benefit on their own (Bergers and Hanahan 2008, Meadows and Hurwitz 2012, Kim, Yang *et al.* 2014). Additionally, in diseases that are characterised by insufficient angiogenesis, RhoJ could be used to promote blood vessel growth. Therapeutic angiogenesis may be used in the treatment of disorders like hypertension and coronary heart disease by stimulating growth of new vessels as a result of gene, protein or cell delivery (Humar, Zimmerli *et al.* 2009, Chu and Wang 2012), and RhoJ could also be delivered in this manner.

Thus far, RhoJ appears to be a promising *in vivo* target for future therapies, however there are limitations. Rho GTPases are very difficult proteins to target *in vivo*, with only one effective drug that directly targets the GTPase confirmed (Gao, Dickerson *et al.* 2004). Early attempts to target Rho proteins sought to modulate C-terminal isoprenylation, however this is not specific for Rho GTPases. The Rac1 specific inhibitor NSC23766 functions by fitting into a surface groove of the protein required for GEF specification, in this case blocking activation by the Rac specific GEF Trio or Tiam1 (Gao, Dickerson *et al.* 2004), however this too has

limitations in that it lacks potency (Lu, Longo *et al.* 2009). More promising is the ability to target other parts of the Rho GTPase signaling pathway, for example downstream effectors. The RhoA effector ROCK has been successfully targeting by numerous inhibitors including Y27632 and Fasudil, and these drugs have been used to effectively treat vascular disorders including cerebral vasospasm in humans (Siasios, Kapsalaki *et al.* 2013) and pulmonary hypertension in rodents (Casey, Badejo *et al.* 2010). The work presented in this thesis has partially elucidated the signalling pathway of RhoJ, and it is possible that aspects of this pathway could be targeted in future therapies.

## References

- Abcouwer, S., P. S. Robinson, C. F. Goochee and M. T. Crow (1989). "Generation of Human Embryonic Kidney Cells with Extended *In Vitro* Life Span through Viral Oncogene Transfection." Nature Biotechnology **7**(9): 939-946.
- Abe, T., M. Kato, H. Miki, T. Takenawa and T. Endo (2003). "Small GTPase Tc10 and its homologue RhoT induce N-WASP-mediated long process formation and neurite outgrowth." J Cell Sci **116**(Pt 1): 155-168.
- Abecassis, I., B. Olofsson, M. Schmid, G. Zalcman and A. Karniguian (2003). "RhoA induces MMP-9 expression at CD44 lamellipodial focal complexes and promotes HMEC-1 cell invasion." Exp Cell Res **291**(2): 363-376.
- Adams, R. H. and K. Alitalo (2007). "Molecular regulation of angiogenesis and lymphangiogenesis." Nat Rev Mol Cell Biol **8**(6): 464-478.
- Adamson, P., C. J. Marshall, A. Hall and P. A. Tilbrook (1992). "Post-translational modifications of p21rho proteins." J Biol Chem **267**(28): 20033-20038.
- Ades, E. W., F. J. Candal, R. A. Swerlick, V. G. George, S. Summers, D. C. Bosse and T. J. Lawley (1992). "HMEC-1: establishment of an immortalized human microvascular endothelial cell line." J Invest Dermatol **99**(6): 683-690.
- Adini, I., I. Rabinovitz, J. F. Sun, G. C. Prendergast and L. E. Benjamin (2003). "RhoB controls Akt trafficking and stage-specific survival of endothelial cells during vascular development." Genes Dev **17**(21): 2721-2732.
- Ahn, S. J., K. W. Chung, R. A. Lee, I. A. Park, S. H. Lee, D. E. Park and D. Y. Noh (2003). "Overexpression of betaPix-a in human breast cancer tissues." Cancer Lett **193**(1): 99-107.
- Aird, W. C. (2012). "Endothelial cell heterogeneity." Cold Spring Harb Perspect Med **2**(1): a006429.
- Alberts, B. (2002). Molecular biology of the cell. New York, Garland Science.
- Allen, W. E., D. Zicha, A. J. Ridley and G. E. Jones (1998). "A role for Cdc42 in macrophage chemotaxis." J Cell Biol **141**(5): 1147-1157.
- Angers-Loustau, A., J. F. Cote, A. Charest, D. Dowbenko, S. Spencer, L. A. Lasky and M. L. Tremblay (1999). "Protein tyrosine phosphatase-PEST regulates focal adhesion disassembly, migration, and cytokinesis in fibroblasts." J Cell Biol **144**(5): 1019-1031.
- Anthis, N. J. and I. D. Campbell (2011). "The tail of integrin activation." Trends Biochem Sci **36**(4): 191-198.
- Aspenstrom, P., A. Fransson and J. Saras (2004). "Rho GTPases have diverse effects on the organization of the actin filament system." Biochem J **377**(Pt 2): 327-337.

Aspenstrom, P., A. Ruusala and D. Pacholsky (2007). "Taking Rho GTPases to the next level: the cellular functions of atypical Rho GTPases." Exp Cell Res **313**(17): 3673-3679.

Audebert, S., C. Navarro, C. Nourry, S. Chasserot-Golaz, P. Lecine, Y. Bellaiche, J. L. Dupont, R. T. Premont, C. Sempere, J. M. Strub, A. Van Dorsselaer, N. Vitale and J. P. Borg (2004). "Mammalian Scribble forms a tight complex with the betaPIX exchange factor." Curr Biol **14**(11): 987-995.

Bae, J. Y., S. J. Ahn, J. E. Lee, J. E. Kim, M. R. Han, W. Han, S. W. Kim, H. J. Shin, S. J. Lee, D. Park and D. Y. Noh (2005). "BetaPix-a enhances the activity of phospholipase Cgamma1 by binding SH3 domain in breast cancer." J Cell Biochem **94**(5): 1010-1016.

Bagrodia, S., D. Bailey, Z. Lenard, M. Hart, J. L. Guan, R. T. Premont, S. J. Taylor and R. A. Cerione (1999). "A tyrosine-phosphorylated protein that binds to an important regulatory region on the cool family of p21-activated kinase-binding proteins." J Biol Chem **274**(32): 22393-22400.

Bagrodia, S., S. J. Taylor, K. A. Jordon, L. Van Aelst and R. A. Cerione (1998). "A novel regulator of p21-activated kinases." J Biol Chem **273**(37): 23633-23636.

Baird, D., Q. Feng and R. A. Cerione (2005). "The Cool-2/alpha-Pix protein mediates a Cdc42-Rac signaling cascade." Curr Biol **15**(1): 1-10.

Bass, M. D., R. C. Williamson, R. D. Nunan, J. D. Humphries, A. Byron, M. R. Morgan, P. Martin and M. J. Humphries (2011). "A syndecan-4 hair trigger initiates wound healing through caveolin- and RhoG-regulated integrin endocytosis." Dev Cell **21**(4): 681-693.

Bayless, K. J. and G. E. Davis (2002). "The Cdc42 and Rac1 GTPases are required for capillary lumen formation in three-dimensional extracellular matrices." J Cell Sci **115**(Pt 6): 1123-1136.

Bayless, K. J. and G. E. Davis (2004). "Microtubule depolymerization rapidly collapses capillary tube networks in vitro and angiogenic vessels in vivo through the small GTPase Rho." J Biol Chem **279**(12): 11686-11695.

Bear, J. E. and F. B. Gertler (2009). "Ena/VASP: towards resolving a pointed controversy at the barbed end." J Cell Sci **122**(Pt 12): 1947-1953.

Bergers, G. and D. Hanahan (2008). "Modes of resistance to anti-angiogenic therapy." Nat Rev Cancer **8**(8): 592-603.

Bertolucci, C. M., C. D. Guibao and J. J. Zheng (2008). "Phosphorylation of paxillin LD4 destabilizes helix formation and inhibits binding to focal adhesion kinase." Biochemistry **47**(2): 548-554.

Billottet, C., P. Rottiers, F. Tatin, C. Varon, E. Reuzeau, J. L. Maitre, F. Saltel, V. Moreau and E. Genot (2008). "Regulatory signals for endothelial podosome formation." Eur J Cell Biol **87**(8-9): 543-554.



- Bishop, A. L. and A. Hall (2000). "Rho GTPases and their effector proteins." Biochem J **348 Pt 2**: 241-255.
- Bishop, E. T., G. T. Bell, S. Bloor, I. J. Broom, N. F. Hendry and D. N. Wheatley (1999). "An in vitro model of angiogenesis: basic features." Angiogenesis **3(4)**: 335-344.
- Blanco, R. and H. Gerhardt (2013). "VEGF and Notch in tip and stalk cell selection." Cold Spring Harb Perspect Med **3(1)**: a006569.
- Boulter, E., S. Estrach, R. Garcia-Mata and C. C. Feral (2012). "Off the beaten paths: alternative and crosstalk regulation of Rho GTPases." FASEB J **26(2)**: 469-479.
- Boureux, A., E. Vignal, S. Faure and P. Fort (2007). "Evolution of the Rho family of ras-like GTPases in eukaryotes." Mol Biol Evol **24(1)**: 203-216.
- Brinas, L., S. Vassilopoulos, G. Bonne, P. Guicheney and M. Bitoun (2013). "Role of dynamin 2 in the disassembly of focal adhesions." J Mol Med (Berl) **91(7)**: 803-809.
- Broussard, J. A., D. J. Webb and I. Kaverina (2008). "Asymmetric focal adhesion disassembly in motile cells." Curr Opin Cell Biol **20(1)**: 85-90.
- Brown, C. M., B. Hebert, D. L. Kolin, J. Zareno, L. Whitmore, A. R. Horwitz and P. W. Wiseman (2006). "Probing the integrin-actin linkage using high-resolution protein velocity mapping." J Cell Sci **119(Pt 24)**: 5204-5214.
- Brown, M. C., L. A. Cary, J. S. Jamieson, J. A. Cooper and C. E. Turner (2005). "Src and FAK kinases cooperate to phosphorylate paxillin kinase linker, stimulate its focal adhesion localization, and regulate cell spreading and protrusiveness." Mol Biol Cell **16(9)**: 4316-4328.
- Brown, M. C. and C. E. Turner (2004). "Paxillin: adapting to change." Physiol Rev **84(4)**: 1315-1339.
- Bryan, B. A. and P. A. D'Amore (2007). "What tangled webs they weave: Rho-GTPase control of angiogenesis." Cell Mol Life Sci **64(16)**: 2053-2065.
- Bryan, B. A., E. Dennstedt, D. C. Mitchell, T. E. Walshe, K. Noma, R. Loureiro, M. Saint-Geniez, J. P. Campaigniac, J. K. Liao and P. A. D'Amore (2010). "RhoA/ROCK signaling is essential for multiple aspects of VEGF-mediated angiogenesis." FASEB J **24(9)**: 3186-3195.
- Burridge, K. and K. Wennerberg (2004). "Rho and Rac take center stage." Cell **116(2)**: 167-179.
- Bustelo, X. R., V. Sauzeau and I. M. Berenjeno (2007). "GTP-binding proteins of the Rho/Rac family: regulation, effectors and functions in vivo." Bioessays **29(4)**: 356-370.
- Carisey, A., R. Tsang, A. M. Greiner, N. Nijenhuis, N. Heath, A. Nazgiewicz, R. Kemkemer, B. Derby, J. Spatz and C. Ballestrem (2013). "Vinculin regulates the recruitment and release of core focal adhesion proteins in a force-dependent manner." Curr Biol **23(4)**: 271-281.
- Carmeliet, P. (2003). "Angiogenesis in health and disease." Nat Med **9(6)**: 653-660.

- Carmeliet, P. (2005). "Angiogenesis in life, disease and medicine." Nature **438**(7070): 932-936.
- Carmeliet, P. and R. K. Jain (2011). "Molecular mechanisms and clinical applications of angiogenesis." Nature **473**(7347): 298-307.
- Carragher, N. O., M. A. Westhoff, V. J. Fincham, M. D. Schaller and M. C. Frame (2003). "A novel role for FAK as a protease-targeting adaptor protein: regulation by p42 ERK and Src." Curr Biol **13**(16): 1442-1450.
- Casey, D. B., A. M. Badejo, J. S. Dhaliwal, J. L. Sikora, A. Fokin, N. H. Golwala, A. J. Greco, S. N. Murthy, B. D. Nossaman, A. L. Hyman and P. J. Kadowitz (2010). "Analysis of responses to the Rho-kinase inhibitor Y-27632 in the pulmonary and systemic vascular bed of the rat." Am J Physiol Heart Circ Physiol **299**(1): H184-192.
- Castillo-Lluya, S., M. H. Tatham, R. C. Jones, E. G. Jaffray, R. D. Edmondson, R. T. Hay and A. Malliri (2010). "SUMOylation of the GTPase Rac1 is required for optimal cell migration." Nat Cell Biol **12**(11): 1078-1085.
- Cau, J. and A. Hall (2005). "Cdc42 controls the polarity of the actin and microtubule cytoskeletons through two distinct signal transduction pathways." J Cell Sci **118**(Pt 12): 2579-2587.
- Chan, K. T., D. A. Bennin and A. Huttenlocher (2010). "Regulation of adhesion dynamics by calpain-mediated proteolysis of focal adhesion kinase (FAK)." J Biol Chem **285**(15): 11418-11426.
- Chang, F., C. A. Lemmon, D. Park and L. H. Romer (2007). "FAK potentiates Rac1 activation and localization to matrix adhesion sites: a role for betaPIX." Mol Biol Cell **18**(1): 253-264.
- Chardin, P. (2006). "Function and regulation of Rnd proteins." Nat Rev Mol Cell Biol **7**(1): 54-62.
- Cherfils, J. and P. Chardin (1999). "GEFs: structural basis for their activation of small GTP-binding proteins." Trends Biochem Sci **24**(8): 306-311.
- Cherfils, J. and M. Zeghouf (2013). "Regulation of small GTPases by GEFs, GAPs, and GDIs." Physiol Rev **93**(1): 269-309.
- Chhabra, E. S. and H. N. Higgs (2007). "The many faces of actin: matching assembly factors with cellular structures." Nat Cell Biol **9**(10): 1110-1121.
- Chiang, S. H., C. A. Baumann, M. Kanzaki, D. C. Thurmond, R. T. Watson, C. L. Neudauer, I. G. Macara, J. E. Pessin and A. R. Saltiel (2001). "Insulin-stimulated GLUT4 translocation requires the CAP-dependent activation of TC10." Nature **410**(6831): 944-948.
- Chiang, S. H., J. C. Hou, J. Hwang, J. E. Pessin and A. R. Saltiel (2002). "Cloning and functional characterization of related TC10 isoforms, a subfamily of Rho proteins involved in insulin-stimulated glucose transport." J Biol Chem **277**(15): 13067-13073.

- Chiang, S. H., J. Hwang, M. Legendre, M. Zhang, A. Kimura and A. R. Saltiel (2003). "TCGAP, a multidomain Rho GTPase-activating protein involved in insulin-stimulated glucose transport." EMBO J **22**(11): 2679-2691.
- Choi, C. K., M. Vicente-Manzanares, J. Zareno, L. A. Whitmore, A. Mogilner and A. R. Horwitz (2008). "Actin and alpha-actinin orchestrate the assembly and maturation of nascent adhesions in a myosin II motor-independent manner." Nat Cell Biol **10**(9): 1039-1050.
- Chu, H. and Y. Wang (2012). "Therapeutic angiogenesis: controlled delivery of angiogenic factors." Ther Deliv **3**(6): 693-714.
- Chuang, Y. Y., A. Valster, S. J. Coniglio, J. M. Backer and M. Symons (2007). "The atypical Rho family GTPase Wrch-1 regulates focal adhesion formation and cell migration." J Cell Sci **120**(Pt 11): 1927-1934.
- Ciobanaru, C., B. Faivre and C. Le Clainche (2012). "Actin dynamics associated with focal adhesions." Int J Cell Biol **2012**: 941292.
- Claing, A., S. J. Perry, M. Achiriloaie, J. K. Walker, J. P. Albanesi, R. J. Lefkowitz and R. T. Premont (2000). "Multiple endocytic pathways of G protein-coupled receptors delineated by GIT1 sensitivity." Proc Natl Acad Sci U S A **97**(3): 1119-1124.
- Cleaver, O. and D. A. Melton (2003). "Endothelial signaling during development." Nat Med **9**(6): 661-668.
- Clemens, M. J. (2005). "Translational control in virus-infected cells: models for cellular stress responses." Semin Cell Dev Biol **16**(1): 13-20.
- Connolly, J. O., N. Simpson, L. Hewlett and A. Hall (2002). "Rac regulates endothelial morphogenesis and capillary assembly." Mol Biol Cell **13**(7): 2474-2485.
- Cortesio, C. L., L. R. Boateng, T. M. Piazza, D. A. Bennin and A. Huttenlocher (2011). "Calpain-mediated proteolysis of paxillin negatively regulates focal adhesion dynamics and cell migration." J Biol Chem **286**(12): 9998-10006.
- Cote, J. F. and K. Vuori (2007). "GEF what? Dock180 and related proteins help Rac to polarize cells in new ways." Trends Cell Biol **17**(8): 383-393.
- Cross, M. J., J. Dixelius, T. Matsumoto and L. Claesson-Welsh (2003). "VEGF-receptor signal transduction." Trends Biochem Sci **28**(9): 488-494.
- D'Souza-Schorey, C. and P. Chavrier (2006). "ARF proteins: roles in membrane traffic and beyond." Nat Rev Mol Cell Biol **7**(5): 347-358.
- Davis, G. E., K. J. Bayless and A. Mavila (2002). "Molecular basis of endothelial cell morphogenesis in three-dimensional extracellular matrices." Anat Rec **268**(3): 252-275.
- De Spiegelaere, W., C. Casteleyn, W. Van den Broeck, J. Plendl, M. Bahramsoltani, P. Simoens, V. Djonov and P. Cornillie (2012). "Intussusceptive angiogenesis: a biologically relevant form of angiogenesis." J Vasc Res **49**(5): 390-404.

- de Toledo, M., F. Senic-Matuglia, J. Salamero, G. Uze, F. Comunale, P. Fort and A. Blangy (2003). "The GTP/GDP cycling of rho GTPase TCL is an essential regulator of the early endocytic pathway." Mol Biol Cell **14**(12): 4846-4856.
- Deramaudt, T. B., D. Dujardin, A. Hamadi, F. Noulet, K. Kolli, J. De Mey, K. Takeda and P. Ronde (2011). "FAK phosphorylation at Tyr-925 regulates cross-talk between focal adhesion turnover and cell protrusion." Mol Biol Cell **22**(7): 964-975.
- Disanza, A., A. Steffen, M. Hertzog, E. Frittoli, K. Rottner and G. Scita (2005). "Actin polymerization machinery: the finish line of signaling networks, the starting point of cellular movement." Cell Mol Life Sci **62**(9): 955-970.
- Donaldson, J. G. and C. L. Jackson (2000). "Regulators and effectors of the ARF GTPases." Curr Opin Cell Biol **12**(4): 475-482.
- Dorn, T., U. Kuhn, G. Bungartz, S. Stiller, M. Bauer, J. Ellwart, T. Peters, K. Scharffetter-Kochanek, M. Semmrich, M. Laschinger, B. Holzmann, W. E. Klinkert, P. T. Straten, T. Kollgaard, M. Sixt and C. Brakebusch (2007). "RhoH is important for positive thymocyte selection and T-cell receptor signaling." Blood **109**(6): 2346-2355.
- Drake, C. J. (2003). "Embryonic and adult vasculogenesis." Birth Defects Res C Embryo Today **69**(1): 73-82.
- Efimov, A. and I. Kaverina (2009). "Significance of microtubule catastrophes at focal adhesion sites." Cell Adh Migr **3**(3): 285-287.
- Egginton, S., A. L. Zhou, M. D. Brown and O. Hudlicka (2001). "Unorthodox angiogenesis in skeletal muscle." Cardiovasc Res **49**(3): 634-646.
- Eitel, J., M. Krull, A. C. Hocke, P. D. N'Guessan, J. Zahlten, B. Schmeck, H. Slevogt, S. Hippenstiel, N. Suttorp and B. Opitz (2008). "Beta-PIX and Rac1 GTPase mediate trafficking and negative regulation of NOD2." J Immunol **181**(4): 2664-2671.
- Eleniste, P. P., L. Du, M. Shivanna and A. Bruzzaniti (2012). "Dynamin and PTP-PEST cooperatively regulate Pyk2 dephosphorylation in osteoclasts." Int J Biochem Cell Biol **44**(5): 790-800.
- Ellenbroek, S. I. and J. G. Collard (2007). "Rho GTPases: functions and association with cancer." Clin Exp Metastasis **24**(8): 657-672.
- Engers, R., E. Springer, F. Michiels, J. G. Collard and H. E. Gabbert (2001). "Rac affects invasion of human renal cell carcinomas by up-regulating tissue inhibitor of metalloproteinases (TIMP)-1 and TIMP-2 expression." J Biol Chem **276**(45): 41889-41897.
- Espert, L., C. Rey, L. Gonzalez, G. Degols, M. K. Chelbi-Alix, N. Mechti and C. Gongora (2004). "The exonuclease ISG20 is directly induced by synthetic dsRNA via NF-kappaB and IRF1 activation." Oncogene **23**(26): 4636-4640.

- Ezratty, E. J., M. A. Partridge and G. G. Gundersen (2005). "Microtubule-induced focal adhesion disassembly is mediated by dynamin and focal adhesion kinase." Nat Cell Biol **7**(6): 581-590.
- Feil, S., N. Valtcheva and R. Feil (2009). "Inducible Cre mice." Methods Mol Biol **530**: 343-363.
- Feng, Q., J. G. Albeck, R. A. Cerione and W. Yang (2002). "Regulation of the Cool/Pix proteins: key binding partners of the Cdc42/Rac targets, the p21-activated kinases." J Biol Chem **277**(7): 5644-5650.
- Feng, Q., D. Baird and R. A. Cerione (2004). "Novel regulatory mechanisms for the Dbl family guanine nucleotide exchange factor Cool-2/alpha-Pix." EMBO J **23**(17): 3492-3504.
- Feng, Q., D. Baird, X. Peng, J. Wang, T. Ly, J. L. Guan and R. A. Cerione (2006). "Cool-1 functions as an essential regulatory node for EGF receptor- and Src-mediated cell growth." Nat Cell Biol **8**(9): 945-956.
- Feng, Q., D. Baird, S. Yoo, M. Antonyak and R. A. Cerione (2010). "Phosphorylation of the cool-1/beta-Pix protein serves as a regulatory signal for the migration and invasive activity of Src-transformed cells." J Biol Chem **285**(24): 18806-18816.
- Fong, G. H., J. Rossant, M. Gertsenstein and M. L. Breitman (1995). "Role of the Flt-1 receptor tyrosine kinase in regulating the assembly of vascular endothelium." Nature **376**(6535): 66-70.
- Franco, S. J., M. A. Rodgers, B. J. Perrin, J. Han, D. A. Bennin, D. R. Critchley and A. Huttenlocher (2004). "Calpain-mediated proteolysis of talin regulates adhesion dynamics." Nat Cell Biol **6**(10): 977-983.
- Frank, S. R. and S. H. Hansen (2008). "The PIX-GIT complex: a G protein signaling cassette in control of cell shape." Semin Cell Dev Biol **19**(3): 234-244.
- Fukushima, Y., M. Okada, H. Kataoka, M. Hirashima, Y. Yoshida, F. Mann, F. Gomi, K. Nishida, S. Nishikawa and A. Uemura (2011). "Sema3E-PlexinD1 signaling selectively suppresses disoriented angiogenesis in ischemic retinopathy in mice." J Clin Invest **121**(5): 1974-1985.
- Gao, Y., J. B. Dickerson, F. Guo, J. Zheng and Y. Zheng (2004). "Rational design and characterization of a Rac GTPase-specific small molecule inhibitor." Proc Natl Acad Sci U S A **101**(20): 7618-7623.
- Garcia-Mata, R., E. Boulter and K. Burridge (2011). "The 'invisible hand': regulation of RHO GTPases by RHOGDIs." Nat Rev Mol Cell Biol **12**(8): 493-504.
- Garcia-Mata, R. and K. Burridge (2007). "Catching a GEF by its tail." Trends Cell Biol **17**(1): 36-43.

- Gavina, M., L. Za, R. Molteni, R. Pardi and I. de Curtis (2010). "The GIT-PIX complexes regulate the chemotactic response of rat basophilic leukaemia cells." *Biol Cell* **102**(4): 231-244.
- Goehler, H., M. Lalowski, U. Stelzl, S. Waelter, M. Stroedicke, U. Worm, A. Droege, K. S. Lindenberg, M. Knoblich, C. Haenig, M. Herbst, J. Suopanki, E. Scherzinger, C. Abraham, B. Bauer, R. Hasenbank, A. Fritzsche, A. H. Ludewig, K. Bussow, S. H. Coleman, C. A. Gutekunst, B. G. Landwehrmeyer, H. Lehrach and E. E. Wanker (2004). "A protein interaction network links GIT1, an enhancer of huntingtin aggregation, to Huntington's disease." *Mol Cell* **15**(6): 853-865.
- Gringel, A., D. Walz, G. Rosenberger, A. Minden, K. Kutsche, P. Kopp and S. Linder (2006). "PAK4 and alphaPIX determine podosome size and number in macrophages through localized actin regulation." *J Cell Physiol* **209**(2): 568-579.
- Guasch, R. M., P. Scambler, G. E. Jones and A. J. Ridley (1998). "RhoE regulates actin cytoskeleton organization and cell migration." *Mol Cell Biol* **18**(8): 4761-4771.
- Gumienny, T. L., E. Brugnera, A. C. Tosello-Trampont, J. M. Kinchen, L. B. Haney, K. Nishiwaki, S. F. Walk, M. E. Nemergut, I. G. Macara, R. Francis, T. Schedl, Y. Qin, L. Van Aelst, M. O. Hengartner and K. S. Ravichandran (2001). "CED-12/ELMO, a novel member of the CrkII/Dock180/Rac pathway, is required for phagocytosis and cell migration." *Cell* **107**(1): 27-41.
- Gupta, K. and J. Zhang (2005). "Angiogenesis: a curse or cure?" *Postgrad Med J* **81**(954): 236-242.
- Haendeler, J., G. Yin, Y. Hojo, Y. Saito, M. Melaragno, C. Yan, V. K. Sharma, M. Heller, R. Aebersold and B. C. Berk (2003). "GIT1 mediates Src-dependent activation of phospholipase Cgamma by angiotensin II and epidermal growth factor." *J Biol Chem* **278**(50): 49936-49944.
- Hall, A. (2012). "Rho family GTPases." *Biochem Soc Trans* **40**(6): 1378-1382.
- Hamadi, A., M. Bouali, M. Dontenwill, H. Stoeckel, K. Takeda and P. Ronde (2005). "Regulation of focal adhesion dynamics and disassembly by phosphorylation of FAK at tyrosine 397." *J Cell Sci* **118**(Pt 19): 4415-4425.
- Hanein, D. and A. R. Horwitz (2012). "The structure of cell-matrix adhesions: the new frontier." *Curr Opin Cell Biol* **24**(1): 134-140.
- Heasman, S. J. and A. J. Ridley (2008). "Mammalian Rho GTPases: new insights into their functions from in vivo studies." *Nat Rev Mol Cell Biol* **9**(9): 690-701.
- Heath, V. L., S. L. Shaw, S. Roy and M. S. Cyert (2004). "Hph1p and Hph2p, novel components of calcineurin-mediated stress responses in *Saccharomyces cerevisiae*." *Eukaryot Cell* **3**(3): 695-704.
- Hillen, F. and A. W. Griffioen (2007). "Tumour vascularization: sprouting angiogenesis and beyond." *Cancer Metastasis Rev* **26**(3-4): 489-502.

Hippenstiel, S., B. Schmeck, P. D. N'Guessan, J. Seybold, M. Krull, K. Preissner, C. V. Eichel-Streiber and N. Suttrop (2002). "Rho protein inactivation induced apoptosis of cultured human endothelial cells." Am J Physiol Lung Cell Mol Physiol **283**(4): L830-838.

Ho, H., J. Aruri, R. Kapadia, H. Mehr, M. A. White and A. K. Ganesan (2012). "RhoJ regulates melanoma chemoresistance by suppressing pathways that sense DNA damage." Cancer Res **72**(21): 5516-5528.

Ho, H., A. Soto Hopkin, R. Kapadia, P. Vasudeva, J. Schilling and A. K. Ganesan (2013). "RhoJ modulates melanoma invasion by altering actin cytoskeletal dynamics." Pigment Cell Melanoma Res **26**(2): 218-225.

Ho, V. C., L. J. Duan, C. Cronin, B. T. Liang and G. H. Fong (2012). "Elevated vascular endothelial growth factor receptor-2 abundance contributes to increased angiogenesis in vascular endothelial growth factor receptor-1-deficient mice." Circulation **126**(6): 741-752.

Hoang, M. V., M. C. Whelan and D. R. Senger (2004). "Rho activity critically and selectively regulates endothelial cell organization during angiogenesis." Proc Natl Acad Sci U S A **101**(7): 1874-1879.

Hoefen, R. J. and B. C. Berk (2006). "The multifunctional GIT family of proteins." J Cell Sci **119**(Pt 8): 1469-1475.

Hsu, Y. H., W. L. Lin, Y. T. Hou, Y. S. Pu, C. T. Shun, C. L. Chen, Y. Y. Wu, J. Y. Chen, T. H. Chen and T. S. Jou (2010). "Podocalyxin EBP50 ezrin molecular complex enhances the metastatic potential of renal cell carcinoma through recruiting Rac1 guanine nucleotide exchange factor ARHGEF7." Am J Pathol **176**(6): 3050-3061.

Hu, G. D., Y. H. Chen, L. Zhang, W. C. Tong, Y. X. Cheng, Y. L. Luo, S. X. Cai and L. Zhang (2011). "The generation of the endothelial specific cdc42-deficient mice and the effect of cdc42 deletion on the angiogenesis and embryonic development." Chin Med J (Engl) **124**(24): 4155-4159.

Huck, B., R. Kemkemmer, M. Franz-Wachtel, B. Macek, A. Hausser and M. A. Olayioye (2012). "GIT1 phosphorylation on serine 46 by PKD3 regulates paxillin trafficking and cellular protrusive activity." J Biol Chem **287**(41): 34604-34613.

Humar, R., L. Zimmerli and E. Battegay (2009). "Angiogenesis and hypertension: an update." J Hum Hypertens **23**(12): 773-782.

Hussain, A., M. Steimle, H. Hoppeler, O. Baum and S. Egginton (2012). "The vascular-disrupting agent combretastatin impairs splitting and sprouting forms of physiological angiogenesis." Microcirculation **19**(4): 296-305.

Huveneers, S. and E. H. Danen (2009). "Adhesion signaling - crosstalk between integrins, Src and Rho." J Cell Sci **122**(Pt 8): 1059-1069.

- Ispanovic, E., D. Serio and T. L. Haas (2008). "Cdc42 and RhoA have opposing roles in regulating membrane type 1-matrix metalloproteinase localization and matrix metalloproteinase-2 activation." Am J Physiol Cell Physiol **295**(3): C600-610.
- Jaffe, A. B. and A. Hall (2005). "Rho GTPases: biochemistry and biology." Annu Rev Cell Dev Biol **21**: 247-269.
- Jain, R. K. (2003). "Molecular regulation of vessel maturation." Nat Med **9**(6): 685-693.
- James, P., J. Halladay and E. A. Craig (1996). "Genomic libraries and a host strain designed for highly efficient two-hybrid selection in yeast." Genetics **144**(4): 1425-1436.
- Jamieson, J. S., D. A. Tumbarello, M. Halle, M. C. Brown, M. L. Tremblay and C. E. Turner (2005). "Paxillin is essential for PTP-PEST-dependent regulation of cell spreading and motility: a role for paxillin kinase linker." J Cell Sci **118**(Pt 24): 5835-5847.
- Jones, M. C., K. Machida, B. J. Mayer and C. E. Turner (2013). "Paxillin kinase linker (PKL) regulates Vav2 signaling during cell spreading and migration." Mol Biol Cell **24**(12): 1882-1894.
- Jones, N. P. and M. Katan (2007). "Role of phospholipase Cgamma1 in cell spreading requires association with a beta-Pix/GIT1-containing complex, leading to activation of Cdc42 and Rac1." Mol Cell Biol **27**(16): 5790-5805.
- Karlsson, R., E. D. Pedersen, Z. Wang and C. Brakebusch (2009). "Rho GTPase function in tumorigenesis." Biochim Biophys Acta **1796**(2): 91-98.
- Kaur, S., K. Leszczynska, S. Abraham, M. Scarcia, S. Hiltbrunner, C. J. Marshall, G. Mavria, R. Bicknell and V. L. Heath (2011). "RhoJ/TCL regulates endothelial motility and tube formation and modulates actomyosin contractility and focal adhesion numbers." Arterioscler Thromb Vasc Biol **31**(3): 657-664.
- Kawaji, A., M. Nishizuka, S. Osada and M. Imagawa (2010). "TC10-like/TC10betaLong regulates adipogenesis by controlling mitotic clonal expansion." Biol Pharm Bull **33**(3): 404-409.
- Kepner, E. M., S. M. Yoder, E. Oh, M. A. Kalwat, Z. Wang, L. A. Quilliam and D. C. Thurmond (2011). "Cool-1/betaPIX functions as a guanine nucleotide exchange factor in the cycling of Cdc42 to regulate insulin secretion." Am J Physiol Endocrinol Metab **301**(6): E1072-1080.
- Kilarski, W. W., B. Samolov, L. Petersson, A. Kvanta and P. Gerwins (2009). "Biomechanical regulation of blood vessel growth during tissue vascularization." Nat Med **15**(6): 657-664.
- Kim, C., H. Yang, Y. Fukushima, P. E. Saw, J. Lee, J. S. Park, I. Park, J. Jung, H. Kataoka, D. Lee, W. D. Heo, I. Kim, S. Jon, R. H. Adams, S. Nishikawa, A. Uemura and G. Y. Koh (2014). "Vascular RhoJ Is an Effective and Selective Target for Tumor Angiogenesis and Vascular Disruption." Cancer Cell **25**(1): 102-117.



- Kim, S., J. Ko, H. Shin, J. R. Lee, C. Lim, J. H. Han, W. D. Altmann, C. C. Garner, E. D. Gundelfinger, R. T. Premont, B. K. Kaang and E. Kim (2003). "The GIT family of proteins forms multimers and associates with the presynaptic cytomatrix protein Piccolo." J Biol Chem **278**(8): 6291-6300.
- Kim, S., S. H. Lee and D. Park (2001). "Leucine zipper-mediated homodimerization of the p21-activated kinase-interacting factor, beta Pix. Implication for a role in cytoskeletal reorganization." J Biol Chem **276**(14): 10581-10584.
- Kiosses, W. B., S. J. Shattil, N. Pampori and M. A. Schwartz (2001). "Rac recruits high-affinity integrin alphavbeta3 to lamellipodia in endothelial cell migration." Nat Cell Biol **3**(3): 316-320.
- Klinger, J. R., S. H. Abman and M. T. Gladwin (2013). "Nitric oxide deficiency and endothelial dysfunction in pulmonary arterial hypertension." Am J Respir Crit Care Med **188**(6): 639-646.
- Koerselman, J., Y. van der Graaf, P. P. de Jaegere and D. E. Grobbee (2003). "Coronary collaterals: an important and underexposed aspect of coronary artery disease." Circulation **107**(19): 2507-2511.
- Koh, C. G., E. Manser, Z. S. Zhao, C. P. Ng and L. Lim (2001). "Beta1PIX, the PAK-interacting exchange factor, requires localization via a coiled-coil region to promote microvillus-like structures and membrane ruffles." J Cell Sci **114**(Pt 23): 4239-4251.
- Koh, C. G., E. J. Tan, E. Manser and L. Lim (2002). "The p21-activated kinase PAK is negatively regulated by POPX1 and POPX2, a pair of serine/threonine phosphatases of the PP2C family." Curr Biol **12**(4): 317-321.
- Kouklis, P., M. Konstantoulaki, S. Vogel, M. Broman and A. B. Malik (2004). "Cdc42 regulates the restoration of endothelial barrier function." Circ Res **94**(2): 159-166.
- Kraynov, V. S., C. Chamberlain, G. M. Bokoch, M. A. Schwartz, S. Slabaugh and K. M. Hahn (2000). "Localized Rac activation dynamics visualized in living cells." Science **290**(5490): 333-337.
- Kuo, J. C., X. Han, C. T. Hsiao, J. R. Yates, 3rd and C. M. Waterman (2011). "Analysis of the myosin-II-responsive focal adhesion proteome reveals a role for beta-Pix in negative regulation of focal adhesion maturation." Nat Cell Biol **13**(4): 383-393.
- Kurokawa, K. and M. Matsuda (2005). "Localized RhoA activation as a requirement for the induction of membrane ruffling." Mol Biol Cell **16**(9): 4294-4303.
- Kusuhara, S., Y. Fukushima, S. Fukuhara, L. M. Jakt, M. Okada, Y. Shimizu, M. Hata, K. Nishida, A. Negi, M. Hirashima, N. Mochizuki, S. Nishikawa and A. Uemura (2012). "Arhgef15 promotes retinal angiogenesis by mediating VEGF-induced Cdc42 activation and potentiating RhoJ inactivation in endothelial cells." PLoS One **7**(9): e45858.
- Kutsche, K., H. Yntema, A. Brandt, I. Jantke, H. G. Nothwang, U. Orth, M. G. Boavida, D. David, J. Chelly, J. P. Fryns, C. Moraine, H. H. Ropers, B. C. Hamel, H. van Bokhoven and A.

- Gal (2000). "Mutations in ARHGEF6, encoding a guanine nucleotide exchange factor for Rho GTPases, in patients with X-linked mental retardation." Nat Genet **26**(2): 247-250.
- Ladomery, M. R., S. J. Harper and D. O. Bates (2007). "Alternative splicing in angiogenesis: the vascular endothelial growth factor paradigm." Cancer Lett **249**(2): 133-142.
- Lahuna, O., M. Quellari, C. Achard, S. Nola, G. Meduri, C. Navarro, N. Vitale, J. P. Borg and M. Misrahi (2005). "Thyrotropin receptor trafficking relies on the hScrib-betaPIX-GIT1-ARF6 pathway." EMBO J **24**(7): 1364-1374.
- Lakka Klement, G., E. Shai and D. Varon (2013). The Role of Platelets in Angiogenesis. Platelets. A. D. Michelson, Elsevier: 487-502.
- Lallemant, Y., V. Luria, R. Haffner-Krausz and P. Lonai (1998). "Maternally expressed PGK-Cre transgene as a tool for early and uniform activation of the Cre site-specific recombinase." Transgenic Res **7**(2): 105-112.
- Lamallice, L., F. Le Boeuf and J. Huot (2007). "Endothelial cell migration during angiogenesis." Circ Res **100**(6): 782-794.
- Le Clainche, C. and M. F. Carlier (2008). "Regulation of actin assembly associated with protrusion and adhesion in cell migration." Physiol Rev **88**(2): 489-513.
- Lee, C. S., C. K. Choi, E. Y. Shin, M. A. Schwartz and E. G. Kim (2010). "Myosin II directly binds and inhibits Dbl family guanine nucleotide exchange factors: a possible link to Rho family GTPases." J Cell Biol **190**(4): 663-674.
- Lee, S. H. and R. Dominguez (2010). "Regulation of actin cytoskeleton dynamics in cells." Mol Cells **29**(4): 311-325.
- Lee, S. J., S. J. Yang, D. H. Kim, J. H. Pak, K. H. Lee, K. H. Choi, D. Park and S. Rhee (2011). "Interaction of microtubules and actin with the N-terminus of betaPix-b(L) directs cellular pinocytosis." Mol Cell Biochem **351**(1-2): 207-215.
- Li, X., X. Bu, B. Lu, H. Avraham, R. A. Flavell and B. Lim (2002). "The hematopoiesis-specific GTP-binding protein RhoH is GTPase deficient and modulates activities of other Rho GTPases by an inhibitory function." Mol Cell Biol **22**(4): 1158-1171.
- Liu, J., S. D. Fraser, P. W. Faloony, E. L. Rollins, J. Vom Berg, O. Starovic-Subota, A. L. Laliberte, J. N. Chen, F. C. Serluca and S. J. Childs (2007). "A betaPix Pak2a signaling pathway regulates cerebral vascular stability in zebrafish." Proc Natl Acad Sci U S A **104**(35): 13990-13995.
- Liu, J., L. Zeng, R. M. Kennedy, N. M. Gruenig and S. J. Childs (2012). "betaPix plays a dual role in cerebral vascular stability and angiogenesis, and interacts with integrin alphavbeta8." Dev Biol **363**(1): 95-105.
- Liu, S., R. T. Premont and D. C. Rockey (2012). "G-protein-coupled receptor kinase interactor-1 (GIT1) is a new endothelial nitric-oxide synthase (eNOS) interactor with functional effects on vascular homeostasis." J Biol Chem **287**(15): 12309-12320.

Lombardo, L. J., F. Y. Lee, P. Chen, D. Norris, J. C. Barrish, K. Behnia, S. Castaneda, L. A. Cornelius, J. Das, A. M. Doweiko, C. Fairchild, J. T. Hunt, I. Inigo, K. Johnston, A. Kamath, D. Kan, H. Klei, P. Marathe, S. Pang, R. Peterson, S. Pitt, G. L. Schieven, R. J. Schmidt, J. Tokarski, M. L. Wen, J. Wityak and R. M. Borzilleri (2004). "Discovery of N-(2-chloro-6-methyl- phenyl)-2-(6-(4-(2-hydroxyethyl)- piperazin-1-yl)-2-methylpyrimidin-4- ylamino)thiazole-5-carboxamide (BMS-354825), a dual Src/Abl kinase inhibitor with potent antitumor activity in preclinical assays." *J Med Chem* **47**(27): 6658-6661.

Loo, T. H., Y. W. Ng, L. Lim and E. Manser (2004). "GIT1 activates p21-activated kinase through a mechanism independent of p21 binding." *Mol Cell Biol* **24**(9): 3849-3859.

Lu, Q., F. M. Longo, H. Zhou, S. M. Massa and Y. H. Chen (2009). "Signaling through Rho GTPase pathway as viable drug target." *Curr Med Chem* **16**(11): 1355-1365.

Ma, J., Y. Xue, W. Cui, Y. Li, Q. Zhao, W. Ye, J. Zheng, Y. Cheng, Y. Ma, S. Li, T. Han, L. Miao, L. Yao, J. Zhang and W. Liu (2012). "Ras homolog gene family, member A promotes p53 degradation and vascular endothelial growth factor-dependent angiogenesis through an interaction with murine double minute 2 under hypoxic conditions." *Cancer* **118**(17): 4105-4116.

Ma, J., Y. Xue, W. Liu, C. Yue, F. Bi, J. Xu, J. Zhang, Y. Li, C. Zhong and Y. Chen (2013). "Role of activated rac1/cdc42 in mediating endothelial cell proliferation and tumor angiogenesis in breast cancer." *PLoS One* **8**(6): e66275.

Machacek, M., L. Hodgson, C. Welch, H. Elliott, O. Pertz, P. Nalbant, A. Abell, G. L. Johnson, K. M. Hahn and G. Danuser (2009). "Coordination of Rho GTPase activities during cell protrusion." *Nature* **461**(7260): 99-103.

Maciag, T., J. Cerundolo, S. Ilsley, P. R. Kelley and R. Forand (1979). "An endothelial cell growth factor from bovine hypothalamus: identification and partial characterization." *Proc Natl Acad Sci U S A* **76**(11): 5674-5678.

Manabe, R., M. Kovalenko, D. J. Webb and A. R. Horwitz (2002). "GIT1 functions in a motile, multi-molecular signaling complex that regulates protrusive activity and cell migration." *J Cell Sci* **115**(Pt 7): 1497-1510.

Manser, E., T. H. Loo, C. G. Koh, Z. S. Zhao, X. Q. Chen, L. Tan, I. Tan, T. Leung and L. Lim (1998). "PAK kinases are directly coupled to the PIX family of nucleotide exchange factors." *Mol Cell* **1**(2): 183-192.

Masiero, M., F. C. Simoes, H. D. Han, C. Snell, T. Peterkin, E. Bridges, L. S. Mangala, S. Y. Wu, S. Pradeep, D. Li, C. Han, H. Dalton, G. Lopez-Berestein, J. B. Tuynman, N. Mortensen, J. L. Li, R. Patient, A. K. Sood, A. H. Banham, A. L. Harris and F. M. Buffa (2013). "A core human primary tumor angiogenesis signature identifies the endothelial orphan receptor ELTD1 as a key regulator of angiogenesis." *Cancer Cell* **24**(2): 229-241.

Mattheyses, A. L., S. M. Simon and J. Z. Rappoport (2010). "Imaging with total internal reflection fluorescence microscopy for the cell biologist." *J Cell Sci* **123**(Pt 21): 3621-3628.

- Mattila, P. K. and P. Lappalainen (2008). "Filopodia: molecular architecture and cellular functions." Nat Rev Mol Cell Biol **9**(6): 446-454.
- Mazaki, Y., S. Hashimoto, T. Tsujimura, M. Morishige, A. Hashimoto, K. Aritake, A. Yamada, J. M. Nam, H. Kiyonari, K. Nakao and H. Sabe (2006). "Neutrophil direction sensing and superoxide production linked by the GTPase-activating protein GIT2." Nat Immunol **7**(7): 724-731.
- Md Hashim, N. F., N. S. Nicholas, A. E. Dart, S. Kiriakidis, E. Paleolog and C. M. Wells (2013). "Hypoxia-induced invadopodia formation: a role for beta-PIX." Open Biol **3**(6): 120159.
- Meadows, K. L. and H. I. Hurwitz (2012). "Anti-VEGF therapies in the clinic." Cold Spring Harb Perspect Med **2**(10).
- Mellor, H., P. Flynn, C. D. Nobes, A. Hall and P. J. Parker (1998). "PRK1 is targeted to endosomes by the small GTPase, RhoB." J Biol Chem **273**(9): 4811-4814.
- Mendoza, P., R. Ortiz, J. Diaz, A. F. Quest, L. Leyton, D. Stupack and V. A. Torres (2013). "Rab5 activation promotes focal adhesion disassembly, migration and invasiveness in tumor cells." J Cell Sci **126**(Pt 17): 3835-3847.
- Menon, P., R. Deane, A. Sagare, S. M. Lane, T. J. Zarcone, M. R. O'Dell, C. Yan, B. V. Zlokovic and B. C. Berk (2010). "Impaired spine formation and learning in GPCR kinase 2 interacting protein-1 (GIT1) knockout mice." Brain Res **1317**: 218-226.
- Menon, P., G. Yin, E. M. Smolock, M. J. Zuscik, C. Yan and B. C. Berk (2010). "GPCR kinase 2 interacting protein 1 (GIT1) regulates osteoclast function and bone mass." J Cell Physiol **225**(3): 777-785.
- Meyer, M. Z., N. Deliot, S. Chasserot-Golaz, R. T. Premont, M. F. Bader and N. Vitale (2006). "Regulation of neuroendocrine exocytosis by the ARF6 GTPase-activating protein GIT1." J Biol Chem **281**(12): 7919-7926.
- Michaelson, D., J. Silletti, G. Murphy, P. D'Eustachio, M. Rush and M. R. Philips (2001). "Differential localization of Rho GTPases in live cells: regulation by hypervariable regions and RhoGDI binding." J Cell Biol **152**(1): 111-126.
- Millard, T. H., S. J. Sharp and L. M. Machesky (2004). "Signalling to actin assembly via the WASP (Wiskott-Aldrich syndrome protein)-family proteins and the Arp2/3 complex." Biochem J **380**(Pt 1): 1-17.
- Missy, K., B. Hu, K. Schilling, A. Harenberg, V. Sakk, K. Kuchenbecker, K. Kutsche and K. D. Fischer (2008). "AlphaPIX Rho GTPase guanine nucleotide exchange factor regulates lymphocyte functions and antigen receptor signaling." Mol Cell Biol **28**(11): 3776-3789.
- Mitra, S. K., D. A. Hanson and D. D. Schlaepfer (2005). "Focal adhesion kinase: in command and control of cell motility." Nat Rev Mol Cell Biol **6**(1): 56-68.

- Momboisse, F., E. Lonchamp, V. Calco, M. Ceridono, N. Vitale, M. F. Bader and S. Gasman (2009). "betaPIX-activated Rac1 stimulates the activation of phospholipase D, which is associated with exocytosis in neuroendocrine cells." J Cell Sci **122**(Pt 6): 798-806.
- Murphy, C., R. Saffrich, M. Grummt, H. Gournier, V. Rybin, M. Rubino, P. Auvinen, A. Lutcke, R. G. Parton and M. Zerial (1996). "Endosome dynamics regulated by a Rho protein." Nature **384**(6608): 427-432.
- Murphy, C., R. Saffrich, J. C. Olivo-Marin, A. Giner, W. Ansorge, T. Fotsis and M. Zerial (2001). "Dual function of rhoD in vesicular movement and cell motility." Eur J Cell Biol **80**(6): 391-398.
- Nalbant, P., L. Hodgson, V. Kraynov, A. Touthkine and K. M. Hahn (2004). "Activation of endogenous Cdc42 visualized in living cells." Science **305**(5690): 1615-1619.
- Nayal, A., D. J. Webb, C. M. Brown, E. M. Schaefer, M. Vicente-Manzanares and A. R. Horwitz (2006). "Paxillin phosphorylation at Ser273 localizes a GIT1-PIX-PAK complex and regulates adhesion and protrusion dynamics." J Cell Biol **173**(4): 587-589.
- Nishizuka, M., E. Arimoto, T. Tsuchiya, T. Nishihara and M. Imagawa (2003). "Crucial role of TCL/TC10beta L, a subfamily of Rho GTPase, in adipocyte differentiation." J Biol Chem **278**(17): 15279-15284.
- Nobes, C. D. and A. Hall (1995). "Rho, rac, and cdc42 GTPases regulate the assembly of multimolecular focal complexes associated with actin stress fibers, lamellipodia, and filopodia." Cell **81**(1): 53-62.
- Nobes, C. D., I. Lauritzen, M. G. Mattei, S. Paris, A. Hall and P. Chardin (1998). "A new member of the Rho family, Rnd1, promotes disassembly of actin filament structures and loss of cell adhesion." J Cell Biol **141**(1): 187-197.
- Oakes, P. W., Y. Beckham, J. Stricker and M. L. Gardel (2012). "Tension is required but not sufficient for focal adhesion maturation without a stress fiber template." J Cell Biol **196**(3): 363-374.
- Oh, W. K., J. C. Yoo, D. Jo, Y. H. Song, M. G. Kim and D. Park (1997). "Cloning of a SH3 domain-containing proline-rich protein, p85SPR, and its localization in focal adhesion." Biochem Biophys Res Commun **235**(3): 794-798.
- Pandya, N. M., N. S. Dhalla and D. D. Santani (2006). "Angiogenesis--a new target for future therapy." Vascul Pharmacol **44**(5): 265-274.
- Pang, J., R. Hoefen, G. S. Pryhuber, J. Wang, G. Yin, R. J. White, X. Xu, M. R. O'Dell, A. Mohan, H. Michaloski, M. P. Massett, C. Yan and B. C. Berk (2009). "G-protein-coupled receptor kinase interacting protein-1 is required for pulmonary vascular development." Circulation **119**(11): 1524-1532.

- Pang, J., X. Xu, M. R. Getman, X. Shi, S. L. Belmonte, H. Michaloski, A. Mohan, B. C. Blaxall and B. C. Berk (2011). "G protein coupled receptor kinase 2 interacting protein 1 (GIT1) is a novel regulator of mitochondrial biogenesis in heart." J Mol Cell Cardiol **51**(5): 769-776.
- Pang, J., X. Xu, X. Wang, S. Majumder, J. Wang, V. A. Korshunov and B. C. Berk (2013). "G-protein-coupled receptor kinase interacting protein-1 mediates intima formation by regulating vascular smooth muscle proliferation, apoptosis, and migration." Arterioscler Thromb Vasc Biol **33**(5): 999-1005.
- Paris, S., R. Longhi, P. Santambrogio and I. de Curtis (2003). "Leucine-zipper-mediated homo- and hetero-dimerization of GIT family p95-ARF GTPase-activating protein, PIX-, paxillin-interacting proteins 1 and 2." Biochem J **372**(Pt 2): 391-398.
- Park, H. J., D. Kong, L. Iruela-Arispe, U. Begley, D. Tang and J. B. Galper (2002). "3-hydroxy-3-methylglutaryl coenzyme A reductase inhibitors interfere with angiogenesis by inhibiting the geranylgeranylation of RhoA." Circ Res **91**(2): 143-150.
- Parsons, J. T., A. R. Horwitz and M. A. Schwartz (2010). "Cell adhesion: integrating cytoskeletal dynamics and cellular tension." Nat Rev Mol Cell Biol **11**(9): 633-643.
- Passaniti, A. (1992). "Extracellular matrix-cell interactions: Matrigel and complex cellular pattern formation." Lab Invest **67**(6): 804; author reply 804-808.
- Paulis, Y. W., P. M. Soetekouw, H. M. Verheul, V. C. Tjan-Heijnen and A. W. Griffioen (2010). "Signalling pathways in vasculogenic mimicry." Biochim Biophys Acta **1806**(1): 18-28.
- Pavlov, T. S., A. Chahdi, D. V. Ilatovskaya, V. Levchenko, A. Vandewalle, O. Pochynyuk, A. Sorokin and A. Staruschenko (2010). "Endothelin-1 inhibits the epithelial Na<sup>+</sup> channel through betaPix/14-3-3/Nedd4-2." J Am Soc Nephrol **21**(5): 833-843.
- Pearse, G. (2006). "Normal structure, function and histology of the thymus." Toxicol Pathol **34**(5): 504-514.
- Pellinen, T., A. Arjonen, K. Vuoriluoto, K. Kallio, J. A. Fransen and J. Ivaska (2006). "Small GTPase Rab21 regulates cell adhesion and controls endosomal traffic of beta1-integrins." J Cell Biol **173**(5): 767-780.
- Perona, R., S. Montaner, L. Saniger, I. Sanchez-Perez, R. Bravo and J. C. Lacal (1997). "Activation of the nuclear factor-kappaB by Rho, CDC42, and Rac-1 proteins." Genes Dev **11**(4): 463-475.
- Pertz, O., L. Hodgson, R. L. Klemke and K. M. Hahn (2006). "Spatiotemporal dynamics of RhoA activity in migrating cells." Nature **440**(7087): 1069-1072.
- Phee, H., I. Dzhalalov, M. Mollenauer, Y. Wang, D. J. Irvine, E. Robey and A. Weiss (2010). "Regulation of thymocyte positive selection and motility by GIT2." Nat Immunol **11**(6): 503-511.

Potente, M., H. Gerhardt and P. Carmeliet (2011). "Basic and therapeutic aspects of angiogenesis." Cell **146**(6): 873-887.

Premont, R. T., A. Claing, N. Vitale, J. L. Freeman, J. A. Pitcher, W. A. Patton, J. Moss, M. Vaughan and R. J. Lefkowitz (1998). "beta2-Adrenergic receptor regulation by GIT1, a G protein-coupled receptor kinase-associated ADP ribosylation factor GTPase-activating protein." Proc Natl Acad Sci U S A **95**(24): 14082-14087.

Premont, R. T., A. Claing, N. Vitale, S. J. Perry and R. J. Lefkowitz (2000). "The GIT family of ADP-ribosylation factor GTPase-activating proteins. Functional diversity of GIT2 through alternative splicing." J Biol Chem **275**(29): 22373-22380.

Premont, R. T., S. J. Perry, R. Schmalzigaug, J. T. Roseman, Y. Xing and A. Claing (2004). "The GIT/PIX complex: an oligomeric assembly of GIT family ARF GTPase-activating proteins and PIX family Rac1/Cdc42 guanine nucleotide exchange factors." Cell Signal **16**(9): 1001-1011.

Privat, C., F. Lantoin, F. Bedioui, E. Millanvoe van Brussel, J. Devynck and M. A. Devynck (1997). "Nitric oxide production by endothelial cells: comparison of three methods of quantification." Life Sci **61**(12): 1193-1202.

Qiu, R. G., A. Abo and G. Steven Martin (2000). "A human homolog of the C. elegans polarity determinant Par-6 links Rac and Cdc42 to PKCzeta signaling and cell transformation." Curr Biol **10**(12): 697-707.

Raftopoulou, M. and A. Hall (2004). "Cell migration: Rho GTPases lead the way." Dev Biol **265**(1): 23-32.

Ramakers, G. J., D. Wolfer, G. Rosenberger, K. Kuchenbecker, H. J. Kreienkamp, J. Prange-Kiel, G. Rune, K. Richter, K. Langnaese, S. Masneuf, M. R. Bosl, K. D. Fischer, H. J. Krugers, H. P. Lipp, E. van Galen and K. Kutsche (2012). "Dysregulation of Rho GTPases in the alphaPix/Arhgef6 mouse model of X-linked intellectual disability is paralleled by impaired structural and synaptic plasticity and cognitive deficits." Hum Mol Genet **21**(2): 268-286.

Ren, Y., L. Yu, J. Fan, Z. Rui, Z. Hua, Z. Zhang, N. Zhang and G. Yin (2012). "Phosphorylation of GIT1 tyrosine 321 is required for association with FAK at focal adhesions and for PDGF-activated migration of osteoblasts." Mol Cell Biochem **365**(1-2): 109-118.

Ribatti, D. (2009). "Endogenous inhibitors of angiogenesis: a historical review." Leuk Res **33**(5): 638-644.

Ridley, A. J. and A. Hall (1992). "The small GTP-binding protein rho regulates the assembly of focal adhesions and actin stress fibers in response to growth factors." Cell **70**(3): 389-399.

Ridley, A. J., H. F. Paterson, C. L. Johnston, D. Diekmann and A. Hall (1992). "The small GTP-binding protein rac regulates growth factor-induced membrane ruffling." Cell **70**(3): 401-410.

Ridley, A. J., M. A. Schwartz, K. Burridge, R. A. Firtel, M. H. Ginsberg, G. Borisy, J. T. Parsons and A. R. Horwitz (2003). "Cell migration: integrating signals from front to back." Science **302**(5651): 1704-1709.

- Roberts, P. J., N. Mitin, P. J. Keller, E. J. Chenette, J. P. Madigan, R. O. Currin, A. D. Cox, O. Wilson, P. Kirschmeier and C. J. Der (2008). "Rho Family GTPase modification and dependence on CAAX motif-signaled posttranslational modification." *J Biol Chem* **283**(37): 25150-25163.
- Rooney, C., G. White, A. Nazgiewicz, S. A. Woodcock, K. I. Anderson, C. Ballestrem and A. Malliri (2010). "The Rac activator STEF (Tiam2) regulates cell migration by microtubule-mediated focal adhesion disassembly." *EMBO Rep* **11**(4): 292-298.
- Rosenberger, G., A. Gal and K. Kutsche (2005). "AlphaPIX associates with calpain 4, the small subunit of calpain, and has a dual role in integrin-mediated cell spreading." *J Biol Chem* **280**(8): 6879-6889.
- Rosenberger, G. and K. Kutsche (2006). "AlphaPIX and betaPIX and their role in focal adhesion formation." *Eur J Cell Biol* **85**(3-4): 265-274.
- Rossman, K. L., C. J. Der and J. Sondek (2005). "GEF means go: turning on RHO GTPases with guanine nucleotide-exchange factors." *Nat Rev Mol Cell Biol* **6**(2): 167-180.
- Rovini, A., G. Gauthier, R. Berges, A. Kruczynski, D. Braguer and S. Honore (2013). "Anti-migratory effect of vinflunine in endothelial and glioblastoma cells is associated with changes in EB1 C-terminal detyrosinated/tyrosinated status." *PLoS One* **8**(6): e65694.
- Rui, Z., X. Li, J. Fan, Y. Ren, Y. Yuan, Z. Hua, N. Zhang and G. Yin (2012). "GIT1Y321 phosphorylation is required for ERK1/2- and PDGF-dependent VEGF secretion from osteoblasts to promote angiogenesis and bone healing." *Int J Mol Med* **30**(4): 819-825.
- Sakurai, Y., K. Ohgimoto, Y. Kataoka, N. Yoshida and M. Shibuya (2005). "Essential role of Flk-1 (VEGF receptor 2) tyrosine residue 1173 in vasculogenesis in mice." *Proc Natl Acad Sci U S A* **102**(4): 1076-1081.
- Salatino-Oliveira, A., J. P. Genro, R. Chazan, C. Zeni, M. Schmitz, G. Polanczyk, T. Roman, L. A. Rohde and M. H. Hutz (2012). "Association study of GIT1 gene with attention-deficit hyperactivity disorder in Brazilian children and adolescents." *Genes Brain Behav* **11**(7): 864-868.
- Sambrook, J. and D. W. Russell (2001). *SDS-Polyacrylamide Gel Electrophoresis of Proteins. Molecular Biology: A Laboratory Manual*. J. Sambrook and D. W. Russell. New York, Cold Spring Harbor Laboratory Press. **3**: A8.40-48.45.
- Sanders, L. C., F. Matsumura, G. M. Bokoch and P. de Lanerolle (1999). "Inhibition of myosin light chain kinase by p21-activated kinase." *Science* **283**(5410): 2083-2085.
- Saras, J., P. Wollberg and P. Aspenstrom (2004). "Wrch1 is a GTPase-deficient Cdc42-like protein with unusual binding characteristics and cellular effects." *Exp Cell Res* **299**(2): 356-369.
- Schlenker, O. and K. Rittinger (2009). "Structures of dimeric GIT1 and trimeric beta-PIX and implications for GIT-PIX complex assembly." *J Mol Biol* **386**(2): 280-289.



- Schmalzigaug, R., H. Phee, C. E. Davidson, A. Weiss and R. T. Premont (2007). "Differential expression of the ARF GAP genes GIT1 and GIT2 in mouse tissues." J Histochem Cytochem **55**(10): 1039-1048.
- Schmalzigaug, R., R. M. Rodriguiz, P. E. Bonner, C. E. Davidson, W. C. Wetsel and R. T. Premont (2009). "Impaired fear response in mice lacking GIT1." Neurosci Lett **458**(2): 79-83.
- Schmalzigaug, R., R. M. Rodriguiz, L. E. Phillips, C. E. Davidson, W. C. Wetsel and R. T. Premont (2009). "Anxiety-like behaviors in mice lacking GIT2." Neurosci Lett **451**(2): 156-161.
- Schober, M., S. Raghavan, M. Nikolova, L. Polak, H. A. Pasolli, H. E. Beggs, L. F. Reichardt and E. Fuchs (2007). "Focal adhesion kinase modulates tension signaling to control actin and focal adhesion dynamics." J Cell Biol **176**(5): 667-680.
- Schwartz, M. A. (2010). "Integrins and extracellular matrix in mechanotransduction." Cold Spring Harb Perspect Biol **2**(12): a005066.
- Shikata, Y., K. G. Birukov, A. A. Birukova, A. Verin and J. G. Garcia (2003). "Involvement of site-specific FAK phosphorylation in sphingosine-1 phosphate- and thrombin-induced focal adhesion remodeling: role of Src and GIT." FASEB J **17**(15): 2240-2249.
- Siasios, I., E. Z. Kapsalaki and K. N. Fountas (2013). "Cerebral vasospasm pharmacological treatment: an update." Neurol Res Int **2013**: 571328.
- Singh, V. K., K. Munro and Z. Jia (2012). "A novel calmodulin-beta-PIX interaction and its implication in receptor tyrosine kinase regulation." Cell Signal **24**(9): 1790-1796.
- Slack-Davis, J. K., K. H. Martin, R. W. Tilghman, M. Iwanicki, E. J. Ung, C. Autry, M. J. Luzzio, B. Cooper, J. C. Kath, W. G. Roberts and J. T. Parsons (2007). "Cellular characterization of a novel focal adhesion kinase inhibitor." J Biol Chem **282**(20): 14845-14852.
- Staruschenko, A. and A. Sorokin (2012). "Role of betaPix in the Kidney." Front Physiol **3**: 154.
- Stehbens, S. and T. Wittmann (2012). "Targeting and transport: how microtubules control focal adhesion dynamics." J Cell Biol **198**(4): 481-489.
- Stockton, R., J. Reutershan, D. Scott, J. Sanders, K. Ley and M. A. Schwartz (2007). "Induction of vascular permeability: beta PIX and GIT1 scaffold the activation of extracellular signal-regulated kinase by PAK." Mol Biol Cell **18**(6): 2346-2355.
- Strath, J., L. J. Georgopoulos, P. Kellam and G. E. Blair (2009). "Identification of genes differentially expressed as result of adenovirus type 5- and adenovirus type 12-transformation." BMC Genomics **10**: 67.
- Stricker, J., Y. Beckham, M. W. Davidson and M. L. Gardel (2013). "Myosin II-mediated focal adhesion maturation is tension insensitive." PLoS One **8**(7): e70652.

- Su, Z. J., C. N. Hahn, G. J. Goodall, N. M. Reck, A. F. Leske, A. Davy, G. Kremmidiotis, M. A. Vadas and J. R. Gamble (2004). "A vascular cell-restricted RhoGAP, p73RhoGAP, is a key regulator of angiogenesis." Proc Natl Acad Sci U S A **101**(33): 12212-12217.
- Takahashi, T., S. Yamaguchi, K. Chida and M. Shibuya (2001). "A single autophosphorylation site on KDR/Flk-1 is essential for VEGF-A-dependent activation of PLC-gamma and DNA synthesis in vascular endothelial cells." EMBO J **20**(11): 2768-2778.
- Takase, H., K. Matsumoto, R. Yamadera, Y. Kubota, A. Otsu, R. Suzuki, H. Ishitobi, H. Mochizuki, T. Kojima, S. Takano, K. Uchida, S. Takahashi and M. Ema (2012). "Genome-wide identification of endothelial cell-enriched genes in the mouse embryo." Blood **120**(4): 914-923.
- Tan, W., T. R. Palmby, J. Gavard, P. Amornphimoltham, Y. Zheng and J. S. Gutkind (2008). "An essential role for Rac1 in endothelial cell function and vascular development." FASEB J **22**(6): 1829-1838.
- Tcherkezian, J. and N. Lamarche-Vane (2007). "Current knowledge of the large RhoGAP family of proteins." Biol Cell **99**(2): 67-86.
- ten Klooster, J. P., Z. M. Jaffer, J. Chernoff and P. L. Hordijk (2006). "Targeting and activation of Rac1 are mediated by the exchange factor beta-Pix." J Cell Biol **172**(5): 759-769.
- Turner, C. E., M. C. Brown, J. A. Perrotta, M. C. Riedy, S. N. Nikolopoulos, A. R. McDonald, S. Bagrodia, S. Thomas and P. S. Leventhal (1999). "Paxillin LD4 motif binds PAK and PIX through a novel 95-kD ankyrin repeat, ARF-GAP protein: A role in cytoskeletal remodeling." J Cell Biol **145**(4): 851-863.
- Turner, C. E., K. A. West and M. C. Brown (2001). "Paxillin-ARF GAP signaling and the cytoskeleton." Curr Opin Cell Biol **13**(5): 593-599.
- Vader, P., R. van der Meel, M. H. Symons, M. H. Fens, E. Pieters, K. J. Wilschut, G. Storm, M. Jarzabek, W. M. Gallagher, R. M. Schiffelers and A. T. Byrne (2011). "Examining the role of Rac1 in tumor angiogenesis and growth: a clinically relevant RNAi-mediated approach." Angiogenesis **14**(4): 457-466.
- van Nieuw Amerongen, G. P., K. Natarajan, G. Yin, R. J. Hoefen, M. Osawa, J. Haendeler, A. J. Ridley, K. Fujiwara, V. W. van Hinsbergh and B. C. Berk (2004). "GIT1 mediates thrombin signaling in endothelial cells: role in turnover of RhoA-type focal adhesions." Circ Res **94**(8): 1041-1049.
- Vega, F. M., G. Fruhwirth, T. Ng and A. J. Ridley (2011). "RhoA and RhoC have distinct roles in migration and invasion by acting through different targets." J Cell Biol **193**(4): 655-665.
- Vega, F. M. and A. J. Ridley (2007). "SnapShot: Rho family GTPases." Cell **129**(7): 1430.
- Vicente-Manzanares, M. and A. R. Horwitz (2011). "Cell migration: an overview." Methods Mol Biol **769**: 1-24.

- Vignal, E., M. De Toledo, F. Comunale, A. Ladopoulou, C. Gauthier-Rouviere, A. Blangy and P. Fort (2000). "Characterization of TCL, a new GTPase of the rho family related to TC10 and Cdc42." J Biol Chem **275**(46): 36457-36464.
- Vitale, N., W. A. Patton, J. Moss, M. Vaughan, R. J. Lefkowitz and R. T. Premont (2000). "GIT proteins, A novel family of phosphatidylinositol 3,4, 5-trisphosphate-stimulated GTPase-activating proteins for ARF6." J Biol Chem **275**(18): 13901-13906.
- Wacker, A. and H. Gerhardt (2011). "Endothelial development taking shape." Curr Opin Cell Biol **23**(6): 676-685.
- Wang, J., Y. Taba, J. Pang, G. Yin, C. Yan and B. C. Berk (2009). "GIT1 mediates VEGF-induced podosome formation in endothelial cells: critical role for PLCgamma." Arterioscler Thromb Vasc Biol **29**(2): 202-208.
- Wang, J., G. Yin, P. Menon, J. Pang, E. M. Smolock, C. Yan and B. C. Berk (2010). "Phosphorylation of G protein-coupled receptor kinase 2-interacting protein 1 tyrosine 392 is required for phospholipase C-gamma activation and podosome formation in vascular smooth muscle cells." Arterioscler Thromb Vasc Biol **30**(10): 1976-1982.
- Wang, X., S. Liao, E. R. Nelson, R. Schmalzigaug, R. F. Spurney, F. Guilak, R. T. Premont and D. Gesty-Palmer (2012). "The cytoskeletal regulatory scaffold protein GIT2 modulates mesenchymal stem cell differentiation and osteoblastogenesis." Biochem Biophys Res Commun **425**(2): 407-412.
- Wang, Y., H. Cao, J. Chen and M. A. McNiven (2011). "A direct interaction between the large GTPase dynamin-2 and FAK regulates focal adhesion dynamics in response to active Src." Mol Biol Cell **22**(9): 1529-1538.
- Webb, D. J., M. Kovalenko, L. Whitmore and A. F. Horwitz (2006). "Phosphorylation of serine 709 in GIT1 regulates protrusive activity in cells." Biochem Biophys Res Commun **346**(4): 1284-1288.
- Webb, D. J., M. W. Mayhew, M. Kovalenko, M. J. Schroeder, E. D. Jeffery, L. Whitmore, J. Shabanowitz, D. F. Hunt and A. F. Horwitz (2006). "Identification of phosphorylation sites in GIT1." J Cell Sci **119**(Pt 14): 2847-2850.
- Wennerberg, K. and C. J. Der (2004). "Rho-family GTPases: it's not only Rac and Rho (and I like it)." J Cell Sci **117**(Pt 8): 1301-1312.
- Wojciak-Stothard, B., S. Potempa, T. Eichholtz and A. J. Ridley (2001). "Rho and Rac but not Cdc42 regulate endothelial cell permeability." J Cell Sci **114**(Pt 7): 1343-1355.
- Wojciak-Stothard, B., L. Y. Tsang, E. Paleolog, S. M. Hall and S. G. Haworth (2006). "Rac1 and RhoA as regulators of endothelial phenotype and barrier function in hypoxia-induced neonatal pulmonary hypertension." Am J Physiol Lung Cell Mol Physiol **290**(6): L1173-1182.

- Wolfenson, H., Y. I. Henis, B. Geiger and A. D. Bershadsky (2009). "The heel and toe of the cell's foot: a multifaceted approach for understanding the structure and dynamics of focal adhesions." Cell Motil Cytoskeleton **66**(11): 1017-1029.
- Wolfenson, H., I. Lavelin and B. Geiger (2013). "Dynamic regulation of the structure and functions of integrin adhesions." Dev Cell **24**(5): 447-458.
- Won, H., W. Mah, E. Kim, J. W. Kim, E. K. Hahm, M. H. Kim, S. Cho, J. Kim, H. Jang, S. C. Cho, B. N. Kim, M. S. Shin, J. Seo, J. Jeong, S. Y. Choi, D. Kim, C. Kang and E. Kim (2011). "GIT1 is associated with ADHD in humans and ADHD-like behaviors in mice." Nat Med **17**(5): 566-572.
- Worth, D. C. and M. Parsons (2008). "Adhesion dynamics: mechanisms and measurements." Int J Biochem Cell Biol **40**(11): 2397-2409.
- Yin, G., J. Haendeler, C. Yan and B. C. Berk (2004). "GIT1 functions as a scaffold for MEK1-extracellular signal-regulated kinase 1 and 2 activation by angiotensin II and epidermal growth factor." Mol Cell Biol **24**(2): 875-885.
- Yin, G., Q. Zheng, C. Yan and B. C. Berk (2005). "GIT1 is a scaffold for ERK1/2 activation in focal adhesions." J Biol Chem **280**(30): 27705-27712.
- Yu, J. A., N. O. Deakin and C. E. Turner (2009). "Paxillin-kinase-linker tyrosine phosphorylation regulates directional cell migration." Mol Biol Cell **20**(22): 4706-4719.
- Yu, J. A., F. C. Foley, J. D. Amack and C. E. Turner (2011). "The cell adhesion-associated protein Git2 regulates morphogenetic movements during zebrafish embryonic development." Dev Biol **349**(2): 225-237.
- Yuan, L., A. Sacharidou, A. N. Stratman, A. Le Bras, P. J. Zwiers, K. Spokes, M. Bhasin, S. C. Shih, J. A. Nagy, G. Molema, W. C. Aird, G. E. Davis and P. Oettgen (2011). "RhoJ is an endothelial cell-restricted Rho GTPase that mediates vascular morphogenesis and is regulated by the transcription factor ERG." Blood **118**(4): 1145-1153.
- Zaidel-Bar, R., C. Ballestrem, Z. Kam and B. Geiger (2003). "Early molecular events in the assembly of matrix adhesions at the leading edge of migrating cells." J Cell Sci **116**(Pt 22): 4605-4613.
- Zaidel-Bar, R., M. Cohen, L. Addadi and B. Geiger (2004). "Hierarchical assembly of cell-matrix adhesion complexes." Biochem Soc Trans **32**(Pt3): 416-420.
- Zaidel-Bar, R. and B. Geiger (2010). "The switchable integrin adhesome." J Cell Sci **123**(Pt 9): 1385-1388.
- Zhang, H., D. J. Webb, H. Asmussen and A. F. Horwitz (2003). "Synapse formation is regulated by the signaling adaptor GIT1." J Cell Biol **161**(1): 131-142.

Zhang, H., D. J. Webb, H. Asmussen, S. Niu and A. F. Horwitz (2005). "A GIT1/PIX/Rac/PAK signaling module regulates spine morphogenesis and synapse formation through MLC." J Neurosci **25**(13): 3379-3388.

Zhang, N., W. Cai, G. Yin, D. J. Nagel and B. C. Berk (2010). "GIT1 is a novel MEK1-ERK1/2 scaffold that localizes to focal adhesions." Cell Biol Int **34**(1): 41-47.

Zhang, Z. and B. Zhou (2013). "Accelerated coronary angiogenesis by vegfr1-knockout endocardial cells." PLoS One **8**(7): e70570.

Zhao, Z. S., E. Manser, T. H. Loo and L. Lim (2000). "Coupling of PAK-interacting exchange factor PIX to GIT1 promotes focal complex disassembly." Mol Cell Biol **20**(17): 6354-6363.

## **APPENDIX: Re-print of the thesis related publication**

‘RhoJ interacts with the GIT–PIX complex and regulates focal adhesion disassembly’

Eleanor Wilson<sup>\*</sup>, Katarzyna Leszczynska<sup>\*</sup>, Natalie S. Poulter, Francesca Edelmann, Victoria A. Salisbury, Peter J. Noy, Andrea Bacon, Joshua Z. Rappoport, John K. Heath, Roy Bicknell and Victoria L. Heath

J Cell Sci 2014 127:3039-3051; Advance Online Article June 13, 2014, doi:10.1242/jcs.140434

\* These authors contributed equally to this work